Hot and Dense Matter in Compact Stars – From Nuclei to Quarks

Dissertation

submitted to the
Combined Faculties of the Natural Sciences and Mathematics
of the Ruperto-Carola-University of Heidelberg, Germany
for the degree of
Doctor of Natural Sciences

put forward by
Matthias Hempel
born in Frankfurt am Main, Germany
Oral examination date: 19.10.2010

Referees: Prof. Dr. Jürgen Schaffner-Bielich
Prof. Dr. Matthias Bartelmann

Dissertation

submitted to the
Combined Faculties of the Natural Sciences and Mathematics
of the Ruperto-Carola-University of Heidelberg, Germany
for the degree of
Doctor of Natural Sciences

put forward by
Matthias Hempel
born in Frankfurt am Main, Germany
Oral examination date: 19.10.2010

Hot and Dense Matter in Compact Stars – From Nuclei to Quarks

Referees: Prof. Dr. Jürgen Schaffner-Bielich
Prof. Dr. Matthias Bartelmann

Abstract

Hot and Dense Matter in Compact Stars – From Nuclei to Quarks
This dissertation deals with the equation of state of hot and dense matter in compact stars, with special focus on first order phase transitions. A general classification of first order phase transitions is given and the properties of mixed phases are discussed. Aspects of nucleation and the role of local constraints are investigated. The derived theoretical concepts are applied to matter in neutron stars and supernovae, in the hadron-quark and the liquid-gas phase transition.

For the detailed description of the liquid-gas phase transition a new nuclear statistical equilibrium model is developed. It is based on a thermodynamic consistent implementation of relativistic mean-field interactions and excluded volume effects. With this model different equation of state tables are calculated and the composition and thermodynamic properties of supernova matter are analyzed. As a first application numerical simulations of core-collapse supernovae are presented.

For the hadron-quark phase transition two possible scenarios are studied in more detail. First the appearance of a new mixed phase in a proto neutron star and the implications on its evolution. In the second scenario the consequences of the hadron-quark transition in core-collapse supernovae are investigated. Simulations show that the appearance of quark matter has clear observable signatures and can even lead to the generation of an explosion.

Zusammenfassung

Heiße und Dichte Materie in Kompakten Sternen – Von Kernen zu Quarks Diese Dissertation beschäftigt sich mit der Zustandsgleichung heißer und dichter Materie in kompakten Sternen, mit besonderem Fokus auf Phasenübergänge erster Ordnung. Zunächst werden diese allgemein klassifiziert und die Eigenschaften von gemischten Phasen diskutiert. Anschließend werden Aspekte der Nukleation und die Rolle von lokalen Zwangsbedingungen untersucht. Die erarbeiteten theoretischen Konzepte werden dann auf Materie in Neutronensternen und Supernovae im Hadron-Quark- und flüssig-gas-Phasenübergang angewandt.

Zur detaillierten Beschreibung des flüssig-gas-Phasenübergangs wird ein neues nukleares statistisches Gleichgewichtsmodell entwickelt. Dieses basiert auf einer thermodynamisch konsistenten Implementierung von relativistischen Mittel-Feld-Wechselwirkungen und Ausgeschlossenem-Volumen-Effekten. Mit diesem Modell werden verschiedene Zustandsgleichungs-Tabellen berechnet und die Zusammensetzung und thermodynamischen Eigenschaften von Supernova-Materie untersucht. Die Ergebnisse werden mit anderen bestehenden Modellen verglichen. Als erste Anwendung werden numerische Simulationen von Kernkollaps-Supernovae präsentiert.

Für den Hadron-Quark-Phasenübergang werden zwei mögliche Szenarien detaillierter betrachtet. Zum einen das Auftreten einer neue gemischte Phase in einem Proto-Neutronenstern und die zugehörigen Auswirkungen auf dessen Entwicklung und Stabilität. In einem anderen Szenario werden die Konsequenzen des Hadron-Quark-Übergangs in Kernkollaps-Supernovae untersucht. Simulationen zeigen, dass das Auftreten von Quarkmaterie mit klaren beobachtbaren Signaturen verbunden ist und sogar zur Entwicklung einer Explosion führen kann.

Acknowledgements

Here I want to thank all the people who helped me during my Ph.D. studies or who contributed to this work. First of all I want to thank my supervisor Jürgen Schaffner-Bielich. My Ph.D. would not have been possible without him. He introduced me into the research field of compact stars already during my diploma studies. The initial ideas for my Ph.D. studies were given by him and have been worked out under his friendly and liberal supervision. I want to thank him that he was always open for my questions and found time for the discussion of my work. Furthermore, he encouraged me to participate in international conferences, introduced me into the community of compact star physicists and gave advice for my collaborations with other scientists. This was of great help for my research and my future carreer as well.

In this context I am also very grateful for the financial support and the structured doctoral education by the Graduate Program for Hadron and Ion Research (GP-HIR), the Frankfurt Institute for Advanced Studies (FIAS), the Helmholtz Research School for Quark Matter Studies (H-QM) and the Heidelberg Graduate School for Fundamental Physics (HGSFP).

I want to thank all the students and post-docs of our working group and of the villa in the Philosophenweg 16 for the nice time spent together, the friendly and open-minded atmosphere and the stimulating discussions we had. Special thanks go to Giuseppe Pagliara, Irina Sagert, Bruno Mintz and Tillmann Böckel for the amazing common research projects and the everyday exchange of ideas, but also for the fun we had in the office, at lunch, in the oldtown of Heidelberg and at other places all over europe during conferences.

Next I want to acknowledge all my collaborators outside of the Heidelberg University. Tobias Fischer contributed substantially to the development of the model for the supernova equation of state and it was always a pleasure to work with him. The discussions with Igor Mishustin, Gerd Röpke, Alexander Botvina, Stefan Typel and Matthias Liebendörfer were very enlightening. They supported my work and gave useful feedback. I want to thank Joachim Stroth for the time he spent as my co-superviser and the helpful committee-meetings which we had. I am also very grateful for Matthias Bartelmann. It was a great relief for me that he agreed on shirt notice to be the second reviewer of this thesis.

Finally, I want to thank my friends Nils Pelleringhoff, Thomas Illenseer, Heidi König, Katja Müller, Melanie Moog, Domingo Candia, Nathalie Larie Diaz Reyes and Catherine Basford, and my family, Sabrina Hempel, Christina Hempel, Claudia Hempel, Nicole Bauersfeld, Waltraut Schiffczyck, Margit Hempel, Jürgen Bauersfeld, Tjorben Bauersfeld, Marit Bauersfeld, Nicolai Armstrong, and Angelika Hempel, and in particular my parents Ingeborg Hempel and Klaus Hempel. Most of my leisure time I have spent with them, in which we had a lot of fun and enjoyed great experiences together. But they also helped me in the hard times, shared my troubles and sorrows. They gave me motivation and the necessary personal support for my work.

Contents

Chapter 1

Introduction

In 2003, the Committee on the Physics of the Universe, which is part of the National Academies of the USA, published a book with the title "Connecting Quarks with the Cosmos - Eleven Science Questions for the New Century" [CotPotU03]. Most of the eleven questions deal with aspects of cosmology, extensions of the Standard Model and its connection to gravity. However, at least two of the questions are directly related to the main theme of this thesis: the properties of hot and dense matter in the context of compact stars. These two questions are:

"What Are the New States of Matter at Exceedingly High Density and Temperature?

Computer simulations of quantum chromodynamics (QCD) have provided evidence that at high temperature and density, matter undergoes a transition to a state known as the quark-gluon plasma. The existence and properties of this new phase of matter have important cosmological implications. Quark-gluon plasmas may also play a role in the interiors of neutron stars. ... X-ray observations of neutron stars can shed light on how matter behaves at nuclear and higher densities, providing insights about the physics of nuclear matter and possibly even of new states of matter."

"How Were the Elements from Iron to Uranium Made?

While we have a relatively complete understanding of the origin of elements lighter than iron, important details in the production of elements from iron to uranium remain a puzzle. A sequence of rapid neutron captures by nuclei, known as the r-process, is clearly involved, as may be seen from the observed abundances of the various elements. Supernova explosions, neutron-star mergers, or gamma-ray bursters are possible locales for this process, but our incomplete understanding of these events leaves the question open. Progress requires work on a number of fronts. More realistic simulations of supernova explosions and neutron star mergers are essential; they will require access to large-scale

computing facilities. In addition, better measurements are needed for both the inputs and the outputs of these calculations."

These two questions are part of the motivation for this thesis. To put the two questions and the thesis into the appropriate context we want to give an introduction into nuclear astrophysics, nucleosynthesis, stellar evolution and the physics of compact stars. It will also become clear in more detail how the topics of this thesis are connected to the two questions.

1.1 Primordial Nucleosynthesis

At a time of 10^{-5} s after the Big Bang, at a temperature of ~ 190 MeV the QCD phase transition was reached. Before, matter consisted of elementary particles in the so-called quark-gluon-plasma, which is a strongly interacting mixture of free quarks, leptons and photons. After this phase transition the quarks have been confined to hadrons in form of baryons and mesons. At a temperature of 1 MeV, corresponding to the time of 1 s, all mesons decayed and besides electrons, positrons and photons only neutrons and protons remained.

From this point in time on we want to follow the evolution of the baryonic part of the matter in the universe in more detail. In equilibrium, the ratio of neutrons to protons is given by their mass difference Δ of 1.29 MeV:

$$n_n/n_p = e^{-\frac{\Delta}{T}} \ . \tag{1.1}$$

For temperatures much larger than 1 MeV, this ratio is equal to unity, for $T = 1$ MeV one obtains $n_n/n_p = 0.28$.

However, already at $T = 0.8$ MeV the typical weak reaction rates fall below the expansion rate of the universe, and thus weak equilibrium is not established any more. As the neutron lifetime is rather long, $\tau_n \sim 890$ s, at this temperature the neutron abundance freezes out with a value $n_n/n_p \sim 0.2$. At the same time the nuclear reactions set in. Necessarily the first reaction has to be the production of deuterons. As the deuteron is only weakly bound, for $T \gg 0.1$ MeV the deuterons are immediately destroyed after their production by photodisintegration. Only below $T = 0.1$ MeV sufficiently many deuterons survive to be further processed to ^{4}He alpha particles.

At three minutes after the Big Bang and $T \sim 0.01$ MeV the end of the primordial nucleosynthesis is reached. Almost all the neutrons which did not decay ($n_n/n_p \sim 0.13$)

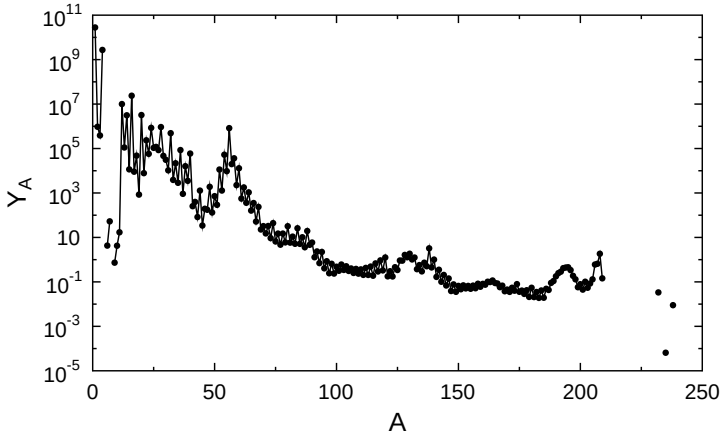

Figure 1.1: The abundance of nuclei by mass number relative to the abundance of silicon as 10^6 in the solar system. Data taken from `www.webnucleo.org`.

are bound to alpha particles, which fixes the alpha particle mass fraction:

$$X_\alpha = \frac{4n_\alpha}{n_B} = \frac{2n_n}{n_B} = 0.24 \,, \tag{1.2}$$

where n_α, n_n and n_B denotes the number density of alphas, neutrons and baryons respectively. Matter after the primordial nucleosynthesis is composed of mainly 76% protons and 24% alphas. In addition only small traces of ^{3}He and D in the order of $10^{-5} - 10^{-4}$ have been produced. A tiny amount of ^{7}Li in the order of $10^{-10} - 10^{-9}$ is also formed. The primordial production of all heavier elements is truly negligible, as there are no stable isotopes with $A = 5$ and $A = 8$, and also because the thermal energies are too low to overcome the increasing Coulomb barrier. We note that these estimated numbers are in agreement with detailed numerical calculations and measurements in old stars and metal-poor gas clouds.

1.2 Today's Element Abundances

The products of the primordial nucleosynthesis represent the initial fuel for the nuclear fusion in stars. The quest of nucleosynthesis is to explain the element abundances which we find in our solar system today as shown in Fig. 1.1. In the context of stellar nucleosynthesis, usually all elements above helium are called "metals". The fraction of metals, the "metallicity" is an indication of the age of the star, as will become clear in the following. Obviously, the first stars of the universe had the vanishingly small metallicity of the primordial nucleosynthesis. We observe that the fraction of hydrogen and helium today is still rather similar as in the early universe. However, it is of fundamental

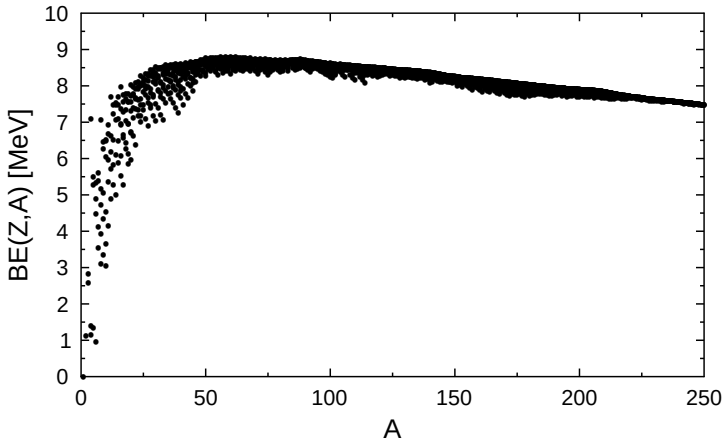

Figure 1.2: The binding energy of nuclei as a function of mass number A. Shown are experimentally measured values of Ref. [AWT03].

relevance to understand the origin of the small fraction (in the order of percent) of the metals, i.e. all the other elements.

The abundance pattern is closely connected to the binding energy of nuclei, which is depicted in Fig. 1.2 for nuclei which have been studied in the laboratory. The binding energy per nucleon has its maximum value for ^{62}Ni. But the nucleus with the lowest energy per nucleon including the rest-mass term is ^{56}Fe. Thus ^{56}Fe is the most stable nucleus. Starting from the initial cosmic fuel consisting of hydrogen and helium, energy can be gained by nuclear fusion until the maximum of the binding energy around $A = 60$ is reached. However, we find elements up to ^{238}U here on earth and in our solar system. As the production of heavier elements than nickel is endothermic, one can expect that there are different physical processes which are involved in the nucleosynthesis.

1.3 Star Formation

The stellar nucleosynthesis and the cycle of matter can be described starting from a cloud of interstellar material, i.e. a mixture of mainly primordial hydrogen and helium and a small fraction of heavier elements in form of atoms, molecules and dust, represented by the violet cloud in Fig. 1.3. Figure 1.4 shows a real image taken with the Hubble Space Telescope of a typical star formation region around the star cluster NGC 3603 in the Milky Way, approximately 20,000 light-years away from our solar system. One can see pillars of dust and gas (Letter A in the figure) which are formed by the interaction with the young stars in the center of the picture.

According to the virial theorem, a cold cloud of interstellar material will collapse under its own gravitational weight if the gravitational energy exceeds twice the kinetic

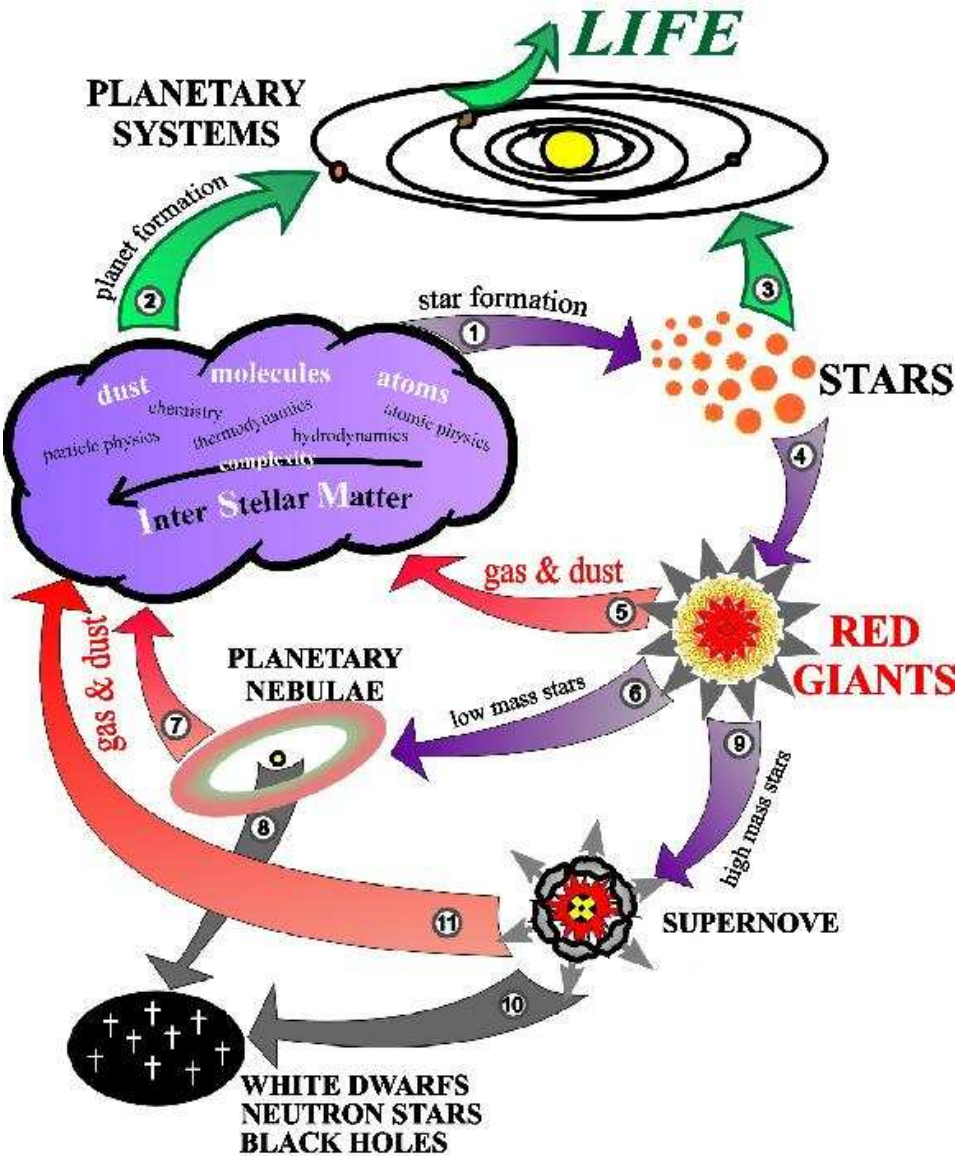

Figure 1.3: The cosmic cycle of matter.

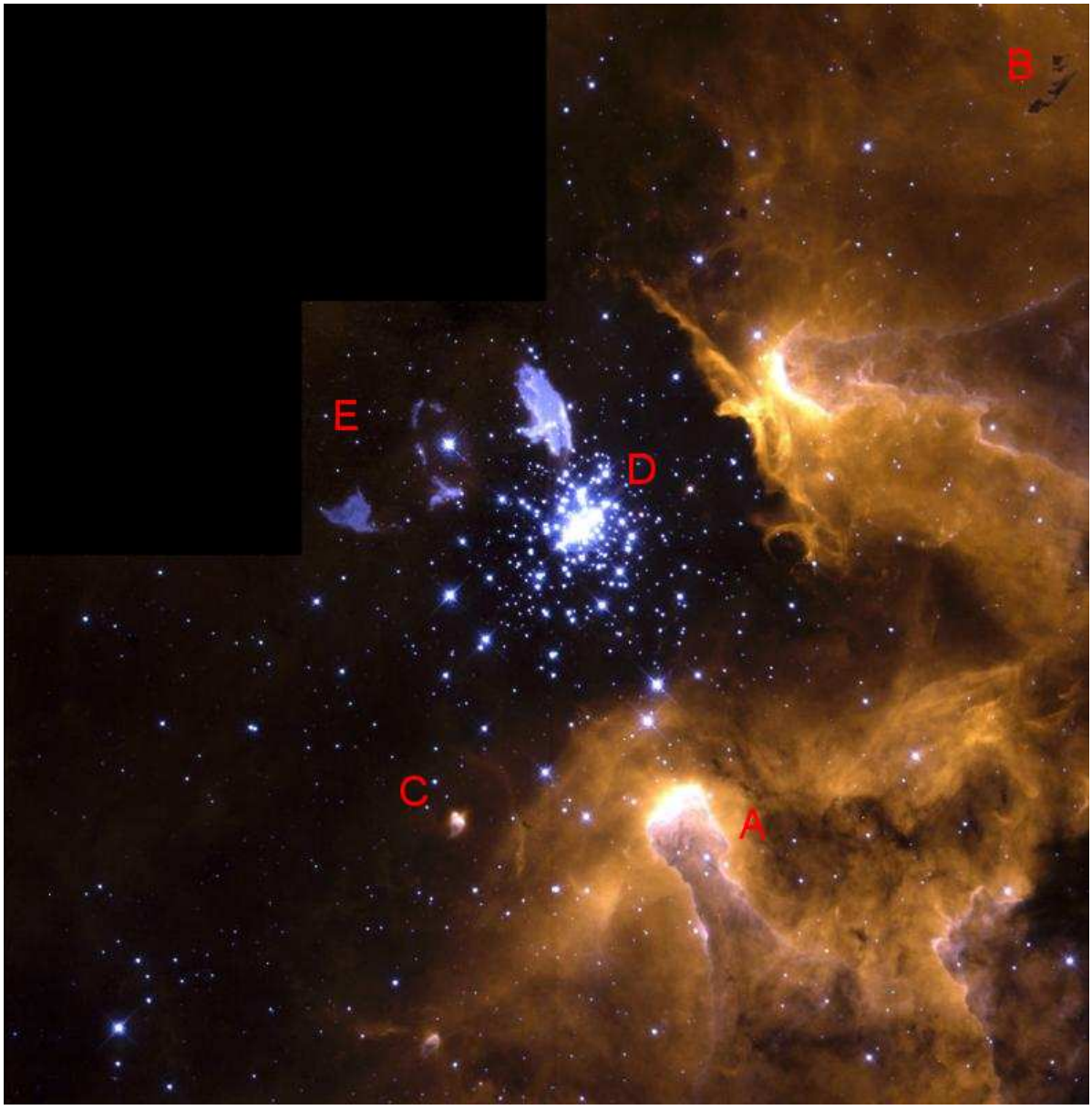

Figure 1.4: Hubble Space Telescope image (true-color) of the giant galactic nebula NGC 3603, 22,000 light-years away from our solar system. A: Gaseous pillars of interstellar material. B: Bok globules: early stages of star formation. C: Gas and dust evaporation from protoplanetary disks. D: Starburst cluster dominated by young, hot Wolf-Rayet stars and early O-type stars. E: Evolved blue supergiant Sher 25 with circumstellar ring and bipolar outflows of chemically enriched material.

energy. This step is depicted by Arrow 1 in Fig. 1.3. An adiabatic collapse follows, which leads to compression and heating of the matter. The small black clouds, called the Bok globules, close to Letter B in Fig. 1.4 show an early stage of this collapse.

The bulk part of the matter in the collapsing cloud will be bound in the central star. A small fraction of the matter can remain in the environment around the star and may evolve to a protoplanetary disk (proplyd). The two compact, tadpole-shaped emission nebulae at Letter C are interpreted as gas and dust evaporation from such protoplanetary disks. Finally, the proplyds may evolve further to a planetary system (Arrows 2 and 3 in Fig. 1.3). Five billion years ago, our own solar system may have looked very similar like the small nebula in Fig. 1.4 C.

1.4 Main Sequence Stars

The temperature in the cloud depends on the collapsing mass and will be the highest in the center, due to the largest compression. For masses greater than 0.1 $M_\odot$ the core temperature will exceed 10^7 K, the critical temperature for which hydrogen burning starts. At this point the high energy tail of the thermal distribution of the hydrogen nuclei becomes large enough to overcome the Coulomb barrier between two protons to form a deuteron in a weak reaction process. In the so-called pp-chain, 4 protons and electrons are burned to an alpha particle, two electrons and two neutrinos. In one such fuel cycle an energy of 26.7 MeV is released, of which an average of 0.26 MeV is directly carried away by the freely escaping neutrinos. The burning energy heats up the star, further enhances the reaction rate and increases the thermal pressure until a new secular equilibrium is reached.

The bottle-neck of the pp-chain is the fusion to deuteron, due to the very small weak reaction cross-section $\sigma < 10^{-21}$ fm^2. This stabilizes the reaction and allows for quasi-static burning. As a consequence, our sun will continue hydrogen burning in the form it does today for the next five billion years. Depending on its mass, a star will spend the longest time of its life in this static burning phase as a so-called main-sequence star. The group of blue stars in the center of Fig. 1.4 at Letter D is a so-called starburst cluster dominated by young, hot Wolf-Rayet stars and early main-sequence O-type stars. At Letter E we see the evolved blue supergiant called Sher 25 which has a unique circumstellar ring of glowing gas.

When the hydrogen in the core is exhausted, the star will further contract until helium burning is ignited for stars more massive than 0.25 $M_\odot$. In this process three

alpha particles are burned to a carbon nucleus. After helium has been ignited, the hydrogen burning continuous in a layer around the core, which is called hydrogen shell burning. Depending on the mass, further burning stages will be reached in which oxygen, neon, magnesium and silicon are produced and burnt to heavier elements. Massive stars will develop an onion-like structure during their evolution. The last possible stage is silicon burning which requires a mass larger than 10 $M_\odot$. The ash of silicon burning consists of iron-like nuclei which accumulate in the core and cannot be processed further.

The nuclei which are involved in the burning chains represent the main outcome of the stellar nucleosynthesis. However, in small portions also other nuclei are produced, including even nuclei beyond iron. Even though the production of heavier nuclei requires energy, there is a way how to form them as a by-product of the stellar nucleosynthesis in the so called s-process. The s-process operates in stellar evolution during helium and carbon burning. "s" abbreviates slow neutron captures. In the s-process neutron captures take place at a rate which is much smaller than the beta-decay rate of the nucleus which is formed after the neutron capture. Immediate beta decay follows, until a stable nucleus is reached. By further subsequent neutron captures and beta decays, heavier elements can be produced along the line of stability. It turns out that the s-process gives characteristic abundance patterns, which alone do not agree with the observed element abundances as shown in Fig. 1.1. Furthermore, nuclei with $A > 209$ undergo very fast alpha decay which suppresses the production of heavier elements by slow neutron captures.

1.5 Explosive Nucleosynthesis

Three nuclei with $A > 209$ are found in the solar system and on earth, which are $^{232}_{90}$Th, $^{235}_{92}$U and $^{238}_{92}$U. The existence of these nuclei and the deviations of the s-process patterns from the observed abundances require that there are additional nucleosynthesis processes. To reach these heavy elements, neutron captures must take place on a timescale which is much shorter than the decay time of the nuclei. A huge neutron flux is required to enable such rapid neutron captures. Thus this process is called the r-process, with "r" standing for rapid. Roughly half of the elements above iron are produced in the r-process. Neutron captures are possible until the neutron dripline is reached, where the neutron separation energy becomes positive. Eventually, the formed nuclei which are located at the dripline will decay to the line of stability. The outcome are r-process abundance patterns with characteristic features which depend on the neutron mass fraction, the temperatures and the involved time-scales. Since the beginning, core-collapse super-

novae are thought to be the ideal candidates for the location of the r-process. However, as noted in the second question, until today it is not clear which astrophysical system actually provides the conditions for a successful r-process.

Besides the r-process another nucleosynthesis process has to exist, as e.g. the existence of three stable isobars for certain mass numbers leads to shielded nuclei which neither can be formed by the r- nor the s-process. This additional process is called the p-process because it deals with the synthesis of nuclei on the proton rich side. Typically 1% of the total element abundance are synthesized by the p-process. These nuclei can be produced by photodisintegration in which a photon is captured and a neutron or alpha-particle is emitted. One thinks that the p-process occurs in explosive neon-oxygen burning in the outer part of core collapse supernovae. In addition there is the rp-process, which involves direct rapid proton-captures. It is expected to take place in X-ray bursts. However, it is not clear how these systems can eject matter into the interstellar medium.

Even with these four processes one cannot explain the strong abundance of light proton-rich nuclei. The observations indicate a lighter element primary process (LEPP). Only very recently the so-called νp-process has been discovered [FML$^+$06]. Progress in core-collapse supernova simulations revealed slightly proton-rich conditions in the early phase of the neutrino wind. Anti-neutrino captures on free and bound protons permit to move upward to nuclei with $A < 100$. For more details about nucleosynthesis we refer to the recent review article [TDF$^+$10].

1.6 The Death of a Star

Every star will finally reach the point where all its burnable fuel is exhausted. This lead to the death of the ordinary burning star and at the same time to the birth of an extremely dense compact star. Depending on its mass, one expects three very different scenarios to happen. For stars below 8 $M_\odot$ a white dwarf forms. More massive stars will collapse to a neutron star. If the progenitor is more massive than 20 $M_\odot$ the mass of the core may exceed the possible maximum mass of a protoneutron star. Then the star further collapses to a stellar black hole.

1.7 White Dwarfs

For stars below 8 $M_\odot$, silicon burning is not reached. Usually a mixture of carbon, nitrogen and oxygen (CNO) accumulates in the core. When the star approach its end,

the outer hydrogen and helium layers are significantly blown up due to shell burning. The star increases in size and becomes a red giant (Arrow 4 in Fig. 1.3).

Eventually, the CNO core will further contract until it is stabilized again by the degeneracy pressure of electrons (Arrow 6). The outer layers further expand and are finally observed as a planetary nebula. The matter of the outer layers which has partly been processed by the stellar nucleosynthesis to a higher metallicity is ejected back into the interstellar space (Arrow 7). The remaining CNO core has a size of roughly 10,000 km and a mass of 1 to 1.4 $M_\odot$. It cools by photon-emission and is observed as a white dwarf (Arrow 8). The central density in a white dwarf is in the order of 10^7 g/cm^3 and has an initial temperature of roughly 10^8 K $\sim$ 0.01 MeV.

1.8 Core-Collapse Supernovae

For stars more massive than 8 $M_\odot$, an iron core forms in the center, which finally collapses under its own weight, leading to a core-collapse supernova (Arrow 9). An enormous amount of gravitational energy of 10^{53} erg is released. Roughly 1 % of this energy has to be transferred into kinetic energy to power the stellar explosion. One of the initial ideas for the explanation of the supernova phenomenon was a direct bounce of the core. In this scenario the nuclear matter in the center compresses during the initial collapse until the large compressibility above saturation density leads to the formation of an outgoing shock wave. The shock wave further accelerates and finally triggers the explosion and ejection of the outer layers. The biggest part of the mass of the star is ejected back into the interstellar space (Arrow 11).

However, the idea of a direct bounce does not work in realistic simulations. So far, even the most comprehensive numerical studies of core-collapse supernovae have difficulties to achieve successful explosions within the progenitor mass range 10 $M_\odot \leq M_{prog} \leq$ 15 $M_\odot$. Explosions in spherical symmetry where accurate three-flavor Boltzmann neutrino transport can be applied, have only been obtained for an 8.8 $M_\odot$ O-Ne-Mg-core [KJH06, FWM$^+$09]. The correct treatment of neutrino transport and weak reactions shows that the shock continuously looses energy by dissociation of heavy nuclei and the emitted neutrinos. The outgoing shock converts into a standing accretion front. The supernova mechanism, which is needed to transform the released gravitational binding energy into an explosion with matter ejection, appears to be much more complex than expected. It represents an outstanding challenge for our current understanding of physics and modeling capabilities.

Multidimensional effects as convection and/or increased neutrino-heating behind the shock may help to revive the shock wave. In general, multidimensional simulations are expected to achieve explosions, but they are computationally very expensive [BDM$^+$06, JMMS08, MJ09]. In more detail, several explosion mechanisms are proposed from different groups: the neutrino-driven [BW85] the magneto-rotational [LW70, Bis71] or the acoustic mechanisms [BLD$^+$06]. In addition to multidimensional effects and the aforementioned mechanisms, an improved equation of state, uncertainties in the neutrino opacities and missing nuclear effects could help to revive the shock wave and finally trigger the explosion.

Since very long core-collapse supernovae have been seen as the ideal candidates to provide conditions for a successful explosive nucleosynthesis. One expects that they contain hot neutron-rich material which is ejected with high velocities. Furthermore, they are frequent and energetic enough to explain the robustness of the observed abundance patterns. In more detail, the later, neutron-rich high entropy phase of the neutrino wind seems to be the most promising site. However, given the difficulties of the simulations to achieve explosions, self-consistent predictions of core-collapse supernova nucleosynthesis are not possible at the moment. To circumvent this problem one can trigger the explosion artificially e.g. by enhancing neutrino heating rates or by depositing additional energy in the core. This makes sense and is fully correct for the outer stellar layers where the p-process takes place, but is incorrect for the innermost layers with the r- and νp-process, which are directly related to the physical explosion mechanism. In general the outcome of the nucleosynthesis and especially the amount of mass which is ejected will depend on the way how the artificial explosion is triggered. In conclusion, the understanding of the supernova mechanism is of great interest by itself but also an essential step to finally answer the second question.

1.9 Neutron Stars

In the progenitor mass range of 8 to 20 $M_\odot$ an extreme new state of matter is formed in the center of the core-collapse supernova. The degeneracy pressure of the electrons is not sufficient to stop the collapse of the core. The densities become so extremely large that the nuclei are dissolved into uniform nuclear matter or even quark matter. Finally, the nuclear interactions and the degeneracy of the nucleons balance the gravitational force again. A neutron star is formed (Arrow 10). During the first ten seconds, in the initial hot stage of the evolution where neutrinos are trapped, one usually calls it a protoneutron star. The neutron star initially cools by neutrinos until at 10^5 years

photon cooling takes over. Neutron stars have typical massess of 1 to 2 $M_\odot$ and radii of 10 to 20 km which makes them to the densest objects of the universe besides black holes. The density in the center of a neutron star may even exceed 10^{15} g/cm^3.

The existence of neutron stars had first been postulated by Landau in 1932 [Lan32]. Baade and Zwicky formulated the idea more precisely in 1934 and even conjectured that they may be born in a supernova [BZ34b, BZ34a]. It took more than 30 years until the existence of neutron stars could be confirmed. Unexpectedly, observations in the radio band lead to the discovery of the first neutron star in the form of a pulsar in 1967 by Jocelyn Bell and Anthony Hewish [HBP$^+$68]. Accidentaly, this group detected a mysterious pulsating source with a very stable frequency of 1,377 ms. Very quickly the origin of the signal could be identified as a rapidly rotating neutron star with a strong magnetic field. In the so-called lighthouse model of Gold [Gol68], the radio-signal is explained in the following way: Due to the conservation of the magnetic flux the magnetic field strength can be increased significantly in the stellar collapse and may easily exceed 10^{13} G in the neutron star. The strong magnetic fields accelerate charged particles which leads to beamed electromagnetic radiation in direction of the magnetic field axis. In general the magnetic field axis is not alined with the rotation axis. If an observer is in the line of sight of one of the rotating radiation cones he observes a pulsating radio signal with the frequency of the rotation frequency. Until today, the radio signal of pulsars belongs to the most important observables of neutron stars and several thousands of radio-pulsars have been identified.

The rotation frequency is so stable and so well understood, that pulsar timing can exceed the preciseness of an atomic clock. If the pulsar is in a binary system, one can deduce the orbital size and period and the total mass of the system. If the system is compact enough general relativistic effects and the emission of gravitational waves even allow to determine the separate masses of the two objects. For some pulsars like the Hulse-Taylor pulsar this can be done so precisely, that the pulsar signal serves as a test of general relativity. The analysis of the Hulse-Taylor pulsar represents the first indirect measurement of gravitational waves, for which Hulse and Taylor received the Nobel prize in 1993. Today, the combined analysis of the timing of several pulsars is also used as a galactic detector of gravitational waves of cosmological origin. So far no signal was detected, which gives an upper limit for the maximum amplitude of gravitational waves in the corresponding frequency band.

Besides in radio, nowadays neutron stars are observed in the optical, X-ray and γ-ray spectrum. Their are many pulsars with well determined mass, however until today there is no reliable direct measurement of the tiny radii of neutron stars which

can be several thousands of lightyears away. It is not possible to deduce the radius of a compact star from the radio signal. Thus the observation in the other bands give important complementary information. For some neutron stars which are in accreting binary systems, so called X-ray bursters, it is possible to deduce the radius based on certain model assumptions. Quite recently in Ref. [SLB10] for the first time a bayesian analysis of several objects was used to get constraints for the mass and radius of neutron stars.

Compact stars provide conditions which cannot be produced in terrestrial laboratories. Compact stars serve as cosmic laboratories for matter at extreme densities, which give complementary information compared to heavy-ion reactions and lattice data. From the opposite point of view, there is of course the fundamental interest to explain the astronomical observations of compact stars with theoretical models.

1.10 Compact Stars and Nucleosynthesis

In Figure 1.3 the remaining compact objects are noted as the "cosmic graveyard", which is misleading from our perspective. Compact stars still can participate in the evolution of the universe and the cosmic cycle of matter. Besides supernovae, also neutron stars and white dwarves may give an important contribution to the observed abundance patterns of the chemical elements. Compared to supernovae, the low proton fraction in neutron star mergers seem to favor a successful r-process. On the other hand, such events are much more rare (every 10^5 years in the Milky way) and less matter is ejected back into space. If a white dwarf ends up in a binary system and accretes matter from the companion star, it might exceed its maximum mass limit. Explosive carbon and oxygen burning sets in, which leads to the complete disruption of the star. This energetic event is observed as a supernova Ia, which also contribute to the nucleosynthesis.

1.11 The Cycle of Matter

In all possible scenarios for the death of the star, the bulk part of the matter is ejected back into space, where it serves again as fuel for the next star formation process. After one of these cycles, the matter has partly been processed in the nucleosynthesis processes and has been enriched with metals. In Figure 1.4 the ring and the bipolar outflows at Letter E (blobs to the upper right and lower left of the star) show such processed ejected matter. The color difference between the supergiant's outflow and the diffuse interstellar

medium in the giant nebula dramatically visualizes the enrichment in heavy elements due to synthesis of heavier elements within stars.

1.12 The Equation of State

Almost all simulations and calculations of the previously mentioned scenarios require thermodynamic information in form of an equation of state (EOS) as an essential input. The EOS contains the interactions of the constituent particles and gives the connection between microphysics and macrophysics. Also to perform simulations of supernova explosions or neutron stars, the thermodynamic properties of matter under the corresponding conditions have to be known. Thus the second question is actually very much connected to the first one. For example to study nucleosynthesis in a core-collapse supernova one first has to construct an EOS which requires certain assumptions for the answer to the first question.

Usually the EOS is calculated for a uniform, infinite thermodynamic system. Such a bulk EOS can contain a thermodynamically unstable region, which leads to a first order phase transition, occurrence of phase separation and thus to the formation of a mixed phase with two phases in coexistence. First order phase transitions are especially interesting because they can lead to extreme effects with clear observable signatures which could help to reveal the true answer to the first question.

It is fascinating that the conditions in typical core-collapse supernovae extend over the huge range from zero to several times saturation density, and temperatures from 0 to 100 MeV, which corresponds to roughly 10^{12} K. These conditions range from the hadron-quark phase transition down to the occurrence of ordinary nuclei. The high density part of the EOS controls the formation of the central core which evolves to a protoneutron star or a black hole. It fixes the gravitational energy which is available for the explosion. But also the low density part plays a crucial role, because there the standing accretion front needs to be transformed into an accelerating shock to launch the explosion. We note that matter in cold compact stars may reach larger densities and larger neutron to proton asymmetries, but otherwise the EOS of cold compact stars is just a special subcase of the most general supernova EOS. Depending on its accuracy, a supernova EOS can also be used for the description of white dwarfs, accretion in binary systems and mergers of compact stars.

1.13 Themes of the Thesis

In this thesis we study the properties of matter in supernovae and compact stars. The physics of compact stars is a wide field of research with an interesting combination of theory, terrestrial experiments and astronomical observations. Furthermore, in these astrophysical objects there is an exciting interplay of quite many and very different physical effects: general relativity, quantum physics, magnetic fields, rotation, superconductivity, hydrodynamics, neutrino physics, weak interactions, QCD, nuclear physics, solid state physics or thermodynamics, just to mention a few. In this thesis we mainly deal with the thermodynamic and nuclear physics aspects of the (supernova) equation of state. Thus we will not address the second question directly. We only deliver the theoretical background which may help to realize the call in the last sentence: "More realistic simulations of supernova explosions and neutron star mergers are essential."

Due to the extreme densities which occur in compact stars we necessarily have to address question number one. Our focus lies on the possible occurrence of first order phase transitions, e.g. to the quark-gluon-plasma, and their correct thermodynamic description. Later we will present two exciting examples for the implications of the phase transition to quark matter in a protoneutron star and a core-collapse supernova. Interestingly, many thermodynamic properties of first order phase transitions can be described rather universal so that the same concepts can be applied to different systems. These general aspects of first order phase transitions are also elaborated in the thesis. The detailed study of the thermodynamics of first order phase transitions also lead to the discovery of some new effects which have not been discussed in the literature to compact stars so far.

At the moment there exist only two realistic EOSs which can be applied in the context of core-collapse supernovae. The reasons for this are the big number of different nuclear effects which come together and the huge parameter range which has to be covered. Furthermore, the calculation of supernova equation of state tables requires huge numerical efforts. As only very few EOS tables are available, the results of the current simulations are somewhat biased and there is a need for new EOS tables. Plenty of effects and possible scenarios have not been investigated so far. For example both of the existing models assume that matter consists of ordinary nucleons up to the largest densities and temperatures. Even if this was true, the supernova EOS is still very much model dependent. First of all, the nuclear interactions are not known at large densities. Second, at densities below saturation density another first order phase transition occurs, the liquid-gas phase transition of nuclear matter. The properties of the low density EOS are dominated by this phase transition, thus its precise description is crucial.

This leads to the main effort of my PhD studies. I developed a new model for a complete supernova equation of state: the excluded volume nuclear statistical equilibrium (EXV-NSE) model. This model has some new features, which are not contained in the two existing EOSs and allows to calculate new equation of state tables rather quickly. New EOS tables enable to explore the role of certain aspects of the EOS in simulations, like e.g. different nuclear interactions which give different symmetry energies. The ExV NSE model can give a consistent bridge from ordinary nuclei like they exist here on earth, to the densities where quark matter is expected to appear. The low density part is based on experimental and theoretical input for the nuclear masses. This may allow an easier connection of core-collapse supernovae simulations with nucleosynthesis calculation. It is convenient that the existing knowledge about the nuclear structure is also used in the EOS. Eventually a better understanding of the EOS may help to solve the question of the supernova-mechanism and the missing site for nucleosynthesis.

Chapter 2

QCD Matter

Quantum Chromodynamics (QCD) is the fundamental theory which in principle describes strongly interacting matter ab initio. However, the complex structure of this theory defies solutions in the non-perturbative regime relevant for compact stars. Thus even though the underlying theory is known, experimental observations and phenomenological models are necessary to understand the properties of matter under such conditions. The high density regime is of special relevance for our fundamental understanding of nature, because one expects that the transition from hadrons to quarks occurs there.

2.1 General Aspects of QCD

First we want to discuss some characteristic aspects of QCD, the quantum field theory of the strong interactions. This theory describes the interactions of particles which carry the conserved baryon quantum number and which are color-charged. Eventually, the strong interactions are also the origin of the nuclear interactions of the color-neutral hadrons.

In the standard model the elementary particles which constitute the matter around us and of which we are made of are electrons and quarks. With the current knowledge, gained from experiments and theories, one expects that there are six different kind of quarks: the up, down, strange, charm, bottom and top quark, (sorted by increasing mass). The interactions of these particles are dominated by the strong interactions which are described by the QCD Lagrangian:

$$\mathcal{L} = \bar{\psi}_f(i\not{D} - m_f)\psi_f - \frac{1}{4}G^a_{\mu\nu}G^{\mu\nu}_a \ , \tag{2.1}$$

where f denotes the quark flavor and m_f the corresponding quark mass. The interaction of the quarks, which are represented by the quark fields ψ_f (Dirac spinors) is mediated

by the exchange of gluons. This can be identified with the appearance of the gauge potential G^a_μ in the covariant derivative:

$$i\not{D}\psi = \gamma^\mu \left(i\partial_\mu + gG^a_\mu \frac{\lambda^a}{2} \right) \psi \ . \tag{2.2}$$

G^a_μ also builds up the gauge invariant gluonic field strength tensor:

$$G^a_{\mu\nu} = \partial_\mu G^a_\nu - \partial_\nu G^a_\mu - g f^{abc} G^b_\mu G^c_\nu \tag{2.3}$$

where the QCD structure constants f^{abc} appear. Compared to the other two fundamental interactions of matter besides gravity, the electromagnetic interactions of Quantum Electrodynamics (QED) and the theory of weak interactions, the structure of the strong interactions exhibits some fundamental complications which so far do not allow to derive solutions at low energy scales.

In a qualitative picture there are mainly two aspects which cause these complications: The charge of QCD is called 'color'. In contrast to electroweak interactions, the interaction-bosons of QCD themselves are also charged, i.e. not only the quarks but also the gluons carry color. Thus the gluons can interact among themselves, which is not possible in electroweak theory, as the photons do not carry electric charge and the massive vector bosons do not carry weak charge. This interaction of the gluons can be identified in Eq. (2.3) by the appearance of the coupling constant g in the gluonic part of the Lagrangian.

This aspect alone would not be a fundamental problem. But in connection with the following property of QCD it leads to principle difficulties. In electroweak theory the coupling constants are small at the energy scales which are of relevance for terrestrial experiments and for today's universe. Conversely, in QCD the coupling constant $\alpha_s = g^2/4\pi$ is of order unity. Thus perturbation theory cannot be applied. Diagrams up to all orders contribute, including the gluon-gluon interactions.

These effects lead to certain characteristic features of QCD matter at densities below several times saturation density. One effect is called 'confinement'. It is related to the fact, that so far no isolated colored objects have been observed. It seems to be that isolated particles have to be color-neutral. If two quarks, which together are color-neutral, are tried to be separated from each other, their potential will rise linearly at large distances. Thus the potential energy will increase until another color-neutral quark-antiquark pair is created, preventing the separation of quarks from antiquarks on large distances. In high energy heavy-ion collisions, this effect can be observed and is called 'string fragmentation'. There exist only two combinations to form a color-neutral

object: pairs of quarks and antiquarks, called mesons, or combinations of three quarks, called baryons. Thus at low energies only mesons and baryons can be observed, but no single quarks. This effect of confining the color charge to color-neutral objects is yet not understood quantitatively and cannot be derived directly from QCD. Besides baryons and mesons, some theories propose that there are additional classes of color-neutral particles: so called penta-quarks, consisting of five quarks, and four-quark-states called 'dibaryons'. However, there is no clear experimental evidence for their actual existence.

Another important aspect of QCD is chiral symmetry. Chirality is a symmetry of the QCD-Lagrangian for massless particles and leads to the conservation of helicity. In QCD, chiral symmetry is spontaneously broken. At low densities/energies the quarks get a large mass which is generated dynamically by the fields. The additional consideration of small 'constituent' quark masses, leads to explicit chiral symmetry breaking so that also at large densities chiral symmetry is restored only approximately.

QCD contains further interesting aspects: With increasing energy scales the coupling constant α_s decreases, which is the opposite behavior compared to the electromagnetic and weak coupling constants. Thus at high momentum, perturbation theory can be applied, and the one-gluon exchange is the dominant interaction. In this regime, confinement is not observed any more and the quarks behave as 'deconfined', free particles. This effect is called 'asymptotic freedom'. However, the required densities at $T = 0$ are orders of magnitude larger than the typical densities in the center of a neutron star, even though they are the most compact objects of the universe. Thus the perturbative description is not of relevance in the context of nuclear astrophysics.

2.2 Phase Transitions in QCD matter

Here we only want to give a brief overview of the possible first order phase transitions in QCD matter, with the focus on compact stars. The detailed description of such phase transitions follows in the subsequent chapters. As the underlying theory of strongly interacting matter cannot be solved, one is left with the possibility to use phenomenological or effective models. From the study of such models one expects that QCD matter undergoes a first order phase transition at large densities and temperatures, the so-called 'QCD phase transition' or 'hadron-quark phase transition', see e.g. [Ito70, HPS93]. This phase transition is due to the aforementioned chiral symmetry restoration within the quark phase, i.e. the quarks become (almost) massless. Also confinement can lead to a first order phase transition. So far, in most theories these two phase transitions coincide, as shown in Fig. 2.1. However, experimentally this is not fixed and some of the

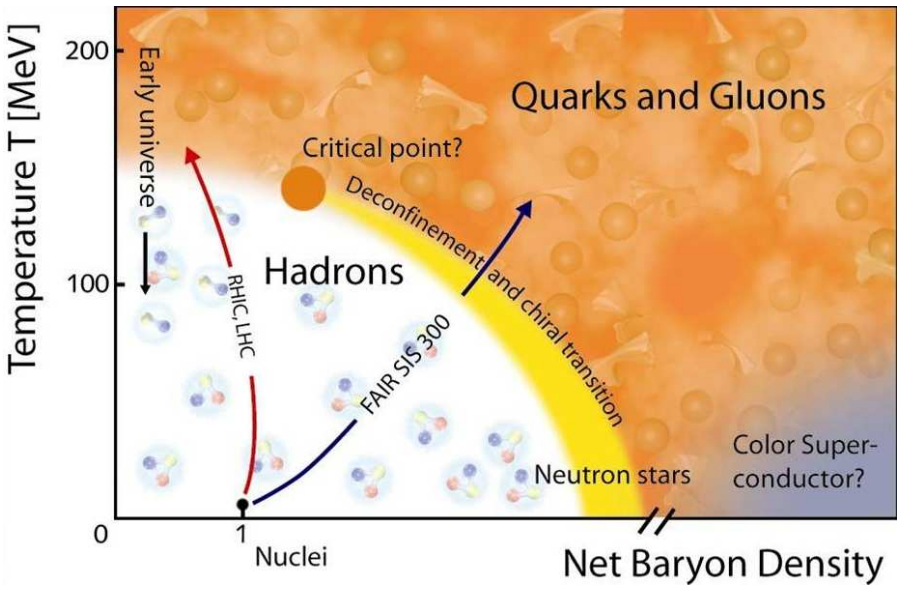

Figure 2.1: An artistic illustration of the QCD phase diagram, as qualitatively expected from phenomenological or effective models.

theories for QCD matter predict a different phase diagram. For example in Ref. [MP07] a new phase of so-called 'quarkyonic' matter was proposed, in which chiral symmetry is restored but quarks are still deconfined.

At large temperatures and vanishing densities numerical solutions of the QCD-Lagrangian exist for finite discretized space-time volumes. This parameter regime is of special interest for cosmology, as the evolution of the early universe went along the temperature-axis according to most of the cosmological models, but different scenarios are also discussed, see e.g. [BS09]. Monte-Carlo calculations are necessary for the evaluation of the QCD equations of motion and thus one also speaks about lattice QCD simulations. These simulations give important information about the QCD phase diagram. Within the last decades one came to the conclusion that the QCD phase transition is actually a cross-over at zero density. It occurs at a temperature of roughly 190 MeV [Kt07]. If at large densities a first order phase transition exists, naturally this leads to the prediction of a critical endpoint at which the phase transition is of second order. Unfortunately, the extension of lattice simulations to large densities exhibits severe problems which so far have not been solved unambiguously. It is one of the major challenges for theoretical as well as experimental research to prove or disprove the existence of the first order phase transition line and to finally find the precise location of the possible critical endpoint.

From an experimental point of view high energy heavy-ion collisions are the best tool to explore the QCD phase diagram. Physicists have big expectations on the largest ex-

periment ever built, the Large Hadron Collider LHC at CERN, which started operation in 2009. Besides proton-proton collisions also an extensive heavy-ion program is planned at this facility. The most important experiments of the past were performed at the Relativistic Heavy Ion Collider RHIC in Brookhaven and at the Super Proton Synchrotron SPS at CERN. Due to the large collision energies evolved, these experiments mainly probe conditions of large temperatures and small baryo-chemical potentials, which were also present in the early universe and where the crossover transition is expected. At the Facility for Antiproton and Ion Research FAIR at GSI Darmstadt one wants to achieve higher densities, to reach the first order region of the QCD phase diagram.

Besides the QCD phase transition plenty of other phase transitions can occur for the typical conditions in a compact star, i.e. at large densities and low temperatures. There is the possibility of a first order phase transition to a kaon condensed phase [FMMT96, GS98, GS99, PRE$^+$00]. The possible phase transition to a pion condensed phase [MCM79, HP82, MSTV90] or to hyperon matter [SHSG02] might also be of first order. Phase transitions between different types of color superconducting quark matter were proposed e.g. in Refs. [RWB$^+$06a, BFG$^+$05, PS08, IRR$^+$08].

A description on the basis of interacting quarks and gluons would be rather impractical on an energy scale of the order of the nuclear interactions. Due to confinement, on this energy scale the relevant degrees of freedom are the baryons and mesons and not the quarks. Anyhow, so far it was not accomplished to describe hadronic matter by quark degrees of freedom. An unified EOS which describes quark and hadronic matter within the same model is not available. This statement is true with one exception: It is possible to develop a model which always includes hadrons and quarks in a chemical mixture, see e.g. [DS10]. At low densities the quark contribution vanishes and at large densities the hadron densities are negligible. Besides such models, usually the quark and the hadronic EOS are calculated with two separate models. They represent the two regions of the phase diagram of the imaginative underlying unified EOS, which are separated from each other by the binodal region of the first order phase transition. At the end of this chapter we will present some of such phenomenological or effective models for the two parts of the QCD bulk EOS, first for quark matter and then for nucleonic matter.

At lower densities around saturation density, $\rho_0 \sim 2 - 3 \times 10^{14}\mathrm{g/cm}^3$ and temperatures lower than ~ 15 MeV, another phase transition occurs: the well-known liquid-gas phase transition of nuclear matter [RPW83, LLPR83, MS95, BGMG01, IOS03, DCG06, DCG07]. It leads to the formation of dense nuclei (the liquid) within a dilute, neutron-rich gas. The stability of nuclei at zero temperature and density can also be seen as a manifestation of this phase transition. It is very interesting that the nuclear matter

EOS, which can be seen as a result of the chiral/deconfinement phase transition, contains another first order phase transition. In contrast to quark matter, its existence and qualitative properties are rather well established by plenty of experimental studies, in particular by low-energy heavy ion collisions. Also from the theoretical side this phase transition is understood in much more detail. It is possible to calculate the uniform nuclear matter EOS with one single model for the nuclear interactions at all relevant densities, including the binodal and spinodal regions. The nuclear interactions lead to phase separation into a more dense and symmetric phase, the nuclear liquid, and the dilute neutron gas phase. The two phases can be calculated with the same model, and only differ in density and asymmetry, which thus are also order parameters of the phase transition. The liquid-gas phase transition is one of the main topics of this thesis. In Chapter 8 we will present a very comprehensive model for its description.

2.3 Implications of Phase Transitions in Compact Stars

The inclusion of a phase transition to exotic degrees of freedoms can substantially alter the stability of a compact star. In general, a phase transition leads to a softening of the EOS and therefore lowers the maximum mass which can be supported by the star. The formation of quark matter in compact stars is mainly discussed in two scenarios, in protoneutron stars already during the first stages after their birth in the supernova explosion [PSPL01] and in old accreting neutron stars [LCC$^+$06, ADRM09]. For the first case, different interesting associated signatures were proposed [PCL95, DT99, SPL00, PMP04, NBBS06]. For example in Ref. [PSPL01] a delayed formation of the quark phase was found. Deleptonization leads to the loss of lepton pressure and therefore to an increase in the central density so that the phase transition takes place, which can trigger the collapse of the protoneutron star to a black hole. An observation of a supernova neutrino signal with a later abrupt cessation of the signal would be a clear confirmation of this scenario. At the end of this thesis we will present a similar study in more detail. Further possible observables are the emission of gravitational waves [LCC$^+$06, ADRM09] due to the contraction of the neutron star or delayed γ-ray bursts [FW98, MHB$^+$03, BBD$^+$03, DPS08].

Besides the mass and stability, also other observables can be linked to phase transitions, e.g. sudden spin ups during the rotational evolution of young pulsars [GPW97, ZBHG06]. Furthermore the appearance and the structure of mixed phases can have important consequences for transport properties like the thermal conductivity or the

neutrino emissivities and opacities [RBP00]. Also the shear modulus and the bulk viscosity can be altered, affecting the glitch phenomena or r-modes [Gle01, BGP01]. Consequently, the occurrence of mixed phases can modify the thermal [PGW06] and rotational evolution of compact stars.

A different scenario has not been studied in the literature very extensively: The phase transition from hadronic to quark matter can occur already in the early postbounce phase of a core-collapse supernova [TS88a, TS88b, GAM$^+$93, DT99, YKaHY07]. For the proper description of the complex dynamical environment of a supernova detailed numerical simulations are necessary. The occurrence of the phase transition in a supernova requires a phase transition onset close to saturation density, which can be realized for high temperatures and low proton fractions. For such a scenario Ref. [GAM$^+$93] found the formation of a second shock as a direct consequence of the phase transition. However, the lack of neutrino transport in their model allowed them to investigate the dynamics only for a few ms after bounce. Very recently, a quark matter phase transition has been considered with Boltzmann neutrino transport for a 100 $M_\odot$ progenitor [NSY08]. The appearance of quark matter shortened the time until black hole formation due to the softening of the equation of state (EOS), but did not lead to the launch of a second shock. Later we will present in more detail that an early appearance of quark matter can lead to very interesting consequences in a core-collapse supernovae.

2.4 Nuclear Matter - The Relativistic Mean-Field Model

In this thesis we will use the relativistic mean-field (RMF) model for the description of the nuclear interactions of the nucleons. It represents a self-consistent, effective field-theoretical model which successfully reproduces experimental nuclear data. It is formulated in a covariant way, and the effects of special relativity are taken into account. Compared to non-relativistic models, it is most important that the relativistic description naturally contains the spin-orbit coupling of the nucleons, which is of great importance for calculations of the nuclear structure. Here we only discuss certain aspects of the RMF model, detailed reviews are given in Refs. [Rei89, BHR03].

The first relativistic description of the nuclear interactions has been the σ-ω-model of J. D. Walecka [Wal74]. As it is based on a field theoretical approach, the interactions are not described by potentials but are generated through the exchange of particles. The scalar, isoscalar σ meson is responsible for a medium-range attraction, the isoscalar ω vector-meson leads to a strong short-range repulsion. With these two interaction bosons one achieves a reasonable description of the saturation properties of nuclear matter and the binding energies of nuclei. For the modeling of isospin-asymmetric matter with an excess of neutrons or protons, the isovector, scalar ρ meson needs to be introduced in the RMF model. If one wants to include Coulomb effects, the photon has to be included in addition. In some models also the isovector, vector δ-meson is taken into account. However, its inclusion does not lead to a better reproduction of experimental data and its properties are not well constrained.

It is important to note that the mesons which are used in such models are not necessarily really existing particles, because the RMF model is only an effective description of the nuclear interactions. For example the σ-meson cannot been identified in experiments. There are only several broad resonances as potential candidates. Furthermore, not all of the known mesons are included. For example the lightest one, the pion, is not taken into account due to parity conservation in finite nuclei. Actually the sigma can be seen as a representation of two pion exchange.

2.4.1 Lagrange Density

The starting point of all relativistic models is a Lagrange density $\mathcal{L}$. It consists of the contributions of the nucleons, the meson-fields, the photons and the coupling of the

mesons with the nucleons:

$$\mathcal{L} = \mathcal{L}_{nucleons} + \mathcal{L}_{mesons} + \mathcal{L}_{photons} + \mathcal{L}_{coupling} \tag{2.4}$$

As being Fermions, the nucleons are described by the Dirac equation:

$$\mathcal{L}_{nucleons} = \bar{\hat{\psi}}(i\gamma^\mu \partial_\mu - m_N)\hat{\psi} \ . \tag{2.5}$$

It is assumed that neutrons and protons have equal masses m_N, so that the nucleon operator $\hat{\psi}$ can be taken as a vector in isospin-space.

For the σ meson the Lagrangian density of the Klein-Gordon equation is applied, for the vector bosons the Proca equation:

$$\begin{aligned} \mathcal{L}_{mesons} = & \tfrac{1}{2}(\partial_\mu \hat{\sigma} \partial^\mu \hat{\sigma} - m_\sigma^2 \hat{\sigma}^2) \\ & - \tfrac{1}{2}(\tfrac{1}{2}\hat{\omega}_{\mu\nu}\hat{\omega}^{\mu\nu} - m_\omega^2 \hat{\omega}_\mu \hat{\omega}^\mu) \\ & - \tfrac{1}{2}(\tfrac{1}{2}\hat{\vec{\rho}}_{\mu\nu} \cdot \hat{\vec{\rho}}^{\mu\nu} - m_\rho^2 \hat{\vec{\rho}}_\mu \cdot \hat{\vec{\rho}}^\mu) \ . \end{aligned} \tag{2.6}$$

With the field-strength tensors of the vector bosons:

$$\hat{\omega}_{\mu\nu} = \partial_\mu \hat{\omega}_\nu - \partial_\nu \hat{\omega}_\mu \ , \qquad \hat{\vec{\rho}}_{\mu\nu} = \partial_\mu \hat{\vec{\rho}}_\nu - \partial_\nu \hat{\vec{\rho}}_\mu \ . \tag{2.7}$$

The Lagrangian density of the photons is given by their field-strength tensor:

$$\mathcal{L}_{photons} = -\tfrac{1}{4}\hat{F}_{\mu\nu}\hat{F}^{\mu\nu} \ , \qquad \hat{F}_{\mu\nu} = \partial_\mu \hat{A}_\nu - \partial_\nu \hat{A}_\mu \ . \tag{2.8}$$

For the interactions usually the ansatz of the minimal coupling is used:

$$\begin{aligned} \mathcal{L}_{coupling} = & - g_\sigma \hat{\sigma} \bar{\hat{\psi}} \hat{\psi} - g_\omega \hat{\omega}_\mu \bar{\hat{\psi}} \gamma^\mu \hat{\psi} - g_\rho \hat{\vec{\rho}}_\mu \cdot \bar{\hat{\psi}} \vec{\tau} \gamma^\mu \hat{\psi} \\ & - e\hat{A}_\mu \bar{\hat{\psi}} \tfrac{1}{2}(1 + \tau_3)\gamma^\mu \hat{\psi} - U_\sigma[\hat{\sigma}] - U_\omega[\hat{\omega}] \ . \end{aligned} \tag{2.9}$$

Here, the RMF model is extended to contain also self-interactions of the σ- and ω-mesons:

$$U_\sigma[\hat{\sigma}] = \tfrac{1}{3}b_2\hat{\sigma}^3 + \tfrac{1}{4}b_3\hat{\sigma}^4 \ , \qquad U_\omega[\hat{\omega}] = \tfrac{1}{4}c_3(\hat{\omega}_\mu \hat{\omega}^\mu)^2 \ . \tag{2.10}$$

These non-linear σ and ω terms are included to achieve a better description of the properties of nuclei and of the equation of state of nuclear matter.

With Hamilton's principle

$$\delta \int \mathcal{L} d^3x \, dt = 0 \tag{2.11}$$

one gets the Euler-Lagrange equations:

$$\frac{\partial}{\partial x^\mu} \left(\frac{\partial \mathcal{L}}{\partial \left(\partial q_i / \partial x^\mu \right)} \right) - \frac{\partial \mathcal{L}}{\partial q_i} = 0 \; . \tag{2.12}$$

They give the equations of motion for the nucleons, mesons and photons. However, a full solution of the general field-theoretical problem is impossible and thus additional approximations are required.

2.4.2 Approximations

Within the mean-field approximation, the field operators of the mesons and photons are replaced by their expectation values, e.g.:

$$\hat{\sigma} \rightarrow \sigma = \langle \sigma \rangle \; . \tag{2.13}$$

Thus the meson fields act as mean potentials generated by the nucleons. Furthermore, the nucleons behave as independent, free particles. The nucleon operator can be expanded in single particle states $\phi_\alpha(x^\mu)$:

$$\hat{\psi} = \sum_\alpha \phi_\alpha(x^\mu) \hat{a}_\alpha \; . \tag{2.14}$$

In the no-sea approximation all states in the Dirac sea with negative energy are neglected. One assumes that the sum of these states cancels the vacuum contribution exactly. Thus vacuum polarizations are not taken into account. This leads to the occupation of single-particle states, ϕ_α, $\alpha = 1, 2, ..., \infty$, which e.g. set the scalar and all other densities:

$$\rho_s = \sum_\alpha \overline{\phi}_\alpha \phi_\alpha \; . \tag{2.15}$$

For the calculation of finite nuclei and uniform nuclear matter, usually only stationary states are being considered. The trivial time dependence of the wave functions is

separated:

$$\phi_\alpha(x^\mu) = \phi_\alpha(\mathbf{r})\, \mathrm{e}^{i\epsilon_\alpha t}\ , \tag{2.16}$$

with ϵ_α denoting the single particle energy. In the stationary case all time derivatives vanish. For homogeneous and isotropic nuclear matter also the spatial components of densities and fields vanish. Furthermore, one assumes that there is no mixing between neutron and proton states. Thus only the $\sigma, \omega_0, \rho_{00}$ and A_0 remain as the relevant non-vanishing fields. With these simplifications the equations of motion for the expectation values of the fields can be determined from the Euler-Lagrange Equations (2.12).

2.4.3 Equations of Motion

For the nucleons one finds a time-independent, single-particle Dirac equation which contains the interactions with the fields:

$$\begin{aligned}\epsilon_\alpha\gamma_0\phi_\alpha = &(-i\vec{\gamma}\cdot\nabla + m_N + g_\sigma\sigma + g_\omega\omega_0\gamma_0 \\ &+\tfrac{1}{2}g_\rho\rho_{00}\gamma_0\tau_0 + \tfrac{1}{2}eA_0\gamma_0(1+\tau_0)\big)\,\phi_\alpha\end{aligned} \tag{2.17}$$

For the fields one gets the following equations:

$$-(\Delta + m_\sigma^2)\sigma + U'(\sigma) = -g_\sigma\bar{\psi}\psi \tag{2.18}$$

$$(-\Delta + m_\omega^2)\omega_0 + U'(\omega_0) = g_\omega\bar{\psi}\gamma_0\psi \tag{2.19}$$

$$(-\Delta + m_\rho^2)\rho_{00} = \tfrac{1}{2}g_\rho\bar{\psi}\tau_0\gamma_0\psi \tag{2.20}$$

$$-\Delta A_0 = \tfrac{1}{2}e\bar{\psi}(1+\tau_3)\gamma_0\psi\ . \tag{2.21}$$

For given nucleon densities the implicit equation of motion for the sigma meson field needs to be solved numerically to achieve self-consistency. With the approximations one arrives at a self-consistent relativistic description which is similar to the non-relativistic Hartree-Fock method. The RMF model is not an ab initio field-theoretical description, but represents a successful effective model. Different mesons, meson masses and different forms of the non-linear couplings can be used. As in non-relativistic Hartree-Fock models, the free parameters of the model, namely the masses of the nucleons and the mesons and their coupling strengths, have to be determined from fits to experimental data.

	n_B^0 [fm^{-3}]	E/A [MeV]	K [MeV]	M^*/M	a_{sym} [MeV]	M_{max} [M$_\odot$]
TM1	0.145	-16.3	281	0.634	36.9	2.2
TMA	0.147	-16.0	318	0.635	30.7	2.0

Table 2.1: Nuclear matter and neutron star properties of the relativistic mean field model TM1 [ST94] and TMA [THS$^+$95]. Listed are the saturation density and binding energy, the incompressibility, the effective mass at saturation, the symmetry energy and the maximum mass of a cold neutron star.

2.4.4 Parameterizations

In this work we use the parameter set TM1 [ST94] and TMA [THS$^+$95]. TM1 was developed together with TM2, which were fitted to binding energies and charge radii of light (TM2) and heavy nuclei (TM1). TMA is based on an interpolation of these two parameter sets. The coupling parameters g_i of the set TMA are chosen to be mass-number dependent of the form $g_i = a_i + b_i/A^{0.4}$, with a_i and b_i being constants, to have a good description of nuclei over the entire range of mass number. For uniform nuclear matter the couplings become constants and are given by a_i.

Table 2.1 lists some characteristic saturation properties of uniform nuclear matter, and the resulting maximum mass of a cold neutron star. The baryon number density with the lowest energy per nucleon is defined as the saturation density n_B^0. As it is a minimum, one can characterize the symmetric nuclear matter EOS, which has an equal amount of neutrons and protons, by a quadratic expansion around saturation density:

$$E/N(n_B) = E/N(n_B^0) + \frac{1}{18} K (1 - n_B/n_B^0)^2 \ , \tag{2.22}$$

with the following definition of the incompressibility K:

$$K = 9 \left. \frac{\partial^2 E/N}{\partial^2 n_B} \right|_{n_B^0} {n_B^0}^2 \ . \tag{2.23}$$

In both parameterizations the saturation density and the binding energy of symmetric nuclear matter are well determined through the fit to ground state nuclei and lie in the usual range. But TM1 has a much larger symmetry energy than TMA. Contrary, in TMA the nuclear incompressibility is rather high, also compared to the value of $K = 240 \pm 20$ MeV [SKC06] or $K = 248 \pm 8$ MeV [Pie04] deduced with theoretical models from experimental data on isoscalar giant monopole resonances (ISGMR) which probe nuclear matter slightly below saturation density. However, it is perceived in the literature

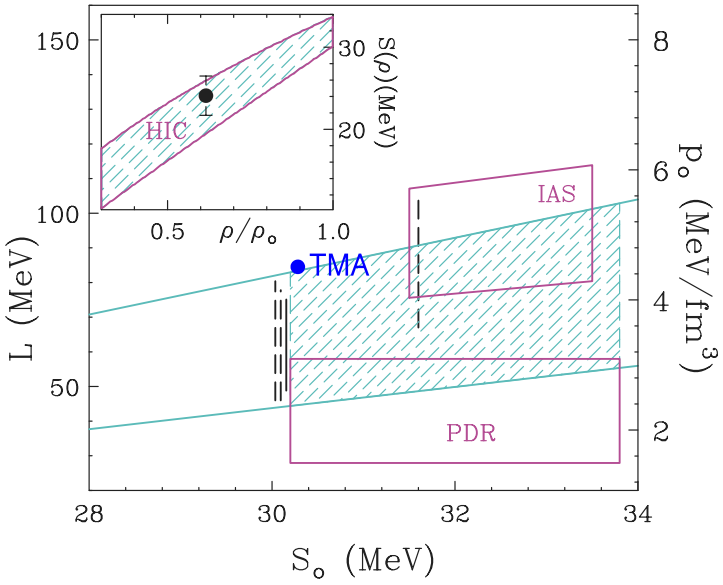

Figure 2.2: Constraints on the parameters S_0 and L from Ref. [TZD$^+$09]. The right axis corresponds to the pressure of neutron matter at saturation density. The region bounded by the diagonal lines and the vertical lines at $S_0 = 30.1$ MeV represent the constraints obtained from isospin diffusion data and proton to neutron ratios. The vertical line at $S_0 = 31.6$ MeV is from Refs. [LC05, LCK08]. The lower and upper boxes are formed by the constraints from data [LAN07] for the pygmy dipole resonance and from symmetry energy analysis on nuclei [DL09], respectively. The inset shows the density dependence of the symmetry energy of the shaded region. The symbol in the inset represents results for the giant dipole resonance. The RMF model TMA is depicted by the blue dot. S_0 of TM1 lies out of the shown range.

that the extraction of K from ISGMR data is not unambiguous as it is dependent on the density dependence of the symmetry energy of the nuclear interactions which are taken for the analysis of the data [SKC06, Pie04, Sha09]. For RMF models without further constraints on the density dependence of the symmetry energy usually similar large values in the range of 250 to 270 MeV are obtained for K [Pie04]. Later we will further illustrate the problems of the classification of an EOS by the incompressibility.

The density dependence of the symmetry energy itself can be probed by different experimental observables, e.g. by isospin diffusion and double neutron to proton ratios in heavy-ion collisions or the precise measurement of the neutron skin thickness of ^{208}Pb [AB00, TB01b]. A recent compilation of various experimental results concerning the density dependence of the symmetry energy is given in Ref. [TZD$^+$09]. The most important constraints of this analysis are shown in Fig. 2.2. In this plot the symmetry energy is characterized by two parameters, S_0 and L. S_0 is the symmetry energy at saturation density and thus equivalent to a_{sym} used in Table 2.1. L is the slope parameter of the

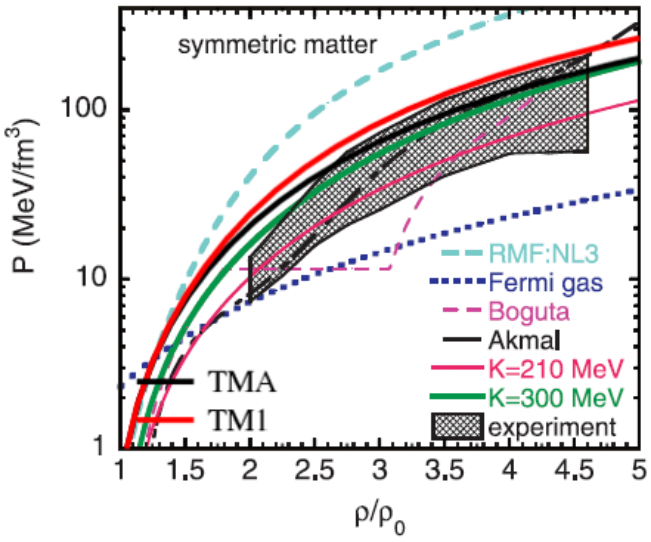

Figure 2.3: Zero-temperature EOS for symmetric nuclear matter. The shaded region corresponds to the region of pressure consistent with the experimental flow data from Ref. [DLL02]. The various curves and lines show predictions for different symmetric matter EOSs. The RMF parameterization TMA is compatible with the experimental constraints, whereas the pressure of TM1 is slightly too large.

symmetry energy at saturation density, which is related to the pressure of neutron matter at saturation density p_0: $L = 3p_0/n_B^0$. With $p_0 = 4.55$ MeV/fm^3 TMA is still within the border of the experimental constraints. The value of S_0 of TM1 is out of the range depicted in Fig. 2.2 which shows that the symmetry energy is unusually large in this model. TM1 gives $p_0 = 5.48$ MeV/fm^3 and would lie in the continuation of the allowed range shown in Fig. 2.2.

At several times saturation density experimental flow data from high-energy heavy ion collisions can be used as a constraint for the EOS. In Figs. 2.3 and 2.4 several EOSs are shown for symmetric and neutron matter, respectively. Here we do not want to discuss all of the EOSs, but are only interested in the comparison of the RMF models TM1 and TMA to the region which is deduced from the experimental flow data of Ref. [DLL02]. For TMA an acceptable agreement is found: it is lying almost completely in the compatible range for an asymmetric stiff EOS. The pressure of TM1 is slightly too large.

The comparison of the pressure-density relation of the two parameterizations shown in Fig. 2.3 with the properties listed in Table 2.1 is very instructive. Usually one associates a large incompressibility with a large pressure, as one can deduce the following

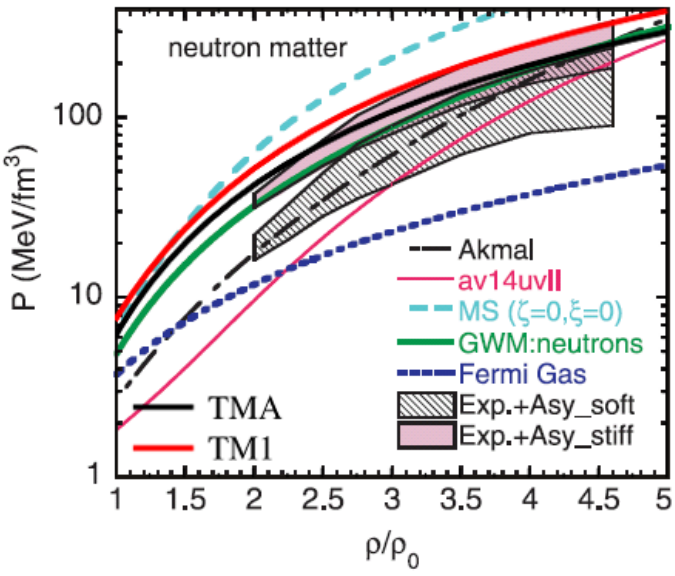

Figure 2.4: Zero-temperature EOS for neutron matter. The upper and lower shaded regions correspond to the pressure regions for neutron matter consistent with the experimental flow data after inclusion of the pressures from asymmetry terms with strong and weak density dependencies, respectively. The results are taken from Ref. [DLL02]. The various curves and lines show predictions for different neutron matter EOSs. The RMF parameterization TMA is compatible with the experimental data for an asymmetric stiff EOS, whereas TM1 barely touches the allowed region.

relation from Eq. (2.22):

$$p = \frac{K}{9}(n_B - n_B^0)\left(\frac{n_B}{n_B^0}\right)^2 \quad . \tag{2.24}$$

However, in Fig. 2.3 we observe that TMA with the larger incompressibility has the lower pressure. Also if the pressure is plotted as a function of the energy density, one observes that TMA has a lower pressure at all densities besides a very small region around saturation density. This is rather surprising, as the two parameterizations belong to the same class of models, have only slightly different saturation densities (difference of 2%) and binding energies and mainly differ in the incompressibility (difference of 10%), see Table 2.1. This comparison shows, that the commonly used classification of the stiffness of an EOS by the incompressibility is not adequate. There are two reasons for the observed behavior. First, close to saturation density the slightly different values of the saturation densities are more important than the value of K itself. Second, even for densities in the vicinity of saturation density, e.g. 1.3 n_B^0 the higher order terms to the expansion used in Eq. (2.22) give a significant contribution to the EOS. The higher order terms are negative above saturation density and are smaller in TM1 than in TMA, leading to the larger total pressure of TM1 at all densities.

Another important constraint for the EOS comes from pulsar timing measurements. By determining post-Keplerian parameters one is able to determine the mass of pulsars with very high precision. Currently, the largest precisely known mass of a pulsar is 1.67 ± 0.01 $M_\odot$, of the pulsar PSR J1903+0327 [Fre09]. Obviously every EOS has to have a maximum mass which is above this value. For TMA the maximum mass of a cold deleptonized neutron star is $M_{max} = 2.0$ $M_\odot$, and thus fulfills this constraint and the maximum mass of TM1, $M_{max} = 2.2$ $M_\odot$, is even larger. From the value of K alone, one would expect the opposite behavior. We already discussed that TM1 has a stiffer symmetric EOS despite the lower value of K. In addition, the symmetry energy of TM1 is much larger. This stiffens the neutron matter EOS which has a large effect on the maximum mass of a neutron star.

Fig. 2.5 shows the phase diagram of bulk nuclear matter calculated with TMA. For symmetric nuclear matter a critical temperature of 17.4 MeV is found. At $T = 0$ MeV the mixed phase ends between $0.63 n_B^0$ and n_B^0 for the shown values of Y_p. At larger densities only the uniform nuclear matter phase is present. The phase diagram depends strongly on Y_p: For lower proton fractions the mixed phase region shrinks considerably and even disappears completely for pure neutron matter.

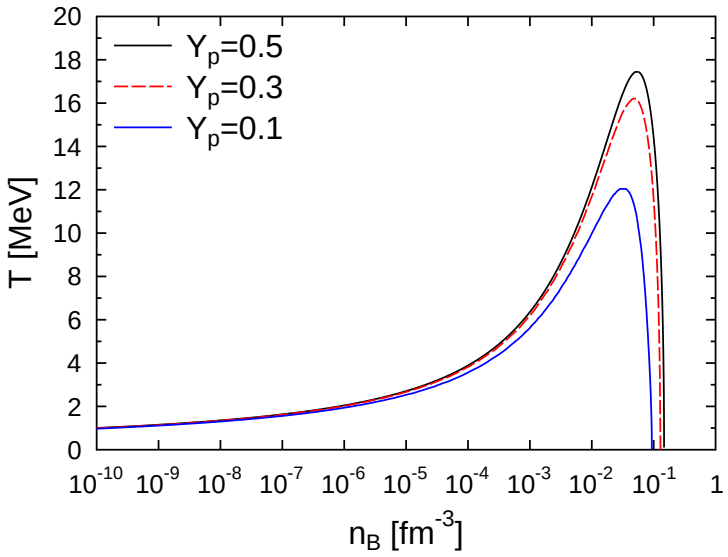

Figure 2.5: The phase diagram of bulk nuclear matter calculated with the RMF model TMA [THS+95]. The lines show the binodals for different Y_p, at which the liquid-gas phase transition of nuclear matter sets in and a mixed phase appears.

2.5 Quark Matter - The Quark Bag Model

The most simple model for the description of quark matter is the so called quark bag model. Based on first ideas of Bogolyubov, it was further developed in the 70s by a group of physicist at the Massachusetts Institute of Technology (MIT) for the description of hadron spectra. In this context one also speaks about the MIT bag model. However, the values of the model parameter (the bag constant) deduced from fits to the hadron masses differ from the values usually applied for infinite quark matter. The quark bag model gives a phenomenological description of confinement: the quarks are confined in a bag in the vacuum. Inside this bag they behave as free particles, but the vacuum exerts a pressure on the bag. Thus the volume of the bag gives a contribution to the energy, due to the mechanical work of the quark bag volume against the vacuum pressure. Thus the energy density is the sum of the energy density of the Fermi-Dirac gas of quarks ϵ_i and the vacuum energy density B, the so called bag constant:

$$\epsilon = \sum_{i=u,d,s} \epsilon_i + B \,, \tag{2.25}$$

with i denoting the different quark flavors. The up and down quarks are rather light, with $m_u \sim 5$ and $m_d \sim 10$ MeV compared to the strange quark with $m_s \sim 100$ MeV. As the other quarks are much heavier, usually only these three flavors are relevant in the astrophysical context. There is no contribution of the vacuum to the entropy, thus:

$$s = \sum_i s_i \,. \tag{2.26}$$

Then the free energy density $f = \epsilon - ts$ is well defined, which allows to evaluate the pressure:

$$p = \sum_i p_i - B \,. \tag{2.27}$$

It becomes apparent that the vacuum pressure reduces the total pressure, as it acts against the Fermi pressure of the quarks.

One can interpret the quark bag model also in a different way, in which it is not necessary to consider a vacuum energy outside of the quark bag. In this different interpretation, the volume which is filled by quarks possesses a constant energy density, representing the non-perturbative contributions of quark-antiquark pairs and gluons. In addition there is the Fermi-Dirac contribution of the three valence quarks. Thus, the

energy density remains in the same form as before. A constant positive energy density always leads to a negative pressure, because

$$p = n\frac{\partial \epsilon}{\partial n} - \epsilon \ . \tag{2.28}$$

If we use $\epsilon = B = const.$, we get $p = -B$ which appears in Eq. (2.27). The vacuum energy of the quark bag can be reduced by decreasing the size of the bag. This force acts like a negative pressure.

For the masses of the quarks one can use experimentally determined values. However, the value of the Bag constant cannot be deduced directly from experiments. The bag constant represents all the non-perturbative features of QCD expressed in one single value. It is usually chosen between $B^{1/4} = 145 - 200$ MeV [SGST00] as there exist some important constraints. First of all, up- and down-quark matter at zero pressure must not be more strongly bound than iron. Otherwise nuclei would decay into quark matter. This gives a lower limit for the bag constant in the order of $B^{1/4} \sim 145$ MeV, depending on the chosen quark masses. There is the controversial hypothesis, that strange quark matter is the true ground state of nuclear matter, see e.g. [Bod71, Wit84]. In this scenario ordinary matter does not decay into strange quark matter, because deconfinement takes place under strong interactions with flavor conservation. A nucleus of A nucleons can only decay into up- and down-quark matter which is less bound. To overcome the barrier, $A/3$ quarks have to be converted into strange quarks at once. As flavor conversion is mediated by weak interactions this process is highly unlikely. Even though it is a very extreme scenario, this possibility is not ruled out yet and is still discussed in the literature.

There are several extensions of the quark bag model. The simplest is to add first order corrections in the strong coupling constants α_S. A different possibility is a density- and/or temperature-dependent bag constant. For our purpose, such extensions are not necessary. We are mainly interested in the general features of first order phase transitions. Of course, the quantitative behavior is governed by the detailed properties of the EOS. But the particular form of the EOS is not relevant for the general thermodynamic conditions for phase equilibrium.

2.6 Phenomenological EOS

In this subsection we want to present another phenomenological EOS which has some interesting features. Namely it allows to tune the characteristic properties of the EOS

by one parameter a so that it can behave like quark matter or like nuclear matter. Furthemore we will show the connection between the EOS and the mass-radius relation of compact stars. The EOS has the following form:

$$p' = \mu'^4 - a\mu'^2 + a - 1 \tag{2.29}$$
$$\epsilon' = 3\mu'^4 - a\mu'^2 - a + 1 \, . \tag{2.30}$$

Here we use a dimensionless form of the pressure and of the chemical potentials:

$$p' = p/\mu_c^4 \tag{2.31}$$
$$\mu' = \mu/\mu_c \, . \tag{2.32}$$

With this formulation the dimensionless mass-radius $M'(R')$ relation becomes independent of the parameter μ_c, with the following scaling behavior:

$$M' = M/M_0 \tag{2.33}$$
$$M_0 = \frac{M_{Pl}^3}{\mu_c^2} \tag{2.34}$$
$$R' = R/R_0 \tag{2.35}$$
$$R_0 = \frac{M_{Pl}}{\mu_c^2} \, , \tag{2.36}$$

with $M_{Pl} = 1.22 \times 10^{22}$ MeV denoting the Planck mass. Reasonable values for μ_c are between 150 and 250 MeV. If we set $a = 0$, the EOS is identical to the quark bag EOS with massless quarks and μ_c^4 is equivalent to the bag constant. It is interesting to note that the maximum mass decreases with increasing μ_c, i.e. the bag constant. $a = 2$ instead represents a hadronic EOS.

In Fig. 2.6 the dimensionless mass-radius relation has been calculated for different values of a. We refer to Ref. [SHGS06] for the explanation how the mass-radius curve is calculated, and the discussion of stability. The curve with $a = 2$ shows the typical behavior of a hadronic equation of state: Starting at large radii, the mass increases with decreasing radius, until a maximum mass is reached. Compact stars which lie on the curve on the left of the maximum mass are unstable and will collapse to a black hole. The pure quark EOS with $a = 0$ shows a very different behavior. The mass-radius curve starts at the origin, and the mass increases with the radius until the maximum mass is reached. Usually the mass does not approach zero for large radii. This happens only because no EOS for the low-density region of the neutron star crust is applied. Strange stars are stable up to this point. Thus strange stars of arbitrary size can exist in nature. Very

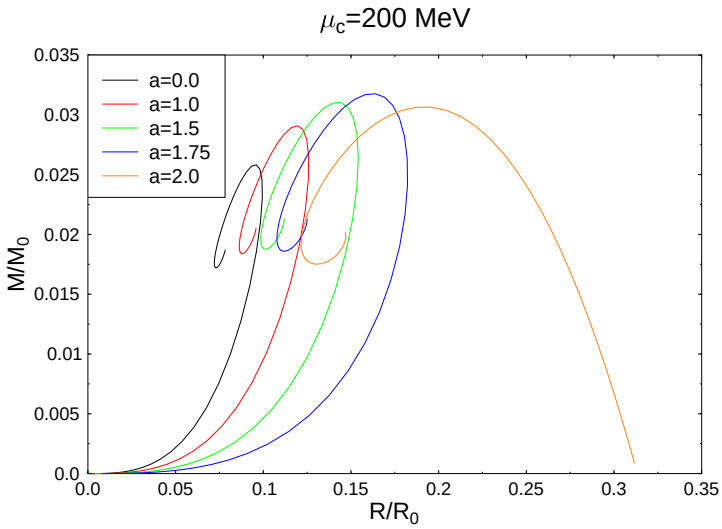

Figure 2.6: The dimensionless mass-radius relation for different values of a.

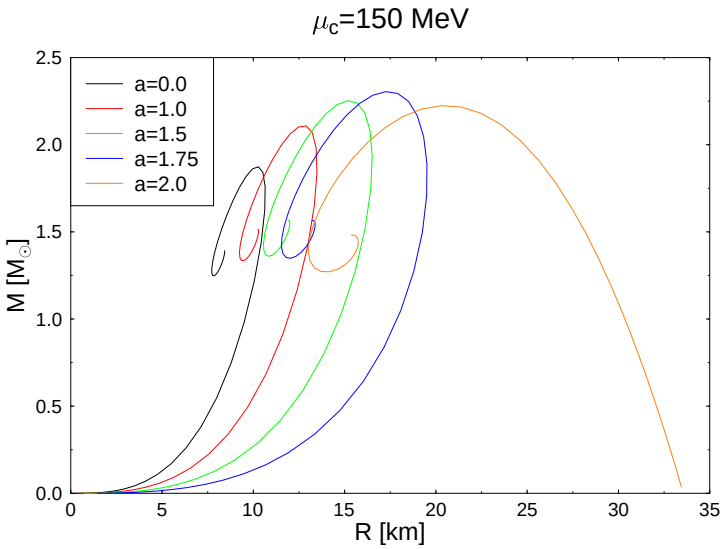

Figure 2.7: The normal mass-radius relation for $\mu_c = 150$ MeV and different values of a.

tiny lumps of quark matter are usually called strangelets. Strange stars and strangelets are not bound by gravity, but by the interactions of the quarks, which are represented by the bag constant. Thus one also speaks about selfbound stars. In contrast, hadronic stars are only bound by gravity and would explode without it, because of the strong repulsive hadronic interactions at large densities. It is very typical for quark stars, that they posses smaller radii. Since very long this is proposed as an observable which allows to distinguish quark and neutron stars. Unfortunately, measurements of radii are quite difficult and so far it was not possible to verify or falsify the actual existence of strange stars.

Figure 2.7 depicts the mass-radius relation in dimensionfull units of solar masses and km. $\mu_c = 150$ MeV gives typical values for the maximum mass of strange stars, $M_{max} = 1.9\mathrm{M}_\odot$, and hadronic stars, $M_{max} = 2.2\mathrm{M}_\odot$. The radii of the EOS with $a = 2$ are rather large, e.g. $R \sim 30$ km for $M = 1.4\mathrm{M}_\odot$. This indicates that $\mu_c = 150$ MeV is not a very reasonable value for $a = 2$. The phenomenological EOS is not used further in the following. We applied it here only to illustrate the connection between the EOS and the mass-radius relation and the characteristic differences between neutron and quark stars.

Chapter 3

General Description of First Order Phase Transitions

In this chapter we want to give a general, system-independent description of first order phase transitions. Our formalism and results can be applied to any first order phase transition, as long as the system is in complete thermodynamic equilibrium. We do not consider any finite size effects, which means that the different phases which appear are always treated in the thermodynamic limit.

3.1 Classification

As in Ref. [DCG06] we will distinguish between the term 'phase transition' and 'phase transformation'. According to the Ehrenfest classification a phase transition is of first order, if at least one of the first derivatives of the grand-canonical potential is discontinuous, and of second order if the first derivatives are continuous, but the second are not. Thus in a first order phase transition the discontinuous first derivatives can serve as an order parameter. According to Landau [LL69], a first order phase transition is defined by the appearance of different phases in phase coexistence, which can be distinguished and are characterized by order parameters. In this theses, we restrict the discussion on first order phase transitions and note only that the phenomenology and properties of second order phase transitions are very different.

In our terminology the term 'phase transformation' refers to a specific path through the phase diagram, characterized by a certain set of state variables (also called control parameters) which are changed in a specific continuous way. As we will show, phase transformations of a first order phase transition can behave continuously as well as discontinuously. This aspect was sometimes not treated very carefully in the literature. For

example in Refs. [MS95, Mue97] a continuous first order phase transition was misinterpreted as a second order phase transition. In this chapter we want to classify and discuss the general properties of first order phase transitions in different phase transformations.

The main idea is, that, contrary to common wisdom, the choice of the state variables and thus the choice of the ensemble is not arbitrary but leads to differences as soon as a first order phase transition occurs. Still, the different ensembles can be transformed into each other, and thus are equivalent. Qualitative differences arise, because we assume that the state variables are changed in a continuous way. Such a continuous change of a certain set of state variables can not always be mapped continuously onto a different set of state variables, i.e. a different thermodynamic ensemble. This is the reason for qualitative differences in phase transformations of different ensembles.

It is important to realize that the choice of state variables is determined by the physical process which one wants to describe. The state variables are the independent parameters that are controlled and fixed externally. In a dynamic (but necessarily quasistatic) process they are the parameters that characterize the evolution of the thermodynamic system. E.g. for an isolated and closed system, only extensive variables can directly be adjusted from outside. If instead a subsystem in a heatbath is investigated, the temperature of the subsystem can directly be set to a certain value, but not the entropy. Only if the exchange of an extensive quantity with the surrounding is possible its conjugate intensive variable can be used as a state variable. However, in a theoretical investigation or in the analysis of experimental data, the state variables or control parameters simply correspond to the variables which are chosen as abscissae.

As will be shown, the qualitative properties of a phase transformation are entirely determined by the number of extensive state variables used and the number of phases which are involved in the phase transformation. Some of the aspects which will be discussed below have already been addressed in the literature, like e.g. the role of additional degrees of freedom which increase the number of extensive state variables. The differences between a single and a multi-component body in the context of neutron stars were extensively studied in Ref. [Gle92] for the first time. For heavy-ion collisions, already in Ref. [GKS87] strangeness conservation was assumed in addition to baryon number conservation, leading to the phase transition of a multi-component body.

3.2 Thermodynamic Variables and Possible Phases

Consider a thermodynamic system with $\mathcal{G}$ globally conserved charges $C_k, k = 1, ..., \mathcal{G}$. With 'charge' we mean any kind of conserved, extensive quantity in addition to the en-

tropy and the volume, like e.g. particle numbers or e.g. the total electric dipole moment. In Chapter 5 we will show how to connect a set of particle numbers with a set of different conserved charges. With 'global conservation' it is meant here, that if there are several phases in equilibrium the charge can be shared among the different phases, and only the total sum of the entire system has to be conserved. There exist $2(\mathcal{G}+2)$ thermodynamic variables in total, in $\mathcal{G}+2$ conjugate pairs. $\mathcal{G}+2$ of the variables are intensive (also called non-additive): the $\mathcal{G}$ chemical potentials $\mu_k, k = 1, ..., \mathcal{G}$, the temperature T and the pressure p. $\mathcal{G}+2$ are extensive (also called additive) variables: the $\mathcal{G}$ charges C_k, the entropy S and the volume V. Of each of the $\mathcal{G}+2$ pairs either the extensive or the intensive variable has to be chosen as one of the $\mathcal{G}+2$ independent state variables. These state variables completely define the state of the system. Let $\mathbf{X} = (X_i)$, $i = 1, ..., \mathcal{E}$ and $\mathbf{Y} = (Y_j)$, $j = 1, ..., \mathcal{I}$ denote the vector of the $\mathcal{E}$ chosen independent extensive and the $\mathcal{I}$ chosen independent intensive state variables, respectively, whereas

$$\mathcal{E} + \mathcal{I} = \mathcal{G} + 2\,. \tag{3.1}$$

Here and in the following, bold symbols will always denote vectors.

When the state variables are specified, there remain $\mathcal{E}$ dependent intensive and $\mathcal{I}$ dependent extensive quantities $\tilde{Y}_i$ and $\tilde{X}_j$ respectively, which are determined by the EOS. We denote the vector of the dependent extensive variables by $\tilde{\mathbf{X}} = (\tilde{X}_j)$ and the vector of the dependent intensive variables by $\tilde{\mathbf{Y}} = (\tilde{Y}_i)$. They are given as partial derivatives of the thermodynamic potential $\Phi(\mathbf{X}, \mathbf{Y})$ with respect to the corresponding conjugate state variable:

$$\begin{aligned} (\tilde{Y}_i) &= \left(\frac{\partial \Phi}{\partial X_i}\right) \\ (\tilde{X}_j) &= -\left(\frac{\partial \Phi}{\partial Y_j}\right)\,. \end{aligned} \tag{3.2}$$

Opposite signs (e.g. as it is the case in the standard definition of the pressure) can be absorbed in the definition of $\tilde{Y}_i$.

For $\mathcal{E} = \mathcal{G} + 2$ the thermodynamic potential is the internal energy:

$$E(\mathbf{X}) = \sum_{i=1}^{\mathcal{G}+2} \tilde{Y}_i(\mathbf{X}) X_i\,. \tag{3.3}$$

In the general case where $\mathcal{I}$ of the extensive variables are replaced by their conjugate intensive variables through Legendre transformations, the thermodynamic potential be-

comes:

$$\Phi(\mathbf{X},\mathbf{Y}) = \sum_{i=1}^{\mathcal{E}} \tilde{Y}_i(\mathbf{X},\mathbf{Y}) X_i \ . \tag{3.4}$$

If all the intensive variables are used as state variables ($\mathcal{E} = 0$), we obtain $\Phi \equiv 0$ which implies $V \equiv 0$. If no extensive state variables are used the size of the system is not specified and we get the result that the system actually does not exist. We want to interpret this result further and give a physical explanation for it. In this case we would consider a subsystem which was controlled by all of the intensive variables. For this, the exchange of all extensive quantities with the surrounding main system (the bath) has to be possible (charges, energy and volume). But then there is nothing which distinguishes the subsystem from the bath, leading to the meaningful result that the subsystem does not exist. From a different point of view, there is the Gibbs-Duhem relation among the intensive variables, so that not all of the $\mathcal{G}+2$ intensive variables are independent. One of the intensive state variables is fixed through the EOS by the other intensive variables. Thus only $\mathcal{E} \geq 1$ is relevant.

Next the case $\mathcal{E} = 1$ is discussed in more detail. There is only one extensive state variable X_1, and the potential is then $\Phi = \tilde{Y}_1(X_1,\mathbf{Y})X_1$. $\tilde{Y}_1$ is the only unknown intensive variable and as an intensive variable it can actually not depend on X_1: $\tilde{Y}_1 = \tilde{Y}_1(\mathbf{Y})$, because of the Gibbs-Duhem relation. X_1 only specifies the size of the system and to do so $X_1 \neq 0$, necessarily. If $X_1 = 0$ then $\Phi \equiv 0$, so that the system would not exist, similar to the case $\mathcal{E} = 0$ discussed before. X_1 could e.g. be the volume or a non-vanishing net number of particles. For simplicity, we assume in the following that X_1 cannot be negative. It is easy to deduce all possible kind of mixed phases from the case $\mathcal{E} = 1$ which we want to do now.

Let us consider that there exist $\mathcal{P}$ different (intrinsically stable) single homogeneous phases (SHP). In reality, there should be only one generic equation of state containing all the possible phases. For simplicity we assume in the following that the different phases can always be distinguished from each other and that they are described by different EOSs, i.e. thermodynamic potentials Φ^κ, $\kappa = 1,...,\mathcal{P}$ in the entire region of the state variables under investigation. With this assumption we exclude any critical points, where the distinction of the different phases would not be possible any more. Let us assume further that the potential of each SHP exists and behaves continuously, independent of which state variables are used.

For $\mathcal{E} = 1$, each of the $\mathcal{P}$ EOSs $\Phi^\kappa(X_1,\mathbf{Y})$ gives a relation $\tilde{Y}_1^\kappa = \tilde{Y}_1^\kappa(\mathbf{Y})$. Because $\tilde{Y}_1^\kappa$ is an intensive variable it can not depend on the size of the phase, as noted before.

$\tilde{Y}_1^\kappa$ also fixes the thermodynamic potential of each phase: $\Phi^\kappa = \tilde{Y}_1^\kappa(\mathbf{Y})X_1$. Thus it is convenient to investigate the $\mathcal{G}+2$ dimensional parameter space of all intensive variables $\{Y_j, \tilde{Y}_1\}$ to analyze the phase diagram. In this parameter space the $\mathcal{P}$ phases will form $\mathcal{P}$ different $\mathcal{G}+1$ dimensional surfaces[1] of possible physical states. From the second and first law of thermodynamics it follows that Φ has to be minimal in equilibrium. Thus for fixed state variables $(X_1, \mathbf{Y})$ the SHP with the lowest $\tilde{Y}_1$ will be the favored phase. Φ will then be piecewise made up of one of the $\mathcal{P}$ SHPs. A typical example would be the minimization of the negative pressure for given temperature, chemical potentials and volume.

In the intensive parameter space $\{Y_j, \tilde{Y}_1\}$ the coexistence regions of $\mathcal{K}$ different phases are the $\mathcal{G}+2-\mathcal{K}$-dimensional intersections of $\mathcal{K}$ different $\mathcal{G}+1$-dimensional surfaces belonging to the different phases. Gibbs' phase rule is recovered, that at most $\mathcal{G}+2$ phases can be in equilibrium:

$$\mathcal{K} \leq \mathcal{G}+2\ . \tag{3.5}$$

On the intersection surfaces the $\mathcal{K}$ phases have the same value of $\tilde{Y}_1$ and the rest of the intensive variables Y_j are used as state variables and are therefore equal by construction. The $\mathcal{K}$ phases are indeed in equilibrium, as all intensive variables are equal in the participating phases, satisfying Gibbs' conditions for phase equilibrium:

$$\begin{aligned}(Y_j^1) = (Y_j^2) = ... = (Y_j^\mathcal{K}) =: (Y_j)\\ (\tilde{Y}_i^1) = (\tilde{Y}_i^2) = ... = (\tilde{Y}_i^\mathcal{K}) =: (\tilde{Y}_i) \quad .\end{aligned} \tag{3.6}$$

These conditions directly follow from the minimization of the thermodynamic potential. They express chemical, thermal and mechanical equilibrium between all the $\mathcal{K}$ phases. We note that in such a phase coexistence the different SHPs are spatially separated from each other.

If we return to the parameter space of the state variables $\{X_1, Y_j\}$, we get the following phase diagram. It fragments into $\mathcal{G}+2$ dimensional volumes in which only one SHP is present. The $\mathcal{G}+3-\mathcal{K}$ dimensional surfaces where $\mathcal{K}$ of these phases intersect are the coexistence regions. The dimensions increased by one compared to the intensive parameter space $\{Y_j, \tilde{Y}_1\}$, because the intensive variables are independent of the size of the system in the thermodynamic limit.

[1] We call every parameter region a surface if it has a dimension $\mathcal{D}$ lower than the dimensionality $\mathcal{G}+2$ of the space of the state variables. If $\mathcal{D} = \mathcal{G}+2$ the region is called a volume.

3.3 Properties of Mixed Phases

Now we assume that a specific set of state variables with a certain $\mathcal{E}$, $1 \leq \mathcal{E} \leq \mathcal{G}+2$, has been selected. We want to analyze the properties of a (mixed) phase K which consists of $\mathcal{K}$ SHPs, with $1 \leq \mathcal{K} \leq \mathcal{P}$. For this we are investigating a certain point $(\mathbf{X}, \mathbf{Y})$ in the phase diagram where $\mathcal{K}$ SHPs are indeed in equilibrium. Because of thermodynamic equilibrium, Eqs. (3.6), one never needs to consider that intensive variables are different in different SHPs. It is always sufficient to use the $\mathcal{G}+2$ intensive variables Y_j and $\tilde{Y}_i$ of Eqs. (3.6), namely the $\mathcal{G}$ chemical potentials, the temperature and the pressure which are equal in all SHPs. Furthermore, each equation of state of each SHP gives one relation among the intensive variables, so actually only $\mathcal{G}+2-\mathcal{K}$ of the intensive variables are independent in the coexistence of $\mathcal{K}$ SHPs. This reflects that a mixed phase of $\mathcal{K}$ SHPs has the dimensionality $\mathcal{G}+2-\mathcal{K}$ in the intensive parameter space $\{Y_j, \tilde{Y}_i\}$.

Let us first discuss the case $\mathcal{K} > \mathcal{E}$, for which more SHPs are in equilibrium than extensive quantities are used as state variables. From Equations (3.1) and (3.5) it follows that $\mathcal{I} = \mathcal{G}+2-\mathcal{E} \geq 1$, so at least one of the state variables is an intensive quantity in this case. Furthermore $\mathcal{I} > \mathcal{G}+2-\mathcal{K}$, which means that the number of intensive state variables is larger than the dimensionality of the $\mathcal{K}$-phase intersection in the intensive parameter space $\{Y_j, \tilde{Y}_i\}$. If one is inside such a mixed phase the intensive variables are actually overdetermined, which means that only special intensive state variables $\mathbf{Y} = (Y_j)$ allow to have the $\mathcal{K}$ phases in equilibrium. Due to this over-determination the dependent intensive variables $\tilde{Y}_i$ are fixed by the independent variables $\mathbf{Y}$ without the need to consider the extensive state variables:

$$(\tilde{Y}_i) = (\tilde{Y}_i(\mathbf{Y})) \; . \tag{3.7}$$

Furthermore, the overdetermination means that every change of a single intensive state variable will in general lead to the leaving of the mixed phase into a different (mixed) phase. Because $\mathcal{I} > \mathcal{G}+2-\mathcal{K}$, the mixed phase occupies also only a $\mathcal{G}+2-\mathcal{K}$-dimensional surface of the $\mathcal{I}$-dimensional space of the intensive state variables $\{Y_j\}$, like in the space of all intensive variables $\{Y_j, \tilde{Y}_i\}$.

Next we want to discuss the extension of the mixed phase with respect to the extensive state variables and the boundaries of the mixed phase further. The total value of the

extensive quantity X_i is given by the sum over the SHPs:

$$\begin{aligned} X_i &= \sum_{\kappa=1}^{\mathcal{K}} X_i^\kappa \\ &= \sum_{\kappa=1}^{\mathcal{K}} X_1^\kappa \frac{X_i^\kappa}{X_1^\kappa} \end{aligned} \tag{3.8}$$

In the last line we simply expanded with X_1^κ, the variable which is meant to fix the size of the phase, like e.g. the volume. Now we can use that the ratio $x_i^\kappa = X_i^\kappa / X_1^\kappa$ (e.g. an energy density) of the two extensive quantities of the same SHP can only depend on the intensive variables:

$$X_i = \sum_{\kappa=1}^{\mathcal{K}} X_1^\kappa x_i^\kappa(\mathbf{Y}, \tilde{\mathbf{Y}}) \,, \tag{3.9}$$

where we also used that the phases are in equilibrium $\tilde{\mathbf{Y}}^\kappa = \tilde{\mathbf{Y}}$. We note that Eq. (3.9) becomes trivial for $i = 1$, because $x_1^\kappa \equiv 1$. With Eqs. (3.7) there remain only the $\mathcal{K}$ unknowns X_1^κ in the set of the $\mathcal{E}$ Eqs. (3.9). As $\mathcal{E} < \mathcal{K}$, the volumes of $\mathcal{K} - \mathcal{E}$ SHPs remain unconstrained by the state variables and the equilibrium conditions. Vice versa, the extensive state variables can in general be varied at constant intensive state variables without leaving the mixed phase. Together with Eqs. (3.7) this shows that the intensive variables $\tilde{Y}_i$ are indeed independent of the extensive state variables inside the mixed phase.

We conclude that the mixed phase will be extended in all of the variables X_i. The boundaries in the space of extensive state variables $\{X_i\}$ for fixed $\mathbf{Y}$ is set by the constraint that the X_1^κ (e.g. the volumes) have to be positive and non-zero. According to Eqs. (3.9) the maximum (minimum) possible value of the extensive variable X_i for fixed $\mathbf{Y}$, and thus fixed $(\tilde{Y}_i(\mathbf{Y}))$ is reached when the volumes of all SHPs but the one with the largest (smallest) x_i^κ go to zero. Thus we know that for given $\mathbf{Y}$ the points with the largest and smallest value of each extensive variable actually do not belong to the mixed phase K, but to one of the SHPs.

There is the very unlikely possibility that by chance for one particular extensive variable X_i the x_i^κ are equal in all the SHPs κ: $x_i^1 = x_i^2 = ... = x_i^{\mathcal{K}} =: x_i$. Then for a fixed system size X_1 the mixed phase exists only for one particular value of X_i:

$$\begin{aligned} X_i &= \sum_{\kappa=1}^{\mathcal{K}} X_1^\kappa x_i^\kappa(\mathbf{Y}, \tilde{\mathbf{Y}}) \\ &= X_1 x_i(\mathbf{Y}, \tilde{\mathbf{Y}}) \,. \end{aligned} \tag{3.10}$$

We want to exclude this unlikely case in the following discussion.

One can summarize that if there are $\mathcal{K} > \mathcal{E}$ phases in equilibrium the volume fractions of the SHPs remain unconstrained and all intensive quantities are independent of the extensive state variables. The mixed phase has the dimension $\mathcal{G} + 2 - \mathcal{K}$ in the space of the intensive state variables $\{Y_j\}$ and is extended in the direction of the extensive state variables, thus forming a $\mathcal{G} + 2 - \mathcal{K} + \mathcal{E}$-dimensional surface in the space of the state variables $\{X_i, Y_j\}$.

Next the case $\mathcal{K} \leq \mathcal{E}$ will be analyzed, in which less or equal SHPs are in equilibrium than extensive quantities are chosen as state variables. By using the $\mathcal{I}$ externally fixed intensive state variables, there remain $\mathcal{G} + 2 - \mathcal{K} - \mathcal{I} = \mathcal{E} - \mathcal{K} \geq 0$ unknown intensive variables $\tilde{Y}_i$. This means that for $\mathcal{K} < \mathcal{E}$ also the extensive state variables X_j need to be considered to determine all intensive variables. The $\mathcal{E}$ Eqs. (3.9) involve exactly $\mathcal{K}$ additional unknowns X_1^κ, so that at the end no unknown variables remain. For $\mathcal{K} \leq \mathcal{E}$ all intensive variables, the X_1^κ and thus all extensive and intensive quantities can be determined from the state variables $(\mathbf{X}, \mathbf{Y})$ and are therefore fixed.

We want to specify the dependency of the unknown variables on the state variables inside the mixed phase further. In the special case $\mathcal{E} = \mathcal{K}$ the unknown intensive variables $\tilde{Y}_j$ do not depend on the extensive state variables X_j, so Eqs. (3.7) remain valid. The intensive state variables $\mathbf{Y}$ solely fix $\tilde{\mathbf{Y}}$. The extensive state variables can be varied, without affecting the dependent intensive variables. The extensive state variables are only needed to determine the X_1^κ and by that the extensive dependent variables $(\tilde{X}_j) = (\tilde{X}_j(\mathbf{X}, \mathbf{Y}))$.

Contrary, for $\mathcal{K} < \mathcal{E}$ also the unknown intensive variables depend on all state variables, including the extensive ones:

$$(\tilde{Y}_i) = (\tilde{Y}_i(\mathbf{X}, \mathbf{Y})) \; . \tag{3.11}$$

A variation in one of the state variables X_i or Y_j will lead to a change in all of the non-fixed variables $\tilde{X}_j$ and $\tilde{Y}_i$.

Now we want to discuss the dimensionality of a mixed phase with $\mathcal{K} \leq \mathcal{E}$ in the space of state variables $\{X_i, Y_j\}$. The important point is, that the number of intensive state variables $\mathcal{I}$ is lower or equal to the dimension of the $\mathcal{K}$-SHP-coexistence surface in the space of all intensive variables, $\mathcal{G} + 2 - \mathcal{K}$. Thus inside the mixed phase each of the intensive state variables can be varied individually without leaving the $\mathcal{K}$-phase coexistence. The system is not overdetermined as in the case $\mathcal{K} > \mathcal{E}$ any more. Thus even though a change of X_i implies a change of $\tilde{\mathbf{Y}}$ also the extensive state variables

case	dimension in $\{X_i, Y_j\}$	dependent variables		
$\mathcal{K} < \mathcal{E}$	$\mathcal{G}+2$	$\tilde{Y}_i = \tilde{Y}_i(\mathbf{X}, \mathbf{Y})$	$\tilde{X}_j = \tilde{X}_j(\mathbf{X}, \mathbf{Y})$	$X_1^\kappa = X_1^\kappa(\mathbf{X}, \mathbf{Y})$
$\mathcal{K} = \mathcal{E}$	$\mathcal{G}+2$	$\tilde{Y}_i = \tilde{Y}_i(\mathbf{Y})$	$\tilde{X}_j = \tilde{X}_j(\mathbf{X}, \mathbf{Y})$	$X_1^\kappa = X_1^\kappa(\mathbf{X}, \mathbf{Y})$
$\mathcal{K} > \mathcal{E}$	$\mathcal{G}+2-\mathcal{K}+\mathcal{E}$	$\tilde{Y}_i = \tilde{Y}_i(\mathbf{Y})$	$\tilde{X}_j$ undetermined	X_1^κ undetermined

Table 3.1: Properties of mixed phases with $\mathcal{K}$ SHPs in coexistence. Such a mixed phase has the dimension $\mathcal{G}+2-\mathcal{K}$ in the state of all intensive variables $\{Y_i, \tilde{Y}_j\}$. The dimension in the space of state variables is given in the second column. The third, fourth and fith column show the dependency of the dependent intensive variables $\tilde{Y}_i$, of the dependent extensive variables $\tilde{X}_j$ and of the sizes of the SHPs X_1^κ on the extensive and intensive state variables $(X_i) = \mathbf{X}$ and $(Y_j) = \mathbf{Y}$. Note that in the case $\mathcal{K} > \mathcal{E}$ the $\tilde{Y}_i$ are overdetermined because of the equilibrium conditions Eqs. 3.6.

can be varied within a certain range without leaving the mixed phase. For $\mathcal{K} \leq \mathcal{E}$ in general the mixed phase will be extended in all the variables X_i, Y_j filling a certain $\mathcal{G}+2$-dimensional volume of the parameter space of the state variables $\{X_i, Y_j\}$. The results for the properties of mixed phases are summarized in Table 3.1.

3.4 Properties of Phase Transformations

We showed now, that (mixed) phases with $\mathcal{K} \leq \mathcal{E}$ extend over a volume of the parameter space $\{X_i, Y_j\}$, and (mixed) phases with $\mathcal{K} > \mathcal{E}$ have a lower dimension. Only such extended phases with $\mathcal{K} \leq \mathcal{E}$ will be considered in the following as the relevant phases which can actually be accessed for a finite time. For the occurrence of mixed phases with $\mathcal{K} > \mathcal{E}$ at least one intensive state variable has to be tuned to an exact value. Any infinitesimal change of one of the intensive variables would lead to the leaving of the mixed phase. From a practical point of view, these phases can not be seen as permanent states of the system.

In the following we will not only consider phase transformations between two SHPs but also between two extended mixed phases. Inside extended (mixed) phases, specified by $\mathcal{K} \leq \mathcal{E}$, everything will change continuously because of the assumption of continuous potentials of the SHPs. It remains to determine the properties of a phase transformation from one particular (mixed) phase A consisting of the $\mathcal{K}^A \leq \mathcal{E}$ different SHPs A_κ, $\kappa = 1, ..., \mathcal{K}^A$, into a different neighboring (mixed) phase B with $\mathcal{K}^B \leq \mathcal{E}$ different SHPs B_λ, $\lambda = 1, ..., \mathcal{K}^B$. Let us denote the set of SHPs which are present in phase A by $A = \{A_\kappa\}$ and those of phase B by $B = \{B_\lambda\}$. Even though mixed phases with

$\mathcal{K} > \mathcal{E}$ cannot be accessed for a finite time, they can be crossed in such a transformation. Indeed, we will show that the qualitative properies of the phase transformation depend on the number of SHPs on the boundary layer which separates phases A and B. For a systematic classification it is sufficient to consider $\mathcal{E} \geq \mathcal{K}^B \geq \mathcal{K}^A$, i.e. phase B consists of more or equal SHPs than phase A. To be more precise we are now investigating a certain path $\Gamma : (\mathbf{X}(t), \mathbf{Y}(t))$ through the parameter space $\{X_i, Y_j\}$ so that the phase transition from phase A to phase B occurs at t^{pt} with $(\mathbf{X}(t^{pt}), \mathbf{Y}(t^{pt})) = (\mathbf{X}^{pt}, \mathbf{Y}^{pt})$. We require the path to start inside the volume of phase A and to end inside the volume of phase B. For the classification we first describe the properties and necessary conditions for the two possible cases, continuous and discontinuous phase transformations, and will then draw the connection to the phases A and B.

At the transition point, the state variables X_i and Y_j have to be equal in the two phases by construction, and thus change continuously. Furthermore at t^{pt} Gibbs' conditions for phase equilibrium have to be fulfilled between the (mixed) phases A and B, leading to

$$\lim_{t^{<} \to t^{pt}} \left(\tilde{Y}_i^A(\mathbf{X}^t, \mathbf{Y}^t) \right) =: \left(\tilde{Y}_i^A(\mathbf{X}^{pt}, \mathbf{Y}^{pt}) \right) = \left(\tilde{Y}_i^B(\mathbf{X}^{pt}, \mathbf{Y}^{pt}) \right) := \lim_{t^{>} \to t^{pt}} \left(\tilde{Y}_i^B(\mathbf{X}^t, \mathbf{Y}^t) \right) . \tag{3.12}$$

Dependent variables evaluated at $(\mathbf{X}^{pt}, \mathbf{Y}^{pt})$ shall refer to the limit of the variable by approaching the phase transition point within the corresponding phase. These limiting values are always well defined, also for the extenstive dependent variables, because we assumed $\mathcal{E} \geq \mathcal{K}^B \geq \mathcal{K}^A$. We see above that the intensive variables change continuously across the transition and are therefore continuous in the whole parameter space $\{X_i, Y_j\}$. The continuous path in $\{X_i, Y_j\}$ is always mapped onto a continuous path in $\{\tilde{Y}_i, Y_j\}$. Thus the only variables which can be different in the two phases at the transition point are the dependent extensive variables $\tilde{X}_j$.

A phase transformation is continuous, if in addition to the intensive variables also all of the extensive state variables are equal at the transition point:

$$\begin{aligned} \left(\tilde{X}_j^A(\mathbf{X}^{pt}, \mathbf{Y}^{pt}) \right) &= \sum_{\kappa=1}^{\mathcal{K}^A} \left(\tilde{X}_j^{A_\kappa}(\mathbf{X}^{pt}, \mathbf{Y}^{pt}) \right) \\ = \left(\tilde{X}_j^B(\mathbf{X}^{pt}, \mathbf{Y}^{pt})) \right) &= \sum_{\lambda=1}^{\mathcal{K}^B} \left(\tilde{X}_j^{B_\lambda}(\mathbf{X}^{pt}, \mathbf{Y}^{pt})) \right) , \end{aligned} \tag{3.13}$$

whereas $\tilde{X}_j^{A_\kappa}$ denotes the contribution of the SHP A_κ to $\tilde{X}_j^A$, and analog for the SHPs of phase B. Each term in the sums is uniquely fixed by the state variables. We can write

this equation also in the following way:

$$\sum_{\kappa=1}^{\mathcal{K}^A} X_1^{A_\kappa}(\mathbf{X}^{pt},\mathbf{Y}^{pt})\left(\tilde{x}_j^{A_\kappa}(\tilde{\mathbf{Y}}^{pt},\mathbf{Y}^{pt})\right)=\sum_{\lambda=1}^{\mathcal{K}^B} X_1^{B_\lambda}(\mathbf{X}^{pt},\mathbf{Y}^{pt})\left(\tilde{x}_j^{B_\lambda}(\tilde{\mathbf{Y}}^{pt},\mathbf{Y}^{pt}))\right)\ , \quad (3.14)$$

by using an equivalent relation to Eq. (3.9). Contrary, for a discontinuous phase transformation, for which Eq. (3.14) is not fulfilled, in general all of the $\tilde{X}_j$ will behave discontinuously:

$$\tilde{X}_j^A(\mathbf{X}^{pt},\mathbf{Y}^{pt}) \neq \tilde{X}_j^B(\mathbf{X}^{pt},\mathbf{Y}^{pt})\ . \quad (3.15)$$

Then each of the dependent extensive variables can serve as an order parameter.

It is possible that some of the SHPs of the two mixed phases A and B disappear when the transition point is reached. The SHPs of phases A and B which are still present at t^{pt} constitute the boundary layer between the two phases. This boundary layer can be seen as a new mixed phase C, because all the non-vanishing SHPs of phase A and B are in equilibrium with each other. Let us denote the set of $\mathcal{K}^C$ SHPs of phase C, given by the different SHPs of the phases A and B which are still present at t^{pt}, by C:

$$C=\{A_\kappa : X_1^{A_\kappa}(\mathbf{X}^{pt},\mathbf{Y}^{pt})\neq 0\}\cup\{B_\lambda : X_1^{B_\lambda}(\mathbf{X}^{pt},\mathbf{Y}^{pt})\neq 0\}\ . \quad (3.16)$$

Note that some of the SHPs of phase A and B can be identical, i.e. it is possible that the element A_κ is identical to B_λ. Obviously,

$$C\subseteq A\cup B\ . \quad (3.17)$$

To fulfill Eq. (3.14) to achieve a continuous phase transformation all SHPs which A and B do not have in common necessarily have to disappear at t^{pt}:

$$C\subseteq A\cap B\ , \quad (3.18)$$

because all terms in Eq. (3.14) are fixed by the state variables. On the other hand, if Eq. (3.18) is fulfilled both phases A and B go over to phase C by approaching the phase transition point. Because $\mathcal{K}^A\leq\mathcal{E}$ and $\mathcal{K}^B\leq\mathcal{E}$ the two phases are always well defined, with respect to all variables. Thus, the two phases will become identical when approaching t^{pt}, i.e. all volumes of the remaining SHPs will approach the same values in phase A and phase B. All limiting values of the dependent variables become identical. Thus the condition of Eq. (3.18) is equivalent to a continuous phase transformation.

Thus, if the condition is not fulfilled, we have a discontinuous phase transformation. However, it still remains to identify which of the SHPs of

$$M := A \cup B \tag{3.19}$$

do not disappear at t^{pt}, i.e. we have to relate phase C to phase A and B. In the following we use $\mathcal{K}^M$ for the number of all different SHPs of phase A and B.

To continue with the discussion we assume now that only two extended mixed phases, namely phases A and B are in contact at the transition point, which is the most likely situation. The boundary surface between two phases has the dimension $\mathcal{G}+1$, but the boundary layer between a larger number of extended phases has a lower dimensionality. The latter case would require that at least one of the state variables is tuned to an exact value. This makes it almost impossible to hit such a special phase transition point. With the assumption that no other extended mixed phases than A and B are in contact at t^{pt} we arrive at a contradiction: We realized above that the set C of the non-vanishing SHPs of phases A and B at t^{pt} can actually be seen as a separate mixed phase. This contradiction has to be resolved.

Let us consider now a discontinuous phase transformation, i.e. $C \not\subseteq A \cap B$. Obviously, then phase C is different from phase A and B. Thus it is necessary that $\mathcal{K}^C > \mathcal{E}$ so that phase C is not extended which resolves the contradiction. Because $C \subseteq M := A \cup B$, $\mathcal{K}^C \leq \mathcal{K}^M$. Thus it is necessary for a discontinuous phase transformation that $\mathcal{K}^M > \mathcal{E}$:

$$\text{discontinuous PT} \Longrightarrow \mathcal{K}^M > \mathcal{E}\ . \tag{3.20}$$

This result leads to an interesting consequence for phase transformations of isolated systems. For an isolated system only extensive state variables can be used, $\mathcal{E} = \mathcal{G}+2$. Because of Gibbs' phase rule, Eq. (3.5), we see that $\mathcal{K}^M \leq \mathcal{E}$ in this case. Thus, we can conclude that all phase transformations of isolated systems have to be continuous.

Let us turn back to the general discussion. In a continuous phase transformation where $C \subseteq A \cap B$, we get $\mathcal{K}^C < \mathcal{E}$, because $\mathcal{K}^A \leq \mathcal{E}$ and $\mathcal{K}^B \leq \mathcal{E}$ and at least one of the SHPs of A and B have to be different. If all SHPs of phase A and B were the same there was no phase transition. $\mathcal{K}^C < \mathcal{E}$ means that C is an extended mixed phase which is in contradiction to our assumption. The only solution is, that C is identical to A or B, and because we assumed $\mathcal{K}^A \leq \mathcal{K}^B$ we get $C{=}A$. This means that the boundary layer between phases A and B where the phase transition occurs actually belongs to phase A. At the phase transition point the additional SHPs of phase B appear continuously. Because $A = C \subseteq A \cap B$ we have $M = A \cup B = B$, so that $\mathcal{K}^M = \mathcal{K}^B \leq \mathcal{E}$ and we can

conclude:

$$\text{continuous PT} \Longrightarrow \mathcal{K}^M \leq \mathcal{E} \; . \tag{3.21}$$

Thus we showed that

$$\text{continuous PT} \Longleftrightarrow \mathcal{K}^M \leq \mathcal{E} \; , \tag{3.22}$$

if no other extended mixed phases than A and B are in contact at $(\mathbf{X}^{pt}, \mathbf{Y}^{pt})$, and with $\mathcal{K}^M$ denoting the number of different SHPs of phase A and B.

We can constrain the properties of the two phases in a continuous transformation even further. Imagine that phase B has more than one SHP in addition to phase A, $\mathcal{K}^B \geq \mathcal{K}^A + 2$. Then it must also be possible to go from the transition point into another phase D which consists of the SHPs of phase A with only one of the additional SHPs of phase B. This would also be a contradiction to the assumption that only phase A and B are in contact at the transition point. We conclude: in a continuous phase transformation, in general the phases A and B differ only in one of the SHPs, which appears in a continuous way after passing the transition point.

Also in a discontinuous phase transformation the phases A and B have to fulfill some additional specific properties. Phase C has the dimension $\mathcal{G}+2+\mathcal{E}-\mathcal{K}^C$ in the space of the state variables which has to be equal to the dimension $\mathcal{G}+1$ of the coexistence surface between the volumes of phases A and B, and thus $\mathcal{K}^C = \mathcal{E}+1$. On C, the intensive variables are independent of the extensive state variables, see Table 3.1. If we keep the intensive variables fixed but move on phase C to slightly different extensive state variables (X_i') the neighboring phases still have to be phases A and B. This requires that also inside phases A and B the intensive variables have to be independent of the extensive state variables, which is only possible if $\mathcal{K}^A = \mathcal{K}^B = \mathcal{E}$. In general, in a discontinuous phase transformation a set of $\mathcal{E}$ different SHPs is replaced by a different set of $\mathcal{E}$ SHPs. From the structure of the phase diagram one can conclude, that phase A and B differ only in one SHP. Finally we note that because of Eqs. (3.7) at least one intensive variables has to be varied along the path to trigger the phase transition, because we excluded that we are at the boundary of the surface which separates phases A and B (phase C). As the maximum possible number of phases in coexistence is $\mathcal{G}+2 = \mathcal{I}+\mathcal{E} \geq \mathcal{K}^{\mathcal{M}} > \mathcal{E}$ at least one intensive variable is indeed also always used as a state variable.

Next we want to investigate the latent heat Q released or absorbed during the phase transformation. It is given by the change of the internal energy of the system,

$$Q = E^B(\mathbf{X}^{pt}, \mathbf{Y}^{pt}) - E^A(\mathbf{X}^{pt}, \mathbf{Y}^{pt}) \ , \tag{3.23}$$

where the internal energy is related to the thermodynamic potential, Eq. (3.4), by:

$$E(\mathbf{X}, \mathbf{Y}) = \Phi(\mathbf{X}, \mathbf{Y}) + \sum_{j=1}^{\mathcal{I}} \tilde{X}_j(\mathbf{X}, \mathbf{Y}) Y_j \ . \tag{3.24}$$

With the equality of the two thermodynamic potentials of the two phases and Gibbs' equilibrium conditions we get:

$$Q = \sum_{j=1}^{\mathcal{I}} Y_j \left(\tilde{X}_j^B(\mathbf{X}^{pt}, \mathbf{Y}^{pt}) - \tilde{X}_j^A(\mathbf{X}^{pt}, \mathbf{Y}^{pt}) \right) \ . \tag{3.25}$$

In a continuous phase transformation this becomes zero. In a discontinuous phase transformation, because of Eq. (3.15), $Q \neq 0$ in general. Only a discontinuous phase transformation leads to the release or absorption of latent heat, i.e. energy. We found before that all phase transformations of isolated systems are continuous. Furthermore, a discontinuous phase transformation can only be triggered by a change of the intensive state variables. The intensive state variables refer to properties of the surrounding heat/particle/pressure bath. Thus we conclude, that the discontinuous energy change of the subsystem, i.e. the appearance of latent heat, is caused by a change of the intensive properties of the bath. The energy is taken from the bath and put into the system directly (for $Q > 0$, i.e. the absorption of latent heat). If the system was isolated, this would not be possible because no surrounding exists, in agreement with our previous considerations.

Prof. I. Iosilevskiy from the Joint Institute of High Temperature in Moscow submitted an unpublished article to the author of this thesis. This article is a very interesting complement to some aspects discussed above. In his work the phase transition of a one-component substance with $\mathcal{G} = 1$ is called a "congruent" phase transition, and of a multi-component substance with $\mathcal{G} \geq 2$ a "non-congruent" phase transition. Only the free enthalpy is considered, so that there are two intensive state variables, $\mathcal{I} = 2$, the temperature T and pressure p. The extensive state variables are all the conserved charges, $\mathcal{E} = \mathcal{G}$, which are kept constant. Only the intensive state variables are varied. Consequently, the congruent phase transitions are discontinuous and the non-congruent ones are continuous phase transformations. Iosilevskiy especially emphasizes the implications

on the dimensionality of the mixed phase regions in the phase diagram. In the congruent case, the coexistence surface is two-dimensional in $\{T, p, N\}$, leading to a coexistence line in $\{T, p\}$. In the non-congruent case, the mixed phase fills a four-dimensional volume in $\{T, p, N_1, N_2\}$, leading to a two-dimensional coexistence region in $\{T, p\}$. In his article Iosilevskiy presents a typical "banana-like" region for the non-congruent phase transition of a chemically reacting uranium-oxygen plasma and anticipates that such higher-dimensional phase coexistence regions should also occur in astrophysical environments. This study is in full agreement with the results derived above.

Let us close with some final remarks to the classification of phase transitions and phase transformations. The Ehrenfest classification of phase transitions refers to the grand-canonical potential $\Phi(V, T, \mu)$, in which only one extensive state variable, namely the volume, is used. Thus it refers to a specific set of state variables with $\mathcal{E} = 1$ and by this to a specific phase transformation. According to the Ehrenfest classification a phase transition is of first order, if at least one of the first derivatives of the grand-canonical potential is discontinuous, and of second order if the first derivatives are continuous, but the second are not[2]. We can directly confirm, that the first order phase transitions investigated here correspond to discontinuous phase transformations of the grand-canonical ensemble, because $\mathcal{K} \geq 2 > \mathcal{E} = 1$. We showed that the $\tilde{X}_j$, which are first derivatives of the corresponding potential, are discontinuous in a discontinuous phase transformation, in agreement with the Ehrenfest classification. Even though phase transformations with different state variables may be continuous, they are still phase transitions of first order. However, we want to stress that it is necessary for this consistency that the grand-canonical potential is used for the classification of phase transitions. For a one-component system with only one conserved charge the situtation is easier, and e.g. also the free enthalpy $G = G(T, p, N)$ gives a well-defined classification.

However, the behavior of the thermodynamic variables in a continuous phase transformation resembles very much a second order phase transition (according to the Ehrenfest classification). In the continuous phase transformations, the $\tilde{X}_j$ are continuous. Thus all first derivatives of the thermodynamic potential are continuous. Also the volume fractions of the SHPs change continuously. The second derivatives of the thermodynamic potential which are derivatives of the $\tilde{X}_j$ involve derivatives of the volumes of the SHPs. The volumes of the non-common SHPs of phase A and B are zero at the transition point, but the derivatives of these volumes are in general not equal in the two different phases A and B, leading to discontinuous second derivatives. However, even though the

[2]Very often second order phase transitions are actually characterized by continuous, but divergent second derivatives of the thermodynamic potential (λ-transition). An example is the critical point of the liquid-gas phase transition or the superfluid transition of ^{4}He.

continuous phase transformations look very similar to second order phase transitions, it also comes to the coexistence of several SHPs which are spatially separated from each other. The SHPs can always be distinguished from each other, e.g. by ratios of extensive variables like the energy density. The occurrence of phase coexistence could be seen as the characteristic of a first order phase transition.

Finally we note that the globally conserved charges are only important as degrees of freedoms, if they are actually explored by the single phases. For example in the liquid-gas phase transition of symmetric nuclear matter both phases will stay symmetric even in the coexistence region. Thus the proton fraction is not relevant as a globally conserved charge. Such a substance, which does not change its charge concentrations by boiling, is called an azeotrope. A different example would be large mixed phase structures which drive the system to be locally charge neutral. In a practical point of view also the extension of the mixed phase with respect to the state variables matters. In a strict sense, for $\mathcal{K} \leq \mathcal{E}$ the phase transformation always remains continuous, but for very small mixed phases (compared to the typical scale of the underlying physical process), the dependent variables may change actually very rapidly so that a continuous phase transformation could appear rather discontinuously.

3.5 Applications and Examples

Our general results can be applied to any thermodynamic system without finite-size effects which is always in full equilibrium. In the following we want to discuss some examples. We start with the phase transitions of a one-component substance like ordinary water, for which we will analyze the phase diagram and the possible phase transformations in detail. Based on the general results we then examine the properties of phase transformations if only two SHPs are in coexistence. Furthermore we address the implications of first order phase transitions in heavy ion collisions and in hydrodynamic simulations. First order phase transitions in compact stars will be discussed in full detail in Chap. 7.

3.5.1 "Water"

Ordinary water consists of one sort of particles, $\mathcal{G} = 1$, and the parameter space is three-dimensional. Water is a very interesting substance, as at the triple-point the maximum possible number of three different SHPs are in coexistence. Thus all different kind of

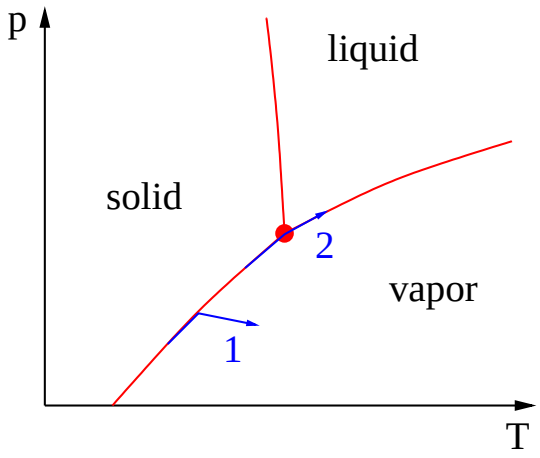

Figure 3.1: The phase diagram of water for constant number of particles N, and for the pressure p and the temperature T as the independent control parameters. Red lines show lines of discontinuous phase transformations, where two different single homogeneous phases (SHPs) are in equilibrium. The red dot marks the triple point of water, where all three SHPs are in equilibrium. The arrows show examples of different phase transformations, belonging to the control parameters of Fig. 3.2, which are discussed in the text.

possible scenarios can occur. For simplicity, we exclude the critical point of the liquid-gas transition and we only study a small region around the triple-point, where liquid water, ice and water vapor are in equilibrium. We are only interested in the topology of the phase diagram, i.e. the dimensionalities of the phase boundaries. The shapes and slopes of phase boundaries are irrelevant for the following discussion. We note that the shown phase diagrams are actually not in full agreement with the true phase diagram of water.

Let us start with $\mathcal{E} = 1$, where e.g. a fixed number of molecules N are in a container of variable size inside a heatbath. A different possibility would be a container with fixed volume V which is permeable for the water molecules in a particle and heat bath. In the following we will always use the molecule number N and set it to be constant. Therefore it is sufficient to plot the phase diagram for the remaining two state variables, which is done in Fig. 3.1. In the parameter space $\{T, p\}$ there exist the three areas of the SHPs, separated from each other by the three different coexistence lines of two SHPs which intersect in the triple point, where all three SHPs coexist. No extended mixed phases exist and all possible phase transformations are discontinuous because $\mathcal{K}^M = 2 > 1 = \mathcal{E}$. We note that it is very unlikely to hit the triple point, as it requires to adjust both the pressure and the temperature of the surrounding medium to an exact value.

The arrows which are drawn in Fig. 3.1 belong to phase transformations with the different set of control parameters in which the pressure is replaced by the volume V,

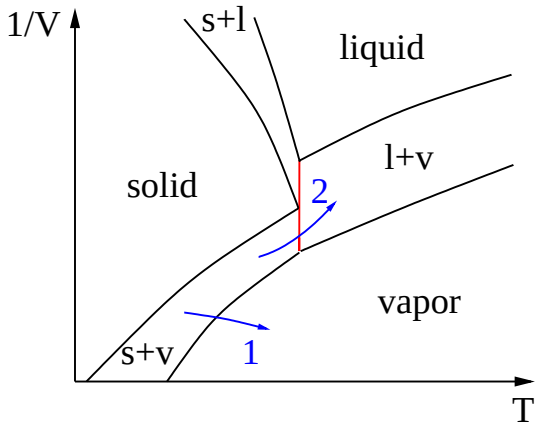

Figure 3.2: The phase diagram of water for constant number of particles N, and for the volume V and the temperature T as the independent control parameters. "s" denotes the solid, "l" the liquid and "v" the vapor SHP in the corresponding extended mixed phases. Black lines show lines of continuous phase transformations. The red line is the discontinuous triple line, on which all three SHPs are in equilibrium. The arrows show examples of different phase transformations which are discussed in the text. Phase transformation No. 1 is continuous, No. 2 is discontinuous.

so that one gets $\mathcal{E} = 2$. Now we are investigating a non-permeable particle container of fixed size inside the heat bath. The corresponding phase diagram is plotted in Fig. 3.2. The three mixed phases of two different SHPs become now areas in the plot. The triple-point becomes a triple line at constant temperature, but now extended in V. It is the line where the extended mixed phases meet. From Sec. 3.4 we know, that the lines of continuous phase transformations actually always belong to the phase with the lower number of SHPs. Thus in Fig. 3.2 the black lines belong to one SHP, e.g. the line between "s+v" and "v" belongs to "v". Next we will discuss two characteristic examples for the two different types of phase transformations in more detail.

Let us begin with phase transformation No. 1. We start with a mixture of the solid and the vapor SHP, whereas each SHP has a certain finite volume fraction. By increasing the temperature and slightly increasing the volume we are manipulating the system and approach the phase transformation into the pure vapor phase. Gradually the solid transforms into vapor until only the vapor is left at the transition point. Obviously, this phase transformation is continuous. In the phase transformation No. 2 we start at a similar state with a mixture of the solid and the vapor. But this time we heat and compress the system in such a way, that we end up in a mixture of the liquid and the vapor. Because no other phases are in contact at the transition point, we know that the phase transformation is discontinuous, because $\mathcal{K}^M = 3 > 2 = \mathcal{E}$. By approaching the transition point the volumes of the solid and the vapor part approach a certain (non-vanishing) value. When we have passed the transition point, the solid is

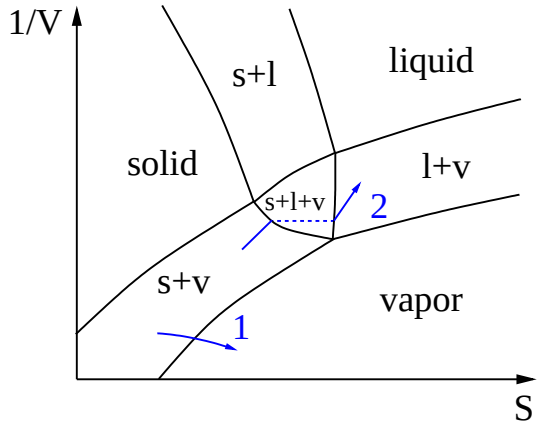

Figure 3.3: The phase diagram of water for constant number of particles N, and for the volume V and the entropy S as the independent control parameters. Black lines show lines of continuous phase transformations. There are no discontinuous phase transformations for this set of control parameters. The arrows show examples of different phase transformations, belonging to the control parameters of Fig. 3.2, which are discussed in the text.

replaced by the liquid and the vapor part jumps to a new value of the volume fraction. At the transition point, all three SHPs are in contact, with arbitrary volume fraction. However, this happens only at one single point, which is not observable and thus not really relevant. It is interesting to study the paths of the discussed phase transformations in the $\{T, p\}$-plane, which is shown in Fig. 3.1. One sees that all intensive variables change continuously.

For $\mathcal{E} = 3$ the volume V, the number of particles N and the entropy S are used as state variables and are therefore fixed externally. the corresponding phase diagram is shown in Fig. 3.3. We are investigating a completely isolated system, which is the easiest scenario to realize. For the phase transformation we can imagine all kind of paths, where heat is put into the system leading to a change in S, and/or changes of the volume V. The following extended phases exist: First the three different SHPs. Again, between each pair of these a common mixed phase of the corresponding two SHPs exists. Between these three mixed phases, there is the region where all three phases are coexisting, $\mathcal{K} = 3$. This mixed phase of three SHPs also occupies a certain area. Because $\mathcal{E} = \mathcal{G} + 2 = 3$, all possible phase transformations are continuous. As already discussed for Fig. 3.2 we know that the states on the lines actually belong to the extended (mixed) phase with the lower number of SHPs. The points where the triple phase is in contact with a phase consisting only of one SHP must actually belong to this SHP, due to the same reasons.

It is very enlightening to investigate the example phase transformations of Fig. 3.2 in the parameter space of extensive variables of Fig. 3.3. Now it becomes obvious, why the two examples are continuous and discontinuous. The entropy S is the only variable which can behave discontinuously for the set of state variables of Fig. 3.2. In example No. 2 the temperature was changed continuously. Thus the entire triple phase region is crossed at once, because the three SHPs can coexist only at one single temperature. This is visualized by the dashed line in Fig. 3.3. In example No. 1 there is no discontinuous change of the entropy.

3.5.2 Two Single Homogeneous Phases

For only two SHPs, the derived formalism simplifies a lot. If $\mathcal{E} = 1$ there exist only two extended phases in the parameter space $\{X_1, Y_j\}$, namely the two SHPs. The two volumes are separated from each other by the $\mathcal{G}+1$-dimensional coexistence surface, in which the volume fraction of the two SHPs remains arbitrary. The phase transformation is always discontinuous, unless the two equations of states give the same $(\tilde{X}_j)$ at the transition point, meaning that all the first derivatives are equal. Actually this would correspond to a critical point, because then the two SHPs could not be distinguished from each other any more. If $\mathcal{E} \geq 2$, the two SHPs are separated from each other by their extended mixed phase, which fills a volume in $\{X_i, Y_j\}$. The transition from one SHP into the mixed phase is continuous, and the volume of the other SHP is zero at the onset of the mixed phase. After crossing the phase transformation surface, the volume fraction of the second SHP increases continuously. When it goes to unity, the first phase has disappeared and the end of the mixed phase is reached. Obviously, the transition from the mixed phase into the second SHP is also continuous.

3.5.3 Heavy Ion Collisions

The results of this chapter could also be relevant for the description of the first order QCD phase transition in relativistic heavy ion collisions which e.g. may be explored at FAIR at GSI in the future. In the central collision region of a heavy ion experiment one expects that quark matter is formed at large enough collision energies. After its generation the central fireball expands and cools. Depending on the densities which are reached inside the colliding system the phase transition from quarks to hadrons may be of first order. In general, the state of the system could be described by the internal energy, the volume, and the baryon and the proton number (U, V, N_B, N_p). There does not exist any surrounding heat or particle bath, so it is most natural to describe the

fireball as an isolated system with evolving state parameters. N_B and N_p could be treated as constants, whereas the temporal evolution of U and V have to be calculated in numerical simulations or require further simplifying assumptions. However, it is very natural to assume that they change continuously. If thermodynamic equilibrium was reached during all stages of the heavy ion collision and if the thermodynamic limit is appropriate for this small system, we can apply our results. Because $\mathcal{E} > 2$, an extended mixed phase would always form and exist over a finite period of time. The hadron-quark transition would be continuous regarding global observables.

3.5.4 Hydrodynamics

There are two formulations of hydrodynamics, the Eulerian form in which the evolution of small stationary cells with fixed volume V is considered, and the Lagrange form which describes gas packages with fixed number of particles N in comoving frames. In both formulations the equations of motion are based on the exchange of the conserved quantities particle number, entropy and momentum between neighboring cells. The entropy, volume and number of particles of each cell are always known. The concept of separated subsystems automatically introduces an entirely extensive description of the cells, $\mathcal{E} = \mathcal{G} + 2$. If a phase transition happened in one of the cells, it would always be continuous and would lead to the formation of a mixed phase. Discontinuities would never occur which directly lead to the appearance of shocks. For the formation of the mixed phase inside the hydrodynamic cell it is necessary, that the typical structures within the mixed phase are much smaller than the size of the cell. This is in agreement with the statement that hydrodynamics describe the large scale evolution of a system.

For astrophysical simulations of the hadron-quark phase transition this is usually well fulfilled, because the typical size of the hydrodynamic cells of $\sim$ 10 m to 1 km are much larger than the mixed phase structures of order 10^{-14} m. Contrary, in the hydrodynamic description of a heavy ion collision this may not be the case, because there the typical cells in a hydrodynamic simulation are usually very small of order $\sim$ 0.1 fm. Thus it could be more realistic to exclude the possibility of a mixed phase in the construction of the EOS for the hydrodynamic simulation. This could be done by assuming additional local constraints for the phase transition, so that there is a direct transition between the two phases. We will present this method in Chapters 5 and 7. Each cell would then always consist only of one of the SHPs. The phase transition in one cell would then automatically be discontinuous and would depend on how the EOSs of the two SHPs were connected with each other, i.e. which conditions were assumed for the phase transition. Some of the thermodynamic variables would behave discontinuously locally.

Global entropy, energy, momentum and particle number conservation is assured by the hydrodynamic description. This procedure would be only a very crude description of the phase transition. In fact, first order phase transition have to be treated in much more detail, if the structures of the mixed phase are of similar size as the hydrodynamic cells, see e.g. [SV09a, SV09b].

Chapter 4

Nucleation

In the previous chapter we studied the implications and properties of first order phase transitions in full equilibrium. Now some non-equilibrium aspects of nucleation shall be addressed, in the case of the phase transition between two single homogeneous phases (SHPs). Nucleation describes the onset and initial formation of the newly appearing phase. Here, we restrict the discussion on classical thermal nucleation, i.e. we do not consider any quantum effects, like quantum fluctuations or tunneling which can be more important than thermal effects at very small temperatures. Furthermore we use only a thermodynamic description which assumes separable bulk and finite-size parts. Our approach is based on several chapters of Ref. [LL69], and is mainly only a compact reformulation and generalization to multi-component systems with $\mathcal{G}$ conserved charges C_k, $k = 1, ..., \mathcal{G}$, denoted by the vector $\mathbf{C} = (C_k)$, and more general finite-size effects.

In Chap. 3 we assumed that the phase transition sets in, as soon as the transition point t^{pt} is reached along the path Γ in the parameter space of the state variables. In case of a continuous phase transformation, starting from the first SHP, the mixed phase of the two SHPs begins at t^{pt} with a gradual appearance of the second SHP. In case of a discontinuous phase transformation we directly jump to the second SHP after t^{pt}. In the last chapter we treated the SHPs as two different EOS. However, we want to remind the reader, that the two different SHPs actually only represent different states of the same underlying unified EOS. Usually there will be a barrier between the two states of the two phases, which has to be overcome, before the second phase can be formed. This can be done by local thermal fluctuations, which can become the seed nuclei for the newly appearing phase. This effect is called nucleation. Small fluctuations will decrease the entropy so that they will be dissipated. Only above a certain critical fluctuation (the barrier) the entropy will increase by further increasing the fluctuation.

The parameter space in which phase coexistence is possible is enclosed by the so-called binodal surface. In our case, the phase transition point t^{pt} is located on the

binodal surface. If the system is driven very far away from the phase transition point and kept in the first SHP, which is now only metastable, it will eventually reach a spinodal instability, where the barrier for nucleation vanishes. Any initial fluctuation will be enhanced and grow further. The states which are between the corresponding binodal and spinodal are the metastable states. In this metastable region nucleation is relevant. Spinodal stability is a local criterion, binodal a global one. The metastable states are locally stable (i.e. for small fluctuations) but a different global minimum of the thermodynamic potential exists. Local stability is lost at the spinodal, meaning that any small fluctuation is unstable. However, also in this case the growth time is finite, see e.g. [Ran09], so that it takes some time until the true equilibrium is established.

Obviously, fluctuations of large size, e.g. changes of a large volume, encounter strong exponential suppression, thus the question of nucleation cannot be addressed in the thermodynamic limit. Instead only fluctuations of a small sub-volume will be considered. Because of the small size of the seed nuclei, surface and other finite-size effects are crucial and need to be taken into account explicitly. If the finite-size effects are known, one can give good estimates for the nucleation rate, i.e. the number of critical fluctuations per unit time and unit volume.

4.1 Fluctuations

In this section we want to describe a certain small fluctuation in a small subsystem within a much larger particle and heat bath. For simplicity, we consider that the bath is isolated and closed. This means the system as a whole is treated micro-canonically. As we will show, only the initial intensive variables (temperature T^0, pressure p^0, and chemical potentials μ_k^0) of the heat bath in the meta-stable state are relevant for the probability that a certain fluctuation occurs. Thus the micro-canonical formulation is not necessary, but it gives the most comprehensible description of the fluctuations.

The entropy of the total system shall be denoted by S^{tot}, which is the sum of the entropy of the bath S^{bath} and of the subsystem S, $S^{tot} = S^{bath} + S$. Here and in the following all variables without index denote the subsystem of the fluctuation. In equilibrium the total entropy is constant. Now we consider that a certain fluctuation takes place which decreases the total entropy for a short moment of time by $\Delta S^{tot} < 0$, because the system is slightly out of equilibrium. The probability for this to happen is given by the corresponding change of the total entropy:

$$P \propto \exp(\Delta S^{tot}) \; . \tag{4.1}$$

This is the thermodynamic probability to be in a different state than its groundstate after an infinitely long time in the sense of the ergodic hypothesis.

The constant of proportionality could e.g. be determined from a proper normalization, so that the sum over all fluctuations gives unity. If the expression above is used for a rate, the factor of proportionality has to have dimensions of MeV^4. Usually the rate is dominated by the exponential term. Thus, quite often one simply takes T^4 for the prefactor. Furthermore, the exponential term contains the physical aspects of nucleation which are easy to understand. Thus we will neglect the constant of proportionality in the following discussion and only speak about the exponential.

Next we have to specify the form of the fluctuation in more detail. Here we assume the most general case of a subsystem in the equilibrium configuration with size V^0, internal energy E^0 and conserved charges C_k^0 which encountered a fluctuation to a new local equilibrium state with changed volume, energy and conserved charges:

$$\begin{aligned} V &= V^0 + \Delta V \\ E &= E^0 + \Delta E \\ \mathbf{C} &= \mathbf{C}^0 + \Delta\mathbf{C} \quad . \end{aligned} \tag{4.2}$$

Here and in the following the index 0 shall always refer to the equilibrium configuration of the metastable state without any fluctuation. Variables without index correspond to the state with the fluctuation. We adopt a microcanonical description of the fluctuation in the subsystem. It does not matter, how the fluctuation was actually formed. It is only necessary, that a new local equilibrium state is reached in the subsystem, so that we can apply thermodynamics. The new entropy of the subsystem is then given by the new values of its state variables:

$$S = S(E, V, \mathbf{C}) \, . \tag{4.3}$$

The fluctuation shall conserve the total volume, energy and charges. Thus we get:

$$\begin{aligned} \Delta V &= -\Delta V^{bath} \\ \Delta E &= -\Delta E^{bath} \\ \Delta\mathbf{C} &= -\Delta\mathbf{C}^{bath} \quad , \end{aligned} \tag{4.4}$$

i.e. the changes of the subsystem correspond to the negative changes of the bath.

The total change of the entropy $\Delta S^{tot} = S^{tot} - S^{tot\ 0}$ splits into the parts of the bath and the subsystem, $\Delta S^{tot} = \Delta S + \Delta S^{bath} = S - S^0 + S^{bath} - S^{bath\ 0}$. We assume that the

relative changes of the main system are vanishingly small, so that the intensive properties of the bath do not change. Furthermore, in the initial equilibrium configuration, the subsystem and the bath have the same pressure, temperature and chemical potentials:

$$\begin{aligned} T^{bath} &= T^{bath\ 0} = T^0 \\ p^{bath} &= p^{bath\ 0} = p^0 \\ \boldsymbol{\mu}^{bath} &= \boldsymbol{\mu}^{bath\ 0} = \boldsymbol{\mu}^0 \quad . \end{aligned} \tag{4.5}$$

Then we can use the first law of thermodynamics to substitute ΔS^{bath}:

$$\Delta S^{tot} = \Delta S + \frac{1}{T^0}\left(\Delta E^{bath} + p^0 \Delta V^{bath} - \sum_k \mu_k^0 \Delta C_k^{bath}\right) \ . \tag{4.6}$$

Using Eqs. (4.4) and $\Delta S = S(E,V,\mathbf{C}) - S^0$ we obtain:

$$\Delta S^{tot} = S(E,V,\mathbf{C}) - S^0 - \frac{1}{T^0}\left(\Delta E + p^0 \Delta V - \sum_k \mu_k^0 \Delta C_k\right) \ . \tag{4.7}$$

By realizing that

$$S^0 = \frac{1}{T^0}\left(E^0 + p^0 V^0 - \sum_k \mu_k^0 C_k^0\right) \ , \tag{4.8}$$

because finite-size effects do not exist for a state without any fluctuation, and using Eqs. (4.2) one gets:

$$\Delta S^{tot} = S(E,V,\mathbf{C}) - \frac{1}{T^0}\left(E + p^0 V - \sum_k \mu_k^0 C_k\right) \ . \tag{4.9}$$

The probability of a general fluctuation is readily obtained:

$$P_{fluc}(E,V,\mathbf{C}) \propto \exp\left(S(E,V,\mathbf{C}) - \frac{1}{T^0}(E + p^0 V - \sum_k \mu_k^0 C_k)\right) \ . \tag{4.10}$$

The entropy change is entirely expressed by the set of $\mathcal{G}+2$ state variables of the subsystem, and the intensive variables of the heat bath. Thus the choice of a different description for the entire system, e.g. a grand-canonical description, would not affect our results, as long as the bath can be treated in the thermodynamic limit and the fluctuation is small. We also find that the initial state of the subsystem $(E^0, V^0, \mathbf{C}^0)$ is irrelevant.

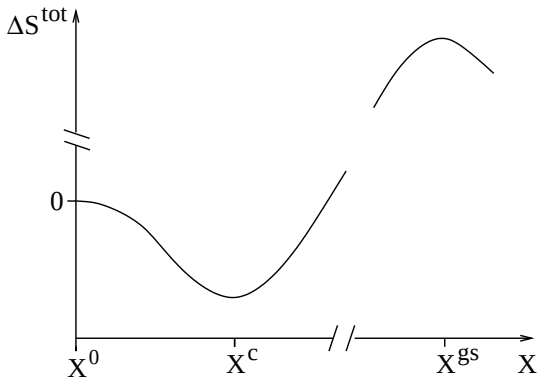

Figure 4.1: Illustration of the change of the total entropy with a fluctuation of the variable X from its equilibrium value X^0. For small fluctuations the entropy has to decrease quadratically. X^c shows the critical fluctuation and X^{gs} the value of the variable in the true groundstate which is a global maximum of the total entropy.

4.2 Conditions for Nucleation

Next we have to ask for the criteria, that a certain fluctuation will grow further and not be dissipated away. In a stable system the entropy is decreased by the fluctuation, and the system can only increase the entropy again by dissipating the fluctuation. In a stable equilibrium configuration, the entropy has to decrease quadratically in all directions for any small fluctuation and the probability distribution is a multi-dimensional gaussian [LL69].

Nucleation can only occur if the system is not in its true ground state but in a metastable state. Thus it is necessary, that the system has been driven beyond the equilibrium phase transition point, which we assume in the following. Initially, the system shall remain in the first phase which is only metastable. Because we assume that we have passed the equilibrium transition point, we know that there is a different global configuration with a larger entropy. Thus it is clear, that there exist some over-critical fluctuations, for which the system develops to the true ground state with the global maximum of the entropy, once they are produced.

In case of a continuous phase transformation the ground state will usually be the mixed phase with phase coexistence. For a discontinuous phase transformation, the ground state belongs to the second SHPs, because no extended mixed phase exists. Obviously, the groundstate is intrinsically stable. Thus we know, that the total entropy of the final configuration also decreases quadratically in all directions. In Figure 4.1 the behavior of ΔS^{tot} is illustrated for the one-dimensional case.

Equation 4.1 gives the probability for the system to be in the arbitrary state with ΔS^{tot}. Obviously, the probability to be in the groundstate is larger than to be in the

initial state. This apparent contradiction arises because Eq. (4.1) is the thermodynamic occupation probability of the state after an infinitely long evolution time of the system. To deduce the nucleation rate from the probability, we need some additional handwaving arguments.

Let us denote the set of state variables $(E, V, \mathbf{C})$ by $\mathbf{X} = (X_i)$, $i = 1, ..., \mathcal{G} + 2$ in the following. We cannot follow the dynamical evolution from the nucleation to the true groundstate, because this is a non-equilibrium process. However, this is not what we are interested in. We describe the entire nucleation and phase transition process by three steps, each of them being a (local) equilibrium state: Necessarily, we have to start any fluctuation from the metastable equilibrium configuration $\mathbf{X}^0$ in the initial phase. Then follows the intermediate state of the fluctuation in local equilibrium, denoted by $\mathbf{X} = \mathbf{X}^{nucl}$. For such a critical fluctuation, the system will develop to $\mathbf{X}^{gs}$, the true groundstate (mixed phase or the second SHP) in full equilibrium.

The nucleation rate is given by the critical fluctuation which has the largest probability, i.e. the largest ΔS^{tot}. However, it would not make sense to assume that the state $\mathbf{X}^{nucl}$ is a maximum of ΔS^{tot} because then this state would be metastable and would not evolve to the groundstate. Thus we assume only that it is a maximum with respect to all fluctuation variables but one, here denoted by X_1:

$$\begin{aligned} \left.\frac{\partial \Delta S^{tot}}{\partial X_i}\right|_{\mathbf{X}=\mathbf{X}^{nucl}} &= 0 \;\forall\; i \neq 1 \\ \left.\frac{\partial^2 \Delta S^{tot}}{(\partial X_i)^2}\right|_{\mathbf{X}=\mathbf{X}^{nucl}} &< 0 \;\forall\; i \neq 1 \quad . \end{aligned} \tag{4.11}$$

These conditions fix only $\mathcal{G}+1$ of the $\mathcal{G}+2$ fluctuation variables X_i^{nucl}. One fluctuation variable, e.g. X_1^{nucl} remains unconstrained. This means we need one further condition to fix the state of the nucleation $\mathbf{X}^{nucl}$.

To do so, let us assume that $X_1^0 < X_1^{nucl} < X_1^{gs}$. If $\left.\frac{\partial \Delta S^{tot}}{\partial X_1}\right|_{\mathbf{X}=\mathbf{X}^{nucl}} < 0$ the system would increase the entropy by going back to the groundstate configuration so that nucleation would not occur. This corresponds to fluctuations which are to the left of X^c in Fig. 4.1. If instead $\left.\frac{\partial \Delta S^{tot}}{\partial X_1}\right|_{\mathbf{X}=\mathbf{X}^{nucl}} > 0$ the system can increase its entropy by further enhancing the fluctuation. The system can in principle develop to its true ground state by alone by "rolling up" the entropy hill and nucleation is possible. In Figure 4.1 all fluctuations to the right of the minimum X^c are overcritical. However, it would not make sense to calculate the rate of nucleation by a fluctuation which is to the right of X^c. Every fluctuation X^{oc} to the right of X^c has a larger probability than X^c, but for the formation of such a fluctuation it is necessary to pass through X^c. Thus we require

that the nucleation occurs via the fluctuation which is a minimum of ΔS^{tot} with respect to X_1, corresponding to X^c in Fig 4.1.

From these considerations we conclude that ΔS^{tot} has to be a minimum with respect to one of the state variables of the fluctuation, but a maximum of the entropy with respect to all others. The nucleation occurs via a special multi-dimensional saddle-point of the total entropy. This gives the following necessary conditions for nucleation:

$$\left.\frac{\partial \Delta S^{tot}}{\partial X_i}\right|_{\mathbf{X}=\mathbf{X}^{nucl}} = 0 \;\forall i \; . \tag{4.12}$$

There is still the possibility that several solutions for Eq. (4.12) exist. Obviously, then the solution with the largest entropy gives the largest contribution to the rate of nucleation.

Now we want to evaluate the conditions of Eqs. (4.12) for ΔS^{tot} further. Let us define the temperature, pressure and chemical potentials of the entire subsystem in the usual manner:

$$\begin{aligned} T &= \left.\frac{\partial S}{\partial E}\right|_{V,\mathbf{C}} \\ p &= T \left.\frac{\partial S}{\partial V}\right|_{E,\mathbf{C}} \\ (\mu_k) &= -\left(T \left.\frac{\partial S}{\partial C_k}\right|_{E,V,\{C_{l\neq k}\}} \right) \; . \end{aligned} \tag{4.13}$$

Note that E contains bulk and finite-size contributions, thus the Euler equation of thermodynamics, $E = TS - pV + \sum_k C_k \mu_k$, is not valid in general. By realizing that the intensive variables of the heat bath are constant, we then get the following total differential of ΔS^{tot}:

$$d\Delta S^{tot} = \left(\frac{1}{T} - \frac{1}{T^0}\right) dE + \left(\frac{p}{T} - \frac{p^0}{T^0}\right) dV - \sum_k \left(\frac{\mu_k}{T} - \frac{\mu_k^0}{T^0}\right) dC_k \; . \tag{4.14}$$

From the total differential given in Eq. (4.14) we can read off the partial derivatives, which have to be zero because of Eqs. (4.12). This gives the following conditions for nucleation:

$$\begin{aligned} T &= T^0 \\ p &= p^0 \\ \boldsymbol{\mu} &= \boldsymbol{\mu}^0 \; . \end{aligned} \tag{4.15}$$

Nucleation occurs via a state which is in unstable quasi-equilibrium with the initial phase. These conditions fix the fluctuation variables E, V, and $\mathbf{C}$ so that the nucleation rate can be calculated with Eq. (4.10). The conditions only involve intensive variables, but due to finite-size effects, also the size of the critical bubble can be determined.

4.3 Finite-Size Effects

To calculate the nucleation rate, i.e. the probability of a fluctuation corresponding to the conditions of Eqs. (4.15) we first need to specify the finite-size contribution further. Here we use the simplest approach that the energy of the bubble, i.e. the subsystem, can be split into a bulk and a finite-size part:

$$E = E^B + E^{FS} \quad . \tag{4.16}$$

It is not guaranteed that this is always possible and in certain cases this approach will fail. In fact, the nucleation rate depends crucially on the assumed form of the finite-size effects.

4.3.1 Nucleation With Finite-Size Entropy

In case there is a contribution of the finite-size effects to the entropy (i.e. the finite-size energy is temperature dependent), we assume that also the entropy can be split into a bulk and a finite-size part, whereas the bulk entropy depends only on the bulk energy and the finite-size entropy only on the finite-size energy:

$$S(E, V, \mathbf{C}) = S^B(E^B, V, \mathbf{C}) + S^{FS}(E^{FS}, V, \mathbf{C}) \tag{4.17}$$

Because the intensive properties of the heat bath are constant, we can also assume that the finite-size entropy depends additionally on T^0, p^0 and $\boldsymbol{\mu}^0$, so that actually $S^{FS} = S^{FS}(E^{FS}, V, \mathbf{C}, T^0, p^0, \boldsymbol{\mu}^0)$. Because this additional dependence on constants does not lead to any changes, we can suppress the additional arguments which refer to the heat bath.

In addition to the intensive variables of the entire subsystem of the fluctuation, Eqs. (4.13), we introduce the following bulk and finite-size variables:

$$\begin{aligned} T^{B/FS} &= \left.\frac{\partial S^{B/FS}}{\partial E^{B/FS}}\right|_{V,\mathbf{C}} \\ p^{B/FS} &= T^{B/FS}\left.\frac{\partial S^{B/FS}}{\partial V}\right|_{E^{B/FS},\mathbf{C}} \\ (\mu_k^{B/FS}) &= -\left(T^{B/FS}\left.\frac{\partial S^{B/FS}}{\partial C_k}\right|_{E^{B/FS},V,\{C_{l\neq k}\}}\right) . \end{aligned} \tag{4.18}$$

The maximization of the entropy S with respect to the internal variables E^B and E^{FS} leads to:

$$T^B = T^{FS} = T \ , \tag{4.19}$$

which means that the finite-size and bulk part have the same temperature. Contrary, the pressure and chemical potentials have a bulk and finite-size contribution:

$$\begin{aligned} p &= p^B + p^{FS} \\ \boldsymbol{\mu} &= \boldsymbol{\mu}^B + \boldsymbol{\mu}^{FS} \ . \end{aligned} \tag{4.20}$$

In this approach the bulk part is treated in the thermodynamic limit so that all the usual thermodynamic relations can be applied. Starting from Eq. (4.9), thus we can replace S^B in $S = S^B + S^{FS}$ to get:

$$\Delta S^{tot} = \frac{1}{T}\left(E^B + p^B V - \sum_k \mu_k^B C_k\right) + S^{FS} - \frac{1}{T^0}\left(E + p^0 V - \sum_k \mu_k^0 C_k\right) \ . \tag{4.21}$$

With Eq. (4.16) this can be written as:

$$\Delta S^{tot} = E\left(\frac{1}{T} - \frac{1}{T^0}\right) + V\left(\frac{p^B}{T} - \frac{p^0}{T^0}\right) - \sum_k C_k\left(\frac{\mu_k^B}{T} - \frac{\mu_k^0}{T^0}\right) + S^{FS} - \frac{E^{FS}}{T} \ , \tag{4.22}$$

which further simplifies by applying Eqs. (4.20):

$$\begin{aligned} \Delta S^{tot} = \quad & E\left(\frac{1}{T} - \frac{1}{T^0}\right) + V\left(\frac{p}{T} - \frac{p^0}{T^0}\right) - \sum_k C_k\left(\frac{\mu_k}{T} - \frac{\mu_k^0}{T^0}\right) \\ & + \frac{1}{T}(TS^{FS} - E^{FS} - p^{FS}V + \sum_k \mu_k^{FS} C_k) \ . \end{aligned} \tag{4.23}$$

We note that the Euler equation in general does not apply for the finite-size part, otherwise the last line in the equation would be zero.

4.3.2 Nucleation Without Finite-Size Entropy

If there is no direct entropy contribution (i.e. the finite-size effects are temperature-independent) we have to modify our approach slightly because $S^{FS} \equiv 0$. Let us keep the definitions of Eqs. (4.13) for the total subsystem and Eqs. (4.18) for the bulk part. For the finite-size part, one now has use the finite-size energy $E^{FS} = E^{FS}(V, \mathbf{C})$ instead:

$$\begin{aligned} p^{FS} &= -\left.\frac{\partial E^{FS}}{\partial V}\right|_{\mathbf{C}} \\ (\mu_k^{FS}) &= \left(\left.\frac{\partial E^{FS}}{\partial C_k}\right|_{V,\{C_{l\neq k}\}}\right) . \end{aligned} \tag{4.24}$$

We note again that the finite-size energy may also depend additionally on the constant parameters T^0, p^0 and μ_k^0, without any changes arising. With the above definitions one gets:

$$\begin{aligned} T &= T^B \\ p &= p^B + p^{FS} \\ \boldsymbol{\mu} &= \boldsymbol{\mu}^B + \boldsymbol{\mu}^{FS} . \end{aligned} \tag{4.25}$$

By comparing with the previous subsection, we realize that Eqs. (4.21) – (4.23) can also be applied if the finite-size effects do not depend on temperature, by simply setting S^{FS} to zero.

4.3.3 Nucleation Rate

By inserting the conditions for nucleation of Eqs. (4.15) in Eq. (4.23), we obtain the following form of the nucleation rate:

$$P_{nucl} \propto \exp\left(\frac{1}{T}(TS^{FS} - E^{FS} - p^{FS}V + \sum_k \mu_k^{FS} C_k)\right) . \tag{4.26}$$

All variables in this expression are fixed by the nucleation conditions and Eqs. (4.19) and (4.20) in the case if there is a finite-size entropy and Eqs. (4.25) if there is not.

It is also interesting to study the case where finite-size contributions are neglected. Then the conditions for nucleation are the same as for stable phase equilibrium and the volume of the fluctuation remains arbitrary. If these conditions can be fulfilled one gets $\Delta S^{tot} = 0$ which means that the probability for nucleation is equal to the probability that the system remains in the metastable state without any fluctuations. This is a reasonable result, because we can choose an arbitrary small volume $V \longrightarrow 0$ for the nucleation, as the subsystem is treated like in the thermodynamic limit. Obviously, such a vanishing small fluctuation takes place immediately. This shows explicitly that the nucleation rate is exceedingly large if surface effects are neglected.

Let us discuss the conditions for nucleation with finite-size effects a little bit further. Besides temperature and pressure equilibrium (including the finite-size part), they contain complete chemical equilibrium with respect to all the conserved charges. We want to stress that still all charges (and the total volume and the total energy as well) are strictly conserved, see Eqs. (4.4). The total system is treated microcanonically. The fluctuation with conditions corresponding to unstable phase equilibrium including the finite-size contributions, Eqs. (4.15), is only the most likely one which leads to nucleation. These conditions are not in contradiction to the conservation of all charges, because the size of the fluctuation is negligible small compared to the bath. This aspect was sometimes confused in the literature, e.g. in [LB98, LDGS10] only partial chemical equilibrium was assumed to describe the nucleation of a quark phase under the constraint of flavor conservation. Instead of full chemical equilibrium the same up- and down-quark fraction was assumed in the hadronic and in the quark phase. However, as we showed, this is not necessary, because the derived formulation is always based on the strict conservation of all charges during the nucleation.

We can also apply our formalism if some charges are actually not conserved in the initial phase. We will show later in Eq. (5.29) that if the conservation law of the charge l is lifted, this leads to $\mu_l^0 = 0$. Even though the initial value of the total charge $C_l^{tot\ 0} = C_l^{tot\ 0}(\mu_l^0 = 0)$ remains constant during the nucleation, the equilibrium condition $\mu_l^0 = 0$ applies also for the most likely nucleation, because $\mu_l = \mu_l^0$. Of course it is necessary for every fluctuation ΔC_k, that the charge exists already in the heat bath, and not $C_k^{tot\ 0} = 0$. For example if there is no strangeness in the hadronic phase at all, it is not possible that there is a thermal fluctuation in the strange quark density. But any finite $C_k^{tot\ 0} \neq 0$ is enough to produce a fluctuation and our formalism is correct as long the assumption is fulfilled, that the heatbath is not modified by the fluctuation.

It is possible to suppress fluctuations of certain degrees of freedom. One could allow only fluctuations in one of the state variables, or alternatively suppress the fluctuations of

certain particle ratios. The corresponding variable is then fixed by a certain assumption, and its change does not appear in Eq. (4.7) any more. The corresponding condition for maximization also drops out of Eqs. (4.12). The artificial suppression of the fluctuations of some degrees of freedom just give a lower nucleation rate. However, there might be reasons why to suppress fluctuations, e.g. if the charge does not exist at all, as noted before, or to simulate forces which are not included in the thermodynamic description. One such scenario is the assumption of local charge neutrality. To be able to neglect the Coulomb forces, it is necessary that the fluctuation is strictly charge neutral. Let us denote this by $Q^{bath} = 0$, $Q = 0$. Thus the charge chemical potential will not be equal in the subsystem and the heatbath, $\mu_Q^0 \neq \mu_Q$. Instead we could allow the fluctuation to be charged, but still neglect the Coulomb forces in S^{FS}. Then we would obtain $Q^{bath} = 0 \neq Q$, with Q fixed by $\mu_Q^0 = \mu_Q$. If we included the Coulomb energy of the bubble the last two relations would still hold, but the expression for μ_Q would be modified by the Coulomb contribution, as we will show in the last section of this chapter.

4.4 Nucleation with Surface Energy

Now we want to calculate the nucleation rate for the example of the simplest form of the finite-size energy, namely a surface energy which depends only on the surface area. Furthermore, we assume spherical geometry. For the notation of this case we use the index S instead of FS. To achieve a correct description implicitly we consider the locally charge neutral case, so that the Coulomb energy does not have to be taken into account. In this case the index k, which denotes the globally conserved charges, does not include the electric charge Q. Alternatively we could allow for charged fluctuations but completely neglect the Coulomb energy, as discussed before. Then we would get the equality of the charge chemical potentials in addition.

For the surface energy belonging to the surface area S we use $E^S = \sigma S$, with σ denoting a constant surface tension, which may be a function of T^0, p^0 and $\boldsymbol{\mu}^0$. Expressed by the volume we get:

$$E^S(V) = \sigma(36\pi)^{1/3} V^{2/3} \,. \tag{4.27}$$

The only other finite-size contribution is the surface pressure:

$$p^S = -\frac{2}{3}\sigma(36\pi)^{1/3} V^{-1/3} = -\frac{2}{3}\frac{E^S}{V} \,. \tag{4.28}$$

The nucleation rate Eq. (4.26) can be expressed as:

$$P^S_{nucl} \propto \exp\left(-\frac{E^S}{3T}\right) . \tag{4.29}$$

The conditions for the most likely nucleation take on the following explicit form:

$$\begin{aligned} T &= T^0 \\ \boldsymbol{\mu}^B &= \boldsymbol{\mu}^0 \\ p^B - \sigma\tfrac{2}{3}(36\pi)^{1/3}V^{-1/3} &= p^0 . \end{aligned} \tag{4.30}$$

Compared to bulk equilibrium, only the surface pressure appears. The intensive variables of the heat bath are fixed and the EOS gives a relation $p^B = p^B(T, (\mu^B_k))$, which allows to derive the size of the most likely nucleation. Thus all properties of the subsystem can be determined. Finally, we can express the nucleation rate in the following way:

$$P^S_{nucl} \propto \exp\left(-\frac{16\pi}{3}\frac{\sigma^3}{T^0(p^B(T^0,(\mu^0_k)) - p^0)^2}\right) . \tag{4.31}$$

It follows from Eqs. (4.30) that $p^B > p^0$ to get a positive volume V. The case $p^B = p^0$ is also interesting. This situation occurs only at the equilibrium phase transition point denoted by t^{pt} before. In this case we get $V \longrightarrow \infty$ and $P^S_{nucl} \longrightarrow 0$. At the phase transition line (where the system just begins to become metastable) a fluctuation which leads to nucleation has to have infinite size and thus has zero probability. From the opposite point of view, the result $V \longrightarrow \infty$ for bulk phase equilibrium shows explicitly that the normal conditions for full phase equilibrium correspond to two phases which are treated in the thermodynamic limit. In the case of a constant surface tension, after the nucleation has occurred the nuclei of the new phase will grow in size to minimize the thermodynamic potential. Finally when the groundstate is reached, the thermodynamic limit $V \longrightarrow \infty$ applies and the surface energy becomes negligible compared to the bulk energy.

4.5 Nucleation with Surface and Coulomb Energy

Now we want to go beyond the complete neglect of Coulomb forces, or the other extreme of strict local charge neutrality. For the notation of this case we use SC. Now the finite-

size energy consists in addition to the surface energy E^S of the Coulomb energy E^C:

$$E^{SC} = E^S + E^C \ . \tag{4.32}$$

Here we use the simplest case of a uniformly charged sphere, so that

$$E^C = \alpha \frac{3}{5} \frac{Q^2}{R} \tag{4.33}$$

with the fine-structure constant α, the total electric charge number Q and the radius R of the subsystem. Because the fluctuation is small, the Coulomb energy of the heat bath can be neglected. Actually the charge density of the bath is vanishingly small, because the bath is assumed to be infinitely large compared to the fluctuation. Expressed by V and Q We get:

$$E^{SC}(V,Q) = \sigma(36\pi)^{1/3}V^{2/3} + \alpha\frac{3}{5}\left(\frac{4\pi}{3}\right)^{1/3} Q^2 V^{-1/3} \ . \tag{4.34}$$

The following contributions of the finite-size effects arise:

$$\mu_Q^{SC} = \alpha\frac{6}{5}\left(\frac{4\pi}{3}\right)^{1/3} QV^{-1/3} = 2\frac{E^C}{Q} \tag{4.35}$$

$$p^{SC} = -\sigma\frac{2}{3}(36\pi)^{1/3}V^{-1/3} + \alpha\frac{1}{5}\left(\frac{4\pi}{3}\right)^{1/3} Q^2 V^{-4/3} = -\frac{2}{3}\frac{E^S}{V} + \frac{1}{3}\frac{E^C}{V} \ . \tag{4.36}$$

The nucleation rate then simplifies to:

$$P_{nucl}^{SC} \propto \exp\left(\frac{1}{3}\frac{2E^C - E^S}{T}\right) \ . \tag{4.37}$$

The conditions for nucleation read in explicit form:

$$\begin{gathered} T = T^0 \\ \mu_k^B = \mu_k^0 \text{ for } k \neq Q \\ \mu_Q^B + \alpha\tfrac{6}{5}\left(\tfrac{4\pi}{3}\right)^{1/3} QV^{-1/3} = \mu_Q^0 \\ p^B - \sigma\tfrac{2}{3}(36\pi)^{1/3}V^{-1/3} + \alpha\tfrac{1}{5}\left(\tfrac{4\pi}{3}\right)^{1/3} Q^2V^{-4/3} = p^0 \end{gathered} \tag{4.38}$$

The charge chemical potentials are not equal in the two phases, but are shifted by the Coulomb contribution. Similarly, the pressure is shifted by a negative surface and a positive Coulomb contribution. One obtains the following implicit equation which has

to be solved numerically to determine μ_Q^B:

$$p^B(T^0, \mu_Q^B, \{\mu_{k\neq Q}^0\}) - 4\sigma \left(\frac{2\pi}{5} \frac{\alpha\ n_Q}{\mu_Q^0 - \mu_Q^B} \right)^{1/2} + \frac{1}{6}(\mu_Q^0 - \mu_Q^B) n_Q = p^0 \tag{4.39}$$

with the charge density $n_Q = Q/V$ which is also a function of T^0, μ_Q^B and $\mu_{k\neq Q}^0$, $n_Q = n_Q(T^0, \mu_Q^B, \{\mu_{k\neq Q}^0\})$. Then the volume of the fluctuation

$$V = \frac{5}{12} \left(\frac{5}{2\pi} \right)^{1/2} \left(\frac{\mu_Q^0 - \mu_Q^B}{\alpha\ n_Q} \right)^{3/2} \tag{4.40}$$

and all other thermodynamic variables are fixed. In terms of the intensive variables, the nucleation rate becomes:

$$P_{nucl}^{SC} \propto \exp \left(\frac{1}{T_0} \left\{ \frac{5}{36} \left(\frac{5}{2\pi} \frac{(\mu_Q^0 - \mu_Q^B)^5}{\alpha^3 n_Q} \right)^{1/2} - \frac{5}{6}\sigma \frac{\mu_Q^0 - \mu_Q^B}{\alpha\ n_Q} \right\} \right) . \tag{4.41}$$

Here we end with the discussion of nucleation, without calculating any examples. The formalism is derived, and it would be an interesting continuation to study the nucleation quantitatively for specific EOSs. For example one could compare the nucleation rates for different conditions, e.g. local charge neutrality, charged nucleation with Coulomb and without Coulomb or with locally fixed fractions.

Chapter 5

Equilibrium Conditions with Local Constraints

In this chapter, we extend the general formalism of Chap. 3 and derive the more concrete conditions for phase equilibrium for the set of state variables which is relevant for compact stars. The results of this and the following chapter have been partly published in Ref. [HPS09]. We assume that not the single particle numbers of the system but only some particular charges like e.g. baryon number are conserved. It will derived how the particle numbers are fixed by the conserved charges through the equilibrium conditions. In addition to globally conserved charges we analyze the implications of locally conserved charge fractions, like e.g. local electric charge neutrality or locally fixed proton or lepton fractions. Such local constraints have not been considered in Chap. 3. We will show that neither internal degrees of freedom nor locally conserved fractions do not influence the qualitative behavior of the mixed phase. Thus all the results of Chap. 3 apply also for a system with local constraints and/or internal degrees of freedom.

Consider a thermodynamic system with volume V and temperature T composed of two different, spatially separated phases. The numbers of the $\mathcal{N}^I$ different particle species of phase I are denoted by $\mathbf{N}^I = (N_i^I)$, the $\mathcal{N}^{II}$ particles of phase II by $\mathbf{N}^{II} = (N_j^{II})$. To distinguish the two phases we introduce the index $\kappa = I, II$. To avoid a complicated notation in some cases we will also use the index i for the particles of phase II. Furthermore, for a clear denotation it will later be necessary that i and j are not integer numbers. For the entire set of particle numbers we introduce $\mathbf{N} = (\mathbf{N}^I, \mathbf{N}^{II})$. The thermodynamic potential of the system is the Helmholtz free energy $F(T, V, \mathbf{N})$. We chose this canonical formulation, because we will apply it later in the description of phase transitions in compact stars. However, the relations which are found for the chemical potentials of the particles can also be used for other thermodynamic ensembles.

In many cases, there exist some conserved charges, but the single particle numbers are not conserved. Then it will be more convenient to use these conserved charges as the independent degrees of freedom for the description of the state of the system, instead of specifying all the single particle numbers. In this subsection the equilibrium conditions in terms of the chemical potentials of the particles shall be derived. Let us assume there are $\mathcal{C}$ conserved charges C_k, $k = 1, ..., \mathcal{C}$, for which a conservation law of the following form exists:

$$\begin{aligned} C_k(\mathbf{N}^I, \mathbf{N}^{II}) &= C_k^I(\mathbf{N}^I) + C_k^{II}(\mathbf{N}^{II}) = \text{const.} , \\ C_k^\kappa(\mathbf{N}^\kappa) &= \sum_i \alpha_{ik}^\kappa N_i^\kappa \end{aligned} \tag{5.1}$$

with α_{ik}^κ denoting the amount of charge C_k carried by particle i of phase κ. The total conserved charge consists of the charge in phase I, C_k^I, and in phase II, C_k^{II}. To achieve a general description applicable for all kind of local and global constraints we will first assume, that all of the local charges are taken as state variables and are thus fixed locally. Usually instead of using the charges directly, one takes charge fractions as the independent degrees of freedom:

$$Y_t^\kappa(\mathbf{N}^\kappa) = \frac{C_t^\kappa}{C_1^\kappa} = \frac{1}{C_1^\kappa} \sum_i \alpha_{it}^\kappa N_i^\kappa, \tag{5.2}$$

which is the local charge fractions of the conserved charge C_t, $t = 2, ...\mathcal{C}$. Obviously, it would not make sense to define the charge fraction $Y_1^\kappa \equiv 1$ of charge C_1^κ. C_1^κ shall be a positive, non-vanishing quantity so that it is suitable to characterize the size of the phases. In some cases we will also use the vector $\mathbf{Y}^\kappa = (Y_t^\kappa)$ for the notation of the local charge fractions of phase κ. Our state variables are then $(T, V, C_1^I, C_1^{II}, \mathbf{Y}^I, \mathbf{Y}^{II})$.

In the following we want to derive the equilibrium conditions for the internal dependent degrees of freedom N_i^κ if only these state variables are specified $F(T, V, \mathbf{N}) = F(T, V, \mathbf{N}(T, V, C_1^I, C_1^{II}, \mathbf{Y}^I, \mathbf{Y}^{II}))$ and are kept constant. Thus:

$$C_1^\kappa = \text{const.} \tag{5.3}$$

$$Y_t^\kappa = \text{const.} \quad . \tag{5.4}$$

As the temperature is one of the state variables of the two phases it is set equal by construction, so that thermal equilibrium between the two phases is assured. Only the total volume $V = V^I + V^{II}$ is kept constant, but the two subvolumes can vary, leading

to pressure equality as the condition for mechanical equilibrium:

$$p^I = p^{II} \ . \tag{5.5}$$

From the first and second law of thermodynamics we get for the total differential of the free energy F expressed by the particle numbers N_i^κ

$$0 = dF = \sum_{i,\kappa} \frac{\partial F}{\partial N_i^\kappa} dN_i^\kappa \ , \tag{5.6}$$

if the volume and the temperature are kept constant. With

$$\mu_i^\kappa = \frac{\partial F(\mathbf{N})}{\partial N_i^\kappa} \tag{5.7}$$

Eq. (5.6) becomes

$$\sum_{i,\kappa} \mu_i^\kappa dN_i^\kappa = 0 \ . \tag{5.8}$$

The constraints of Eqs. (5.3) and (5.4) can be implemented by the means of Lagrange multipliers $\lambda_1^\kappa, \lambda_t^\kappa$, by adding

$$\lambda_1^\kappa dC_1^\kappa = \lambda_1^\kappa \textstyle\sum_i \alpha_{i1}^\kappa dN_i^\kappa = 0 \quad , \tag{5.9}$$

and

$$\begin{aligned} &\lambda_t^\kappa dY_t^\kappa = \lambda_t^\kappa \tfrac{1}{C_1^\kappa}(dC_t^\kappa - Y_t^\kappa dC_1^\kappa) = 0 \\ \Leftrightarrow\ &\lambda_t^\kappa \tfrac{1}{C_1^\kappa} \left(\textstyle\sum_i \alpha_{it}^\kappa dN_i^\kappa - Y_t^\kappa \sum_i \alpha_{i1}^\kappa dN_i^\kappa\right) = 0 \ , \end{aligned} \tag{5.10}$$

to dF. This leads to:

$$\mu_i^\kappa = \lambda_1^\kappa \alpha_{i1}^\kappa + \sum_t \lambda_t^\kappa \frac{1}{C_1^\kappa} \left(\alpha_{it}^\kappa - Y_t^\kappa \alpha_{i1}^\kappa\right) \ . \tag{5.11}$$

dF can also be expressed as a function of the C_1^κ and Y_t^κ:

$$0 = dF \ = \ \sum_\kappa \frac{\partial F}{\partial C_1^\kappa} dC_1^\kappa + \sum_{\kappa,t} \frac{\partial F}{\partial Y_t^\kappa} dY_t^\kappa \ . \tag{5.12}$$

We introduce the chemical potential of the conserved charges C_1^κ,

$$\mu_1^\kappa = \frac{\partial}{\partial C_1^\kappa} F(C_1^I, C_1^{II}, \mathbf{Y}^I, \mathbf{Y}^{II}) \ , \tag{5.13}$$

and of the conserved fractions Y_t^κ:

$$\mu_{Y_t}^\kappa = \frac{\partial}{\partial Y_t^\kappa} F(C_1^I, C_1^{II}, \mathbf{Y}^I, \mathbf{Y}^{II}) \ . \tag{5.14}$$

Then it is easy to realize, that the Lagrange multipliers are equal to the chemical potentials of the corresponding charges: $\lambda_1^\kappa = \mu_1^\kappa, \lambda_t^\kappa = \mu_{Y_t}^\kappa$, so that:

$$\mu_i^\kappa = \mu_1^\kappa \alpha_{i1}^\kappa + \sum_t \mu_{Y_t}^\kappa \frac{1}{C_1^\kappa} \left(\alpha_{it}^\kappa - Y_t^\kappa \alpha_{i1}^\kappa\right) \ . \tag{5.15}$$

It is interesting to see, that the chemical potentials of the particles depend now directly on the value of the locally fixed charge fractions and the unknown value of C_1^κ. $1/C_1^\kappa$ appears because a change in Y_t^κ implies a change in the corresponding particle numbers of phase κ proportional to C_1^κ. With

$$\begin{aligned} \mu_{Y_t}^\kappa &= C_1^\kappa \frac{\partial}{\partial C_t^\kappa} F(C_1^I, C_1^{II}, \mathbf{Y}^I, \mathbf{Y}^{II}) \\ &= C_1^\kappa \frac{\partial}{\partial C_t^\kappa} F(C_1^I, C_1^{II}, (C_t^I), (C_t^{II})) = C_1^\kappa \mu_t^\kappa \ , \end{aligned} \tag{5.16}$$

one can see that $\mu_{Y_t}^\kappa$ is proportional to C_1^κ and the chemical potential of the charge C_t^κ. In fact the local chemical potentials of the particles can only depend on other local intensive variables, so C_1^κ has to drop out of Eq. (5.15).

By using this result we get the following expression for the equilibrium conditions for the chemical potentials of the particles:

$$\mu_i^\kappa = \mu_1^\kappa \alpha_{i1}^\kappa + \sum_{t=2}^{\mathcal{C}} \mu_t^\kappa \left(\alpha_{it}^\kappa - Y_t^\kappa \alpha_{i1}^\kappa\right) \ . \tag{5.17}$$

The first two of the three terms simply state that the chemical potential of particle (i, κ) is given by the sum over the amount of conserved charges that the particle carries multiplied by the corresponding chemical potentials. The term proportional to Y_t^κ appears only for particles which contribute to C_1^κ. It is due to the change in the charge C_t^κ implied by dC_1^κ if Y_t^κ is kept constant. It would not appear if instead of the fractions the charges were used for the description of the state of the system. This shows the im-

portance in the definition of the chemical potentials of which other quantities are kept constant.

It is important to realize that the local chemical potentials $\mu_1^\kappa, \mu_t^\kappa$ will in general be different in the two phases, leading to different chemical potentials of all particles. Only particles of the same phase which carry the same quantum numbers will have equal chemical potentials. All together there are $2\mathcal{C} + \mathcal{N}^I + \mathcal{N}^{II} + 1$ unknown variables: the chemical potentials $\mu_1^\kappa, \mu_t^\kappa, \mu_i^\kappa$ and one of the two subvolumes V^κ. They can be determined from the $\mathcal{N}^I + \mathcal{N}^{II}$ chemical equilibrium conditions (5.17), pressure equilibrium (5.5) and the $2\mathcal{C}$ conservation laws (5.3) and (5.4) for the fixed state $(C_1^I, C_1^{II}, \mathbf{Y}^I, \mathbf{Y}^{II})$. If all the relations $N_i^\kappa = N_i^\kappa(T, V^\kappa, \mu_i^\kappa)$ are known, the system is determined completely.

Equation (5.17) can also be applied for a single phase κ, by setting $V^{\bar\kappa} = 0$ for the other phase, equivalent to $\mathbf{N}^{\bar\kappa} = 0$, with $\bar\kappa$ denoting the phase different to κ. Then pressure equilibrium is not required any more, and the whole system of equations can be solved and all thermodynamic quantities can be determined, too. If the number of conserved charges $\mathcal{C}$ is equal to the number of particles $\mathcal{N}^\kappa$ in this phase, then the conserved charges directly fix all the $\mathcal{N}^\kappa$ particle numbers N_i^κ. If $\mathcal{C} < \mathcal{N}^\kappa$, $\mathcal{N}^\kappa - \mathcal{C}$ equilibrium conditions between the chemical potentials of the particles will exist.

So far, there are only two equilibrium conditions between two phases: pressure equilibrium (Eq. (5.5)) and temperature equilibrium (by construction). Because all charges are fixed locally, there is only the volume and the total entropy as globally conserved extensive variables. The conjugate intensive variables of these two variables have to be equal in the two phases, in agreement with the results of Chap. 3. Next we want to understand the consequences if not all of the charges are fixed locally. This means we are lifting some of the local constraints. First of all we assume that C_1 is conserved only globally and no longer constrained locally. Furthermore, also $\mathcal{G} - 1$ of the other charges shall be conserved only globally. We will denote the fractions which are no longer constrained locally but only globally by Y_g, $g = 2, ..., \mathcal{G}$. With C_1 this gives $\mathcal{G}$ lobally conserved charges. For the fractions Y_l^κ which are still fixed locally, we introduce the index $l = \mathcal{G}, ..., \mathcal{C}$. We then have $\mathcal{C} = \mathcal{G} + \mathcal{L}$. Because the volume is also one of the state variables we now have $\mathcal{E} = \mathcal{G} + 1$ extensive state variables and only $\mathcal{I} = 1$ intensive state variables, the temperature.

To be more specific, we only consider local constraints which require equal local charge fractions in the two phases:

$$Y_l^I = Y_l^{II} \quad . \tag{5.18}$$

If we introduce the global charge fraction Y_l,

$$Y_l = C_l/C_1 = \text{const.} \,, \tag{5.19}$$

we find:

$$Y_l^\kappa = Y_l = \text{const.} \,. \tag{5.20}$$

Eq. (5.20) is the reason why we can evaluate the constraint of Eq. (5.18) independently for the two phases. The constraint for global conservation of C_1 can be written as:

$$\lambda_1 dC_1 = \lambda_1 \sum_{i,\kappa} \alpha_{i1}^\kappa dN_i^\kappa = 0 \,. \tag{5.21}$$

All the global charge fractions $Y_g = C_g/C_1$ are also conserved:

$$\begin{aligned} &\lambda_g \tfrac{1}{C_1}(dC_g - Y_g dC_1) = 0 \\ \Leftrightarrow\ &\lambda_g \tfrac{1}{C_1}\left(\textstyle\sum_{i,\kappa} \alpha_{ig}^\kappa dN_i^\kappa - Y_g \sum_{i,\kappa} \alpha_{i1}^\kappa dN_i^\kappa\right) = 0 \,. \end{aligned} \tag{5.22}$$

We already implemented the new Lagrange multipliers λ_1, λ_g. By comparing Eqs. (5.9) and (5.10) with (5.21) and (5.22), one finds that the local conservation laws lead to the same constraints (5.21) and (5.22) which are added to dF if we set:

$$\lambda_1^I = \lambda_1^{II} = \lambda_1 \quad , \tag{5.23}$$

$$\frac{\lambda_g^I}{C_1^I} = \frac{\lambda_g^{II}}{C_1^{II}} = \frac{\lambda_g}{C_1} \quad , \tag{5.24}$$

which is equivalent to:

$$\mu_1^I = \mu_1^{II} =: \mu_1 \quad , \tag{5.25}$$

$$\begin{aligned} &\tfrac{\mu_{Y_g}^I}{C_1^I} = \tfrac{\mu_{Y_g}^{II}}{C_1^{II}} \\ \Leftrightarrow\ &\mu_g^I = \mu_g^{II} =: \mu_g \quad , \end{aligned} \tag{5.26}$$

where we used Eq. (5.16) in the last line. Equations (5.25) and (5.26) are the new additional equilibrium conditions for the globally conserved charges in terms of the local chemical potentials. This is in complete agreement with Chap. 3 where we showed that every globally conserved extensive variable induces a corresponding equilibrium condition for the conjugate intensive variable. To express the equality of the chemical potentials we introduced the variables μ_1, μ_g, which are the global chemical potentials of the corresponding charges. If a local conservation law is lifted, an additional condition for

chemical equilibrium between the two phases appears, and the whole set of equilibrium equations can still be solved. Equations (5.25) and (5.26) is the expected result that local chemical potentials become equal in the two phases when the corresponding local constraint is lifted. Then the two local fractions can adjust to minimize the free energy. After equilibrium is reached, the two phases can be separated from each other without any changes arising.

We want to comment on Eq. (5.17), which was derived for the situation in which all charge fractions were fixed locally. In the general case which we discussed here the local fractions of the globally conserved charges will be different in the two phases and are not part of the state variables any more. But also in this case we can use Eq. (5.17), because the new equilibirum conditions still determine all thermodynamic variables, including the local fractions of globally conserved charges. It is only the dependency of the variables in Eq. (5.17) which has changed.

If one of the globally conserved charges, denoted by $C_{g'}$ in the following, is actually not conserved any more this means that

$$\frac{\partial F}{\partial C_{g'}} = 0 \tag{5.27}$$

to minimize the free energy, leading to

$$\mu^I_{g'} = \mu^{II}_{g'} = 0 \ . \tag{5.28}$$

A non-conserved charge gives two local constraints for the chemical potentials. The two Eqs. (5.28) replace the equilibrium condition (5.25). With this additional information the whole system can be determined, even though the value of $C_{g'}$ is not fixed any more. This is in agreement with our previous conclusion that all thermodynamic quantities can be determined, independently of the number of conserved charges $\mathcal{C}$ and the number of particles $\mathcal{N}^I$ and $\mathcal{N}^{II}$. We note that with the new information of Eqs. (5.28) the chemical potentials of the remaining conserved charges can possibly be written in a different simplified form. This procedure for non-conserved charges can also be applied for a single phase κ, in which only one chemical potential $\mu^\kappa_{g'}$ exists, leading to:

$$\mu^\kappa_{g'} = 0 \ . \tag{5.29}$$

All other conclusions are also analog to the mixed phase.

These are very practical results. It allows to construct an EOS for the most general case that all possible quantum numbers are conserved, and then apply this EOS to all

cases in which some of the quantum numbers are actually not conserved any more, by simply setting the corresponding chemical potential to zero. We will use this procedure later.

From Eq. (5.17) it follows immediately, that two particles i and j of the same phase have equal chemical potentials if they carry the same quantum numbers:

$$\mu_i^\kappa = \mu_j^\kappa \text{ if } \alpha_{ik}^\kappa = \alpha_{jk}^\kappa \; \forall \; k = 1, ...\mathcal{C} \; . \tag{5.30}$$

If particles i and j of two different phases carry the same quantum numbers, e.g. if some of the particles in the two different phases are identical, this is no longer true in general. The local chemical potentials of locally fixed fractions will in general be different in the two phases. Consequently, if a particle carries global and local charges, its chemical potential will also be different in the two phases. Only if they do not contribute to the locally conserved charges it follows from Eqs. (5.17), (5.25) and (5.26) that the chemical potentials of such particles are equal:

$$\mu_i^I = \mu_j^{II} \; . \tag{5.31}$$

This means that, since such particles can be exchanged freely between the two phases, in equilibrium always the same amount of energy is needed when the number of particles N_i^I or N_j^{II} is varied in one of the two phases. If no local constraints are applied, the chemical potentials of all identical particles become equal, which is a well-known form of the Gibbs conditions for phase equilibrium.

For fixed temperature T, pressure p and particle numbers $\mathbf{N}$, the correct thermodynamic potential is the Gibbs potential G, which is also called the Gibbs free enthalpy. With Eqs. (5.17), (5.25) and (5.26) we get the following relations inside the mixed phase:

$$\begin{aligned} G\left(T, p, \mathbf{N}(C_1, (Y_g), (Y_l))\right) &= \sum_{i,\kappa} \mu_i^\kappa N_i^\kappa \\ &= \mu_1 C_1 = \mu_1^I C_1^I + \mu_1^{II} C_1^{II} \; , \end{aligned} \tag{5.32}$$

independently of how many charges are constrained locally. For a single phase κ with $C_1^\kappa = C_1$ and $V^\kappa = V$, Eq. (5.17) leads to:

$$G\left(T, p, \mathbf{N}^\kappa(C_1, (Y_g), (Y_l))\right) = \sum_i \mu_i^\kappa N_i^\kappa = \mu_1^\kappa C_1 \; . \tag{5.33}$$

In this case in principle the index κ can also be suppressed because only one single phase exists. These two relations can also be used in other thermodynamic potentials or

in the fundamental relation of thermodynamics. These results are interesting, because they show explicitly that we derived a formulation in which the Gibbs free enthalpy is independent of the local constraints which are actually applied.

Chapter 6

Description of Matter in Compact Stars

Before we turn to the discussion of phase transitions in compact stars we want to introduce the state variables which are used for the different stages of the evolution of a compact star. Furthermore, we want to give the explicit equilibrium conditions for single phases consisting of quarks or nucleons, if only some charges but not all of the particle numbers are conserved. There can be different conserved quantum numbers (denoted by C_k in the previous chapters) in a small closed subsystem of compact star matter. In all cases, the baryon number N_B has to be conserved. Because compact stars are macroscopic objects, electric charge neutrality has to be fulfilled, which we express by the total electric charge number $N_C = 0$ (denoted by Q in Chap. 4). Furthermore, there are two additional conserved charges possible, the lepton number N_L if neutrinos are trapped and the total isospin if weak equilibrium is not established. For nucleon matter, conservation of isospin and baryon number leads to the conservation of the proton number N_p, which we will use instead of isospin. Obviously, for up and down quark matter the conservation of isospin is equivalent to flavor conservation. For a consistent and easy notation we also use N_p to express isospin conservation in the quark phase. N_p in the quark phase could be seen as the electric charge of the particles with baryon number, i.e. of the protons in the nucleon phase, and of the quarks in the quark phase. In total there are $\mathcal{G} = 4$ possible conserved charges.

We consider that the system is either in a hadronic or in a quark phase. As an example we assume that the hadronic phase consists of N_ν neutrinos, N_e electrons, N_p protons and N_n neutrons (net numbers, including antiparticles). The two-flavor quark phase shall be composed of N_e electrons, N_ν neutrinos, N_u up and N_d down quarks. Furthermore, at the end of the section we will discuss strange quark matter, too, in

conserved charge	hadron phase	quark phase
baryon number	$N_B = N_n + N_p$	$N_B = 1/3(N_u + N_d)$
clectric charge	$N_C = N_p - N_e$	$N_C = 1/3(2N_u - N_d) - N_e$
baryonic electric charge	N_p	$N_p = 1/3(2N_u - N_d)$
lepton number	$N_L = N_e + N_\nu$	$N_L = N_e + N_\nu$

Table 6.1: The possible conserved quantum numbers expressed by the particle numbers of a nucleon and a two-flavor quark phase.

which N_s strange quarks are also part of the system. We note that the inclusion of other particle species (e.g. muons, hyperons, kaons, or hadron resonances) is straightforward and does not lead to conceptual differences. The particle numbers of the two considered phases relate to the conserved quantum numbers as shown in Table 6.1.

Usually instead of fixing (N_B, N_C, N_L, N_p), an intensive formulation in terms of the proton and lepton fractions $Y_p = n_p/n_B$ and $Y_L = (n_e + n_\nu)/n_B$, the baryon number density n_B and charge density $n_C = n_p - n_e = 0$ are used, like e.g. in Refs. [LD91a, STOS98a, STOS98b]. In the thermodynamic limit, the size of the system becomes irrelevant, so that we can assume that the volume V is also known. Obviously then it is completely equivalent to fix (n_B, n_C, Y_p, Y_L, V) instead of (N_B, N_C, N_p, N_L, V). We note that $n_C = 0$ is equivalent to zero electric charge per baryon fraction $Y_C = 0$. Thus we can apply the results of Chap. 5 also for the case of local charge neutrality.

In Table 6.2 we show the equilibrium conditions for the most general case, that all four of the charges are conserved in a way that the fractions are kept constant. The chemical potentials of the conserved charges N_B, N_C, N_p and N_L are expressed in terms of the chemical potentials of the particles. The opposite relation which expresses the chemical potentials of the particles in terms of the chemical potentials of the conserved charges is given by Eq. (5.17). We included the index κ denoting different phases, because we will use the shown results for phase transitions later. For two phases in equilibrium, Table 6.2 shows the case that the baryon number and all fractions are conserved locally. As long as only one single homogeneous phase exists, local conservation laws are identical to global ones. In this chapter we only describe single homogenous phases, thus the index κ can be suppressed.

The unusual form of the chemical potentials of the conserved charges/fractions, e.g. μ_{N_B}, can be understood in a simple way. μ_{N_B} gives the change of the free energy with the change of the charge N_B for constant proton and lepton fraction and electric charge neutrality. The combination of chemical potentials of the particles which is found

	chemical potentials	
conserved charge	hadron phase	quark phase
N_B^κ	$\mu_{N_B}^\kappa = (1-Y_p)\mu_n^\kappa + Y_p\mu_p^\kappa$ $+Y_p\mu_e^\kappa + (Y_L - Y_p)\mu_\nu^\kappa$	$\mu_{N_B}^\kappa = (2-Y_p)\mu_d^\kappa + (1+Y_p)\mu_u^\kappa$ $+Y_p\mu_e^\kappa + (Y_L - Y_p)\mu_\nu^\kappa$
Y_C^κ	$\mu_{N_C}^\kappa = \mu_\nu^\kappa - \mu_e^\kappa$	$\mu_{N_C}^\kappa = \mu_\nu^\kappa - \mu_e^\kappa$
Y_p^κ	$\mu_{N_p}^\kappa = \mu_p^\kappa - \mu_n^\kappa - \mu_\nu^\kappa + \mu_e^\kappa$	$\mu_{N_p}^\kappa = \mu_u^\kappa - \mu_d^\kappa - \mu_\nu^\kappa + \mu_e^\kappa$
Y_L^κ	$\mu_{N_L}^\kappa = \mu_\nu^\kappa$	$\mu_{N_L}^\kappa = \mu_\nu^\kappa$

Table 6.2: The local chemical potentials of the baryon number N_B, electric charge N_C, proton number (or baryonic electric charge number) N_p and lepton number N_L in terms of the chemical potentials of the particles in one phase if the baryon number and all fractions are kept constant. The second column is for a hadronic phase composed of neutrons, protons, electrons and neutrinos and the third column for a phase of up quarks, down quarks, electrons and neutrinos. The results also apply for strange quark matter, with $\mu_d = \mu_s$. For a single phase the index κ can be suppressed. For two phases in equilibrium the table shows the results if the baryon number and all fractions are conserved locally. For global baryon number conservation $\mu_{N_B}^I = \mu_{N_B}^{II}$ follows. If some of the fractions are conserved only globally and are no longer restricted by local constraints, the corresponding chemical potentials become equal, too: $\mu_g^I = \mu_g^{II}$.

for μ_{N_B} corresponds to the change of the particle numbers induced by the change of N_B under the chosen constraints. The form of a chemical potential depends on which other quantities are kept constant. For example the baryon chemical potential μ_{N_B} would be equal to μ_n (for nuclear matter) if instead of the fractions the charges themselves were used as the other state variables which are kept constant. However, the final equilibrium conditions are not (and cannot be) affected by the choice of the state variables. Thus we can use the description presented here, which is most convenient for our purpose as it can be applied for single phases as well as for all possible combinations of locally conserved fractions inside mixed phases later.

Table 6.2 corresponds to the special situation of completely trapped neutrinos, but with too short dynamical timescales to change the proton number by weak reactions. Next we will discuss the different possibilities in which some of the charges are actually not conserved any more and will discuss their physical realization. As was shown before, for every charge becoming not conserved an additional equilibrium condition appears, see Eq. (5.29). With this new information the chemical potentials of the remaining conserved charges can possibly be written in a different simplified form.

For non-conserved lepton number from Eq. (5.29) and Table 6.2 $\mu_\nu = 0$ follows. In this case neutrinos are completely untrapped/free streaming. We discuss now the

meaning and some interesting consequences of the result $\mu_\nu = 0$ for matter with neutrinos but without lepton number conservation further. If a particle i carries no conserved charges ($\alpha_{ik} = 0\ \forall k$) with Eq. (5.17) one finds immediately that its chemical potential is zero. If neutrinos can be described as an ideal gas in equilibrium it follows that $N_\nu = 0$, which means that the number of neutrinos equals the number of antineutrinos. Only if $T = 0$ both contributions vanish. Non-conserved Y_L would correspond to the situation when the neutrino mean free path was much larger than the size of the compact star so that neutrinos could leave the neutron star freely. Thus the energy of the system was not conserved, but could be carried away by neutrinos as long as they are abundant. As a logical consequence the neutron star would cool immediately to $T = 0$ if weak reaction rates were fast enough (infinitely large emissivities) to allow to describe the neutrinos as an ideal gas as part of the thermodynamic description. In reality it takes some 10^5 years until the neutron star has cooled to a core temperature of ~ 10 keV and the photon cooling era is reached. The neutrinos are far away from equilibrium, their emissivities have to be calculated, and the description of the cooling process requires detailed numerical simulations [PGW06].

6.1 Supernova Matter

Matter in supernova occurs under very different conditions. In the central regions the densities and temperatures are so high, that neutrinos are completely trapped, so that the lepton number is conserved. Usually, then the neutrinos are also in weak equilibrium. However, in the outer regions above the neutrino spheres, the neutrinos become free streaming. Then in general weak reactions are not in equilibrium any more because the timescales for the weak reactions can become too slow compared to the dynamical timescales of e.g. fast ejecta. Thus we consider the most general case, that weak-equilibrium is not established and the proton fraction is conserved.

Usually for fixed Y_p the electrons and neutrinos are not included in the construction of the EOS but are treated separately. Y_p and n_B directly set the electron density which are usually described as an uniform ideal Fermi-Dirac gas. The neutrino dynamics play a crucial role in supernovae and protoneutron stars. To describe the evolution of such systems it is necessary to handle the neutrinos with a detailed dynamical transport scheme in which their emission, scattering and absorption is calculated. Like the electrons, the neutrinos can also be separated from the non-leptonic EOS: n_B and Y_p directly fix the particle number densities of the hadrons, respectively of the quarks. The non-neutrino part of the EOS does not change, if neutrinos are not included as part of the thermody-

namic system, e.g. because they are out of equilibrium. At the same time, the neutrino contribution is also independent of the non-neutrino EOS: If the lepton fraction is conserved, i.e. if they are completely trapped, the neutrino density is directly specified by $n_\nu = (Y_L - Y_p)n_B$. Without lepton number conservation, $\mu_\nu = 0$ also directly sets the neutrino contribution. An EOS with fixed Y_p can also be used if weak equilibrium is actually reached, by simply determining the proper Y_p for which $\mu_{N_p} = 0$. Thus we conclude that an EOS with fixed proton fraction Y_p can be used for all possible conditions under which the neutrinos appear. In Chap. 7 we will show that the neutrinos also do not affect the equilibrium conditions in mixed phases as long as the lepton fraction is conserved globally. Table 6.2 describes the general case of supernova matter, if we ignore the neutrino part and the lepton number conservation.

Even though most of the matter is characterized by a constant entropy per baryon, usually the temperature is used as a state variable. This is mainly due to numerical reasons, because the calculation of an EOS table in terms of the entropy per baryon is very demanding. Thus we assume in the following that the state variables of a typical supernova EOS including the electrons are $(T, n_B, Y_p, n_C = 0)$. If the electrons are described as an ideal gas they can be separated from the EOS, and (T, n_B, Y_p) are sufficient to fix the nucleon or quark part. In the thermodynamic limit we can assume any arbitrary volume V. Thus fixing $(T, n_B, Y_p, n_C = 0)$ is equivalent to fixing $(T, N_B, N_p, N_C = 0, V)$, giving $\mathcal{G} = 3$, $\mathcal{I} = 1$ and $\mathcal{E} = 4$. Without electrons we have (T, N_B, N_p, V) as state variables, giving $\mathcal{G} = 2$, $\mathcal{I} = 1$ and $\mathcal{E} = 3$.

6.2 Protoneutron Stars

A protoneutron star is the newly formed compact object in the center of a supernova. It is characterized by completely trapped neutrinos. Because the central object behaves rather static there is enough time for the weak reactions to reach equilibrium. This stage lasts for the first 10 seconds of the evolution of the star. One assumes that lepton number is conserved but the proton number not. Then from Table 6.2 with $\mu_{N_p} = 0$ the well known weak equilibrium conditions

$$\mu_p - \mu_n - \mu_\nu + \mu_e = 0 \tag{6.1}$$

for nuclear matter and

$$\mu_u - \mu_d - \mu_\nu + \mu_e = 0 \tag{6.2}$$

for quark matter are found.

Because weak equilibrium is assumed, the neutrinos have to be included in the EOS, thus Y_L is used as a state variable instead of Y_p. Representative static configurations of protoneutron stars are characterized by a fixed entropy per baryon, because matter is opaque for neutrinos and photons, see e.g. [PCL95, PBP+97]. In stable hydrostatic configurations, like in a protoneutron star, the pressure has to be strictly monotonic. Thus one of the natural state variables for matter in a compact star is the pressure p. Thus usually instead of the baryon density the pressure is used, because then the EOS can be used directly in the calculation of the structure of the protoneutron star. This is a nice example where one of the control parameters is an intensive quantity which is not the temperature T. The commonly used state variables for protoneutron stars are $(S/N_B, p, Y_L, n_C = 0)$. This is equivalent to fixing $(S, p, N_B, N_L, N_C = 0)$, giving $\mathcal{G} = 3$, $\mathcal{I} = 1$ and $\mathcal{E} = 4$. At an intermediate stage the lepton number is not conserved any more. If the neutron star is still isentropic, the state variables are $(S/N_B, p, n_C = 0)$ which is equivalent to $(S, p, N_B, N_C = 0)$. In this case only $\mathcal{G} = 2$ conserved charges and $\mathcal{E} = 3$ extensive variables would remain.

6.3 Cold Neutron Stars

At a later stage in the evolution, the neutrinos become completely untrapped and the lepton number is not conserved any more. After roughly 10^5 years the star can be described by zero temperature, because the typical densities and chemical potentials are very large. Thus the temperature is used as one of the state variables, set to the value $T = 0$.

The star has reached full weak equilibrium and only baryon number and electric charge remain as conserved charges. Without lepton number conservation $\mu_\nu = 0$, and the neutrinos drop out in the β-equilibrium conditions

$$\mu_e + \mu_p - \mu_n = 0 \tag{6.3}$$

for nucleons and

$$\mu_u - \mu_d - \mu_e = 0 \tag{6.4}$$

for quarks. For both sets of particles $\mu_{N_C} = -\mu_e$. The baryon chemical potential can also be expressed in a simpler way: $\mu_{N_B} = \mu_n$ for nucleons and $\mu_{N_B} = 2\mu_d + \mu_u$ for

quarks. For cold neutron stars it is more convenient to use the pressure instead of the density, thus the appropriate state variables are $(T, p, n_C = 0)$. This time the baryon number N_B fixes the size of the system, but its value is arbitrary in the thermodynamic limit. Thus fixing $(T, p, n_C = 0)$ is equivalent to fixing $(T, p, N_C = 0, N_B)$, giving $\mathcal{G} = 2$, $\mathcal{I} = 2$ and $\mathcal{E} = 2$..

6.4 Strange Matter

In strange quark matter, in addition to the up and down quarks, N_s strange quarks are part of the thermodynamic system. In principle, strange quarks carry the additional quantum number of strangeness. There exist two possibilities to handle this additional quantum number: First, one can use the total strangeness of the system indeed as an additional conserved charge, increasing $\mathcal{G}$ by one. If strangeness is not taken to be identical to zero, it is necessary to calculate the EOS for all possible strangeness fractions $Y_S = N_S/N_B$. The strangeness chemical potential μ_{N_S} would appear in addition to the chemical potentials of the other conserved charges. This approach was e.g. used in Ref. [GKS87] to describe strangeness separation in heavy ion collisions. Here we will not discuss the scenario of conserved strangeness any further but will leave it for future discussion.

Second, there exists a simpler and more commonly used description of strange matter, by assuming equilibrium with respect to strangeness changing reactions. This means that strangeness is not conserved, so that $\mu_{N_S} = 0$, and $\mathcal{G}$ is not changed by the additional strange quark degree of freedom. In this case the conserved quantum numbers of the strange quark are identical to the ones of the down quark, so that $\mu_d = \mu_s$ because of Eq. (5.30). Then all results presented for two-flavor quark matter in this article can also be applied to strange quark matter, with the baryon number given by $N_B = 1/3(N_u + N_d + N_s)$ and the electric charge number by $N_C = 1/3(2N_u - N_d - N_s) - N_e$.

The only subtlety arises when Y_p is conserved. First of all, it is necessary to reconsider the meaning of Y_p for strange matter. One possibility would be to interpret Y_p as the net electric charge carried by baryons, $N_p = 1/3(2N_u - N_d - N_s)$, so that $N_p = N_e$ still gives charge neutrality. In combination with baryon number conservation, the conservation of Y_p leads then to a fixed number of up quarks, but only the sum of down and strange quarks is fixed, i.e. reactions which change down into strange quarks are still in equilibrium. This means one implicitly assumes that these reactions happen on a much shorter timescale than reactions which change the number of up quarks (semileptonic reactions).

The argumentation followed in Ref. [SHP+09], and which we will also use in Sec. 9.1, is a different one. The EOS is calculated for fixed Y_p. But within the application in a core-collapse supernova, quark matter appears only at such large densities and temperatures, that neutrinos are completely trapped and weak equilibrium is established. Hence Y_p is actually not conserved but only Y_L remains approximately constant. Within the numerical simulation for a given Y_L the proper Y_p is determined for which $\mu_{N_p} = 0$. If the EOS is used in this way, it is not necessary to assume different timescales of the different reactions.

The whole discussion of this subsection applies also for hyperonic matter, i.e. hadronic matter with strangeness, and the conclusions are analog.

Chapter 7

Phase Transitions in Compact Stars

The general results which have been found in the previous chapters shall now be applied to the liquid-gas phase transition of nuclear matter and the hadron-quark phase transition for typical astrophysical environments like in supernovae, protoneutron or neutron stars, as presented in Chap. 6. Other possible first order phase transitions in compact stars and their implications were mentioned in the introduction. Here we restrict the discussion on the thermodynamic aspects of the two examples.

The description of first order phase transitions in cold, deleptonized neutron stars is rather well understood and extensively discussed in the literature. Because cold neutron stars are well described by $T = 0$ and the pressure has to change continuously inside a compact star, there are two intensive state variables, $\mathcal{I} = 2$, compare also with Sec. 6.3. With charge neutrality and baryon number conservation there are two conserved charges, $\mathcal{G} = 2$, which are also used as extensive state variables, $\mathcal{E} = 2$. In our previous formulation the relevant path for the phase transformation corresponds to the pressure profile of the neutron star, i.e. only the pressure is varied and all the other state variables are kept constant. Because $2 = \mathcal{E} = \mathcal{G} = 2$ for two phases in coexistence, the phase transformation is continuous and an extended mixed phase has to be calculated. In the context of neutron stars this case of a multi-component system is usually called the Gibbs construction. In other areas of physics it is also called a non-congruent phase transition. However, as we will discuss in more detail later, it is also a reasonable assumption that the two phases are actually locally charge neutral. Then the electric charge is not a globally conserved charge any more, so that one gets $\mathcal{G} = 1$ and $\mathcal{E} = 1$ With this assumption the phase transformation becomes discontinuous. There is no extended mixed phase which has to be calculated, and the transition pressure can easily be determined from well-known equililbrium conditions of the pressure and the baryon chemical potential. The pressure, temperature and chemical potential change continuously across the transition, but there will be discontinuities in the energy, number and

entropy densities. The one-component case is usually called the Maxwell construction. In other areas of physics one also calls it a congruent phase transition. It was first realized in Ref. [Gle92], that global charge neutrality leads to the appearance of an extended mixed phase and a continuous phase transformation. References [Mue97] and [BMG10] also deal with these aspects.

If we look at the other important scenario of protoneutron stars (Sec. 6.2), the situation is more complicated because additional conserved charges exist and some of the intensive state variables are replaced by extensive state variables, further increasing $\mathcal{E}$. In the protoneutron star stage with trapped neutrinos and roughly constant entropy, we have $\mathcal{G} = 3$, and $\mathcal{E} = 4$ for global charge neutrality and $\mathcal{G} = 2$, $\mathcal{E} = 3$ for local. In both cases $\mathcal{E} > 2$ so that there will always be a mixed phase of e.g. nucleons and nuclei or at larger densities of hadrons and quarks. For the supernovae EOS including electrons but not neutrinos, as introduced in Sec. 6.1, one also has $\mathcal{G} = 3$, $\mathcal{E} = 4$ for global charge neutraliy and $\mathcal{G} = 2$, $\mathcal{E} = 3$ for local. In both systems all phase tranformations are continuous, even if one assumes local charge neutrality.

Until now, the conditions for phase equilibrium and the role of local constraints for matter in supernovae and protoneutron stars were not discussed in detail in the literature. Without local constraints, one can use the results of [Gle92] for the Gibbs construction. However, in some cases the Gibbs conditions for phase equilibrium cannot be fulfilled at all. Furthermore, sometimes the simple Maxwell construction is wanted, i.e. one wants a discontinuous phase transformation. This could be motivated by physical reasons or just by the sake of simplicity, as e.g. in Ref. [BP08, IRR$^+$08], because then there exists no extended mixed phase. One only has to determine the transition point and the demanding calculation of an extended mixed phase is not necessary.

Obviously, the Maxwell construction for cold deleptonized neutron stars cannot be used for protoneutron stars. The requirement of conservation of lepton and/or proton number in addition to baryon number leads to significant differences in the equilibrium conditions, which was not taken into account in several previous publications, like e.g. in [YT01, NBBS06, YK09]. It is only possible to obtain a discontinuous phase transformation if in addition to local charge neutrality some other charges are fixed locally to lower $\mathcal{E}$ to unity. Additional local constraints result in particular new conditions for phase equilibrium. Because of the additional conserved charges involved, there is a large variety of different descriptions of the phase transition, all of them representing different physical scenarios. In this chapter, all relevant possibilities of local and global conservation of the different conserved charges will be analyzed and the corresponding equilibrium conditions will be presented. Several new kinds of mixed phases are presented, with new, interesting properties.

7.1 Local Constraints

If a mixed phase exists, it is crucial whether a charge is conserved globally or locally. In general the more local constraints are applied, the less extended the mixed phase will be. Depending on the remaining number of globally conserved charges, the phase transformation can become discontinuous and the mixed phase may even disappears completely. Contrary, if all local constraints are lifted, one can expect that the mixed phase will be most extended. Furthermore the more globally conserved charges exist, the smoother the phase transformation will be. We expect that the discontinuity in the second derivatives will become less, if more globally conserved charges exist.

In the following we will assume that each of the conserved charges is either conserved globally, or its fraction is conserved locally with equal values in the two phases, as before. Before we start to discuss all relevant combinations of locally and globally conserved charges, we will analyze the physical meaning of the different local constraints.

7.1.1 Local charge neutrality

There are two possibilities for the implementation of electric charge neutrality. Either one assumes local charge neutrality, which means that each phase is charge neutral itself. Or one assumes global charge neutrality, then the two phases can be charged, so that Coulomb forces will in principle be present. We note that the assumption of global charge neutrality is in contradiction to the thermodynamic limit in a strict sense, as the Coulomb energy would diverge for an infinite, electrically charged system [DHN$^+$07].

If one wants to go beyond the bulk limit, finite size effects in form of surface and Coulomb energies need to be included, as was done in [HPS93, VYT03, MCST07, MCST08b, MCST08a] for a mixed phase of (hyperonic) hadronic matter and quark matter. The optimal size and shape of a structure at fixed density is determined by the competition between the surface and the Coulomb energy, ϵ_S, respectively ϵ_C. The minimization of the total energy gives the well known relation: $\epsilon_S = 2\epsilon_C$. Under certain conditions, spherical symmetry does not represent the ground state any more, but exotic structures, the so called "pasta phases" appear [HPS93, GP95]. It was pointed out in Refs. [VYT03, EMCT06] that also the effect of charge screening and the rearrangement of charged particles in presence of the Coulomb interactions must be taken into account for a realistic description of the mixed phase. Then in the most simple approach there are three parameters which determine the size of the structures: the Debye screening lengths of the two phase, given by the charge susceptibilities, and the surface tension σ of

the interface between the two phases. Presently, the value of σ is not known. The possibility that it has a large value, of say $\sigma \sim 100$ MeV/fm^2, cannot be excluded [ARRW01]. In this section we do not want to include any finite size effects in the mixed phases, but rather want to show how different physical situations can be properly described in the thermodynamic limit by the choice of appropriate equilibrium conditions.

Already in [VYT03] it was pointed out, that depending on the surface tension and the Debye-screening length, local charge neutrality might be the better approximation for the description of the phase transition. If a large surface tension drives the system to sizes much larger than the Debye screening length, only a negligible small charged surface layer in the order of the Debye screening length remains and the bulk of the matter becomes locally charge neutral. Most calculations for the phase transition to quark matter indicate that this is indeed the case. Then also global properties, like the mass-radius relation of cold neutron stars, resemble more the results of the Maxwell construction. The mixed phase window shrinks considerably and it approaches the constant-pressure Maxwell construction [VYT03, EMCT06]. This effect in turn would imply the absence of the mixed phase in cold and deleptonized hybrid stars. Already in [HPS93] it was estimated, that for $\sigma > 70$ MeV/fm^2 the Maxwellian case is recovered, recently validated by [MCST08b]. In [MTV$^+$06] a first order phase transition to a kaon condensed phase was studied and similar results are found. In contrast to these results, in most of the publications about the hadron-quark phase transition global charge neutrality is used and finite size effects are completely neglected, as e.g. in Ref. [PSPL01].

Global charge neutrality is the more reasonable assumption only if the surface tension is so small that the typical structures are smaller than the Debye screening length. This applies to the liquid-gas phase transition of nuclear matter, as the Debye screening length is large and only low densities are involved [MTV$^+$05]. However, in a strict sense for structures smaller than the Debye screening length only the charge screening can be neglected, but the finite size effects still can be important. There will always be a surface and Coulomb energy which can give an important contribution to the EOS. Contrary, local charge neutrality represents always a consistent assumption. Then the Coulomb energy is exactly zero. Thus the structures can grow arbitrary in size to lower the surface energy, which then is also negligible small compared to the bulk contribution.

Even though it is not appropriate (because of the large Debye length), we include the assumption of local charge neutrality for the nuclear phase transition in the following discussion, because it is instructive and the corresponding equilibrium conditions can easily be devolved to other kind of phase transitions of nuclear matter.

If one requires that both of the two phases have to be locally charge neutral, two different local electric charge chemical potentials appear in Eq. (5.17) leading to different chemical potentials of all electrically charged particles (electrons, quarks and protons) in the two phases. If one would do the full calculation including finite-size (surface and Coulomb) effects and without the constraint of local electric charge neutrality, the total chemical potential of charged particles would be shifted by the local electric potential, e.g. $\tilde{\mu}_p^I = \mu_p^I + eV^I$ leading to full chemical equilibrium, $\tilde{\mu}_p^I = \tilde{\mu}_p^{II}$, see [VYT03]. In Section 4.5 we found the same result, that the electric charge chemical potential including the Coulomb contribution is equal in the two phases. In this chapter we are discussing infinite matter without Coulomb forces, so that the electric potential cannot be determined and the artificial inequality of the chemical potentials of charged particles remains.

7.1.2 Locally fixed Y_p, Y_L or n_B

In general, there is no physical reason why the proton fraction, the lepton fraction or the baryon number density should be conserved locally or should be equal in the two phases, as there is no long range force between the two phases which is associated with these charges. This would imply that the readjustment of the local proton fraction, lepton fraction and/or baryon density does not take place. Such a situation would occur only if the system can not lower its potential by readjusting the local charges. This is the case for isospin symmetric matter for changes with respect to the proton fraction in the liquid-gas phase transition without Coulomb energies and in some cases also for the quark-hadron phase transition. Such a substance is called an azeotrope. Besides this special case, chemical equilibrium with respect to a locally conserved charge is not established between the two phases. Thus, local constraints may be used to simulate a non-equilibrium situation with respect to certain reactions.

A non-vanishing locally fixed density (e.g. $n_B^I = n_B^{II} = n_B$) influences the condition for mechanical equilibrium so that pressure equilibrium is not obtained from the first and second law of thermodynamics any more. For these constraints a change of the subvolumes would imply a change of the local baryon numbers, too. Instead of pressure equilibrium only a combination of the local pressures and the local chemical potentials are equal in the two phases. Consequently, the pressure would change discontinuously at the phase transition. Thus, we will not use constraints of non-vanishing locally fixed densities.

The special assumptions of locally fixed Y_p or Y_L might be wanted because they allow to achieve a Maxwell construction of the mixed phase at the cost of only partial

chemical equilibrium. Because of the additional conserved charges besides N_B local charge neutrality alone is not sufficient for that (as in the case of cold neutron stars) and at least one other of the conserved charges needs to be fixed locally. This is another motivation why to investigate locally fixed Y_p or Y_L and we will focus on this aspect when discussing different scenarios in the following subsections.

7.2 Properties of Phase Transformations in Compact Stars

Depending on the number of globally conserved charges the properties of a phase transformation are qualitatively different, as showed in Chap. 3. Here we derive parts of these general results again, but in a completely different way which is adapted for the case of compact stars. We only discuss the three relevant phase transformations the supernova EOS, cold neutron stars and protoneutron stars. Furthermore we will show that locally fixed charge fractions do not influence the qualitative behavior of the phase transformation.

7.2.1 Isothermal Compression of a Canonical System

To discuss the properties of a phase transformation we have to specify the state variables (also called control parameters) which are changed externally in a continuous way. As in Chap. 5, in this subsection we consider again the general case of a canonical system in which $\mathcal{L} \leq \mathcal{C} - 1$ of the fractions are fixed locally in the form: $Y_l^I = Y_l^{II} = Y_l$. They are denoted by $\mathbf{Y} = (Y_l)$. For the globally conserved charges $\mathbf{C} = (C_g)$ we will continue to use the index g instead. The number of globally conserved charges is then $\mathcal{G} = \mathcal{C} - \mathcal{L}$. The state variables are $(T, V, \mathbf{C}, \mathbf{Y})$, which is equivalent to $(T, V, (C_g), (Y_l))$ and $(T, V, C_1, (Y_g), (Y_l))$. The Helmholtz free energy is the appropriate potential: $F = F(T, V, \mathbf{C}, \mathbf{Y})$. These state variable correspond to the supernova EOS (Sec. 6.1).

Besides the state variables we have to define our path Γ through the space of state variables. We consider an isothermal compression, in which only the volume is changed and all other state variables are kept constant. This is typical for an equation of state in tabular form which is used in numerical simulations of protoneutron stars and supernovae, as e.g. in Refs. [LD91a, STOS98a, STOS98b]. We note that the chosen path belongs to the numerical procedure to calculate such an EOS table, and not to a physical process a priori.

Already from an intuitive point of view one can expect that we can apply all the results of Chap. 3 without the need to worry about the local constraints. We anticipate that an extended mixed phase of the two SHPs will always form, because the number of extensive state variables $\mathcal{E} = 1 + \mathcal{G}$ is always larger or equal than $\mathcal{K} = 2$, the number of phases in equilibrium (as long as $\mathcal{G} \geq 1$, and only two phases are involved in the phase transition). Thus the phase transformation will be continuous. In the case $\mathcal{G} = 1$, we have the special case $\mathcal{E} = 2 = \mathcal{K}$ and all intensive variables are independent of the extensive state variables, as was shown in Sec. 3.3, see Table 3.1. Because we are only varying the volume V, for $\mathcal{G} = 1$ the intensive variables will remain constant across the phase transformation. This allows a very simple construction of the mixed phase: Once the intensive variables are fixed by the intensive state variable T and the coexistence conditions, the extensive state variables V and C_1 directly set all other dependent thermodynamic variables.

Next we will show all this explicitly in a much more explicit and applicable than in Chap. 3 and with the consideration of the local constraints. To do so we analyze the condition for pressure equilibrium further. The pressure in each phase can only depend on the local chemical potentials of the particles in this phase:

$$p^I(T, (\mu_i^I)) = p^{II}(T, (\mu_j^{II})) \; . \tag{7.1}$$

In the discussion of Eq. (5.17) we argued that also for a single phase the knowledge of the conserved charges, the temperature and the volume is sufficient to determine all thermodynamic quantities. Obviously, the chemical potentials of the particles cannot depend on the size of the phase, so that they have to be determinable by the local densities $c_g^\kappa = C_g^\kappa / V^\kappa$ and the local fractions Y_l^κ alone:

$$p^\kappa(T, (\mu_i^\kappa)) = p^\kappa(T, (c_g^\kappa), (Y_l^\kappa)) \; . \tag{7.2}$$

Next, we can use (μ_g^κ) to replace the unknown local parts (c_g^κ) of the densities c_g which are conserved only globally by their local chemical potentials:

$$p^\kappa = p^\kappa(T, (\mu_g^\kappa), (Y_l^\kappa)) \; . \tag{7.3}$$

According to Eqs. (5.25) and (5.26) the chemical potentials which appear in Eq. (7.3) have to be equal in the two phases, and the locally fixed fractions are equal, too (by construction). Thus:

$$p^I(T, (\mu_g), (Y_l)) = p^{II}(T, (\mu_g), (Y_l)) \; . \tag{7.4}$$

This formulation, in which the chemical potentials of the globally conserved charges are treated as known state variables, is most convenient to discuss the properties of the phase transformation. Of course, the chemical potentials in this equation are actually fixed by the values of the density c_g, the fractions Y_l and the chosen local constraints.

First we will analyze the case in which no other globally conserved charges besides C_1 exist, $\mathcal{G} = 1$. Eq. (7.4) then leads to a relation

$$\mu_1 = \mu_1^{coex}(T, \mathbf{Y}) \; , \tag{7.5}$$

with $\mathbf{Y} = (Y_l)$ denoting the locally fixed charge fractions. The relation above also fixes the coexistence pressure:

$$p = p^{coex}(T, \mathbf{Y}) \; . \tag{7.6}$$

This means that for fixed T and $\mathbf{Y}$ there is only one value of the pressure p^{coex} and the chemical potential μ_1^{coex}, where the two phases can coexist. All other local intensive variables are also fixed by the local constraints and the equilibrium conditions and remain constant in the mixed phase, too. This is in complete agreement with the results of Chap. 3 for mixed phases with $\mathcal{E} = \mathcal{K}$ (remember that the volume and C_1 are the only two extensive state variables).

We continue with some practical comments regarding the construction of a supernova EOS table. A simple way to determine the phase transition pressure is to see where the $p^\kappa(T, \mu_1, \mathbf{Y})$-curves of the two phases intersect. The transition from phase I to phase II occurs, when the pressure is equal in the two phases. The mixed phase will extend over a certain range in the density c_1, with the onset given by $c_1^I(T, \mu_1^{coex}, \mathbf{Y})$ and the end by $c_1^{II}(T, \mu_1^{coex}, \mathbf{Y})$. Inside the mixed phase, the intensive variables are independent of c_1 and c_1 is only used to specify the volume fraction $0 < \chi = V^{II}/(V^I + V^{II}) < 1$ of the two phases:

$$c_1 = (1 - \chi) c_1^I(T, \mu_1^{coex}, \mathbf{Y}) + \chi c_1^{II}(T, \mu_1^{coex}, \mathbf{Y}) \; . \tag{7.7}$$

All extensive variables change linearly with the volume fraction in the same way. E.g. the energy density is given by:

$$\epsilon = (1 - \chi) \epsilon^I(T, \mu_1^{coex}, \mathbf{Y}) + \chi \epsilon^{II}(T, \mu_1^{coex}, \mathbf{Y}) \; . \tag{7.8}$$

Therefore the calculation of the mixed phase becomes trivial. After the coexistence pressure is found it is given by a linear interpolation in the volume fraction between

the onset and endpoint of the mixed phase. This case corresponds to the well known Maxwell construction, because the system has only one consered charge.

For $\mathcal{G} \geq 2$ globally conserved charges, giving $\mathcal{E} \geq 3$ the dependent intensive variables depend also on the extensive state variables, see Table 3.1. Eq. (7.4) is not sufficient to determine all chemical potentials μ_g. This equilibrium condition only allows to fix one of the chemical potentials, e.g. $\mu_1 = \mu_1(T, \mathbf{Y}, \{\mu_{g\neq 1}\})$ and $\mathcal{G} - 1$ chemical potentials remain unknown. But besides the equilibrium conditions, also the total volume and the globally conserved charges have to have the correct value:

$$\begin{aligned} V &= V^I + V^{II} \\ C_g &= C_g^I(V^I, T, (\mu_g), \mathbf{Y}) + C_g^{II}(V^{II}, T, (\mu_g), \mathbf{Y}) \quad . \end{aligned} \tag{7.9}$$

These $\mathcal{G} + 1$ Eqs. involve only two further unknowns V^I and V^{II} so that the whole system of Eqs. (7.4) and (7.9) can be solved for given (arbitrary) volume V, and all thermodynamic variables can be determined. Consequently in this case all quantities (including the pressure) will depend on the values of the densities c_g and $c_g = C_g/V$. A change in the density c_g will also imply a change in the pressure. Thus for $\mathcal{G} \geq 2$ there will be an extended range in pressure in which the two phases can coexist. The simple Maxwell construction cannot be applied, as the system does not behave linearly any more. Instead it is necessary to calculate the mixed phase at every point $(T, V, \mathbf{C}, \mathbf{Y})$ explicitly. Also for $\mathcal{G} \geq 2$ all our general predictions have been confirmed.

In both cases ($\mathcal{G} = 1$ or $\mathcal{G} \geq 2$) we have a continuous phase transformation for the chosen state variables. An extended mixed phase between the two phases forms. At the onset of the mixed phase the volume of the newly appearing phase is zero. Similarly, at the end of the mixed phase only the second phase remains. Thus the mixed phase becomes identical to the neighboring single phases when approaching the onset or end of the mixed phase. Inside the mixed phase the volume fraction changes continuously from 0 to 1, and consequently all global thermodynamic variables up to first derivatives of the thermodynamic potential will change continuously across the whole phase transformation. The second derivatives will in general be discontinuous at the onset and endpoint of the mixed phase, as they involve the derivative of the volume fraction. The thermodynamic potential is the Helmholtz free energy, which also changes continuously and which has the following form inside the mixed phase:

$$\begin{aligned} F &= -pV + \sum_{i,\kappa} N_i^\kappa \mu_i^\kappa \\ &= -pV + \mu_1 C_1 \ , \end{aligned} \tag{7.10}$$

where we used Eq. (5.32). For $\mathcal{G} = 1$ in which the pressure and the chemical potentials are constant, the free energy changes linearly with the volume V.

7.2.2 Compression of an Isothermal-Isobaric Ensemble

Next we want to use the different set of state variables $(T, p, \mathbf{C}, \mathbf{Y})$, in which the volume is replaced by the pressure and we want to analyze the properties of this different phase transformation. Now the Gibbs free enthalpy $G = G(T, p, \mathbf{C}, \mathbf{Y})$, already specified by Eq. (5.32), is the appropriate thermodynamic potential. $\mathcal{G}$, the number of globally conserved charges, is equal to the total number of extensive state variables, $\mathcal{E} = \mathcal{G}$ and thus decreased by one compared to the previous subsection. These state variables are especially important because they can directly be used for the description of isothermal neutron stars, see Sec. 6.3. Furthermore, they illustrate the behavior of matter which is described by a canonical EOS as in the last subsection, if the EOS is applied in a hydrodynamic simulation.

Under the influence of gravity, the pressure in a compact star has to change continuously and has to be strictly monotonic, as long as no shocks are present. In the following we only consider a change of the pressure p and keep all the other state variables constant, which defines the path of the phase transformation through the space of state variables. In the previous example we varied the extensive variable V along the path, but now we vary an intensive variable, which leads to qualitative differences in the case $\mathcal{E} = \mathcal{G} = 2$: The intensive variables are independent of the extensive state variables, which allowed to use a simple linear interpolation for the construction of the mixed phase in the previous example. Now, one of the intensive state variables is varied across the phase transformation, so that all intensive variables will change, too. Thus a linear interpolation can never be used directly for an EOS in which the pressure is varied. We remind the reader that for $\mathcal{E} > 2$ this was anyhow not possible. For $\mathcal{E} < 2$ no extended mixed phase exists at all because the phase transformation is then discontinuous. In the following we will derive and discuss these results in a more explicit way than in Chap. 3, and with the consideration of local constraints.

If $\mathcal{G} = 1$ the mixed phase collapses to one single point at the coexistence pressure p^{coex} introduced above. There is only a point of coexistence, but no extended mixed phase. No mixed phase has to be calculated, only the transition point has to be determined. In the previous formulation we showed that μ_1 is constant across the mixed phase and continuous at the endpoints, thus one gets that the potentials of the two phases are equal at the transition point, $G = G^I = G^{II}$. The equality of $\mu_1^I = \mu_1^{II}$ leads to the

equality of the Gibbs free enthalpy. This equality can also be seen as the reason why the volume fraction of the two phases remains arbitrary at the coexistence point and cannot be determined from the equilibrium conditions. Thus all extensive quantities but those of the externally fixed state variables remain unspecified at the coexistence point.

Because of mechanical, thermal and chemical equilibrium the thermodynamic potential changes continuously across the transition, even though no extended mixed phase exists. For smaller or larger pressures than the transition pressure only the phase with the lower Gibbs free enthalpy will be present. Despite this, the phase transformation is not continuous, as e.g. the volume behaves discontinuously due to the disappearance of the mixed phase:

$$\lim_{p<\to p^{coex}} \left.\frac{\partial G^I}{\partial p}\right|_{T,\mathbf{C},\mathbf{Y}} = V^I \neq V^{II} \lim_{p>\to p^{coex}} \left.\frac{\partial G^{II}}{\partial p}\right|_{T,\mathbf{C},\mathbf{Y}} . \tag{7.11}$$

Therefore the charge densities, defined by C_k/V will change discontinuously, too. Also the entropy jumps in an analogous way at the phase transition, if $T \neq 0$. The internal energy, given by $E = G - pV + TS$ will also behave discontinuously in general. These discontinuities appear in the first derivatives of the thermodynamic potential. The discussed scenario is the familiar case of the Maxwell phase transition of a one-dimensional system (a simple body), e.g. known from the liquid-gas phase transition of water. All this is in agreement to the general properties of phase transformations with $\mathcal{K} > \mathcal{E}$.

For $\mathcal{G} \geq 2$ the system is multi-dimensional (a complex body). There will be an extended range in pressure in which the two phases can coexist and an extended mixed phase forms. As noted before, the simple Maxwell construction cannot be applied. The mixed phase does not behave linearly any more and thus it has to be calculated explicitly for every single pressure. Now the equilibrium conditions and the knowledge of the state variables become sufficient to specify the volume fractions and all other thermodynamic variables of the two phases. This case is usually called the Gibbs construction in the context of cold deleptonized neutron stars with global charge neutrality. The presence of a mixed phases with $\chi = 0$ at the onset and $\chi = 1$ at the endpoint assures that all thermodynamic variables (up to first derivatives) change continuously across the phase transformation, as argued above.

One can conclude that locally conserved charge fractions do not influence the qualitative behavior of a phase transformation. It is only the number of globally conserved charges which determines whether it is continuous or discontinuous. Independently of any locally conserved charge fractions, for $\mathcal{G} = 1$ the system is one-dimensional and behaves like a simple body. By replacing globally conserved charges by adequate local

conservation laws, this allows to reduce the number $\mathcal{G}$ of globally conserved charges. Later we will use this procedure for isothermal phase transformations to arrive at a Maxwell construction, even if in principle multiple conserved charges exist. One can expect that the extension of the mixed phase decreases with the number of local constraints applied. When C_1 remains as the only globally conserved charge, the mixed phase will disappear completely inside a compact star. Furthermore the discontinuity of the second derivatives will increase with the number of local constraints. For $\mathcal{G} = 1$ even the first derivatives become discontinuous then.

7.2.3 Compression of an Isentropic-Isobaric Ensemble

The situation becomes different, if we consider a phase transformation in which the pressure is changed, but the entropy per baryon is kept constant instead of the temperature. This is a common description for protoneutron stars, see Sec. 6.2. Even for $\mathcal{G} = 1$ the Maxwell construction cannot be applied, because $\mathcal{E} \geq 2$. In this case there will always be an extended mixed phase. To keep the entropy constant, necessarily the temperature has to change across the transition with equal temperatures in the two phases at each point of the mixed phase. The change in temperature will lead to a change in all other intensive variables, too. If mechanical and thermal equilibrium between the two phases is required, the mixed phase does not vanish, even if only one globally conserved charge exists. Some other local constraints are needed to achieve a linear interpolation in the mixed phase (e.g. locally fixed entropy) which will influence the conditions for phase equilibrium in a non-trivial way.

7.3 Possible Mixed Phases

In Tables 7.1 and 7.2 all the relevant combinations of local and global conservation laws of the conserved charges for the construction of a mixed phase in supernovae, protoneutron stars and cold neutron stars are listed. We assume that the densities and fractions are either conserved globally, or locally in a form $Y_p^I = Y_p^{II} = Y_p$, $Y_L^I = Y_L^{II} = Y_L$, $n_C^I = n_C^{II} = n_C = 0$, $n_B^I = n_B^{II} = n_B$. The final equilibrium conditions are expressed in terms of the chemical potentials of the particles in the two phases, in Table 7.1 for the liquid-gas phase transition and in Table 7.2 for the hadron-quark phase transition.

	conserved densities/fractions			
case	globally	locally	equilibrium conditions	isothermal mixed phase
0		$n_B, (Y_p), (Y_L), n_C$	-	direct
Ia	n_B	Y_p, Y_L, n_C	$(1-Y_p)\mu_n^I + Y_p(\mu_p^I + \mu_e^I) + (Y_L - Y_p)\mu_\nu^I = (1-Y_p)\mu_n^{II} + Y_p(\mu_p^{II} + \mu_e^{II}) + (Y_L - Y_p)\mu_\nu^{II}$	Maxwell
Ib	n_B	Y_L, n_C	$\mu_n^I + Y_L\mu_\nu^I = \mu_n^{II} + Y_L\mu_\nu^{II}$	Maxwell
Ic	n_B	Y_p, n_C	$(1-Y_p)\mu_n^I + Y_p(\mu_p^I + \mu_e^I) = (1-Y_p)\mu_n^{II} + Y_p(\mu_p^{II} + \mu_e^{II})$	Maxwell
Id	n_B	n_C	$\mu_n^I = \mu_n^{II}$	Maxwell
IIa	n_B, Y_L	Y_p, n_C	$(1-Y_p)\mu_n^I + Y_p(\mu_p^I + \mu_e^I) = (1-Y_p)\mu_n^{II} + Y_p(\mu_p^{II} + \mu_e^{II})$, $\mu_\nu^I = \mu_\nu^{II}$	Maxwell/Gibbs
IIb	n_B, Y_L	n_C	$\mu_n^I = \mu_n^{II}, \quad \mu_\nu^I = \mu_\nu^{II}$	Gibbs
IIIa	n_B, Y_p	Y_L, n_C	$\mu_n^I + Y_L\mu_\nu^I = \mu_n^{II} + Y_L\mu_\nu^{II}$, $\mu_p^I - \mu_n^I - \mu_\nu^I + \mu_e^I = \mu_p^{II} - \mu_n^{II} - \mu_\nu^{II} + \mu_e^{II}$	Gibbs
IIIb	n_B, Y_p	n_C	$\mu_n^I = \mu_n^{II}, \quad \mu_p^I + \mu_e^I = \mu_p^{II} + \mu_e^{II}$	Gibbs
IV	n_B, Y_L, Y_p	n_C	$\mu_n^I = \mu_n^{II}, \quad \mu_\nu^I = \mu_\nu^{II}, \quad \mu_p^I + \mu_e^I = \mu_p^{II} + \mu_e^{II}$	Gibbs
V	n_B, Y_L, Y_p, n_C		$\mu_n^I = \mu_n^{II}, \ \mu_\nu^I = \mu_\nu^{II}, \ \mu_p^I = \mu_p^{II}, \ \mu_e^I = \mu_e^{II}$	Gibbs

Table 7.1: Equilibrium conditions for the liquid-gas phase transition of nuclear matter for fixed baryon number density n_B and charge density n_C. The lepton fraction Y_L and proton fraction Y_p are conserved in addition in some cases. These charge densities/fractions are fixed locally (with equal values in the two phases) or globally. If Y_p is not conserved weak equilibrium (Eq. (6.1)) is established in both phases. If Y_L is not conserved $\mu_\nu^I = \mu_\nu^{II} = 0$ is obtained, leading to the same equilibrium conditions as if neutrinos were not included in the thermodynamic system. The last column denotes whether the Maxwell or the Gibbs construction has to be used for the construction of an isothermal mixed phase.

	conserved densities/fractions			
case	globally	locally	equilibrium conditions	isothermal mixed phase
0		$n_B, (Y_p), (Y_L), n_C$	-	direct
Ia	n_B	Y_p, Y_L, n_C	$(1-Y_p)\mu_n + Y_p(\mu_p + \mu_e^H) + (Y_L - Y_p)\mu_\nu^H =$ $(2-Y_p)\mu_d + (1+Y_p)\mu_u + Y_p\mu_e^Q + (Y_L - Y_p)\mu_\nu^Q$	Maxwell
Ib	n_B	Y_L, n_C	$\mu_n + Y_L\mu_\nu^H = 2\mu_d + \mu_u + Y_L\mu_\nu^Q$	Maxwell
Ic	n_B	Y_p, n_C	$(1-Y_p)\mu_n + Y_p(\mu_p + \mu_e^H) = (2-Y_p)\mu_d + (1+Y_p)\mu_u + Y_p\mu_e^Q$	Maxwell
Id	n_B	n_C	$\mu_n = 2\mu_d + \mu_u$	Maxwell
IIa	n_B, Y_L	Y_p, n_C	$(1-Y_p)\mu_n + Y_p(\mu_p + \mu_e^H) = (2-Y_p)\mu_d + (1+Y_p)\mu_u + Y_p\mu_e^Q,$ $\mu_\nu^H = \mu_\nu^Q$	Maxwell/Gibbs
IIb	n_B, Y_L	n_C	$\mu_n = 2\mu_d + \mu_u, \quad \mu_\nu^H = \mu_\nu^Q$	Gibbs
IIIa	n_B, Y_p	Y_L, n_C	$\mu_n + Y_L\mu_\nu^H = 2\mu_d + \mu_u + Y_L\mu_\nu^Q,$ $\mu_p - \mu_n - \mu_\nu^H + \mu_e^H = \mu_u - \mu_d - \mu_\nu^Q + \mu_e^Q$	Gibbs
IIIb	n_B, Y_p	n_C	$\mu_n = 2\mu_d + \mu_u, \ \mu_p + \mu_e^H = 2\mu_u + \mu_d + \mu_e^Q$	Gibbs
IV	n_B, Y_L, Y_p	n_C	$\mu_n = 2\mu_d + \mu_u, \quad \mu_\nu^H = \mu_\nu^Q, \quad \mu_p + \mu_e^H = 2\mu_u + \mu_d + \mu_e^Q$	Gibbs
V	n_B, Y_L, Y_p, n_C		$\mu_n = 2\mu_d + \mu_u, \quad \mu_\nu^H = \mu_\nu^Q, \quad \mu_p = 2\mu_u + \mu_d, \quad \mu_e^H = \mu_e^Q$	Gibbs

Table 7.2: As Table 7.1, but now for the hadron-quark phase transition. $\mu_d = \mu_s$ is valid if strangeness is in equilibrium. If Y_p is not conserved weak equilibrium (Eqs. (6.1) and (6.2)) is established in both phases.

7.3.1 Case I

In case Ia, besides local charge neutrality the proton and lepton fractions are fixed locally and the system has only one globally conserved charge, the baryon number. The only internal degree of freedom of the two phases is the local baryon density. This case is relevant for supernova matter with trapped neutrinos and suppressed weak reactions. However, the local constraints imply different neutrino densities in the two phases. Thus this case is rather academic and we only show it for completeness. For this case Table 6.1 expresses the local chemical potentials belonging to the conserved charges N_B, N_C, N_p and N_L in terms of the chemical potentials of the particles in the phase.

There is only one global chemical potential with the corresponding equilibrium condition:

$$\mu_{N_B} = \mu^I_{N_B} = \mu^{II}_{N_B} \ . \tag{7.12}$$

This condition, which is shown explicitly in Tables 7.1 and 7.2, expresses that only combinations of particles can be exchanged which do not change the local proton and lepton fractions and are electrically charge neutral to maintain local charge neutrality. Thus in the liquid gas phase transition only a combination of $1-Y_p$ neutrons, Y_p electrons and protons and Y_L-Y_p neutrinos can be exchanged freely between the two phases. In the hadron-quark phase transition only $(1+Y_p)$ up and $(2-Y_p)$ down quarks, Y_p electrons and $Y_L - Y_p$ neutrinos can be exchanged. As there is only one globally conserved charge N_B, the pressure is constant across the phase transformation and the Maxwell construction can be used. The chemical potentials of all particles are different in the two phases, as all particles contribute to the locally conserved fractions. We note that this case was already discussed in Ref. [LB98]. Equivalent equilibrium conditions were found and the same conclusions about the disappearance of the mixed phase in a compact star were drawn.

In the following we will use the results of case Ia in Table 6.1 to derive the equilibrium conditions for all other cases. When a fraction is not conserved locally but only globally, the two local chemical potentials specify the new equilibrium conditions. In Eq. (5.26) it was deduced that by conserving Y_g instead of Y_g^κ, the two local chemical potentials μ_k^κ become equal. If one of the charges is actually not conserved any more, this has to be seen as a global criterion. To minimize the free energy with respect to this charge, in Eq. (5.28) it was derived that a non-conserved fraction leads to two new local constraints for the chemical potentials, $\mu^I_{g'} = \mu^{II}_{g'} = 0$, which replace the two locally fixed fractions used before.

In case Ib Y_p is no longer conserved, but neutrinos are trapped, as e.g. in protoneutron stars. By setting $\mu^{\kappa}_{N_p} = 0$ the weak equilibrium conditions (6.1) respectively (6.2) are obtained which now have to be fulfilled in both phases. Case Ib leads to different neutrino densities in the two phases, as case Ia. However, this case is the only possibility to achieve a Maxwell construction if neutrinos are trapped and in weak equilibrium. In Ic the conservation of Y_L is lifted, leading to $\mu^I_\nu = \mu^{II}_\nu = 0$. The chemical equilibrium conditions are the same if neutrinos are taken out of the thermodynamic description. Thus Ic is relevant for the non-neutrino EOS of supernova matter and we will also use this description of the mixed phase later. If both fractions are not conserved any more as in case Id, the beta-equilibrium conditions (6.3) respectively (6.4) are obtained. The implications of the non-conservation of the lepton and/or proton fraction are independent of the other local or global conservation laws. Thus we do not need to discuss them in the following cases again.

In cases Ia to Id the different conserved charges allow to rewrite the equilibrium condition $\mu^I_{N_B} = \mu^{II}_{N_B}$ in the simplified forms presented in Tables 7.1 and 7.2. Case Id describes a cold, deleptonized neutron star. Only global baryon number conservation and local charge neutrality are considered. The well-known result of the equality of the neutron chemical potentials is found for the Maxwell construction of the liquid-gas phase transition. In all other Maxwell constructions the equality of the baryon chemical potential $\mu^{\kappa}_{N_B}$ takes a different form and involves additional particles besides the neutrons. Because of the inequality of $\mu^{\kappa}_{N_C}$ in the two phases the chemical potentials of the electrically charged particles always remain different in the two phases in all cases Ia to Id.

7.3.2 Case II

In case II lepton number and baryon number are conserved globally. The second equilibrium condition $\mu^I_{N_L} = \mu^{II}_{N_L}$ from the global conservation of lepton number leads to the equality of the neutrino chemical potentials. Neutrinos are the only particles which can be exchanged between the two phases, if the baryon number, the electric charge and the proton fraction were kept constant in both phases.

Case IIa assumes locally fixed Y_p and local charge neutrality in addition. With fixed Y_p it gives a suitable description of e.g. supernova matter which is not in weak-equilibrium. The same equilibrium condition as in case Ic in which Y_L is not conserved is obtained for the non-neutrino part of the EOS. Thus case IIa gives the same description of the non-neutrino EOS as case Ic. If one does not include the neutrinos in the thermodynamic description at all, the same condition as in Ic are found. Once more this shows

explicitly that the non-neutrino EOS is independent of the neutrino contribution. As discussed before, the neutrinos can be calculated separately as long as Y_p is conserved and Y_L is not fixed locally. From this point of view, the non-neutrino EOSs of cases with fixed Y_p and globally conserved Y_L are equivalent to fixed Y_p and non-conserved Y_L.

For the non-neutrino EOS the number of globally conserved charges is $\mathcal{G} = 1$, and the mixed phase without neutrinos can be calculated with the Maxwell construction. The mixed phase would disappear under the influence of gravity in a hydrostatic configuration. But the inclusion of neutrinos leads to an interesting effect on the mixed phase: The neutrino contribution is simply given by $n_\nu(T, \mu_\nu) = (Y_L - Y_p)n_B$. Thus for increasing baryon density also the neutrino density has to increase. Therefore the neutrino pressure is not constant across the phase transition, which is in agreement with our general result for $\mathcal{G} = 2$. If the pressure is used as the continuously varying variable and is changed strictly monotonic (e.g. in a compact star), a mixed phase appears only because of the presence of neutrinos.

It is very interesting to see, that all cases with local charge neutrality in which Y_p or Y_L are conserved globally will lead to an extended mixed phase in a compact star. After the star has cooled to $T = 0$ and has become completely deleptonized, Y_p and Y_L are no longer conserved, and case Id will be reached. Consequently the mixed phase will disappear during the evolution of the star.

If we compare case IIa to case Ia, we see that the same fractions and charges are conserved. In both cases only the Maxwell construction is needed, but in case IIa the additional assumption of a locally fixed lepton fraction is not used so that the neutrino densities become equal in the two phases. This might be more realistic as the neutrino mean free path is much larger than of the other particles. Thus case IIa should be preferred instead of case Ia, if one is only interested in the Maxwell construction.

We conclude that case IIa (or equivalently Ic for the non-neutrino EOS) is the most convenient scenario which leads for fixed Y_p to the desired Maxwell construction of the system without neutrinos. All other cases with conserved proton fraction Y_p involve more than one globally conserved charge for the non-neutrino EOS and the explicit evaluation of phase equilibrium is necessary. Because of the additional global conservation of the proton fraction, only with local charge neutrality a simple Maxwell construction is not possible for matter in supernovae or protoneutron stars.

In case IIb Y_p is no longer conserved, so that the separation of the neutrino EOS is not possible. The Gibbs construction has to be done with the inclusion of neutrinos. Case IIb is physically meaningful, as local charge neutrality is the only local conservation law, applied for a system in weak equilibrium with completely trapped neutrinos, as e.g. in

a protoneutron star. In Section 9.2 we will study this scenario in more detail, by using a concrete EOS to calculate the evolution of the compact star and the properties of the mixed phase.

7.3.3 Case III

The proton fraction is conserved globally in case III. The general equilibrium condition $\mu^I_{N_p} = \mu^{II}_{N_p}$ shown in the second line of case IIIa in Tables 7.1 and 7.2 expresses that only a proton and an electron can be moved from one phase into the other, if at the same time a neutron and a neutrino are converted backwards. All other combinations of particles would change the local baryon number, the electric charge or the lepton fraction.

In case IIIa the neutrino EOS cannot be separated from the rest of the EOS, as the lepton fraction is conserved locally so that the Gibbs construction has to be performed. If one is only interested to achieve the Maxwellian case (without further reasoning why locally fixed Y_L instead of locally fixed Y_p is assumed), the easier case IIa can be applied instead. Furthermore, there is no reason why only the lepton concentration should be equal in the two phases, but all other fractions and the baryon density can vary, leading to different neutrino densities in the two phases. Thus case IIIa is rather academic and included here only for completeness.

In case IIIb the proton fraction is fixed, i.e. weak reactions are suppressed. Y_L is not conserved which gives $\mu^I_\nu = \mu^{II}_\nu = 0$. The condition for chemical equilibrium is the same if Neutrinos are not taken to be part of the thermodynamic system. The only local conservation law in case IIIb is local charge neutrality. Therefore this case gives the proper physical description of a phase transition of supernova matter with sufficiently large surface tension between the two phases. The equilibrium conditions for the local baryon chemical potentials simplify compared to Ic, in which the proton fraction was fixed locally.

7.3.4 Case IV

The non-neutrino constraints of case IV are equivalent to those of case IIIb. Case IV gives the correct description of locally charge neutral supernova matter with completely trapped neutrinos as part of the thermodynamic description, without any weak reactions taking place.

7.3.5 Case V

In case V local electric charge neutrality is not required any more, so that all charges are conserved globally. Equation (5.31) applies now for all particles in the liquid-gas phase transition of nuclear matter, and the chemical potentials of all identical particles become equal. For the hadron-quark phase transition the hadronic chemical potentials directly fix the quark chemical potentials and vice versa.

In Tables 7.1 and 7.2 the cases with global charge neutrality but without the conservation of Y_L and Y_p are not listed. This is not necessary, because the equilibrium conditions remain the same as in case V if one or both of the fractions are actually not conserved, because this is still a global constraint. Additionally, the corresponding chemical potential, see Table 6.1, becomes zero in the two phases. Thus, every non-conserved fraction gives rise to two stronger local constraints. They contain the information about the chemical equilibrium between the two phases with respect to this fraction, so that one of the equilibrium conditions in Tables 7.1 and 7.2 becomes meaningless. If Y_L is not conserved one gets the disappearance of the neutrinos and non-conserved Y_p gives weak-equilibrium, If Y_p is not conserved weak equilibrium, Eqs. (6.1) and (6.2). This is the case in protoneutron stars, or in the core of a supernova. If Y_p and Y_L are both not conserved, the well-known equilibrium conditions of cold deleptonized neutron stars with beta-equilibrium, Eqs. (6.3) and (6.4), and global charge neutrality are recovered.

7.3.6 Case 0

Finally, we want to discuss case 0 in which the phase transition is somewhat constructed by hand. In case 0, all state variables are fixed locally. No mixed phase has to be calculated, as also the baryon density is fixed locally: $n_B^I = n_B^{II} = n_B$. If conserved at all, the three conserved fractions are fixed locally, too. In case 0 there are no globally conserved charges so that no chemical equilibrium condition between the two phases is obtained. Thus, the two equations of state of the two phases can be calculated completely separately and the phase transition point is then set by one freely selectable condition. However, it is possible that the chosen condition can not be fulfilled at all so that no phase transition occurs.

If a phase transition point can be found, the subvolumes of the two phases remain arbitrary there, similarly as at the transition point of a discontinuous phase transformation. Accordingly the extensive variables cannot be determined, too. On the other hand, the local intensive variables remain independent of the volumes of the two phases. Thus

the chemical potentials of the locally conserved charges, the local pressure and the local temperature remain well-defined even without knowing the two subvolumes. The two phases can be treated as independent single homogeneous phases with unknown volume.

Case 0 is interesting if one wants to exclude the possible occurrence of a mixed phase. If pressure equilibrium is taken as the criterion for the determination of the phase transition point the two phases can only coexist at one special density n_B^{coex} if the other state variables are kept constant. No extended mixed phase appears, and the phase transformation is discontinuous. Only if electrons and neutrinos can be treated as ideal gases, $\mu_e^I = \mu_e^{II}$ follows from equal n_B and Y_p and $\mu_\nu^I = \mu_\nu^{II}$ from equal n_B, Y_p and Y_L. If instead of the baryon number density the pressure is used as the continuous state variable no mixed phase forms, either. At the transition point pressure and thermal equilibrium are established, but at least chemical equilibrium of the baryons is not. Case 0 with pressure equilibrium as the additional constraint assumes implicitly that no particles can be exchanged between the two phases. Most importantly, therefore the thermodynamic potential, the free energy $F = -pV + \sum_i N_i \mu_i$, behaves discontinuously. Because of the local constraints, the sum $\sum_i \mu_i N_i$ will not be equal in the two phases. If the pressure is used instead of the volume as one of the state variables, the free enthalpy will also behave discontinuously when the transition point is crossed. Thus, the thermodynamic potential can not be used to determine which of the two phases exists before and which one after the phase transition. The second law of thermodynamics is not fulfilled in Case 0 because there is no chemical equilibration.

Besides pressure equilibrium every other possible coexistence condition can be applied. The conclusions remain the same, and in general all the conditions will lead to a discontinuous thermodynamic potential. The discontinuity of the thermodynamic potential shows the differences to the Maxwell construction. It can only be prevented if the corresponding thermodynamic potential (the free energy F for $(T, V, (C_k))$, the free enthalpy G for $(T, p, (C_k))$) is used directly as the phase coexistence criterion. At the point where the two potentials are equal the phase transition occurs. Before and after the phase transition only the phase with the lower potential is present. However, with this choice the pressure (and all other thermodynamic quantities but the state variables) will behave discontinuously.

We note that case 0 with fixed Y_p would imply for the liquid-gas phase transition, that actually no phase transition occurs, because the same particles appear with equal densities in the two phases. Case 0 is only relevant if some internal degrees of freedom remain which can be different in the two phases.

As proposed in Sec. 3.5.4 case O may be also relevant for hydrodynamic simulations, if the typical hydrodynamical cells are smaller than the structures in the mixed phase. A micro-canonical description with $S = S(E, V, (C_k))$ would conserve energy, charges and entropy. Consequently there would be local jumps in T, p and μ_k when the phase transition occurs, leading to the generation of shocks.

7.4 Adiabatic EOS

Apart from numerical simulations, the EOS is often calculated for the state variables $(S/N_B, p, Y_L, n_C)$. Such an EOS can e.g. directly be used for the description of typical representative configurations of protoneutron stars which are characterized by a constant lepton to baryon ratio and a constant entropy per baryon in a first approximation, see Sec. 6.2.

Because the pressure is chosen to be the independent continuously changing variable, there exist only two possibilities, as we showed in Sec. 7.2.3: Either the phase transition occurs only at one single pressure p^{coex}, or a mixed phase of the two phases forms over an extended range in pressure. In the first case no mixed phase needs to be calculated. If thermal and mechanical equilibrium are required, the direct phase transition point can be found where the temperatures of the two phases become equal $T^I = T^{II}$. This requires locally fixed $S/N_B^I = S/N_B^{II} = S/N_B$, $p^I = p^{II} = p$, $Y_L^I = Y_L^{II} = Y_L$, $n_C^I = n_C^{II} = n_C$ and (arbitrary) globally conserved baryon number N_B which can be shared by the two phases. Pressure equilibrium is automatically given, as the pressure is one of the state variables which is set to equal values in the two phases.

This case is the adiabatic equivalence to case 0 of the isothermal phase transformations, in which all state variables but the volume were fixed locally. Now temperature equilibrium is chosen as the constraint which determines the coexistence point. Even though thermal equilibrium is enforced, the thermodynamic potential, which is the enthalpy $H = TS + \sum_i N_i \mu_i$, will change discontinuously at the transition point. In contrast in the Maxwell construction of the isothermal phase transformations of case I the coexistence pressure is determined by the proper equilibrium conditions of the chemical potentials. We showed that this leads to continuous thermodynamic potentials.

There exists nothing similar for an adiabatic process to the isothermal case IIa, which allows an easy construction of the non-neutrino mixed phase but leads to an extended mixed phase with the inclusion of neutrinos. As explained before, the non-neutrino part of the EOS depends on the neutrino fraction as soon as Y_p is not conserved any more.

Thus it is not possible to separate the neutrino contribution. In the adiabatic case, in all scenarios (except for the direct phase transitions) the Gibbs construction has to be used, with the inclusion of neutrinos and an extended mixed phase is present.

7.5 Role of Neutrinos

In Sec. 6.1 we argued that neutrinos can be separated from the EOS of a single phase, if Y_p is conserved. From the equilibrium conditions discussed in the preceding sections, it becomes obvious that neutrinos also do not have to be included in the non-neutrino equilibrium conditions as long as the lepton fraction is not fixed locally. The only quantum number of the neutrino is the lepton number so that Eq. (5.31) applies for global lepton number conservation, leading to $\mu_\nu^I = \mu_\nu^{II}$. Because we assumed in addition that all locally conserved fractions are equal in the two phases, terms proportional to $Y_l \mu_\nu^\kappa$ (see Table 6.1) drop out in the equilibrium conditions of globally conserved charges. This is also the case if the lepton fraction is not conserved, which directly leads to $\mu_\nu^I = \mu_\nu^{II} = 0$.

The same conditions for chemical equilibrium of the non-neutrino part are obtained, if neutrinos are not taken to be part of the thermodynamic equilibrium. Neutrinos represent a uniform background, which does not influence the chemical equilibrium between the two phases if Y_p is conserved. Then also their pressure contribution in the two phases is exactly the same. Thus it is also sufficient to study the pressure equilibrium without taking neutrinos into account. We conclude it is sufficient to calculate an equation of state for protons, neutrons and electrons (or quarks and electrons) in terms of (T, n_B, Y_p) and this equation of state can be used for all possible conditions under which the neutrinos appear.

Instead if Y_p is not conserved, i.e. one has an EOS in terms of (T, n_B) or (T, n_B, Y_L) the neutrinos influence the rest of the matter via the condition for weak equilibrium. The neutrino contribution has to be taken into account for the evaluation of the non-neutrino EOS. Thus the non-neutrino EOS will also depend on whether lepton number is conserved or not, because the conditions for weak-equilibrium Eqs. (6.1) and (6.2), are different from those for beta-equilibrium, Eqs. (6.3) and (6.4). In the former case the lepton number is conserved and the neutrinos are determined by Y_L. In the latter case neutrinos are completely untrapped and the neutrino contribution becomes trivial, $\mu_\nu = 0$.

Chapter 8

A Statistical Model for a Complete Supernova EOS

The equation of state of uniform nuclear matter is qualitatively very similar to a Van-der-Waals-EOS. Models for the interactions of the nucleons show some long-range attraction and a short-range hard-core repulsion. The latter becomes dominant at large densities. This interplay leads to the occurrence of a first-order phase transition below saturation density, where the binding energy reaches its maximum. Because of the similar behavior to ordinary water, this phase transition is called the liquid-gas phase transition of nuclear matter. In the RMF model presented in Sec. 2.4, the attraction is mediated by the sigma- and the repulsion by the omega-meson. A typical bulk phase diagram was shown in Fig. 2.5. Compared to water, there is one important conceptual difference: nuclear matter is a two-component substance because the densities of neutrons and protons can be varied independently.

Nuclear matter has another very interesting characteristic property. Independent of density and temperature, symmetric nuclear matter has always the lowest energy with respect to changes of the proton fraction Y_p. Nuclear matter thus behaves like a one-component simple body for an equal amount of protons and neutrons. For symmetric nuclear matter the isospin degree of freedom is not explored in two-phase coexistence. In chemistry a mixture of two or more liquids in such a ratio that its composition cannot be changed by simple distillation is called an azeotrope. Thus one can classify symmetric nuclear matter as an azeotrope of the strong interactions. Contrary, in asymmetric nuclear matter isospin distillation occurs. The denser phase, the "liquid", is more symmetric than the more dilute "vapor" phase. Because the interactions are stronger at large densities, it is favorable to concentrate the protons in the denser region.

In this section, a detailed statistical model for the liquid-gas phase transition of nuclear matter is presented. This approach goes far beyond the bulk approximation of

phase equilibrium, as presented in the previous chapters. Indeed, instead of modeling the phase transition by two phases in equilibrium, the picture of a chemical mixture of nucleons and nuclei is used. The nuclei can be interpreted as the more dense and more symmetric liquid phase and the nucleons as the vapor. The model is developed with the intension to describe the equation of state and the composition of supernova matter. Part of the following three sections has already been published in Ref. [HS10].

8.1 Introduction to the supernova EOS

At present, there exist only three (hadronic) EOSs commonly used in the context of core collapse supernovae. One of the first EOSs was developed by Hillebrandt and Wolff [HW85]. More recent EOSs have been developed by Lattimer and Swesty (LS) [LD91b] and Shen et al. [STOS98a, STOS98b]. In the following we will take the Shen and LS EOSs as references for comparison. These two EOSs are based on different models for the nuclear interactions. The former uses a relativistic mean field (RMF) approach, which we will also apply in our model. Nuclei are calculated in the Thomas-Fermi approximation. The latter is based upon a non-relativistic parameterization of the nuclear interactions. Nuclei are described as a compressible liquid-drop including surface effects.

Besides these two, there are plenty of EOSs which focus on particular aspects of nuclear matter but which are restricted to a certain range in temperature, asymmetry or density. In their range of validity they give a much more detailed description of the effects occurring there. The main difficulty in the construction of a complete EOS which is suitable for supernova simulations is the large domain in density 10^4 g/cm^3 $< \rho <$ 10^{15} g/cm^3, temperature $0 < T < 100$ MeV and (total) proton fraction $0 < Y_p < 0.6$ which in principle has to be covered. In this broad parameter range the characteristics of nuclear matter change tremendously: from non-relativistic to ultra-relativistic, from ideal gas behavior to highly degenerate Fermi-Dirac gas, from pure neutron matter to symmetric matter. All possible compositions appear somewhere in the extended phase diagram: uniform nuclear matter, nuclei in coexistence with free nucleons, free nucleons with the formation of light clusters, or an ideal gas mixture of different nuclei, just to mention a few possibilities. Thus one needs a rather simple but reliable model which is able to describe all the different compositions and the phenomenon connected with them. Furthermore, from a numerical point of view the calculation of the EOS table itself is also not trivial.

For uniform nuclear matter plenty of different models for the EOS exist and most of them could in principle be applied in the supernova context. So far, the nuclear EOS

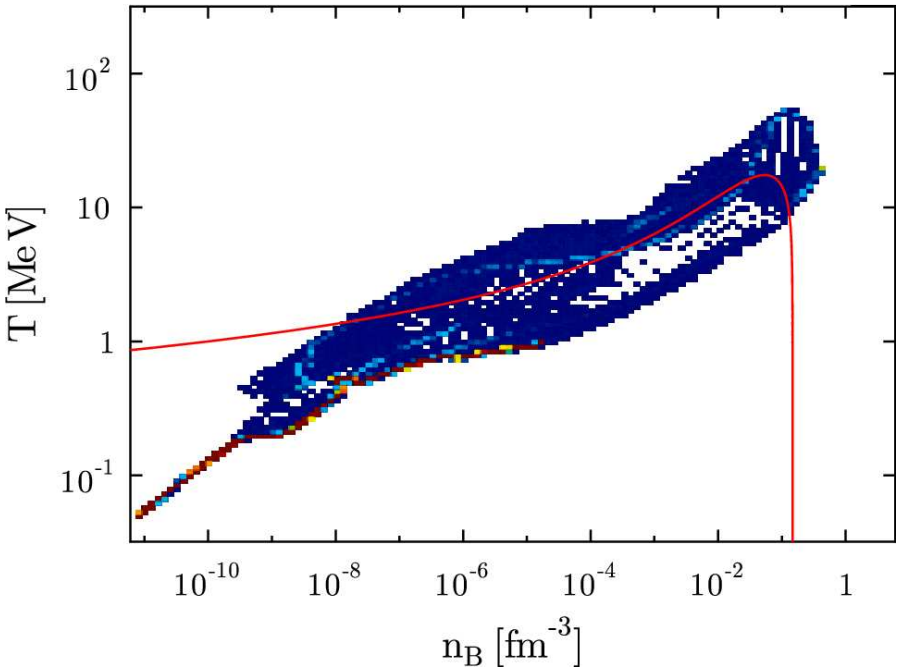

Figure 8.1: The number of calls of density and temperature bins of the EOS in a typical simulation are shown in color coding. Blue shows entries which are called the least, yellow bins are called the most frequent. The red line shows the first order phase transition line for symmetric bulk nuclear matter. Below the line a mixed phase is present.

at large densities is not fixed and is still one of the main fields of current research in high energy physics. From the previous discussion it is clear, that in the application for supernova physics the main difficulties arise below saturation density, where the liquid-gas phase transition of nuclear matter takes place. Matter becomes non-uniform, as light and/or heavy nuclear clusters (nuclei) form within the free nucleon gas. The uniform nuclear matter EOS is only one of the essential input information for the construction of an EOS which is suitable for the description of all possible conditions which typically occur in a core-collapse supernova. For the non-uniform nuclear matter phase further model assumptions are necessary. In this section we focus on the modeling and the resulting properties of non-uniform matter.

We want to emphasize that this low-density part of the EOS plays a special role in core-collapse supernovae. Figure 8.1 shows the number of calls of density and temperature bins of the EOS in a typical simulation. The first order phase transition line for symmetric nuclear matter is plotted on top as an indicator for the occurrence of nuclei. It can be seen that most of the computational time is spent in the low-density regime where nuclei coexist with unbound nucleons.

The subsaturation EOS is not only called quite often but plays also a particular role for the dynamics of a supernova. As mentioned earlier, most supernova simulations fail to achieve successful explosions. The shock front which is initially traveling outwards after the bounce looses energy due to nuclear dissociation and neutrino emission and finally stalls at densities $\sim 10^9$ g/cm^3, see e.g. [BL85, TBP03]. In the neutrino reheating paradigm the high energetic neutrinos of the deeper layers heat the matter between the neutrino-spheres and the stalled shock so that the shock is reenergized until it finally drives of the envelope of the star. Thus the EOS of subsaturation matter is of particular importance for the possible reviving of the shock wave. Furthermore, the neutrino-spheres are located at densities $\sim 10^{11}$ g/cm^3. The neutrino spectra, which belong to the most important observables of a supernova, are formed here and thus carry the information about the properties of low density nuclear matter.

The two EOSs mentioned before have been successfully applied in astrophysical simulations since many years. However, both of them are based on the single nucleus approximation (SNA) assuming that the whole distribution of different nuclei which forms at finite temperature can be represented by only one single nucleus. The single nucleus is found by a minimization procedure of the thermodynamic potential. The SNA has to be seen as a necessary assumption for any microscopic calculation based on one single unit cell with periodic boundary conditions, as e.g. in Ref. [BV81, NS09], too. In such microscopic calculations the nuclei are formed out of the nucleons which are placed in the unit cell just by the nuclear interactions, which is a very convenient aspect of these models. Already in Ref. [BL84] it was shown, that under most conditions the EOS is almost not affected by the SNA. But the SNA gives the composition only in an averaged way, as the spread in the distribution of nuclei can be large. In microscopic calculations quite often several similar minima of the thermodynamic potential are found, also indicating the occurrence of mixtures of different nuclei, in contrast to the SNA, see e.g. [BV81, NS09]. Furthermore, in Ref. [SSL$^+$09] it was presented for some particular EOS models, that the SNA leads to systematically larger nuclei, which was already shown in Ref. [BL84], too. The distribution of nuclei can influence the supernova-dynamics, as e.g. electron capture rates are modified. The electron capture rates are highly sensitive to the nuclear composition and the nuclear structure, see e.g. [LM00, LMS$^+$03, HMM$^+$03, MLF06]. More closely connected to the present work, in Ref. [CHB06] the authors investigated models which are based on a distribution of various nuclei, so called nuclear statistical equilibrium (NSE) models. It was shown with classical molecular dynamics simulations that these models give systematically larger neutrino cross subsections, leading to shorter neutrino mean free paths. In their study also the importance of the remaining uncertainty regarding the composition was pointed out. We want to note that the previously

mentioned systematic change in the composition within the SNA was not analyzed in Ref. [CHB06]. The NSE distribution of nuclei was only compared to a SNA system with a nucleus with the mass and charge of the average of the distribution. The results of Ref. [Saw05] point in the same direction: it was shown that the proper treatment of a multicomponent plasma leads to greatly reduced ion-ion correlations and thus to increased neutrino opacities.

There are further limitations of the previously mentioned EOSs, [STOS98a, STOS98b] and [LD91b]. Both of them do not include any nuclear shell effects. A good description of nuclei is only achieved on an averaged basis. It might be seen as part of the SNA not to attribute any certain shell structure to the single nucleus which only represents the average of the whole distribution of nuclei. But in cases where only very few different or even only one kind of nuclei appears (e.g. at low densities and temperatures), shell effects are important and should definitely be taken into account in a self-consistent way in the composition and in the EOS. Shell effects can substantially alter the composition and are crucial for the evaluation of the weak reaction rates with neutrinos and electrons. In our model we do not want to use the liquid-drop formulation or the Thomas-Fermi approximation, but rather implement as much information gained from experiments about the nuclear masses as possible. Thus our approach is very contrary to the two other EOSs, in which the nuclear interactions are the only input information required in the physical model for non-uniform nuclear matter.

In some supernova EOSs, and also in the LS and in the Shen EOS, the distribution of light clusters is represented only by α-particles, in the same way as the distribution of heavy nuclei is represented by only one heavy single nucleus. In the most simple case the α-particles are described as a non-relativistic, classical ideal gas, without any interactions with the surrounding nucleons. In contrast to this very simplified treatment, there are studies which focus exclusively on the role of light nuclei in supernovae and the medium effects connected with them. A model-independent description of low-density matter is given by the virial equation of state for a gas of light clusters with mass number $A \leq 4$, [HS06b, HS06a, OGH$^+$07]. In Ref. [AMO$^+$08] the composition of this model was compared to the composition of a simple NSE model. Up to densities $\rho \sim 10^{13}$ only small differences were found, mainly an increased α-particle fraction due to attractive nucleon-alpha interactions in the virial EOS. The more elaborated models of Refs. [SR08, Roe09] are based on a quantum statistical approach. In subsection 8.6 we will give a detailed comparison to these two approaches. In all these studies it is found that light clusters in addition to α-particles contribute significantly to the composition, with a particular role of the deuterons. This is also one of the results of Ref. [HSS09], where all stable nuclei with $A \leq 13$ are included, but medium effects are only considered

on a simplified level. The inclusion of the additional degrees of freedom of the light clusters can affect the supernova-dynamics. E.g. in Ref. [AMO+08] the influence of light nuclei on neutrino-driven supernova outflows was studied and a significant change in the energy of the emitted antineutrinos was found. As another example, in Ref. [OGH+07] it was shown, that mass-three nuclei contribute significantly to the neutrino energy loss for $T \geq 4$ MeV. A different topic connected to light clusters is the possible formation of Bose-Einstein condensates, see e.g. [FYH+08, FHR+08, HSS09].

A lot of knowledge about the properties of hot compressed nuclear matter was gained from statistical multifragmentation models (SMM) which are used to analyze low-energy heavy-ion collisions [Gro90, BBI+95]. Later we will give a detailed comparison of our results with the SMM of Botvina and Mishustin. In Refs. [BM04, BM05, Mis08, BM08] it was pointed out that the state reached in these experiments ($T \sim 3 - 6$ MeV, $\rho \sim 0.1\rho_0$, with the saturation density ρ_0) is very similar to the conditions in a core-collapse supernova in the region between the protoneutron star and the shock front. It is very attractive that the same well-established models which are used to describe matter in terrestrial experiments can be applied for matter in some of the most energetic explosions in the universe.

In an astrophysical context such models are usually called NSE models. In this chemical picture the bound states of nucleons are treated as new species of quasi-particles. NSE models are in principle extended Saha-equations, as presented in Ref. [CT65]. Within this approach the whole distribution of light and heavy nuclei can be included by construction. Furthermore, it is very easy to incorporate experimentally measured masses. This classical approach gives an excellent description as long as matter is sufficiently dilute that the nuclear interactions are negligible and if the temperature is so low, that the structure of the nuclei is not changed significantly, see e.g. [IMN+78]. If the whole distribution of nuclei is taken into account, it becomes rather difficult to implement a proper description of the medium effects on the nuclei, which become important at large densities. Thus, especially the transition to uniform nuclear matter which happens around $1/2\rho_0$ leads to difficulties for NSE models. Obviously, in the high density regime close to saturation density, more microscopic SNA-models give a more reliable description. In this high density regime also very exotic nuclear structures, commonly called the "nuclear pasta" phases, appear [SWS+08]. In a recent 3D Skyrme-Hartree-Fock calculation [NS09] it was shown, that this frustrated state of nuclear matter is characterized by a large number of local energy minima, for different mass numbers and for different nuclear configurations. Thus one can expect that many different pasta shapes will coexist at a given temperature and density, which would require a statistical treatment beyond the present capabilities. Furthermore, in SNA models the Coulomb energy of the

considered unit cell is included in the Wigner?Seitz approximation. This always imposes a certain symmetry/periodicity of the system. Also in NSE models the Wigner?Seitz approximation is commonly used. Monte Carlo and Molecular dynamics simulations, as e.g. applied in Refs. [WMS$^+$05, MTV$^+$05] can go beyond these simplifications and incorporate correlations in a more natural way.

In addition to the subtleties at large densities, the assumption of NSE itself, in the sense that chemical equilibrium is established, is only valid for temperatures larger than ~ 0.5 MeV. For lower temperatures, the nuclear reactions are too slow compared to the typical dynamical timescales of ms within a supernova. Anyhow we will present results below $T = 0.5$ MeV for completeness and for the sake of comparison with larger temperatures. For these low temperatures one has to keep in mind that they do not represent the actual conditions in a supernova, but rather the ground state of matter after a sufficiently long time.

Before presenting our own model, we want to review briefly the first studies of NSE models in the context of the supernova EOS. The first publication we are aware of is Ref. [MLB79]. In this NSE model nucleon and Coulomb interactions and internal partition functions are included in a consistent way. Similar works followed [EH80, Mur80], which investigated the different components of NSE models. Excluded volume effects were first considered in Ref. [HM81]. This work also shows the first hydrodynamic simulations of core-collapse supernovae, in which a NSE model had been applied. This NSE model was then further developed in Ref. [HNW84]. More recently, in Ref. [IOS03] Ishizuka et al. included 9000 nuclei from the theoretical mass table of Myers and Swiatecki [MS90]. Excited states of the nuclei are treated with an internal partition function in the same manner as we will do. However, the model of Ishizuka et al. does not consider any nuclear interactions or phenomenological excluded volume corrections. In this sense it is a rather pure NSE model. The SMM model of Botvina and Mishustin [BM04, BM05, Mis08, BM08] does not use any tabulated binding energies, but is based on a liquid-drop parameterization of the nuclear masses. We will discuss this model in more detail in Sec. 8.4 and compare it to our results. The NSE model of Blinnikov et al. [BPRS09] uses the tabulated theoretical nuclear binding energies of Ref. [KTUY05]. In their model interactions of the free nucleons as well as the modification of the nuclear surface energy due to the presence of the free nucleons is taken into account. Nuclear excited states are described by the partition functions of Engelbrecht [EE91]. Besides the use of different nuclear interactions and partition functions, the major difference of this model compared to ours, which will be presented below, is, that excluded volume effects have not been implemented. Nadyozhin and Yudin considered in their NSE calculation only 137 selected nuclei and did not include any nuclear interactions. Instead

they studied elaborated descriptions of the excited states [NY04] and of the Coulomb energy [NY05] in great detail. In the other NSE models discussed above, the Coulomb energies are included in the Wigner-Seitz approximation, which we will also use in our model.

Despite the principle problems NSE models have to cope with at large densities, we want to construct a NSE model which allows to bridge the critical region from some percent of saturation density up to uniform nuclear matter. By using a NSE model we keep the rather simple but accurate description of low-density and low-temperature matter. For uniform nuclear matter an RMF EOS will be applied. Our new NSE model shall be able to give a reasonable description of the transition to uniform nuclear matter, which in the microscopic SNA models is achieved automatically. For that we include the nuclear interactions also in the unbound nucleon contribution below saturation density. In most cases these interactions are not important, but they become crucial where the free nucleons constitute a significant fraction and the interactions are necessary for the liquid-gas phase transition. Furthermore, we develop a thermodynamic consistent description of excluded volume effects, so that we achieve the right asymptotic behavior for very dense and very dilute nuclear matter. We are aware that we apply the NSE description at densities at which we can not control all effects of the nuclear interactions any more, and our very phenomenological description becomes questionable. Anyhow, we want to explore the limits of a NSE model and compare the arising differences to other existing EOSs. So far an NSE model has never been applied close to saturation density and the existing models are not able to describe the transition to uniform nuclear matter at all. We can discuss the whole phase diagram of supernova matter within one consistent model and can address all the aspects which were mentioned above, namely the distribution of heavy nuclei, the importance of the light cluster distribution, or the role of shell effects. As will be presented below, we will apply the same model which was used for the calculation of the nuclear masses for the interactions of the free nucleons, so that all nuclear interactions (apart from excluded volume effects) are based on the same Lagrangian.

8.2 Description of the model

In our model matter consists of nuclei, nucleons, electrons, positrons and photons. As we want to describe the most general case of supernova matter, we do not assume weak equilibrium and thus use the independent state variables (T, n_B, Y_p) (see also Sec. 6.1). As discussed in Sec. 7.5, the neutrinos do not have to be taken into account in the

calculation of the EOS. Electrons are assumed to be distributed uniformly and are described as a general Fermi-Dirac gas, including the positron contribution. All Fermi-Dirac integrals for the electrons as well as for the nucleons were calculated using the very accurate and fast routines from Refs. [Apa98, GZDA01]. Thus the possible degeneracy of the nucleons is fully taken into account. The photon contribution (Stefan-Boltzmann law) is also included in the EOS. The nontrivial part of the model is the description of the baryons, as they are not distributed uniformly and their interactions are significant. For simplicity, for temperatures above or equal 20 MeV matter is assumed to be uniform, i.e. without the presence of nuclear clusters.

8.2.1 Nucleons

For the unbound interacting nucleons (neutrons and protons) the RMF model is applied, which was introduced in Sec. 2.4. We will show results for two different parameter sets, TMA and TM1 (Subsec. 2.4.4). For very low number densities of the nucleon gas ($n_{nuc} < 10^{-5}$ fm^{-3}), where the interactions are negligible, the nucleons are treated as noninteracting ideal Fermi-Dirac gases for simplicity. The photons and their coupling to the nucleons are dropped at this point, because the contribution of the free photon gas is added separately to the EOS and the Coulomb energies will be discussed later.

8.2.2 Nuclei

In our approach we will preferably use experimentally measured masses for the description of nuclei (mass number $A \geq 2$). We take the nuclear data from the atomic mass table 2003 from Audi, Wapstra, and Thibault (AWT) [AWT03] whenever possible. It is very convenient that we directly can use experimental data for the construction of the EOS. We do not take any estimated, non-experimental data of the atomic mass table into account.

For nuclei with experimentally unknown mass we have to use the results of nuclear structure calculations in form of nuclear mass tables. The mass table from Geng et al. [GTM05] is calculated with the relativistic mean field model TMA. Thus all nuclear interactions are consistently based on the same nuclear interactions if the mass table from Geng is combined with the RMF interactions TMA for the unbound nucleons. This mass table lists 6969 even-even, even-odd and odd-odd nuclei, extending from ^{16}O to ^{331}100 from slightly above the proton to slightly below the neutron drip line. The nuclear binding energies are calculated under consideration of axial deformations and

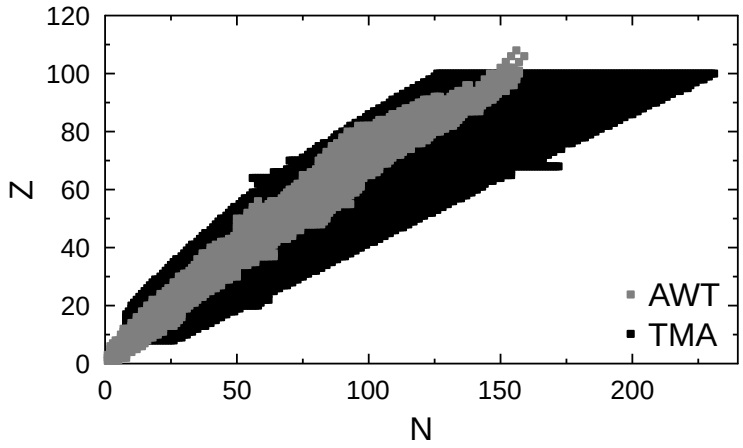

Figure 8.2: The proton number Z and neutron number N of the nuclei taken from the mass table calculated with TMA [THS$^+$95, GTM05] and from the experimental AWT mass table [AWT03].

the pairing is included with a BCS-type δ-force. With these detailed calculations of the nuclear masses a good agreement with the experimental masses is achieved, with a rms deviation $\sigma \sim 2.1$ MeV [GTM05]. For the parametrization TM1 we do not have a suitable mass table at hand, thus we cannot avoid the minor "inconsistency" to use the table of Geng et al. [GTM05], which is based on the TMA parameterization.

As long as a mixed phase of free nucleons and nuclei is favored instead of uniform nuclear matter, our statistical description includes all nuclei which are listed in the experimental AWT table or in the theoretical mass table TMA respectively. Fig. 8.2 shows all the considered nuclei in a nuclear chart.

8.2.3 Excited States

At finite temperature excited states of the nuclei will be populated and consequently the number density $n_{A,Z}$ of a certain nucleus (A, Z) with mass number A and proton number Z will increase. It is given by the sum over all excited states i:

$$n_{A,Z} = \sum_i n^i_{A,Z} \ , \tag{8.1}$$

which can be put into the following form:

$$n_{A,Z} \ = \ n^0_{A,Z} \sum_i g_i (1 + \Delta E^*_i / M_0)^{3/2} \exp(-\Delta E^*_i / T) \ , \tag{8.2}$$

with the excitation energy ΔE_i^* of the excited state i, if a Maxwell-Boltzmann distribution is assumed. $n_{A,Z}^0$ is the number density of the ground state, without its spin degeneracy $g_0 = 2(J_0 + 1)$, which is still included in the sum over i.

Instead of including all excited states explicitly we use a temperature dependent degeneracy function $g_{A,Z}(T)$. It represents the sum over all excited states of a hot nucleus. We choose the simple semi-empirical expression for $g_{A,Z}(T)$ from Ref. [FR82]:

$$g_{A,Z}(T) = g_{A,Z}^0 + \frac{c_1}{A^{5/3}} \int_0^{E_{max}} dE^* e^{-E^*/T} \exp\left(\sqrt{2a(A)E^*}\right) \tag{8.3}$$

$$a(A) = \frac{A}{8}(1 - c_2 A^{-1/3}) \text{ MeV}^{-1} \tag{8.4}$$

$$c_1 = 0.2 \text{ MeV}^{-1}, \;\; c_2 = 0.8 \, , \tag{8.5}$$

with $g_{A,Z}^0$ denoting the degeneracy of the groundstate. $g_{A,Z}^0$ is very small compared to $g_{A,Z}(T)$ and therefore we take $g_{A,Z}^0 = 1$ for even and $g_{A,Z}^0 = 2$ for odd A for simplicity. Only for the deuteron the true groundstate degeneracy $g_{2,1}^0 = 3$ is used, because of its important contribution at large temperatures. For the alpha-particle and most of the other light clusters the previous values are anyhow correct. In this way the only information needed about the nuclei are their ground state masses. In the following, we will use $E_{max} = BE$, i.e. we include excited states up to the binding energy BE to represent that the excited states still have to be bound.

8.2.4 Coulomb energies

For the calculation of the Coulomb energies, which play an important role in the determination of the composition, we assume spherical Wigner-Seitz (WS) cells for every nucleus. For an uniform electron distribution with electrons present inside and outside of a nucleus (A, Z) and zero temperature one gets a simple classical expression for the Coulomb energy of the WS cell:

$$E_{A,Z}^{Coul} = -\frac{3}{5}\frac{Z^2\alpha}{R(A)}\left(\frac{3}{2}x - \frac{1}{2}x^3\right) \tag{8.6}$$

$$x = \left(\frac{n_e}{n_B^0} \frac{A}{Z} \right)^{1/3} , \tag{8.7}$$

where we treated the nuclei as homogeneous spheres with radius $R(A)$ of nucleons at saturation density n_B^0: $R(A) = (3A/4\pi n_B^0)^{1/3}$. n_e is the electron number density, which is fixed by charge neutrality: $n_e = Y_p n_B$. The first term in the brackets corresponds to the Coulomb energy of a point-like nucleus with charge Z within the electron gas. The second term in the brackets arises due to the finite size of the nucleus, with electrons located inside the nucleus.

We do not include the Coulomb energy of the protons because of the following reasons: In principle they could be added within the WS approximation in the same way as for the nuclei, without any further complications. But first of all protons are rather light particles, so that the WS approximation and the above expression for the Coulomb energy would not be very adequate. Next and more important in our context is the following aspect: in uniform charge neutral nuclear matter the Coulomb energy has to be zero. If we included the Coulomb energy of the protons within the approximation above, this would not be the case. Because protons were described as point-like static particles, their WS-Coulomb energy would never vanish, not for a locally charge neutral system either. Instead of the WS approximation one could treat the protons as an uniform background, which would screen the charge of the electrons and interact with the charge of the nuclei. Then the Coulomb energy would vanish for uniform nuclear matter as it has to be. But within our description of the thermodynamic system (which will be presented next) this would lead to numerical complications as an additional implicit equation had to be solved. Thus for simplicity we neglect the anyhow small Coulomb energy of the protons. Then the correct limit of vanishing Coulomb energy for uniform nuclear matter is also achieved.

8.2.5 Thermodynamic model

In our description we distinguish between nuclei and the surrounding interacting nucleons, and we still have to specify how the system is composed of the different particles. For nuclei we will apply the following classical description: All baryons (nucleons in nuclei or unbound nucleons) are treated as hard spheres with the volume $1/n_B^0$ so that the nuclei are uniform hard spheres at saturation density of volume A/n_B^0. Next, a nucleus must not overlap with any other baryon (nuclei or unbound nucleons). Thus the volume in which the nuclei can move is not the total volume of the system, but only the volume which is not filled by baryons. This is illustrated in Fig. 8.3. For the unbound nucleons

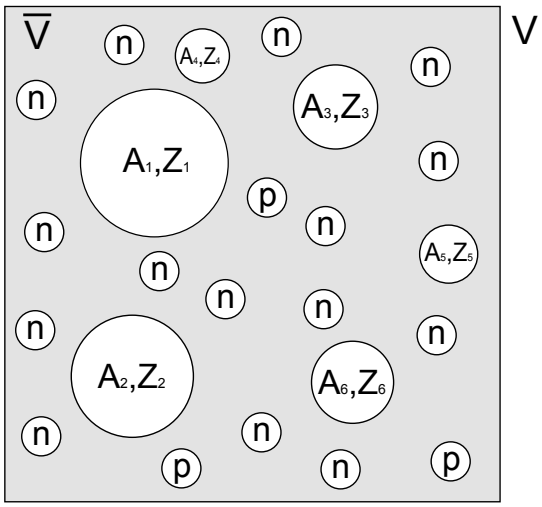

Figure 8.3: Illustration of the excluded volume effects on the nuclei. Each nucleon and nucleus has a proper volume, which reduces the volume in which the nuclei can move to $\bar{V}$, which is given by the grey region.

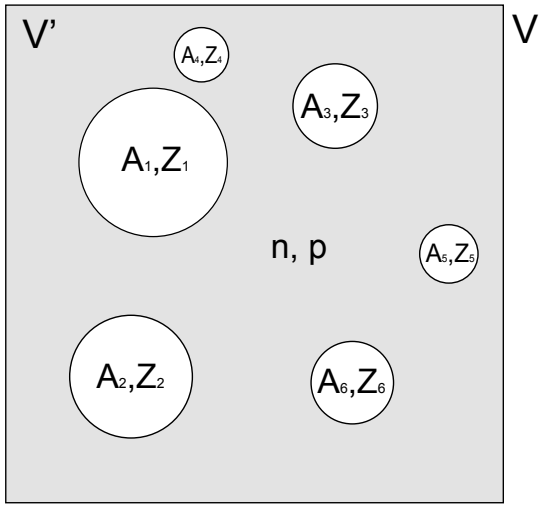

Figure 8.4: Illustration of the excluded volume effects on the nucleons. Nucleons have to be outside of nuclei, thus they only fill the volume V', which is given by the grey region.

we use a different description, because the interactions among them are already included in the RMF model. For unbound nucleons we only assume that they are not allowed to be situated inside the nuclei, which is shown in Fig. 8.4. We will discuss these two different excluded volume corrections in more detail later.

To derive all relevant thermodynamic quantities like e.g. the energy density or the pressure for given (T, n_B, Y_p), we start from the total canonical partition function of the system. To do that we will first consider that the entire set $\{N_i\}$ of all the particle

numbers of electrons N_e, neutrons N_n, protons N_p and all nuclei $\{N_{A,Z}\}$ is fixed (the trivial photon contribution is taken out of the following derivation). In our model the total energy can be split into the contribution of electrons, nucleons, nuclei and the Coulomb energy. Thus the total canonical partition function is given by the product of the partition functions of the four different contributions:

$$Z(T,V,\{N_i\}) = Z_e \; Z_{nuc} \prod_{A,Z} Z_{A,Z} \; Z_{Coul} \; , \tag{8.8}$$

with V denoting the volume of the system. From the canonical partition function the canonical thermodynamic potential follows, which is the Helmholtz free energy:

$$\begin{aligned} F(T,V,\{N_i\}) &= -T\ln Z & (8.9)\\ &= F_e + F_{nuc} + \sum_{A,Z} F_{A,Z} + F_{Coul} \; . & (8.10) \end{aligned}$$

In the following the different contributions to the free energy will be discussed separately in detail.

The free energy of the electrons $F_e = -T\ln Z_e$ is given by a general noninteracting ideal Fermi-Dirac gas, including antiparticle contributions:

$$F_e(T,V,\{N_i\}) = F_e^0(T,V,N_e) \; . \tag{8.11}$$

The electrons are distributed over the entire volume and are not influenced by the excluded volume effects. Then the Coulomb free energy has the following simple form:

$$\begin{aligned} F_{Coul}(T,V,\{N_i\}) &= F_{Coul}(T,V,N_e,\{N_{A,Z}\}) \\ &= \sum_{A,Z} N_{A,Z} E_{A,Z}^{Coul}(V,N_e) \; . & (8.12) \end{aligned}$$

From Eq. (8.6) and (8.7) it is clear that the Coulomb free energy actually depends only on the number density of the electrons, $n_e = N_e/V$, which is fixed by charge neutrality, $n_e = Y_p n_B$, and the numbers of protons N_p and nuclei $\{N_{A,Z}\}$ but not on the volume. Thus the Coulomb free energy is also not modified by the excluded volume corrections.

The volume available to the nucleons is reduced by the volume which is filled by nuclei. Therefore the free energy of the nucleons $F_{nuc} = -T\ln Z_{nuc}$ is the free energy calculated with the unmodified RMF model F_{nuc}^0 for the available volume V' which is

not filled by the volumes of the nuclei:

$$\begin{aligned} F_{nuc}(T,V,\{N_i\}) &= F^0_{nuc}(T,V',N_n,N_p) && (8.13)\\ V' &= V-\sum_{A,Z} N_{A,Z}V_{A,Z} && (8.14)\\ V_{A,Z} &= AV_0 = A/n_B^0\ . && (8.15) \end{aligned}$$

If no nuclei are present we arrive at the unmodified RMF description, as it should be.

Nuclei are treated as non-relativistic classical particles. Also for the nuclei an excluded volume correction is introduced, but one which has a different character than the one for nucleons. The nuclei are allowed to be everywhere in the system as long as they do not overlap with any other baryon (nucleons inside of the other nuclei or the free nucleons). Regarding the effect on the nuclei, the same volume as the one of nucleons in nuclei is attributed to the free nucleons, so that according to Eq. (8.15):

$$V_n = V_p = V_0 = 1/n_B^0\ . \tag{8.16}$$

Every baryon in the system reduces the free volume $\bar{V}$ in which the nuclei can move:

$$\bar{V} = V-\sum_{A,Z} N_{A,Z}V_{A,Z} - N_nV_n - N_pV_p\ . \tag{8.17}$$

Thus within our assumptions, the free energy of the nucleus (A,Z) is the usual Maxwell-Boltzmann expression of a classical ideal gas in the free volume $\bar{V}$:

$$F_{A,Z}(T,V,\{N_i\}) = F^0_{A,Z}(T,\bar{V},N_{A,Z}) \tag{8.18}$$

$$F^0_{A,Z} = N_{A,Z}M_{A,Z} - TN_{A,Z}\left(\ln\left(\frac{g_{A,Z}(T)\bar{V}}{N_{A,Z}}\left(\frac{M_{A,Z}T}{2\pi}\right)^{3/2}\right)+1\right)\quad . \tag{8.19}$$

As the volume appears only in the kinetic part of the free energy, naturally this excluded volume correction does not modify the rest mass term.

The excluded volume correction of the nuclei represents a hard-core repulsion of the nuclei at large densities close to saturation density. Instead the modification of the free energy of the unbound nucleons is purely geometric and just describes that the nucleons fill only a fraction of the total volume. It is important to note that nuclei can not be present at densities larger than saturation density within this picture, which is reasonable and wanted. This is also the reason why we chose $V_0 = 1/n_B^0$ for the value of the volume of a nucleon, which has to be seen as a free parameter of the model.

The volume V of the system can be chosen freely and just determines the size of the system. As its value is completely arbitrary in the thermodynamic limit, a description in which all extensive quantities are replaced by their corresponding densities is more convenient. The total particle number densities are the numbers of particles per total volume:

$$n_{n/p} = N_{n/p}/V \tag{8.20}$$

$$n_{A,Z} = N_{A,Z}/V \ . \tag{8.21}$$

For the nucleons we introduce the local number densities outside of the nuclei, given by the number of neutrons respectively protons per available volume:

$$n'_{n/p} = N_{n/p}/V' \ . \tag{8.22}$$

In the following we will use these local number densities of the nucleons instead of their total number densities, as they directly set the RMF contribution of the nucleons to the EOS. After introducing the filling factor of the nucleons

$$\xi = V'/V = 1 - \sum_{A,Z} n_{A,Z} V_{A,Z} \tag{8.23}$$

$$= 1 - \sum_{A,Z} A \ n_{A,Z}/n_B^0 \tag{8.24}$$

the total number and the electric charge density of the baryons take on the following form:

$$n_B = (N_n + N_p + \sum_{A,Z} A N_{A,Z})/V \tag{8.25}$$

$$= \xi(n'_n + n'_p) + \sum_{A,Z} A \ n_{A,Z} \ , \tag{8.26}$$

$$n_B Y_p = (N_p + \sum_{A,Z} Z N_{A,Z})/V \tag{8.27}$$

$$= \xi n'_p + \sum_{A,Z} Z n_{A,Z} \ . \tag{8.28}$$

$\xi = 1$ corresponds to the case when only free nucleons are present. For $\xi = 0$ the nuclei fill the entire space so that there is no available volume for the free nucleons left.

To replace $\bar{V}$ in the expressions used later the volume fraction κ is introduced:

$$\kappa = \frac{\bar{V}}{V} . \tag{8.29}$$

It is the fraction of the free volume $\bar{V}$ in which the nuclei can move of the total volume V. It depends only on n_B:

$$\kappa = 1 - \frac{1}{n_B^0 V}\left(\sum_{A,Z} N_{A,Z} + N_n + N_p\right) \tag{8.30}$$

$$= 1 - n_B/n_B^0 . \tag{8.31}$$

$1-\kappa$ is the volume fraction which is filled by baryons. If $\kappa = 1$ ($n_B = 0$) then the free volume is equal to the total volume, for $\kappa = 0$ ($n_B = n_B^0$) the entire space is filled by baryons and the free volume vanishes.

After having specified the free energy, all thermodynamic quantities can be derived consistently in the standard manner as derivatives of the free energy. Only the internal energy density $\epsilon = U/V$ has to be determined by the inverse Legendre transformation of the free energy density $f = F/V$, $\epsilon = f + Ts$, with $s = S/V$ denoting the entropy density.

In the intensive formulation the free energy density becomes:

$$\begin{aligned} f &= f_e^0(T, n_e) + \sum_{A,Z} f_{A,Z}^0(T, n_{A,Z}) + f_{Coul}(n_e, \{n_{A,Z}\}) \\ &\quad + \xi f_{nuc}^0(T, n_n', n_p') - T\sum_{A,Z} n_{A,Z}\ln(\kappa) , \end{aligned} \tag{8.32}$$

$$f_{Coul}(n_e, \{n_{A,Z}\}) = \sum_{A,Z} n_{A,Z} E_{A,Z}^{Coul}(n_e) , \tag{8.33}$$

$$f_{A,Z}^0(T, n_{A,Z}) = n_{A,Z}\left(M_{A,Z} - T - T\ln\left(\frac{g_{A,Z}(T)}{n_{A,Z}}\left(\frac{M_{A,Z}T}{2\pi}\right)^{3/2}\right)\right) . \tag{8.34}$$

The first two terms in Eq. (8.32) are the ideal gas expressions of the electrons and the nuclei. The Coulomb free energy of the nuclei appears in addition. The free energy density of the nucleons is weighted with their volume fraction in the fourth term. This can be expected as the free energy is an extensive quantity. The last term arises directly from the excluded volume corrections of the nuclei. Because of this term, as long as nuclei are present, the free energy density goes to infinity when approaching saturation density

($\kappa \to 0$). Thus uniform nuclear matter will always set in slightly before saturation density is reached.

The entropy density can be written in the following form:

$$s = s_e^0(T, n_e) + \sum_{A,Z} s_{A,Z}^0(T, n_{A,Z}) + \xi s_{nuc}^0(T, n_n', n_p') + \sum_{A,Z} n_{A,Z} \ln(\kappa) \ , \quad (8.35)$$

$$s_{A,Z}^0(T, n_{A,Z}) = n_{A,Z} \left(\ln \left(\frac{g_{A,Z}(T)}{n_{A,Z}} \left(\frac{M_{A,Z} T}{2\pi} \right)^{3/2} \right) + \frac{5}{2} + \frac{\partial g_{A,Z}}{\partial T} \frac{T}{g_{A,Z}} \right) \ . \quad (8.36)$$

Analog expressions as in the free energy density appear. As the Coulomb energy is not taken to be temperature dependent it does not give a contribution to the entropy. In the ideal gas expression of the nuclei, Eq. (8.36), an additional contribution from the temperature dependent degeneracy arises. The excluded volume correction term in Eq. (8.35) expresses the reduction of the available number of states for the nuclei with increasing density.

The energy density looks similar:

$$\epsilon = \epsilon_e^0(T, n_e) + \xi \epsilon_{nuc}^0(T, n_n', n_p') + \sum_{A,Z} \epsilon_{A,Z}^0(T, n_{A,Z}) + f_{Coul}(n_e, \{n_{A,Z}\}) \ , \quad (8.37)$$

$$\epsilon_{A,Z}^0(T, n_{A,Z}) = n_{A,Z} \left(M_{A,Z} + \frac{3}{2} T + \frac{\partial g_{A,Z}}{\partial T} \frac{T^2}{g_{A,Z}} \right) \ . \quad (8.38)$$

The total pressure becomes:

$$p = p_e^0(T, n_e) + p_{nuc}^0(T, n_n', n_p') + \frac{1}{\kappa} \sum_{A,Z} p_{A,Z}^0(T, n_{A,Z}) + p_{Coul}(n_e, \{n_{A,Z}\}) \quad (8.39)$$

$$p_{A,Z}^0(T, n_{A,Z}) = T n_{A,Z} \quad (8.40)$$

where the ideal gas pressure of the nuclei is increased by $1/\kappa$ as their free volume is reduced by the excluded volume of the baryons. p_{Coul} denotes the negative Coulomb pressure:

$$p_{Coul}(n_e, \{n_{A,Z}\}) = -\sum_{A,Z} n_{A,Z} \frac{3}{5} \frac{Z^2 \alpha}{R(A)} \left(\frac{1}{2} x - \frac{1}{2} x^3 \right) \ . \quad (8.41)$$

The chemical potential of the electrons is reduced by the Coulomb interactions:

$$\mu_e = \mu_e^0(T, n_e) + \frac{p_{Coul}(n_e, \{n_{A,Z}\})}{n_e} . \tag{8.42}$$

The chemical potential of the neutrons and protons is:

$$\mu_{n/p} = \mu_{n/p}^0(T, n_n', n_p') + \frac{1}{\kappa} \sum_{A,Z} p_{A,Z}^0(T, n_{A,Z}) V_0 . \tag{8.43}$$

Because of the excluded volume corrections mechanical work has to be exerted upon the pressure of the nuclei to add an additional nucleon. The chemical potential of the nuclei encounters an even stronger modification:

$$\mu_{A,Z} = \mu_{A,Z}^0(T, n_{A,Z}) + E_{A,Z}^{Coul}(n_e) \tag{8.44}$$

$$+ \left(p_{nuc}^0(T, n_n, n_p) + \frac{1}{\kappa} \sum_{A,Z} p_{A,Z}^0(T, n_{A,Z}) \right) V_{A,Z} - T\ln(\kappa) , \tag{8.45}$$

$$\mu_{A,Z}^0(T, n_{A,Z}) = M_{A,Z} - T\ln \left(\frac{g_{A,Z}(T)}{n_{A,Z}} \left(\frac{M_{A,Z} T}{2\pi} \right)^{3/2} \right) \tag{8.46}$$

Besides the chemical potential of an ideal gas the Coulomb energy of the nucleus appears. Furthermore to add an additional nucleus volume work has to be performed not only against the pressure of the nuclei, but also against the nucleonic pressure. The last term arises directly from the excluded volume correction and shows the increase of the chemical potential when the density becomes close to saturation density.

The presented approach for the excluded volume corrections is thermodynamically fully consistent and the part for the nuclei is equivalent to the method described in Ref. [RGSG91] in which a grand-canonical formulation was used.

So far, all the particle number densities, n_n, n_p, $\{n_{A,Z}\}$, n_e were treated as fixed variables. In the following the equilibrium conditions for the baryons will be derived for the assumption of baryon number and proton number (or proton fraction) conservation which is equivalent to baryon number and isospin conservation. The electron contribution is fixed by charge neutrality. We note that our procedure, to derive the thermodynamic variables from the thermodynamic potential for given n_n, n_p, $\{n_{A,Z}\}$, n_e first, and to implement chemical equilibrium of the baryons afterwards, gives the correct result and is much simpler than doing it the other way round. The equilibrium con-

ditions only set the baryonic composition but do not change the other thermodynamic functions.

For given n_B and Y_p the internal variables n_n, n_p and $\{n_{A,Z}\}$ are no longer independent. After including the conservation laws with the help of two Lagrange multipliers the first and second law of thermodynamics lead to the following relation which expresses the chemical equilibrium between nuclei and nucleons:

$$\mu_{A,Z} = (A-Z)\mu_n + Z\mu_p \; . \tag{8.47}$$

With this condition only two degrees of freedom (e.g. n_B and Y_p) remain, which have to be specified. Then Eqs. (8.43)–(8.47) can be combined to

$$\begin{aligned} n_{A,Z} &= \kappa \; g_{A,Z}(T) \left(\frac{M_{A,Z} T}{2\pi} \right)^{3/2} \\ &\quad \times \exp\left(\frac{(A-Z)\mu_n^0 + Z\mu_p^0 - M_{A,Z} - E_{A,Z}^{Coul} - p_{nuc}^0 V_{A,Z}}{T} \right) \; . \end{aligned} \tag{8.48}$$

Because all the baryons (including the free nucleons) contribute equally to the excluded volume of the nuclei, the pressure of the nuclei drops out in the equilibrium condition Eq. (8.47) and the number density of the nuclei can be written in this form.

We want to emphasize that μ_n^0 and μ_p^0 contain the RMF interactions of the nucleons. As they appear in Eq. (8.48) the interactions of the free nucleons are thus coupled to the contribution of the nuclei. Compared to the generalized RMF model of Typel et al. [TRK+10], the mutual counteracting in-medium self energy and the Pauli-blocking shifts of the light clusters appear in addition in their model. Furthermore, in our approach the bound nucleons do not contribute to the source term of the meson fields. In our model the Mott effect and the dissolution of clusters at large densities is mimicked only by the excluded volume corrections.

The factors ξ and κ in Eq. (8.48) themselves depend on the number densities of the free nucleons and/or nuclei, and therefore the set of equations (8.23)-(8.31) and (8.48) still has to be solved numerically in a self-consistent way. Within this formulation the values of n_n' and n_p' determine the total baryon number density and the proton fraction. Thus for given n_B and Y_p only two nested root-findings have to be performed, in addition to the root-finding for the RMF equations for the nucleons. Thermodynamic consistency and consistency of the mass fractions is reached on a high level within the calculation and the relative error never exceeds 10^{-6}.

8.2.6 Transition to uniform nuclear matter

For certain temperatures and proton fractions the NSE model as presented above still exhibits a first order phase transition close to saturation density. We want to stress that the liquid-gas phase transition of nuclear matter is almost completely described by the statistical model alone. The first order phase transition occurs only in a very narrow density region in the transition to uniform nuclear matter. This phase transition is triggered by a rather abrupt turnover in the composition, in which nuclei are replaced by unbound nucleons. The first order phase transition is an indication that the model is too restrictive at large densities. We want to illustrate this aspect further.

In the bulk approximation the following behavior for the transition to uniform matter, i.e. close to the endpoint of the liquid-gas phase transition (see Fig. 2.5), is expected: Besides of the restricted parameter-space in (T, Y_p) where retrograde condensation takes place, the volume fraction of the liquid phase (nuclei) grows with increasing density until this phase occupies the entire space, the gas phase disappears and uniform nuclear matter is reached, see [Gle92, MS95]. In our model the mass and charge number of the nuclei is limited by the nuclear mass table and thus the nuclear clusters are not able to grow arbitrary in size. Still it is possible that the volume fraction of nuclei approaches unity, but as the nuclei are described as unchangeable particles they are obviously not able to evolve to uniform nuclear matter. Instead they are replaced by unbound nucleons which leads to the phase transition.

To treat the phase transition correctly we need to construct a mixed phase between the NSE model and uniform nuclear matter. Because we do not want to include Coulomb interactions between the two phases, we require the mixed phase to be locally charge neutral. With this assumption alone we still would have a multi-component system, as the proton fraction and baryon density can be shared by the two phases. A (non-linear) Gibbs construction was required. To avoid additional root-findings, we thus impose the same local proton fraction in both phases in addition, denoted by case Ic in Table 7.1. Then the system becomes a simple body and the Maxwell construction can be used. We note that the same mixed phase construction was used in the LS EOS.

This description of the phase transition leads to a constant total pressure with the electron contribution included. By using these stringent conditions we will get discontinuities in the second derivatives of the free energy. Besides the assumption of locally fixed Y_p another simplification is used: the point at which the pressure in the two phases is equal is determined in an approximative way. To save computational time the two phases are only compared at the density grid-points of the final EOS table. Then the two phases are connected by a thermodynamic consistent interpolation.

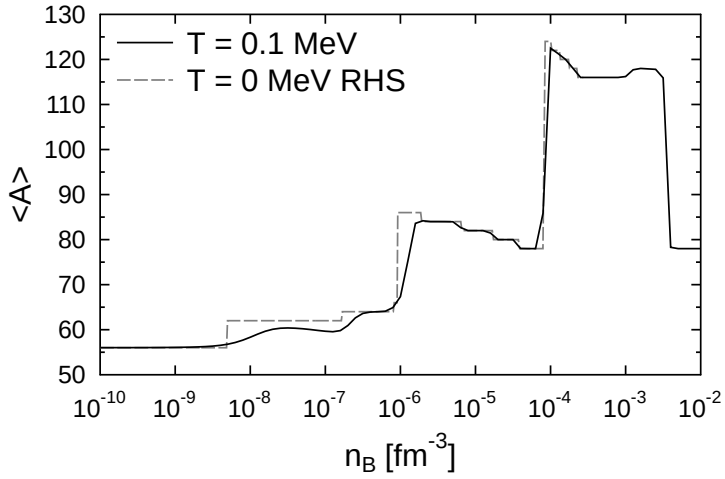

Figure 8.5: The average mass number of heavy nuclei $\langle A \rangle$ as a function of the baryon number density n_B in β-equilibrium. The results of the present work at $T = 0.1$ MeV are compared to the results from Ref. [RHS06] at temperature $T = 0$ MeV, which are also based on the mass table TMA but in which the lattice energy is included explicitly.

With this construction the non-uniform phase consisting of nuclei and nucleons is replaced successively by uniform nuclear matter with increasing density. One can interpret the second phase (uniform nuclear matter) as an infinitely large nucleus which occupies a volume fraction which increases with density. As this nucleus is locally charge neutral it can be treated in the thermodynamic limit, in which the surface energy is negligible compared to the volume part. Thus the use of the mixed phase construction helps to overcome the limitation by the use of nuclear mass table.

This interpretation of the denser phase in the phase transition is also used in Refs. [BGMG00, BGMG01]. In these works an analytic solution of a simplified SMM in the thermodynamic limit was studied, in which excluded volume effects were treated self-consistently. The behavior of the mixed phase in our model is qualitatively similar to their results or of e.g. Ref. [MS95] in which bulk nuclear matter was studied. Interestingly, the results of the recent work [NS09] seem to indicate, that even within a 3D Skyrme-Hartree-Fock calculation the phase transition to uniform nuclear matter requires a mixed phase construction.

8.3 Results

8.3.1 Composition

In the following we will only show and discuss results for the parameterization TMA and the corresponding mass table. We chose this parametrization, because it is the only one for which a consistent mass table was available. To have a general overview of the composition we will distinguish light and heavy nuclei by the charge $Z \leq 5$. The mass fraction of a single particle i is defined by $X_i = A_i n_i / n_B$. For the light and heavy nuclei we will also use the total light, respectively heavy, nuclei mass fraction X_a, respectively X_A, defined by:

$$X_a = \sum_{A\geq 2, Z\leq 5} A n_{A,Z}/n_B \tag{8.49}$$

$$X_A = \sum_{A\geq 2, Z\geq 6} A n_{A,Z}/n_B \ . \tag{8.50}$$

Furthermore we introduce the average heavy nucleus

$$< A > = \sum_{A\geq 2, Z\geq 6} A n_{A,Z} / \sum_{A\geq 2, Z\geq 6} n_{A,Z} \tag{8.51}$$

$$< Z > = \sum_{A\geq 2, Z\geq 6} Z n_{A,Z} / \sum_{A\geq 2, Z\geq 6} n_{A,Z} \tag{8.52}$$

and average light nucleus

$$< a > = \sum_{A\geq 2, Z\leq 5} A n_{A,Z} / \sum_{A\geq 2, Z\leq 5} n_{A,Z} \tag{8.53}$$

$$< z > = \sum_{A\geq 2, Z\leq 5} Z n_{A,Z} / \sum_{A\geq 2, Z\leq 5} n_{A,Z} \tag{8.54}$$

Together with the neutron and proton mass fractions X_n and X_p we achieve:

$$1 = X_n + X_p + X_a + X_A \ , \tag{8.55}$$

which means we have a viable decomposition into four different particle species. Furthermore the density of the average light and heavy nucleus is then correctly given by:

$$n_a = n_B X_A / < A >= \sum_{A \geq 2, Z \leq 5} A n_{A,Z} \tag{8.56}$$

$$n_A = n_B X_a / < a >= \sum_{A \geq 2, Z \geq 6} A n_{A,Z} \; . \tag{8.57}$$

Fig. 8.5 depicts the average mass number of the heavy nuclei $\langle A \rangle$ as a function of n_B for β-equilibrated neutrino-free matter, i.e. $\mu_n = \mu_p - \mu_e$. The results of the present investigation at $T = 0.1$ MeV are compared to a detailed calculation of the outer crust of a neutron star at $T = 0$ [RHS06] which is based on the same nuclear mass table TMA. Instead of the simplified manner described in Secs. 8.2.4 and 8.2.5, in Ref. [RHS06] the Coulomb energy of a body-centered-cubic lattice is incorporated explicitly in the EOS and only the single groundstate nucleus is determined. For $T = 0.1$ MeV the temperature effects are small and only lead to a smoothing of the stepwise change in the composition at $T = 0$. Regarding the composition, the good agreement between the two different calculations shows that the simplified treatment of the Coulomb energies in the statistical model of the present work does not cause any significant differences. We conclude, that an excellent description of nuclear matter composition at low temperatures and densities is achieved, which incorporates shell effects.

In both calculations the system exhibits nuclei with smaller Z/A for increasing density, as the electrons become relativistic and their contribution to the free energy becomes larger. The decrease in Z/A leads to an in overall increasing mass number, up to $n_B \sim 10^{-4}$ fm^{-3}. Shell effects are strongly pronounced: for 10^{-6} fm$^{-3} < n_B < 10^{-4}$ fm^{-3} only nuclei with the magic neutron number 50 are present and around 10^{-4} fm^{-3} only the magic neutron number 82 is populated. It is important to note that up to $\sim 3 \times 10^{-5}$ fm^{-3} the composition is given entirely by nuclei whose mass is taken from experimental data. Around $n_B \sim 2.7 \times 10^{-4}$ fm^{-3} the calculation of Ref. [RHS06] ends, where the so called neutron drip is reached, at which free neutrons begin to appear. In the statistical model the nucleus ^{116}Se initially remains the favored nucleus after the neutron drip. Then ^{118}Se appears and at larger densities ^{78}Ca, a nucleus with very low $Z/A \sim 0.26$ becomes the most abundant nucleus. Obviously, in our statistical model the composition is restricted on the nuclei which are listed in the used nuclear mass table. This could be the reason for the unexpected decrease of $< A >$ at densities close to saturation.

We note that our model is actually not very suitable for the description of neutron star matter in the inner crust, corresponding to the high density part of Fig. 8.5. In

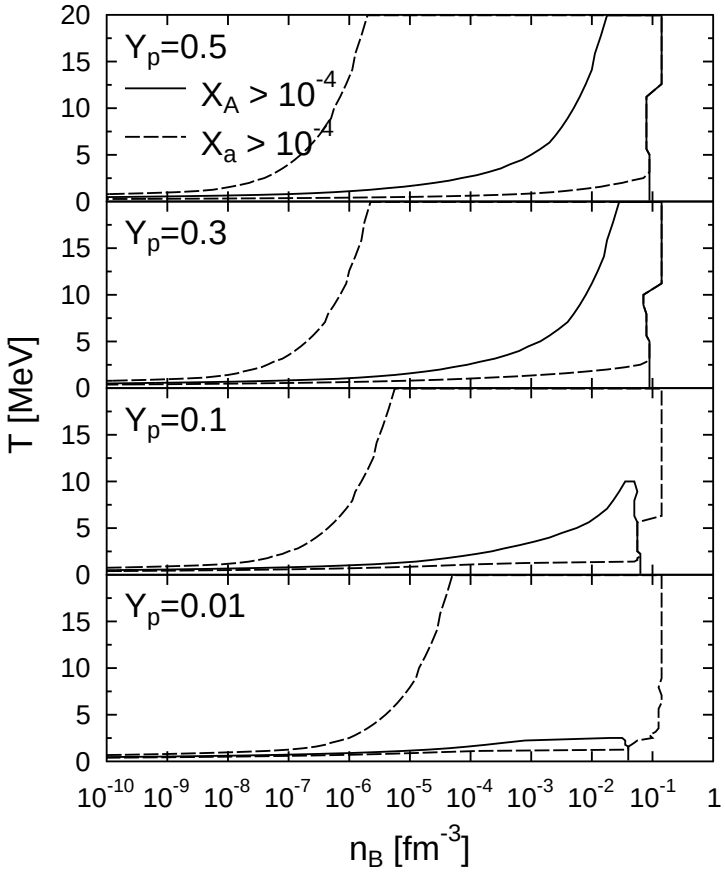

Figure 8.6: The phase diagram of nuclear matter for different proton fractions Y_p in the $T-n_B$ plane. Solid (dashed) lines enclose the region where the mass fraction of heavy nuclei with $Z \geq 6$ (light nuclei with $Z \leq 5$) exceeds 10^{-4}.

contrast to matter in supernovae, in neutron stars the proton fraction is very low causing a large mass fraction of unbound neutrons. Thus the interactions between free neutrons and nuclei, which change the structure of the nuclei, are very important. Later we will discuss this aspect further. We will show that for typical supernova conditions, in the regime where the contribution of the nuclei is important, the mass fraction of free nucleons is low instead.

The phase diagram of nuclear matter, in terms of the composition regarding light and heavy nuclei is depicted in Fig. 8.6. We show the contour lines for a mass fraction 10^{-4} of the light nuclei X_a and of the heavy nuclei X_A, as specified in Eqs. (8.49) and (8.50). At temperatures above $1-2$ MeV and low densities nuclear matter consists almost only of free nucleons. Between 10^{-7} and 10^{-4} fm^{-3} light clusters begin to appear. As will be seen from Fig. 8.17, discussed in more detail later, these first light clusters are mainly deuterons. The more symmetric the system is, the earlier is the onset of the light clusters in form of the isospin symmetric deuterons. For all proton fractions some light

clusters are present up to $n_B \sim 1/2\ n_B^0$ where uniform nuclear matter is reached. Only for temperatures below $1-2$ MeV the system consists almost entirely of heavy nuclei. At the transition to uniform nuclear matter the following observations can be made: At low temperatures, $T \leq 2$ MeV, the transition density where uniform nuclear matter is reached is increasing with the proton fraction from $n_B = 0.3 n_B^0$ to $0.7 n_B^0$, similar as in the bulk nuclear matter phase diagram of Fig. 2.5. Depending on the proton fraction, there is a certain temperature, above which the transition density is significantly increased. At the highest temperatures studied, the uniform nuclear matter appears only slightly below saturation density.

The phase diagram of heavy nuclei in Fig. 8.6 can be seen as a manifestation of the liquid-gas phase transition of bulk nuclear matter, Fig. 2.5. The critical temperature up to which heavy nuclei are abundant increases from roughly 2 MeV at $Y_p = 0.01$ above 20 MeV for symmetric nuclear matter. Obviously, the presented phase diagram depends on the somewhat arbitrary distinction between light and heavy nuclei by the proton number $Z \leq 5$. For example for $T \geq 10$ MeV, the heavy nuclei have actually only very low mass and charge numbers. The appearance of these intermediate nuclei leads to the broad extension of X_A at high temperatures in Fig. 8.6. Nevertheless, if one takes the peculiarities of the different models into account, there is a qualitative agreement with the phase diagrams of e.g. Refs. [LD91b, STOS98b, MS95].

Fig. 8.7 shows again the phase diagram, but this time in the $Y_p - n_B$ plane for some selected temperatures. Contour lines for a mass fraction of 0.5 are shown by the thick lines. With this criterion the dominant phase can directly be identified. For all temperatures, nucleons are the most abundant component for proton fractions below ~ 0.1. In this case there are only few protons in the system and thus only a small amount of nuclear clusters can form. For larger Y_p the phase diagrams show a strong temperature dependence. At the lowest temperature $T = 0.1$ MeV, as expected, the heavy nuclei fill the rest of the $Y_p - n_B$ plane up to $\sim 1/2\ n_B^0$ where uniform nuclear matter is reached. At a temperature of 0.5 MeV a small region in the upper left corner appears which is dominated by light clusters. At such low densities the heavy nuclei are dissolved into lighter clusters, and as these light clusters are mainly α-particles (see Fig. 8.17) because of their relatively strong binding, this happens only at very large proton fractions of ~ 0.5. At a temperature of 1 MeV this light cluster region is shifted to higher densities. Again, the light clusters are mainly α-particles which explains their favorable appearance around $Y_p \sim 0.5$. At the lowest densities even the light clusters are dissolved into free nucleons. At densities larger than $10^{-6} - 10^{-5}$ fm^{-3} the heavy nuclei dominate until uniform nuclear matter is reached. For $T = 5$ and 10 MeV light and heavy nuclei appear only in a very narrow density band between 10^{-3} and 0.1 fm^{-3}.

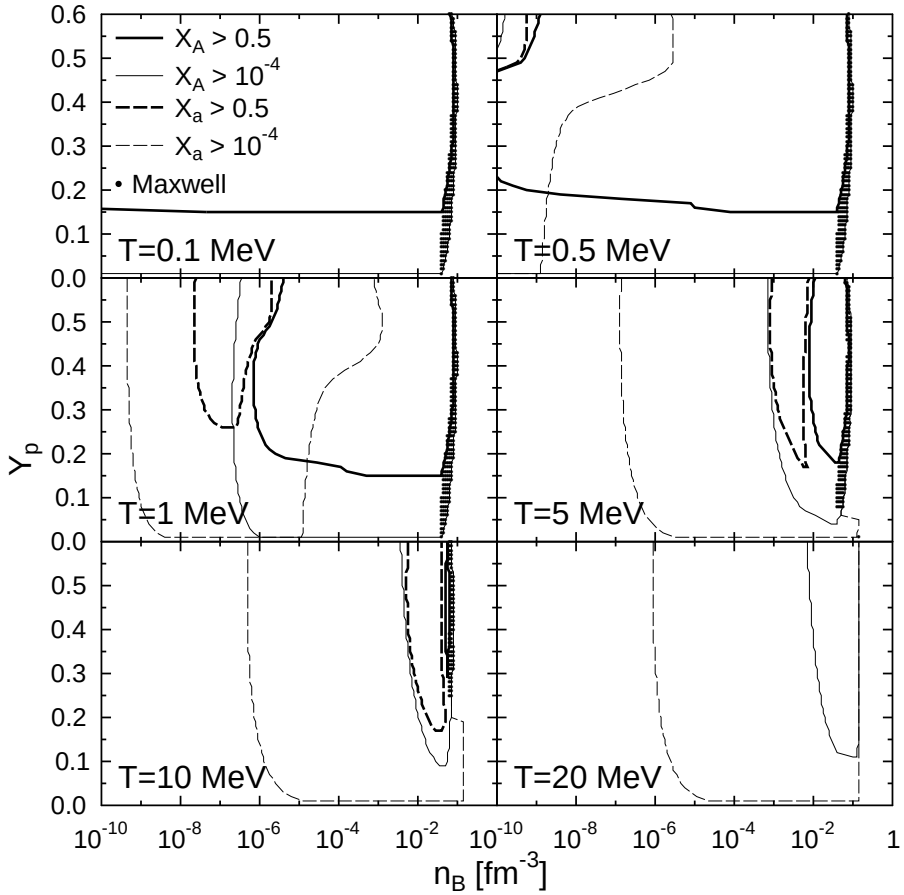

Figure 8.7: The phase diagram of nuclear matter for different temperatures in the $Y_p - n_B$ plane. Thick (thin) solid lines enclose the region where the mass fraction X_A of heavy clusters with $Z \geq 6$ exceeds 0.5 (10^{-4}). The dashed lines correspond to the mass fractions of light clusters X_a with $Z \leq 5$. Dots mark the densities which lie in the mixed phase of the Maxwell-transition from non-uniform to uniform nuclear matter.

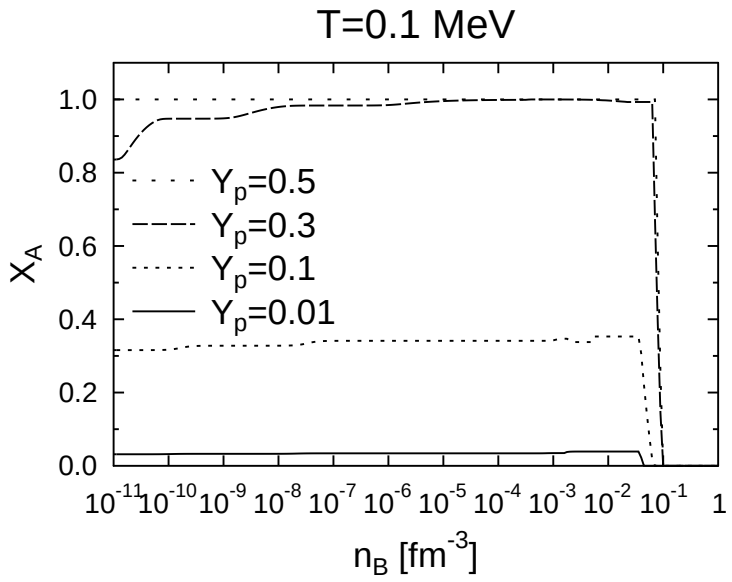

Figure 8.8: The mass fraction of heavy nuclei X_A as a function of the baryon number density n_B for a temperature $T = 0.1$ MeV and different proton fractions Y_p.

The region dominated by heavy nuclei shrinks with increasing temperature. For $T = 20$ MeV the mass fraction of light and heavy nuclei never exceed 0.5.

In Fig. 8.7 also the transition to uniform nuclear matter is illustrated. The dots show the density-grid-points of the calculation which are based on the Maxwell-construction, as explained earlier. We find that with increasing temperature the mixed phase region becomes smaller. It even disappears completely for very low Y_p and temperatures ≥ 5 MeV, because then the mixture of nuclei and nucleons behaves almost like uniform nuclear matter. Due to the same reason the transition is shifted to larger densities. For $T \leq 5$ MeV, where many heavy nuclei exist, the mixed phase becomes most extended at low $Y_p \sim 0.2$. On the contrary, at larger Y_p the Maxwell transition region becomes narrower. This shows that the Maxwell construction is necessary because of the description of the heavy nuclei as unchangeable particles.

The independence of the phase diagram on the density at $T = 0.1$ MeV is further analyzed in Fig. 8.8. There the mass fraction of heavy nuclei is shown as a function of density for various proton fractions. For such low temperatures the mass fraction of heavy nuclei is almost constant throughout all densities. This can be explained in the following way: For all shown values of Y_p free protons are never present and therefore all the protons are concentrated in nuclei. For proton fractions $Y_p \geq 0.3$ the system consists almost only of heavy nuclei. Even though the neutron chemical potential increases slowly with density, the neutron drip ($\mu_n = m_n$) is never reached and as the temperature is low the free neutron density remains vanishingly small. There will be a critical Y_p^{drip},

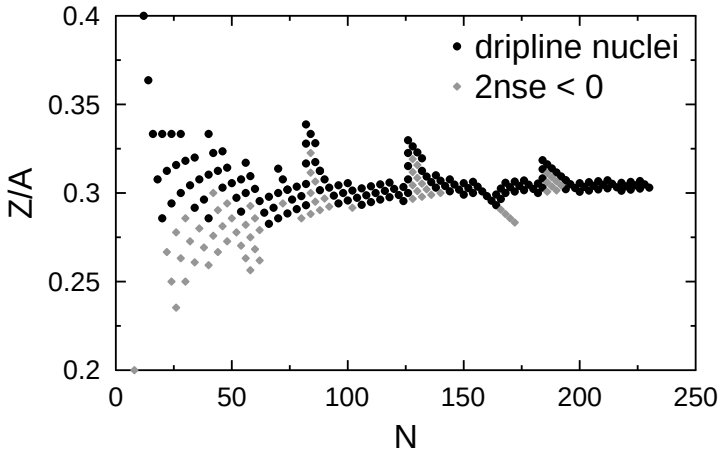

Figure 8.9: The charge to mass ratio Z/A as a function of the neutron number N of nuclei which lie on the neutron drip line (black circles) and which have a negative two neutron separation energy, i.e. which lie behind the neutron drip line (grey diamonds).

below which the neutron drip occurs, with $Y_p^{drip} \sim 0.31$ in our calculations. For proton fractions below this critical value a dilute free neutron gas with $\mu_n \simeq 0$ appears, which leads to the drastic reduction of X_A. Under the condition $\mu_n \simeq 0$ exclusively such nuclei are being populated, whose two-neutron separation energy are close to zero, which means that they are neutron drip nuclei. Fig. 8.9 shows the charge to mass ratio of nuclei which lie on the drip line and of those whose two-neutron separation energy is negative. They all have $Z/A \sim 0.3$. As no free protons are present, the mass fraction of heavy nuclei is directly determined by the total proton fraction, $X_A \sim Y_p/0.3$ for $Y_p < 0.31$, and is independent of density, which is in good agreement with the results of Fig. 8.8.

For higher temperatures the composition changes significantly. Depending on the actual values of temperature, density and proton fraction, free protons, free neutrons and light and heavy nuclei appear in different concentrations. Fig. 8.10 demonstrates that for temperatures of $T = 1$ MeV and densities up to $n_B \sim 10^{-8}$ fm^{-3} mainly only free nucleons are present. At larger densities the protons cluster together to form light nuclei and thus the free proton density vanishes. The light clusters tend to be symmetric and thus the fraction of the free neutrons is reduced by the same value as the one for protons. Due to the same reason, the maximum mass fraction of the light nuclei is roughly twice the proton fraction. At densities larger than 10^{-6} fm^{-3} heavy nuclei appear and replace the lighter nuclei. With increasing density the nuclei grow in size and become more asymmetric so that more neutrons are bound in nuclei. The fraction of heavy nuclei increases further and becomes close to 1 for large proton fractions. As there are no nuclei with $Z/A < 0.1$ in the mass table, some free neutrons have to remain

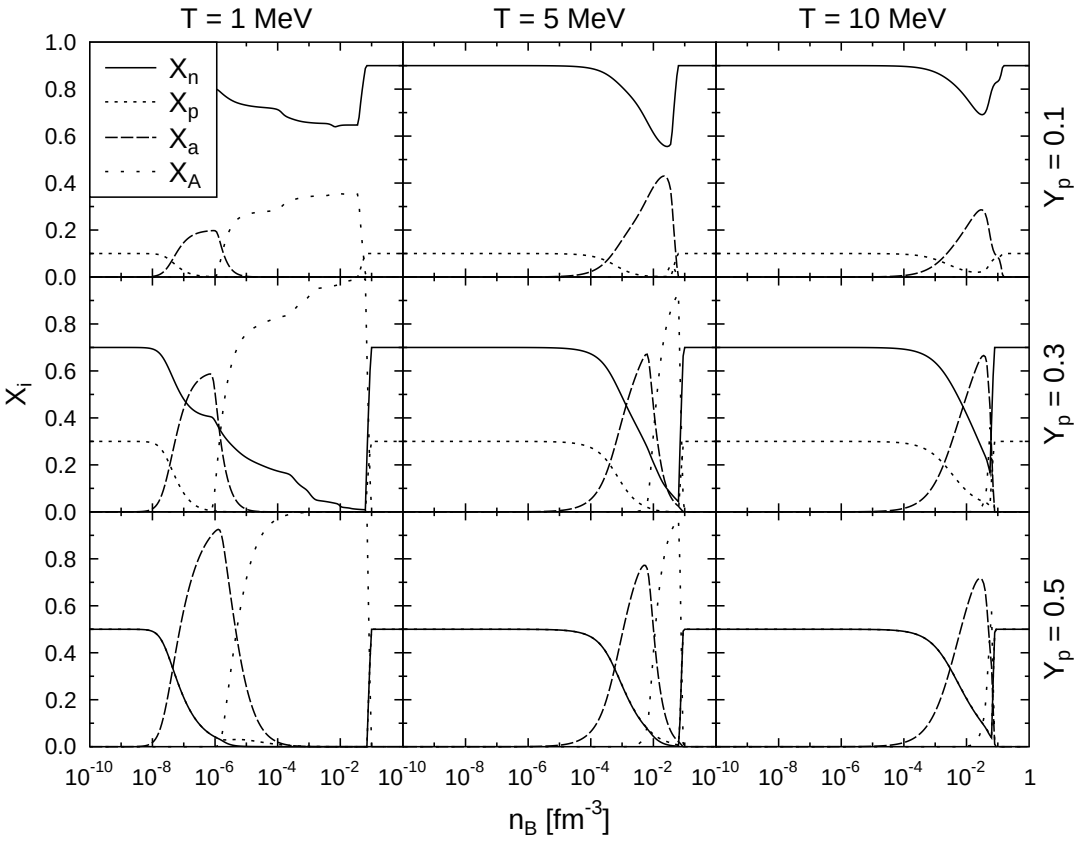

Figure 8.10: The mass fraction of free neutrons X_n, free protons X_p, light nuclei X_a, and heavy nuclei X_A, as a function of the baryon number density n_B. The columns show the different temperatures $T = 1, 5$, and 10 MeV (from left to right), the rows the proton fractions $Y_p = 0.1, 0.3$, and 0.5 (from top to bottom).

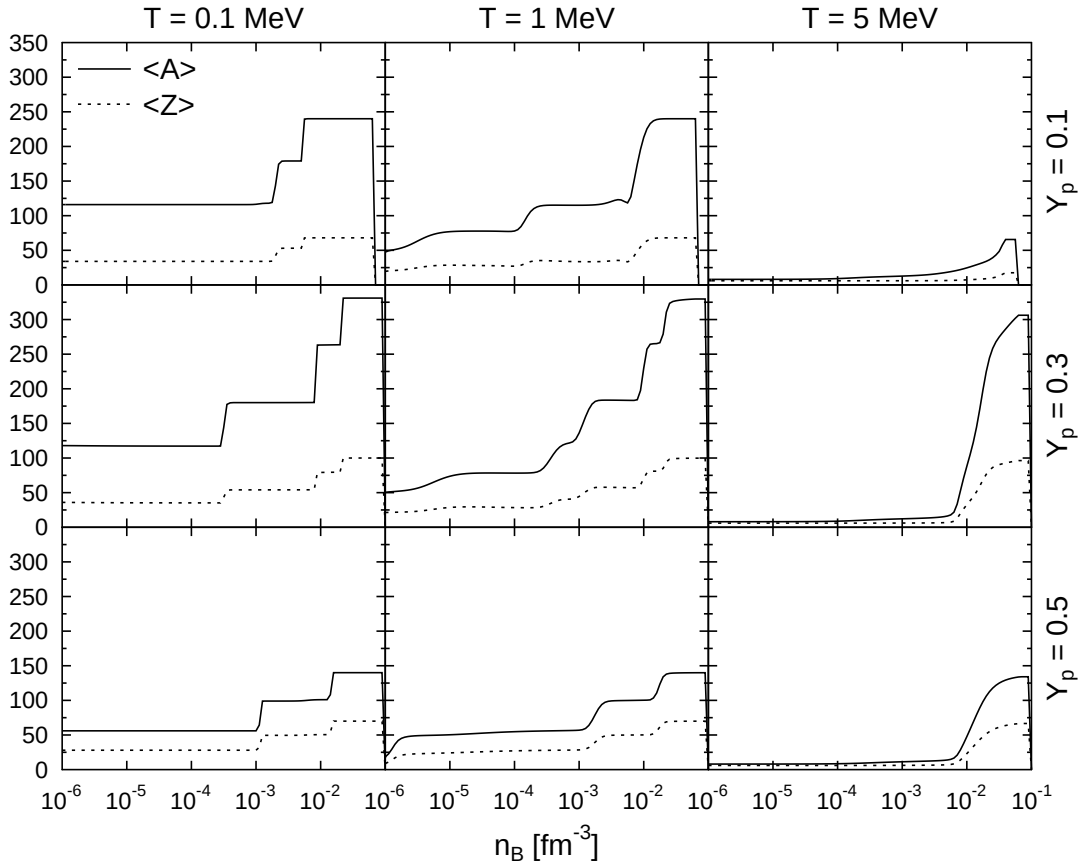

Figure 8.11: The average mass and proton numbers $< A >$ and $< Z >$ of heavy nuclei with $Z \geq 6$.

for $Y_p = 0.1$. The stepwise change of the fractions which can be seen for $Y_p = 0.1$ and 0.3 can be attributed to transitions between different nuclei which give the main contribution to the composition.

At a temperature of $T = 5$ MeV the free nucleon regime extends up to $n_B \sim 10^{-4}$ fm^{-3}. At larger densities the nucleons are successively replaced by light nuclei. For larger proton fractions there are sufficiently many protons in the system that finally all the nucleons can be bound to nuclei. Only in these cases a significant contribution of the heavy nuclei appears, shortly before uniform nuclear matter is reached. At a temperature of 10 MeV the overall composition looks similar. The onset of the light nuclei takes place at roughly the same density, but their presence extends up to higher densities. For $T = 10$ MeV heavy nuclei play only a minor role. Only for large Y_p heavy nuclei appear at all, and then only at densities slightly below the transition to uniform nuclear matter.

The chemical composition regarding the average mass and proton number of heavy nuclei is further analyzed in Fig. 8.11. Temperatures and densities are shown for which

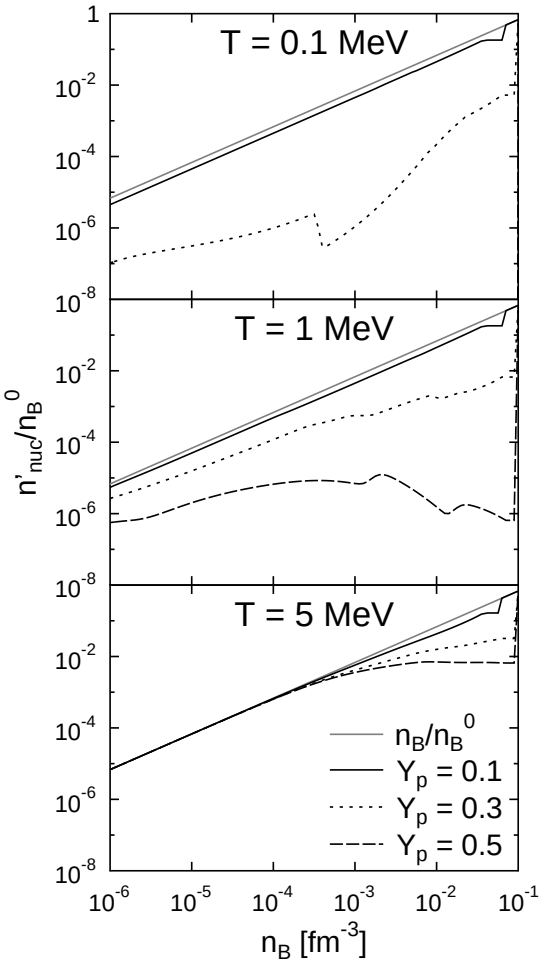

Figure 8.12: The local nucleon number density $n'_{nuc} = n'_n + n'_p$ outside of nuclei in units of the saturation density $n_B^0 = 0.147$ fm^{-3}. Grey lines show the total baryon number density.

their mass fraction is large (see Figs. 8.8 and 8.10). The first thing to note is the stepwise increase of $< A >$ and $< Z >$ for $T = 0.1$ and 1 MeV, which was already seen in Fig. 8.5 before. For such small temperatures the distributions of nuclei are narrow and $< A >$ and $< Z >$ are mainly given by one single nucleus. This causes also the steps in the mass fractions observed in Fig. 8.10 for $T = 1$ MeV. Shells effects are strong, as it comes out that most of these nuclei have neutron magic numbers 28, 50, 82, 126 or 184. This is in strong contrast to models which are based on the Thomas-Fermi approximation [STOS98a, STOS98b] or a liquid-drop parameterization [LD91b], which are not able to reproduce any shell effects. In these models the mass and charge number change continuously. By looking at the different values of Y_p shown in Fig. 8.11, we find that the largest nuclei appear for $Y_p = 0.3$. For $T = 0.1$ and 1 MeV a similar composition is found, differences appear only at low densities. For $T = 5$ MeV and densities below 10^{-2} fm^{-3}, where almost no heavy nuclei exist, the average heavy nucleus is ^{8}C, because it is the lightest nucleus with $Z = 6$. At larger densities, when the fraction of heavy nuclei increases, the nuclei grow in size. For this large temperature we observe a continuous change of the mass and charge number, indicating less pronounced shell effects and broad distributions.

In the present work the shell structure of nuclei is not modified by the medium. The results of Ref. [BMG07] show that the impact of the dense electron gas on nuclear properties is rather small. To estimate the role of free nucleons outside of the nuclei, their local number density $n'_{nuc} = n'_p + n'_n$ is depicted in Fig. 8.12. Only for $Y_p = 0.1$ or at a temperature of 5 MeV the free nucleon density exceeds $0.01 n_B^0$. In the latter case heavy nuclei are only abundant between 10^{-2} fm$^{-3} < n_B < 10^{-1}$ fm^{-3}. At larger temperatures the free nucleon density increases further, but then the heavy nuclei only play a minor role, see Fig. 8.10. At lower temperatures, more heavy nuclei exist in a broader range of density. But then the nucleon density is only significantly large, if the proton fraction is very low. In typical supernova simulations the proton fraction for most of the matter is actually rather high, $0.3 < Y_p$, supporting the neglect of the medium modifications of the nuclei due to the unbound nucleons.

Fig. 8.13 depicts the distributions of nuclei with respect to the mass number A. Here we are showing relative yields $Y_A = \sum_Z n_{A,Z} / \sum_{A,Z} n_{A,Z}$. At a temperature of 0.1 MeV the distributions are sharply peaked. We note that the distributions at $n_B = 10^{-3}$ fm^{-3} and 5×10^{-3} fm^{-3} lie on top of each other for this temperature. The mean value $< A >$ of the heavy nuclei with $Z \geq 6$ coincides with the peak of the distribution. In this case the single nucleus approximation should give almost identical results compared to the NSE description. In Fig. 8.14, which shows the neutron number distribution, one can see that the dominant nuclei at $T = 0.1$ MeV have the neutron magic numbers 126 or

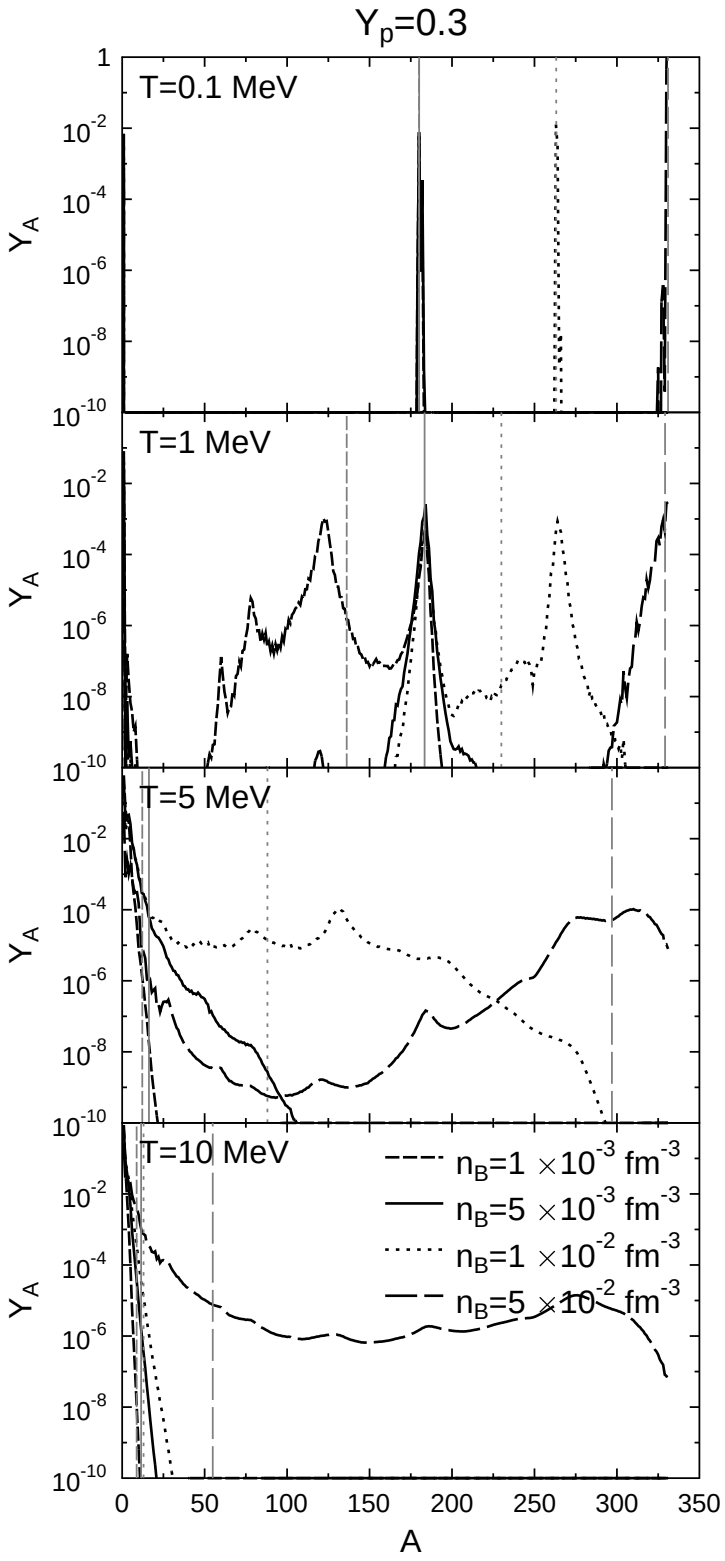

Figure 8.13: Mass distributions for selected temperatures and densities for $Y_p = 0.3$. Vertical lines show the average mass number $< A >$ of the heavy nuclei with $Z \geq 6$.

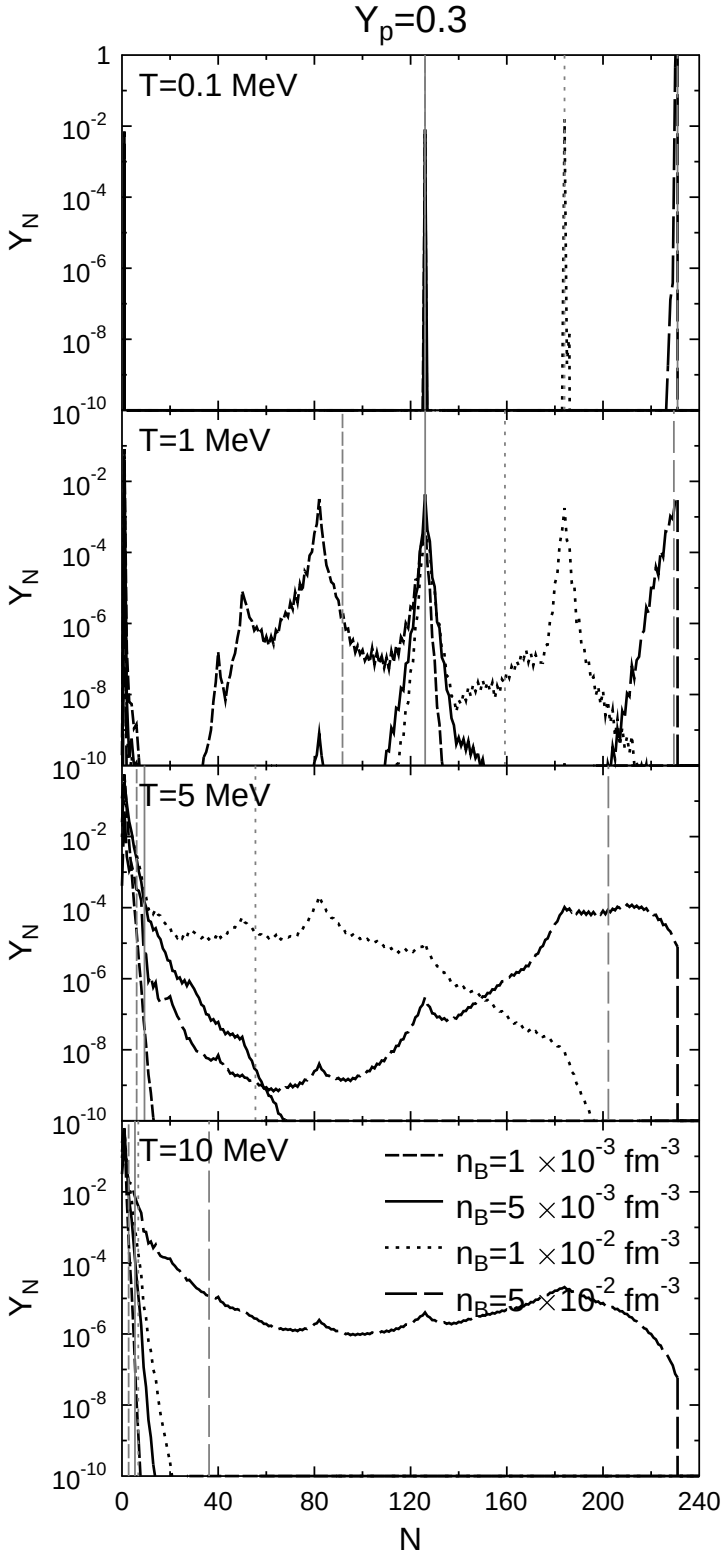

Figure 8.14: As Fig. 8.13, but now for the distribution of the neutron number N.

184. At $n_B = 5 \times 10^{-2}$ fm^{-3} the dominant nucleus is already at the border of the nuclear mass table and therefore no neutron magic number can be identified. At $T = 1$ MeV temperature effects become visible and the distributions broaden. The magic nuclei mentioned before ($N = 126$ and 184) are still strongly populated, but additional peaks appear. E.g. for $n_B = 10^{-3}$ fm^{-3} the strong peaks can be identified with the neutron magic numbers 50, 82 and 126. Nuclei with $N = 40$ also seem to be rather strongly bound in the model TMA. In general most of the peaks in the mass distributions can be assigned to neutron magic numbers. As was already found in Ref. [RHS06] for the outer crust of neutron stars, proton magic numbers do not play a significant role. The proton number determines the Coulomb energy of the nuclei. Thus the charge of the nuclei can not be adjusted as freely as their neutron number. Although for $T = 1$ MeV the distributions are still sharply peaked, because several peaks with similar yields appear, it would not be appropriate to use the mean values to describe the charge and mass distributions. E.g. at $n_B = 10^{-2}$ fm^{-3} the distribution shows two similar maxima, with the mean value $< A >$ lying in between. Compared to statistical models which are based on a liquid-drop formulation without shell corrections the typical Gaussian distributions are not found in the present work because the distributions are dominated by shell effects. In Ref. [BM08] a shell correction was included which resulted in a similar delta-function like distribution. At a temperature of 5 MeV, which is larger than the typical energy associated with shell effects, the neutron magic numbers are still visible, but much weaker. At large densities the distributions become very broad and extend over the whole nuclear chart. With increasing density the typical behavior expected at the liquid-gas phase transition line, compare with Fig. 2.5, can be identified, as it was also discussed in Ref. [BM08]. For $n_B = 10^{-3}$ fm^{-3} the distribution is an exponential. With increasing densities it changes to a flattening power-law. Finally at $n_B = 5 \times 10^{-2}$ fm^{-3} the distribution has the typical U-shaped form. For $T = 10$ MeV mainly light clusters are populated and the distributions are exponential. Only for the largest density which is shown, the U-shaped distribution is reached. This is again an indication for the onset of the liquid-gas phase transition. At this large temperature shell effects are almost not visible any more.

In Figure 8.15 we see the distribution of all nuclei in form of a chart of nuclides, for conditions which have also been shown in the two plots before. The color coding of the mass fraction gives a more qualitative overview of the entire distribution in proton and mass number. As we are in the neutron drip region, there is a strong neutron contribution, but the light nuclei are almost negligible for this low temperature. The neutron magic numbers $N = 82$ and 126 can be clearly identified, and the distribution drops of sharply for nuclei which have a proton fraction which is much different from

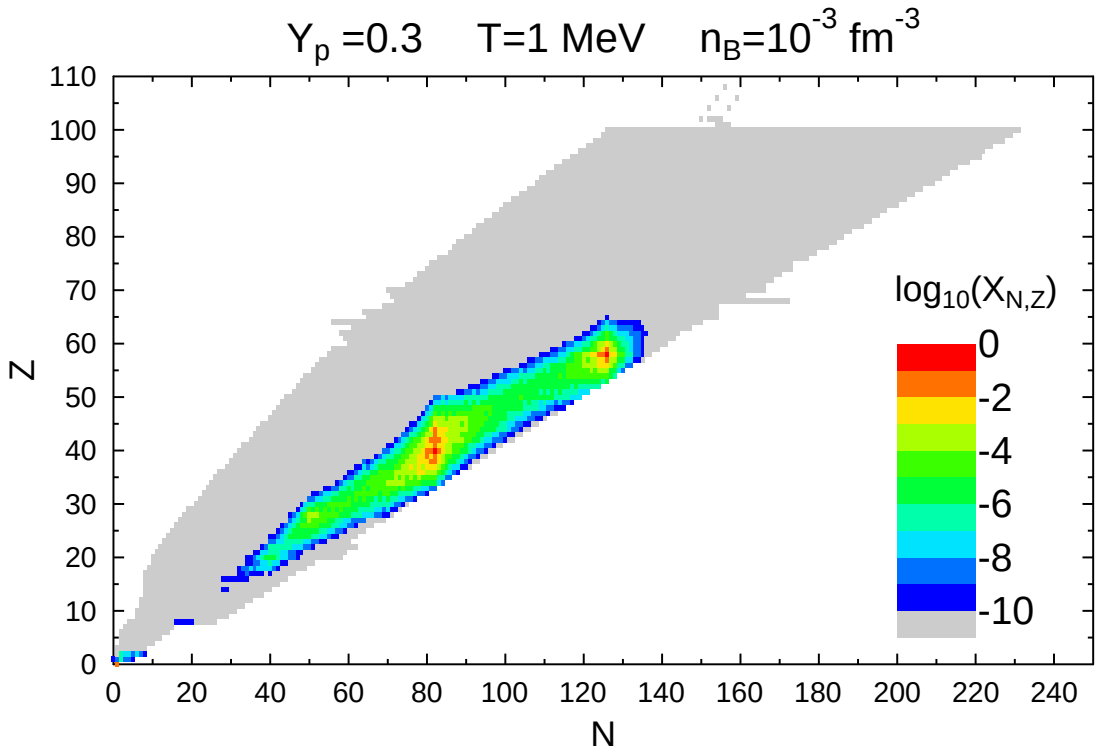

Figure 8.15: The mass fraction of nuclei in color coding in form of a chart of nuclides.

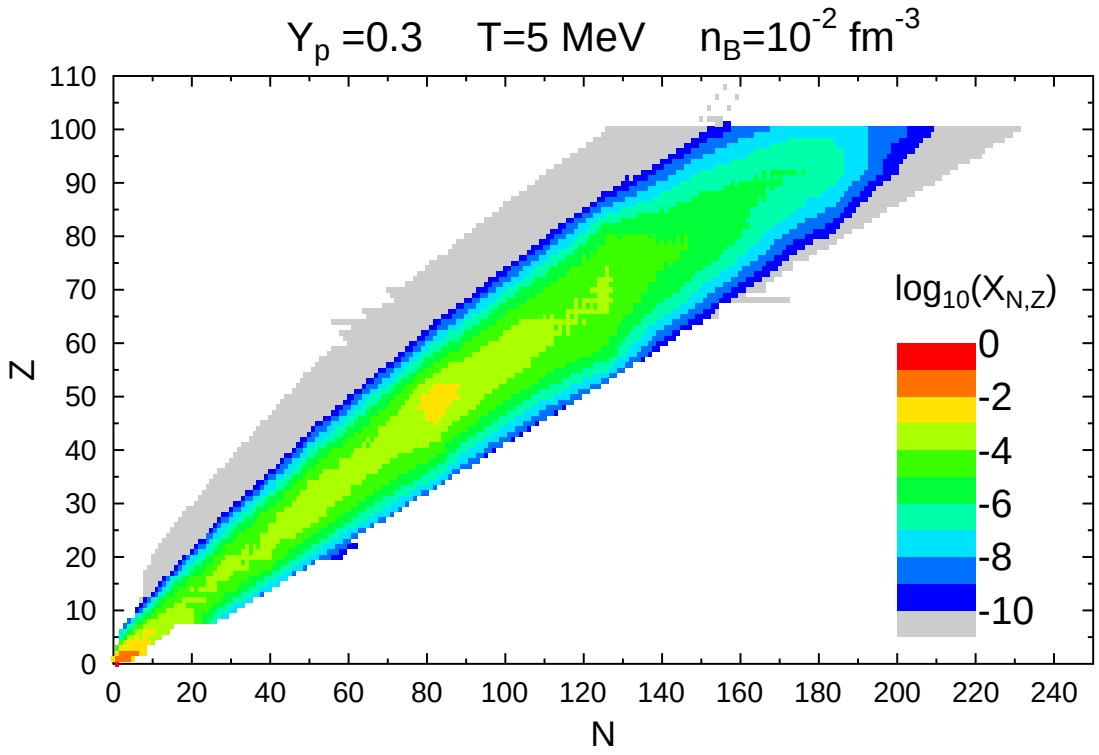

Figure 8.16: As Fig. 8.15 but for different thermodynamic conditions.

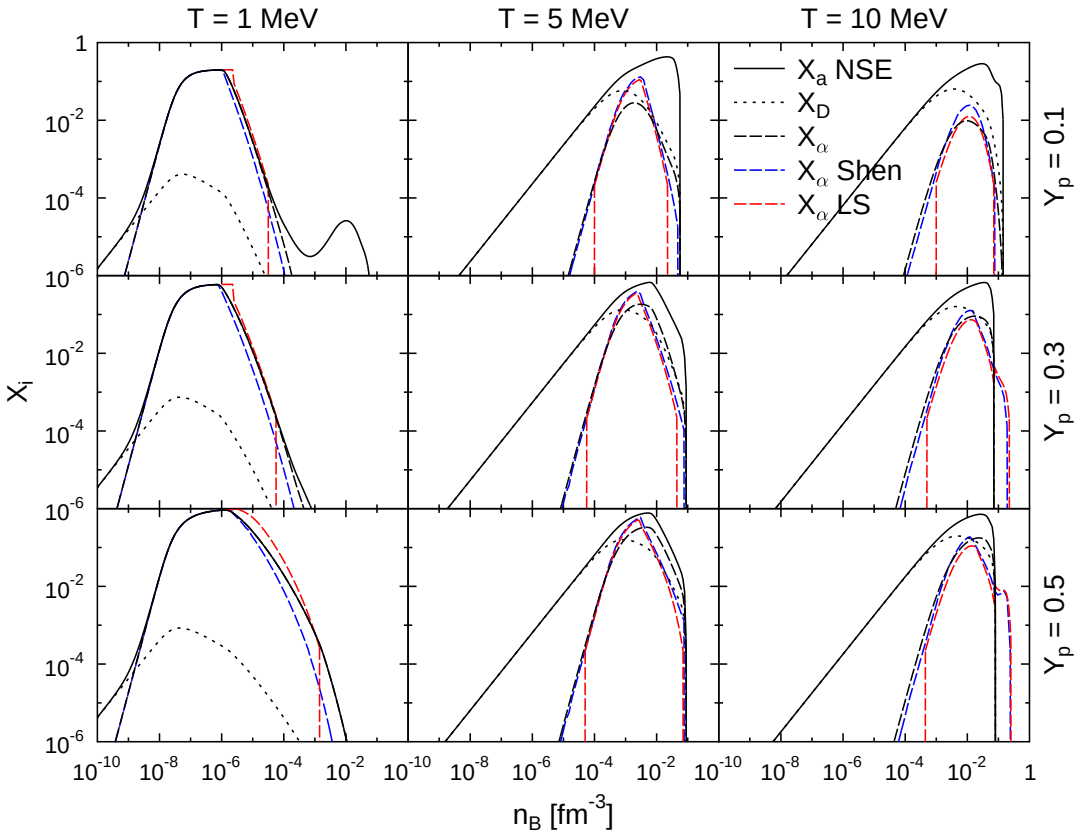

Figure 8.17: The mass fractions of all light nuclei with $Z \leq 5$ X_a (black solid lines), of alpha-particles X_α (black dashed lines), and of deuterons X_D (black dotted lines). Also shown is the alpha particle fraction of the EOSs of Shen et al. [STOS98a, STOS98b] (blue dashed lines) and of Lattimer and Swesty (LS) [LD91b] (red dashed lines).

0.3. In Figure 8.16 the density and temperature have been increased. The distribution becomes very broad and extends over the entire nuclear chart. Shell effects are almost not visible any more. In addition to the heavy and superheavy nuclei, there is still a big contribution of neutrons and light asymmetric nuclei.

The contribution of the light clusters is further analyzed in Fig. 8.17 and compared to the results of the LS and the Shen EOSs. At a temperature $T = 1$ MeV the light clusters are mainly α-particles in the region where they appear in large fractions. The three different models give very similar results for the alpha particle fraction, which thus coincides with the total light cluster fraction. With increasing temperature lighter particles are favored, leading to an increase of the deuteron fraction and a reduction of the α-particles. It is interesting to see, that for low densities the α-particle fraction is still very similar in the three models, even though in the NSE model the deuterons are more abundant. We can conclude that the formation of deuterons occurs through a reduction of unbound protons. For $T = 10$ MeV the deuteron mass fraction surmounts

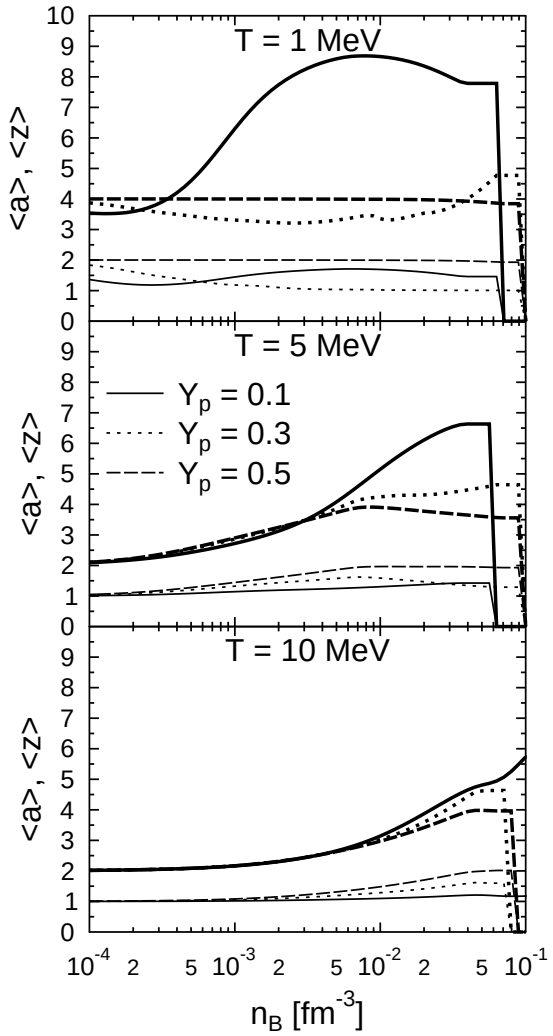

Figure 8.18: The average mass number $< a >$ (thick lines) and average proton number $< z >$ (thin lines) of the light nuclei with $Z \leq 5$.

the α-particle mass fraction at almost all densities. For $T = 5$ and 10 MeV and densities below 10^{-4} fm^{-3} the light clusters are almost exclusively deuterons, but at these densities the light cluster fraction is relatively small, $X_a < 0.01$. For the same temperatures but larger densities from $n_B = 10^{-4}$ fm^{-3} to saturation density not only alphas and deuterons are important, but rather the whole distribution of light nuclei. Then also notable differences of the alpha-particle fraction in the NSE model are observed.

The average mass and charge number of the light clusters are depicted in Fig. 8.18. Note that for $T = 1$ MeV the light nuclei fraction is actually small for the density range which is shown in Fig. 8.18. For symmetric matter at $T = 1$ MeV, the average light cluster is well represented by ^{4}He. For $Y_p = 0.3$, above 10^{-4} fm^{-3} the average mass $< a >$ and charge $< z >$ are in general smaller. Close to the transition to uniform nuclear matter very neutron-rich hydrogen isotopes are formed. The contribution of light, very asymmetric nuclei which form inside the free neutron gas for $Y_p = 0.1$ leads to the second increase of the light cluster fraction seen in Fig. 8.17 for $T = 1$ MeV and $Y_p = 0.1$. For $T = 5$ the light clusters are mainly deuterons at low densities. At larger densities, $< a >$ and $< z >$ again behave differently for different Y_p. For $Y_p = 0.1$ predominantly light clusters with low charge $Z = 1$ appear. With increasing density these hydrogen-isotopes become heavier and more asymmetric, with $< z > / < a > \sim 0.2$ before matter becomes uniform nuclear matter. With increasing Y_p clusters with a higher charge are populated which are more isospin-symmetric. Thus with increasing density, the mass does not increase as much as for low Y_p. The average mass and charge number for $T = 10$ MeV look similar as for 5 MeV, but the distributions are shifted to higher densities. Only above 10^{-3} fm^{-3} the deuterons are replaced by heavier particles. Again, the clusters become more symmetric and have larger proton numbers but lower mass when the proton fraction increases.

8.3.2 Equation of State

The thermodynamic potential for given (T, n_B, Y_p) is the Helmholtz free energy and all other thermodynamic quantities are derived from it. In Fig. 8.19 the total free energy density (including baryons, electrons/positrons and photons) is depicted. As the electron, positron and photon contribution is trivial, we also show the baryonic part of the free energy. We compare it to the results of LS [LD91b] and Shen et al. [STOS98a, STOS98b]. We do not use the routine of the LS EOS but their table for the potential model SkM* [BQB$^+$82], which is publicly available online. For the LS EOS the temperature of 10.67 MeV is shown, because no entry for $T = 10$ MeV exists in the chosen table and we do not want to use any interpolation here. We note

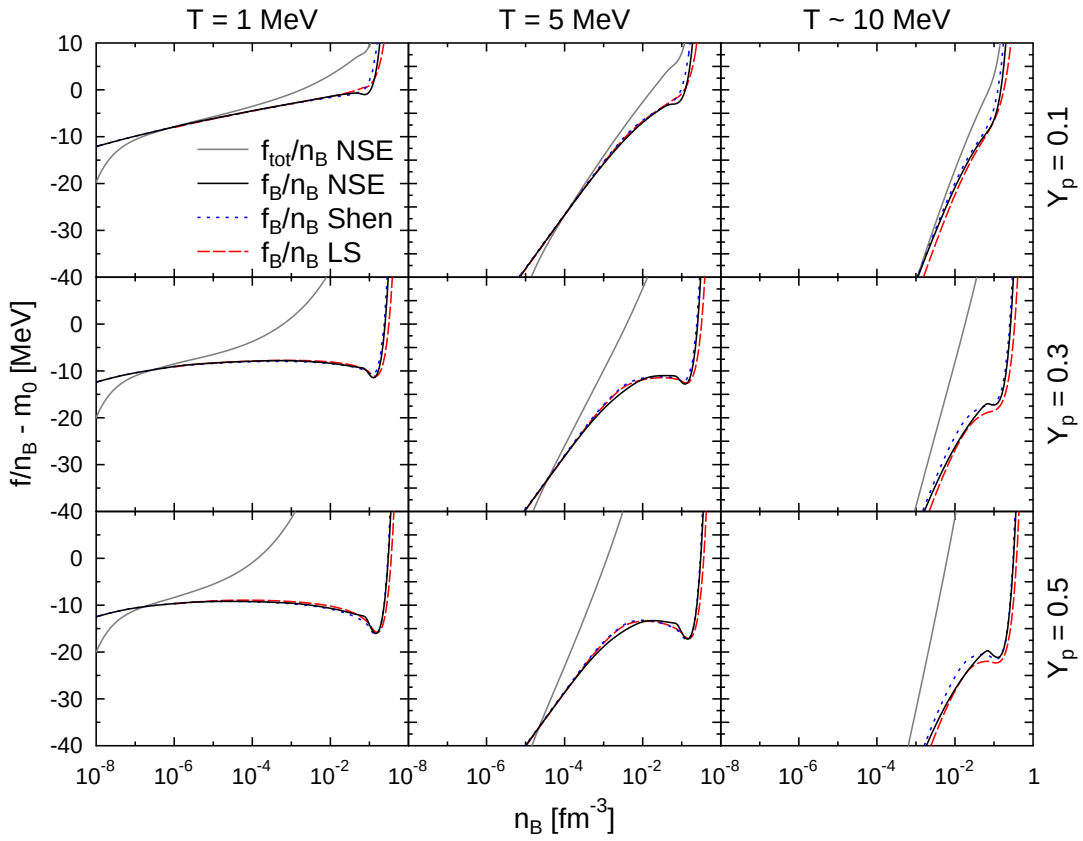

Figure 8.19: The baryonic contribution to the free energy (solid black lines) and the total free energy (solid grey lines) per baryon with respect to the rest mass. The model used in the present investigation (NSE) is compared to the results of Shen et al. [STOS98a, STOS98b] (blue dotted lines) and of Lattimer and Swesty (LS) [LD91b] (red dashed lines).

that the Shen EOS has a higher incompressibility, K =281 MeV, and symmetry energy, a_{sym} = 36.9 MeV, than the LS EOS, which has K =217 MeV and a_{sym} = 31.4 MeV. Thus the Shen EOS represents a stiffer EOS with a higher maximum mass for a cold deleptonized neutron star, $M_{max} = 2.2$ $M_\odot$ [STOS98a], than the LS EOS, $M_{max} = 1.62$ $M_\odot$ [SR07].

It is important that the three different models are based on very different model assumption for the description of non-uniform nuclear matter, as described in the introduction. Furthermore, they use different models for the nuclear interactions with different nuclear matter properties (e.g. saturation density, compressibility, symmetry energy). For the shown temperatures and proton fractions, up to densities of $\sim 10^{-4}$ fm^{-3} the free energies of the three models are almost identical. Above saturation density the different properties of uniform nuclear matter become visible. The RMF model TMA used in the statistical model is more similar to the Shen EOS, which is also based on a RMF model, but on the different parameterization TM1. In the intermediate density range the differences in Fig. 8.19 are small and of similar size as the differences between the EOSs of LS and Shen. It is a surprising result that the present, 'non-microscopic' model is able to give a reasonable description regarding the equation of state across all densities.

One certain feature of the NSE description can be observed at large temperatures, e.g. at $T = 5$ MeV: Although the free energy of uniform nuclear matter is rather large, the free energy is lower than in both of the two single nucleus approximation-models at 10^{-3} fm^{-3} $< n_B < 10^{-2}$ fm^{-3}. As can be seen in Fig. 8.13 the distributions develop from a steep exponential to a very flat power-law shape in this density region. At the beginning of this transition the light clusters become very abundant, see Fig. 8.17. Besides a large fraction of α-particles and deuterons all of the light clusters contribute to the composition. Later we will give further evidence that it is the contribution of light clusters in the NSE model which leads to the reduction of the free energy as seen in Fig. 8.19. In the other two EOSs only α-particles are considered and this behavior can not be observed. However, as was shown in Fig. 8.12, the free nucleon density is rather large under these conditions, so that medium effects could lead to changes in the composition. We will address this aspect further in Subsection 8.6. For a low temperature of 1 MeV there are no systematic differences between the three different models. As can be seen from Fig. 8.17 here the light clusters are very well described by α-particles, which are included in all three models. At $T = 10$ MeV the differences of the different models are in general more pronounced. The lowered free energy of the statistical model is still present, but shifted to slightly larger densities $\sim 10^{-2}$ fm^{-3}.

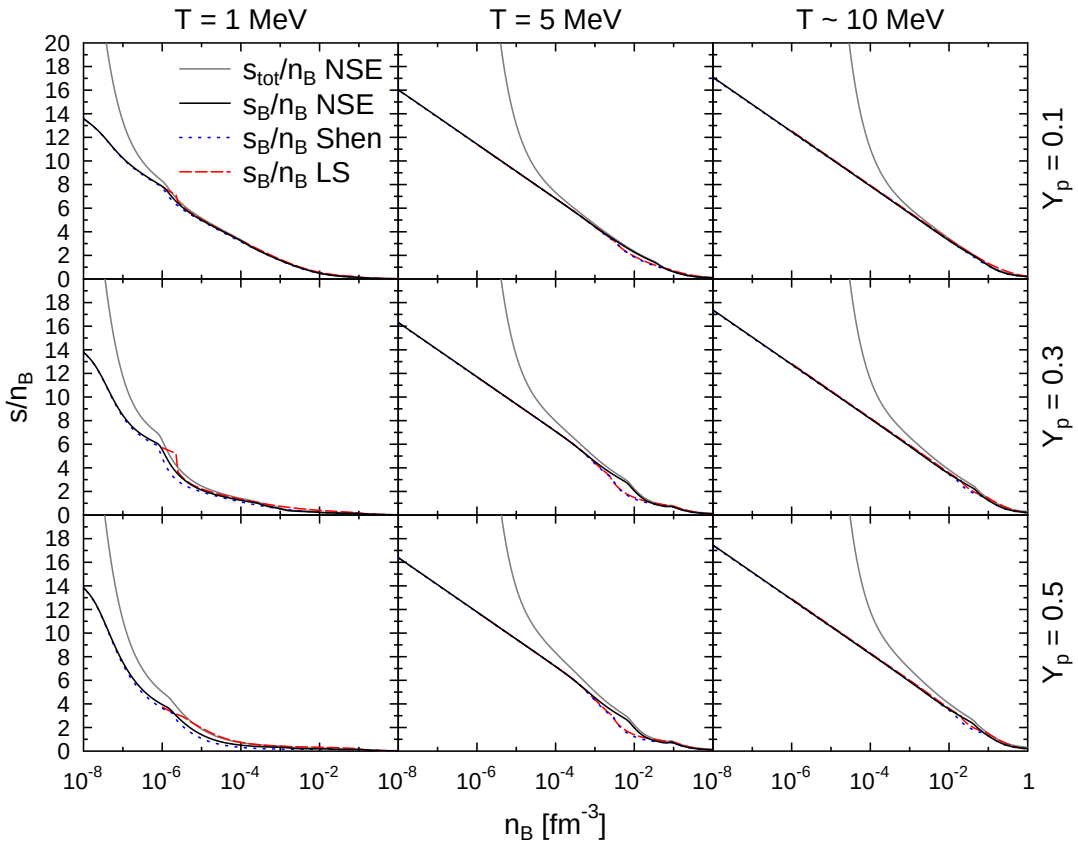

Figure 8.20: As Fig. 8.19, but now for the entropy per baryon.

At densities larger than $\sim 10^{-2}$ fm^{-3} the statistical model has a higher free energy than the other two models. Here the nuclear mass table and the description of the transition to uniform nuclear matter is too restrictive, as the nuclei can not grow arbitrary in size and are limited in Z/A. The kinks in the baryonic contribution which are visible around $\sim 10^{-1}$ fm^{-3} come from the Maxwell-construction which is used here. A Gibbs-construction in which the requirement of local proton fraction conservation would be replaced by global conservation of the proton fraction (as discussed in Sec. 8.2.6) would lead to a more continuous transition with an earlier onset of the uniform nuclear matter phase and a lower free energy. At large temperatures $T \geq 10$ MeV and very low Y_p the transition is smoother, as expected from the discussion of Fig. 8.7, because in this case the contribution of nuclei is low and the non-uniform matter phase behaves very similar to uniform nuclear matter. In contrast, for $Y_p = 0.5$ and $T = 1$ MeV the kink in the baryonic free energy becomes most strongly pronounced. However, these kinks disappear in the total free energy per baryon, when the electrons are added to the baryons. The total free energy and its first derivatives behave continuously, as discussed before and as we will also show in the following.

Fig. 8.20 depicts the entropy per baryon. All models give very similar results for $T = 1$ MeV. The bump around $n_B = 10^{-6}$ fm^{-3} which is most dominant at $Y_p = 0.3$ arises when the large light cluster contribution (mostly alphas) is replaced by heavy nuclei. There the LS EOS shows a rather abrupt change in the entropy. At larger temperatures, the entropy behaves almost like the one of an ideal gas with $s/n_B \propto -ln(n_B) + const.$. Only above $n_B \sim 10^{-4}$ fm^{-3} deviations from the ideal gas behavior appear, when light clusters are formed.

For higher temperatures at densities around $\sim 5 \times 10^{-3}$ fm^{-3} for $T = 5$ MeV and $\sim 5 \times 10^{-2}$ fm^{-3} for $T = 10$ MeV the entropy is significantly higher in the statistical model. As noted before, the whole distribution of light and intermediate clusters is important here and leads to the increased entropy. This increased number of available states is the reason for the lower free energy discussed before.

For comparison also the total entropy is shown in Fig. 8.20. No discontinuities are observed, as expected. The total entropy enables to identify the regions where the nontrivial baryonic contribution is important at all. It is shown only for the statistical model, because the leptons and photons are treated identical in all three models. At densities below 10^{-7} fm^{-3} for $T = 1$ MeV, 10^{-5} fm^{-3} for $T = 5$ MeV, and 10^{-4} fm^{-3} for $T = 10$ MeV, the electron-positron plasma determines the entropy almost completely. But at larger densities it is the baryon contribution which gives the largest contribution to the entropy, and electrons, positrons and photons are negligible. In this density range the different descriptions of the different models become important. Thus we conclude that regarding the entropy the different results for the baryonic EOS also affect the total EOS.

Fig. 8.21 shows the binding energy per baryon, which is directly given by the entropy and the free energy ($\epsilon = f + Ts$). In the third column of Fig. 8.21 the energy density of the LS EOS is higher at low densities, because it is shown for the slightly larger temperature of 10.67 MeV, as mentioned before. At lowest densities the ideal gas limit $\epsilon = 3/2 n_B T$ is reached in all three models. At $T = 1$ MeV the fraction of heavy nuclei becomes already important above $n_B \sim 10^{-8}$ fm^{-3}. Their binding energy leads to a decrease of the baryonic energy density. At $T = 5$ and $T = 10$ MeV the nuclear interactions become visible above $n_B \sim 10^{-4}$ fm^{-3}. In general, the maximum binding energy is achieved close to saturation density.

In the NSE model, around 10^{-2} fm^{-3} for $T = 5$ MeV, the slightly lower free energy is more than compensated by the increased entropy and therefore the energy density becomes larger than in the other two EOSs at these densities. The apparent differences are even more significant than for the free energy and the entropy, because in the ex-

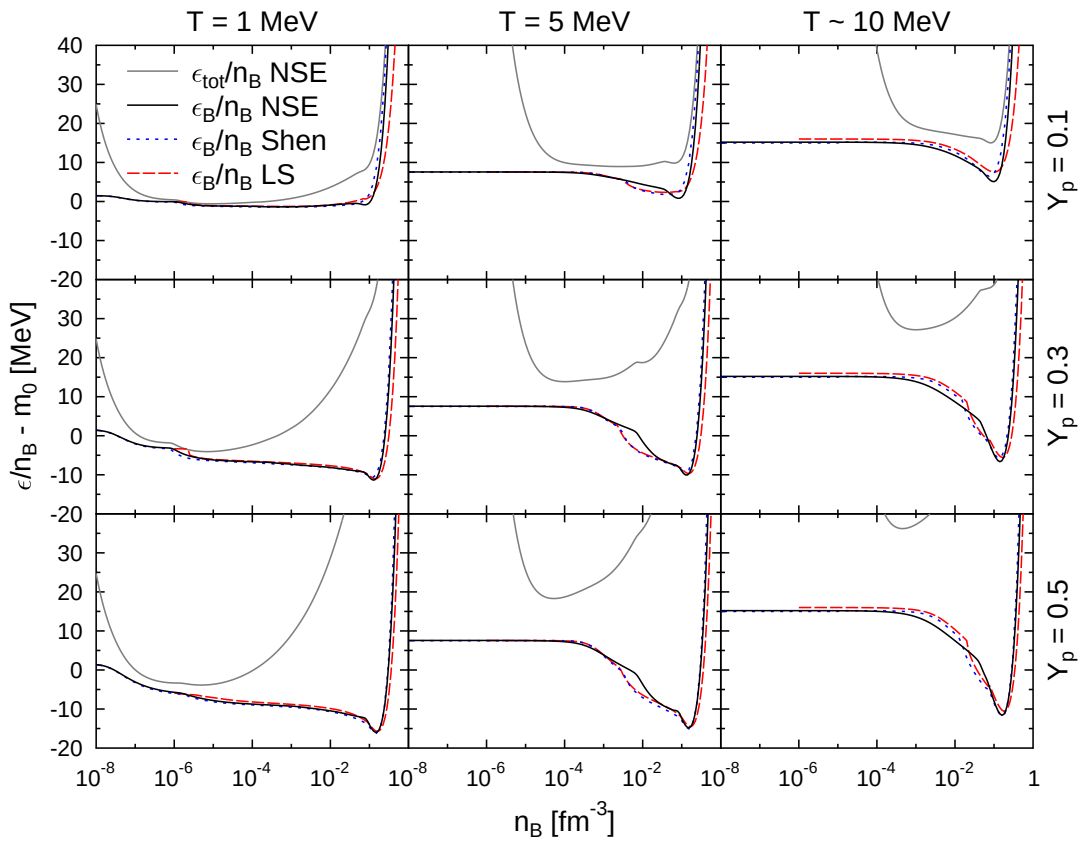

Figure 8.21: As Fig. 8.19, but now for the binding energy per baryon.

pression for the energy density, $\epsilon = f + Ts$, the difference in the entropy is multiplied by the temperature. For $T = 10$ MeV and densities between 10^{-3} and 10^{-2} fm^{-3} the energy density is decreased by roughly 2 MeV in the NSE model. By comparing with Fig. 8.17 one sees that the deuterons and some other light cluster give a strong contribution to the composition and lead to additional binding. Above 10^{-2} fm^{-3} the same increase of the energy density as for $T = 5$ MeV is observed, but is less pronounced.

As can be seen from Fig. 8.21 the baryons are most important for the total energy density at intermediate and very large densities. Again, at low densities, because of the high temperatures, the electron-positron-plasma gives the largest contribution. At larger densities where the positrons have vanished the electrons become degenerate and their energy density rises faster than the one of the attractive nuclear interactions. Obviously, the number density of electrons and their energy density directly depends on the proton fraction Y_p. Thus the baryonic contribution becomes more significant for low Y_p. Above saturation density the nuclear interactions become strongly repulsive and take over to dominate the energy density. The bumps in the nuclear binding energy which appear below saturation density can still be identified in the total energy density.

In Fig. 8.22 the baryonic contribution to the pressure is depicted. It is divided by the baryon density and the temperature is subtracted to see the deviations from the ideal gas pressure more clearly. Presented in this way, the differences of the three different models become very pronounced. The onset of the nuclear interactions appears similarly as in the case for the energy density. At $T = 1$ MeV and high proton fractions an increasing fraction of nucleons is bound to heavy nuclei, which grow in size with density, leading to a decreasing pressure. For larger temperatures nuclei become important only at larger densities. The baryonic contribution to the total pressure is important in the same density range as discussed for the energy density. Though the baryonic pressure is negative in many cases, the total pressure is always positive.

At $T = 1$ MeV and around $n_B = 10^{-1}$ fm^{-3} the pressure increases. Here, matter consists almost exclusively of heavy nuclei. Now the densities are so large that the excluded volume effects significantly increase the pressure of the nuclei, see Eq. (8.39). At even higher densities the "repulsive" excluded volume corrections become so strong, that the transition to uniform nuclear matter takes place. The drop in the pressure (most clearly seen for $Y_p = 0.5$) arises from the Maxwell construction. In the two other EOSs the transition to uniform nuclear matter is described very differently, and thus the behavior of the baryonic pressure is different, too.

The baryonic part of the total pressure is depicted in Fig. 8.23. Here, the pressure is not divided by the baryon density, as done in Fig. 8.22. Now one sees that the

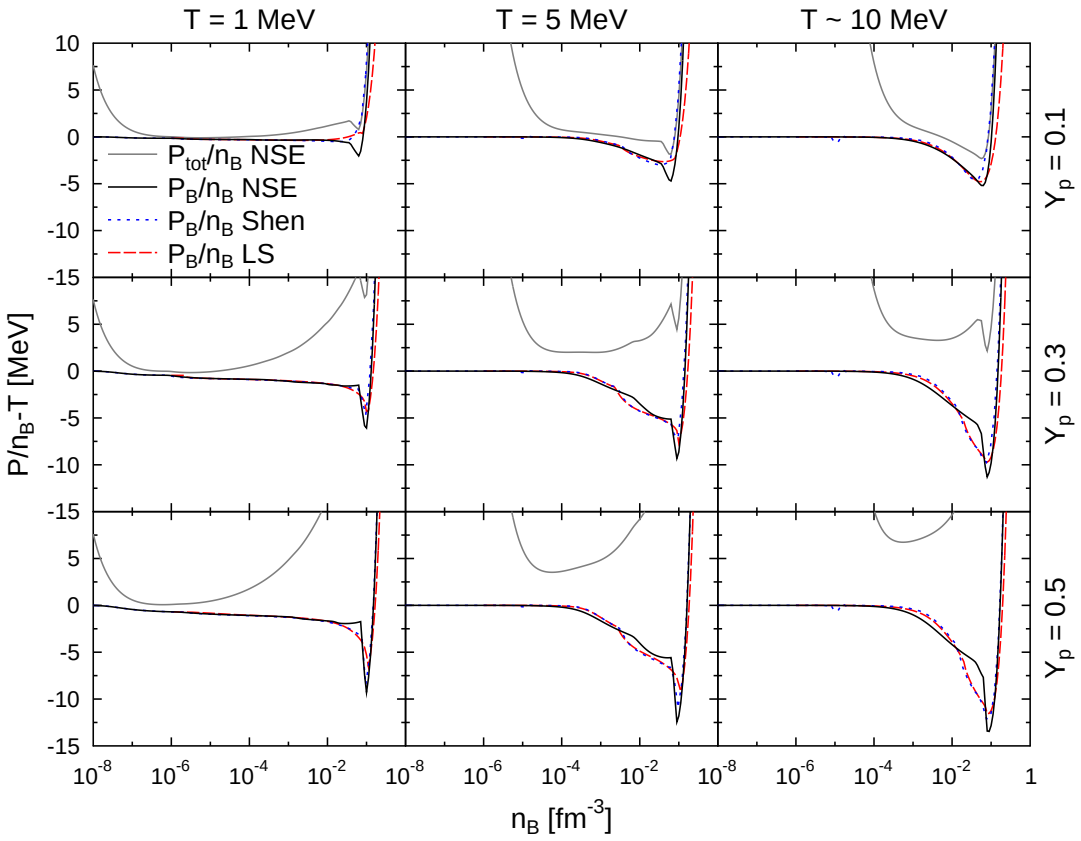

Figure 8.22: As Fig. 8.19, but now for the pressure divided by the baryon density and with the temperature subtracted, to show the deviations from the ideal gas pressure more clearly.

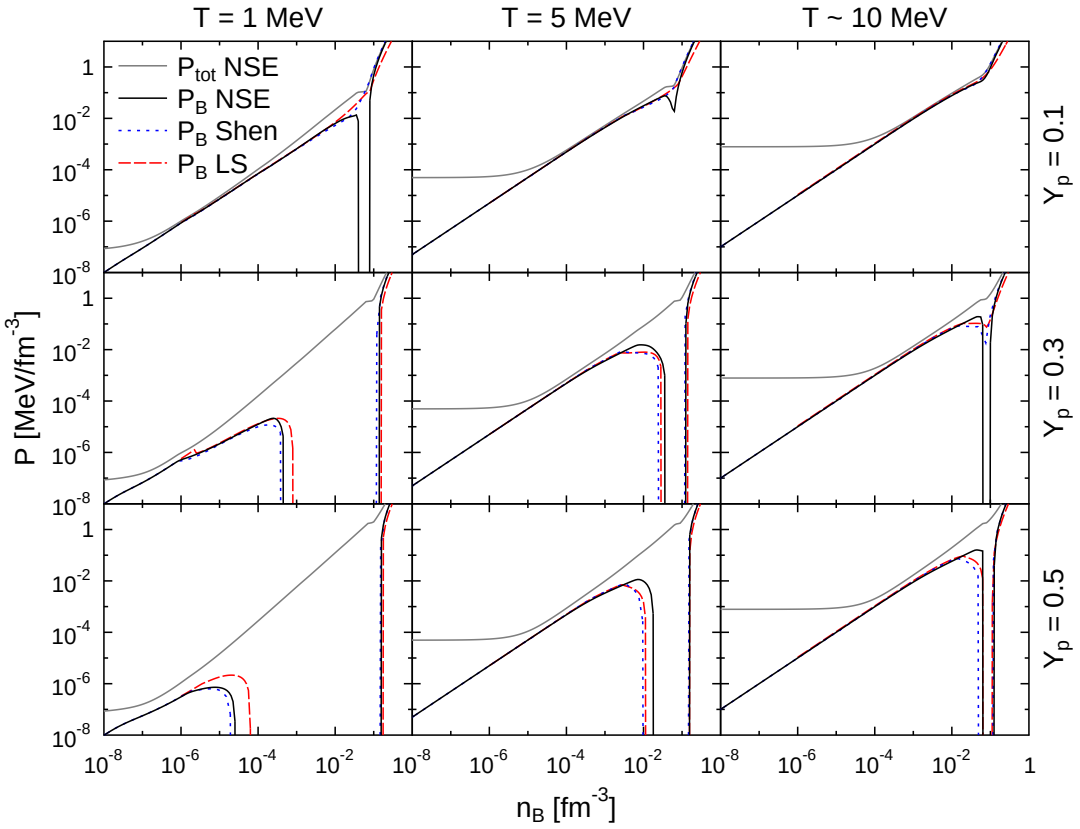

Figure 8.23: As Fig. 8.19, but now for the pressure.

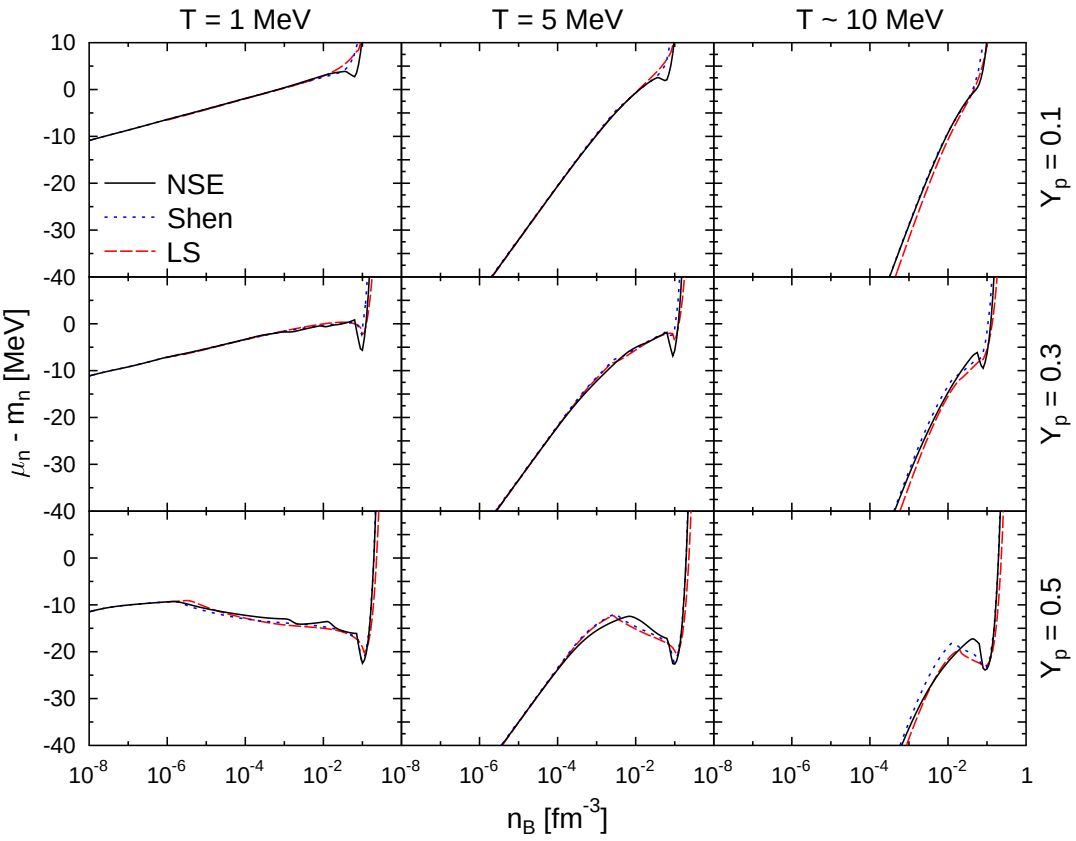

Figure 8.24: As Fig. 8.19, but now for the neutron chemical potential with respect to the neutron rest mass.

total pressure remains constant during the Maxwell transition. This appears as a sharp pressure drop across the transition if not the pressure but $P/n_B - T$ is plotted. The use of a Gibbs-construction with non-locally fixed Y_p would result in a strictly increasing pressure.

The neutron chemical potential is shown in Fig. 8.24, the proton chemical potential in Fig. 8.25. At $T = 1$ MeV the non-monotonic behavior of the chemical potentials of the NSE model is striking. It comes from the rather discontinuous change in the mass and charge number of the heavy nuclei, as temperature effects are weak, see also Figs. 8.11 and 8.13. Besides this, similar results are found as for the other thermodynamic variables. For $T = 5$ MeV around $n_B \sim 10^{-3}$ fm^{-3} the chemical potentials are lower, especially the proton chemical potential at low Y_p. We attribute this to the strong contribution of the light clusters besides alphas. At $T = 10$ MeV this effect happens at $n_B \sim 10^{-2}$ fm^{-3}. At larger densities the excluded volume effects become important and lead to increased chemical potentials until the phase transition sets in. Here the Maxwell construction is visible as a rather sharp drop in the chemical potentials, especially pronounced for the proton chemical potential. In our mixed phase construction, only the

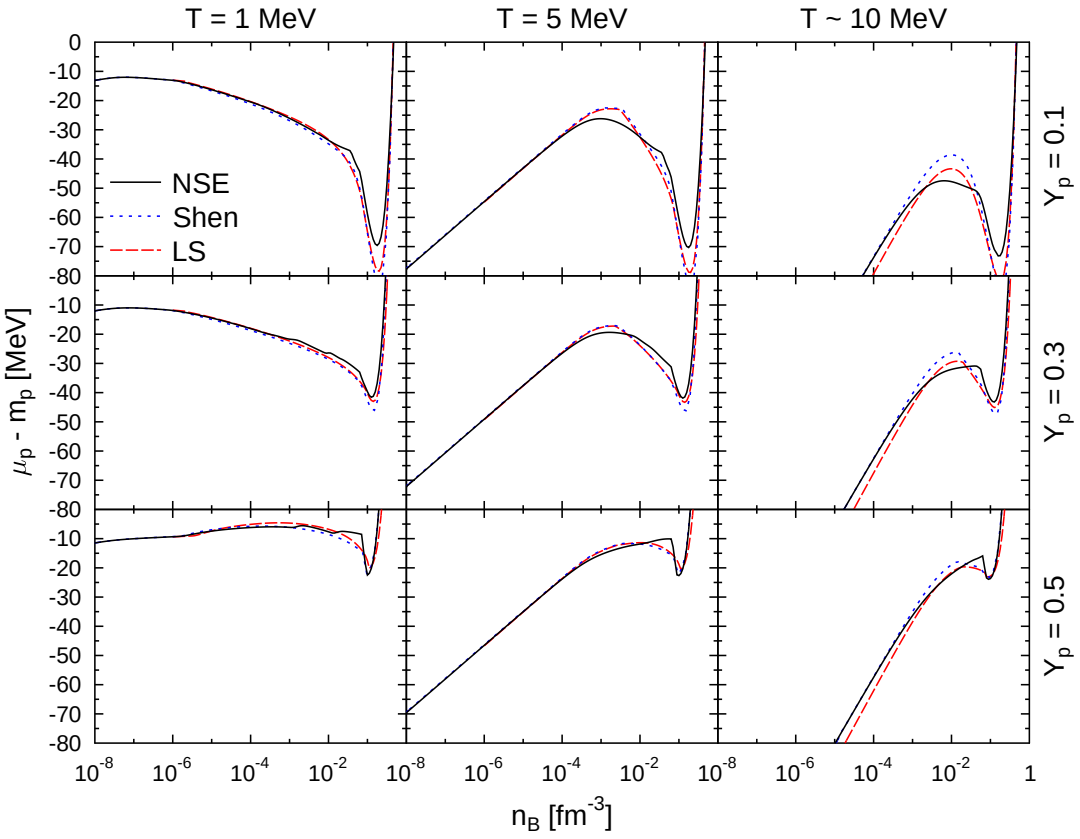

Figure 8.25: As Fig. 8.19, but now for the proton chemical potential with respect to the proton rest mass.

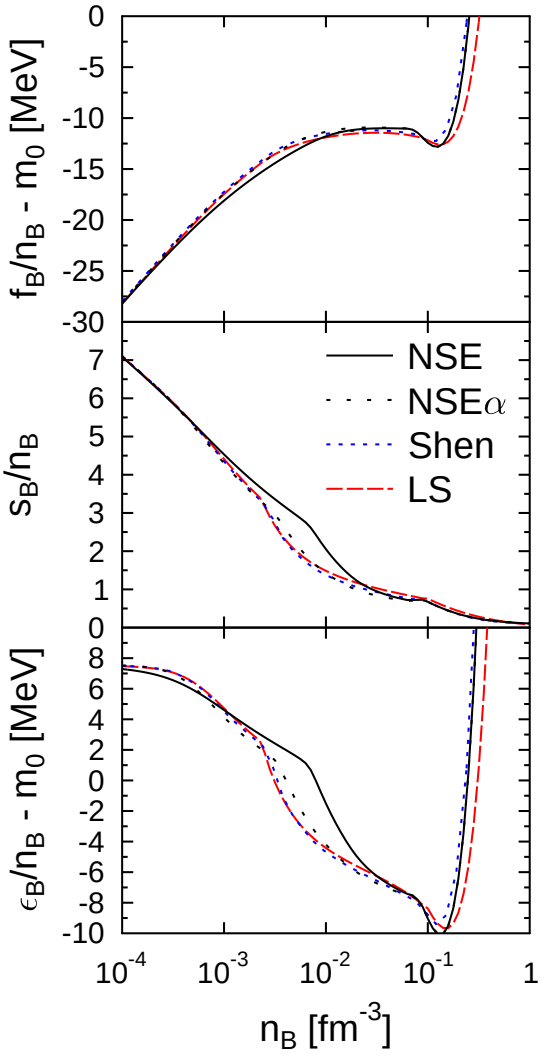

Figure 8.26: The baryonic contribution to the free energy, entropy and energy per baryon as a function of n_B for $T = 5$ MeV and $Y_p = 0.3$. "NSEα" shows the results if all light clusters with $A < 20$ besides α-particles are taken out from the NSE calculation.

total baryon chemical potential for locally fixed Y_p and local electric charge neutrality, $\mu_B = (1-Y_p)\mu_n + Y_p(\mu_p + \mu_e)$, is equal in the two phases and remains constant across the transition, see Chapter 7. The drop of μ_n and μ_p across the transition is compensated by the quickly increasing electron chemical potential μ_e.

To address the origin of the found deviations of the NSE model from the LS and Shen EOS further, the equation of state is shown if all nuclei with $A < 20$ besides nucleons and alphas are taken out in Fig. 8.26. Now one sees that most of the additional entropy and energy density can indeed be attributed to the light clusters. The decrease of the free energy compared to the other two EOSs between $n_B = 10^{-3}$ fm^{-3} and $n_B = 10^{-2}$ fm^{-3} is not visible any more. The increase of the free energy before the transition to

uniform nuclear matter still remains, as it is caused by different reasons (limitation of A and Z/A because of the use of a mass table). Anyhow, by looking at the energy density and the entropy in Fig. 8.26 one observes that some smaller deviations around $n_B \sim 3 \times 10^{-3}$ fm^{-3} remain. The remaining differences are much less pronounced.

8.4 Comparison with the Statistical Multifragmentation Model

The Statistical Multifragmentation Model (SMM) was mainly developed to interpret experimental data on multiple fragment production in different nuclear reactions [BBI+95] and is one of the most established models for this part of nuclear research. Furthermore it is also applied in the context of core-collapse supernovae [BM04, BM05, Mis08, BM08]. In this section we want to compare our results with the SMM model.

The SMM model uses the following liquid-drop parameterization of the nuclear masses for nuclei with $A > 4$:

$$F_{AZ}(T,\rho) = F^B_{AZ} + F^S_{AZ} + F^{\mathrm{sym}}_{AZ} + F^C_{AZ} \,, \tag{8.58}$$

where the different terms denote the bulk, surface, symmetry and Coulomb energies. The first three terms are taken in the following form

$$F^B_{AZ}(T) = \left(-w_0 - \frac{T^2}{\varepsilon_0}\right) A \,, \tag{8.59}$$

$$F^S_{AZ}(T) = \beta_0 \left(\frac{T_c^2 - T^2}{T_c^2 + T^2}\right)^{5/4} A^{2/3} \,, \tag{8.60}$$

$$F^{\mathrm{sym}}_{AZ} = \gamma \frac{(A-2Z)^2}{A} \,, \tag{8.61}$$

where $w_0 = 16$ MeV, $\varepsilon_0 = 16$ MeV, $\beta_0 = 18$ MeV, $T_c = 18$ MeV and $\gamma = 25$ MeV are the model parameters which are extracted from nuclear phenomenology and provide a good description of multifragmentation data. The Coulomb energy is taken in a similar form as Eq. (8.6). Nuclear excited states are not taken into account explicitly. Instead there is a temperature dependent part of the nuclear binding energies, with a separate volume and surface contribution. Shell effects are not included, but in fact they are expected to be weak at the large temperatures for which this model is designed for. One of the purposes of the SMM is that it allows to include arbitrary heavy nuclei and that it is easy to modify to explore certain aspects of the nuclear interactions. In the SMM nuclei are treated as an ideal Maxwell-Boltzmann gas. It also contains an excluded volume correction, which is equivalent to our formulation at low densities.

As a first comparison we chose in Fig. 8.27 a rather low density of $10^{-6} n_B^0$ at $Y_p = 0.4$ and $T = 1$ MeV. Under these conditions, the main contribution is coming from nucleons and alpha particles, and the two models give similar results. In the SMM only for deuterons, helions, tritons and alphas the experimental binding energies are

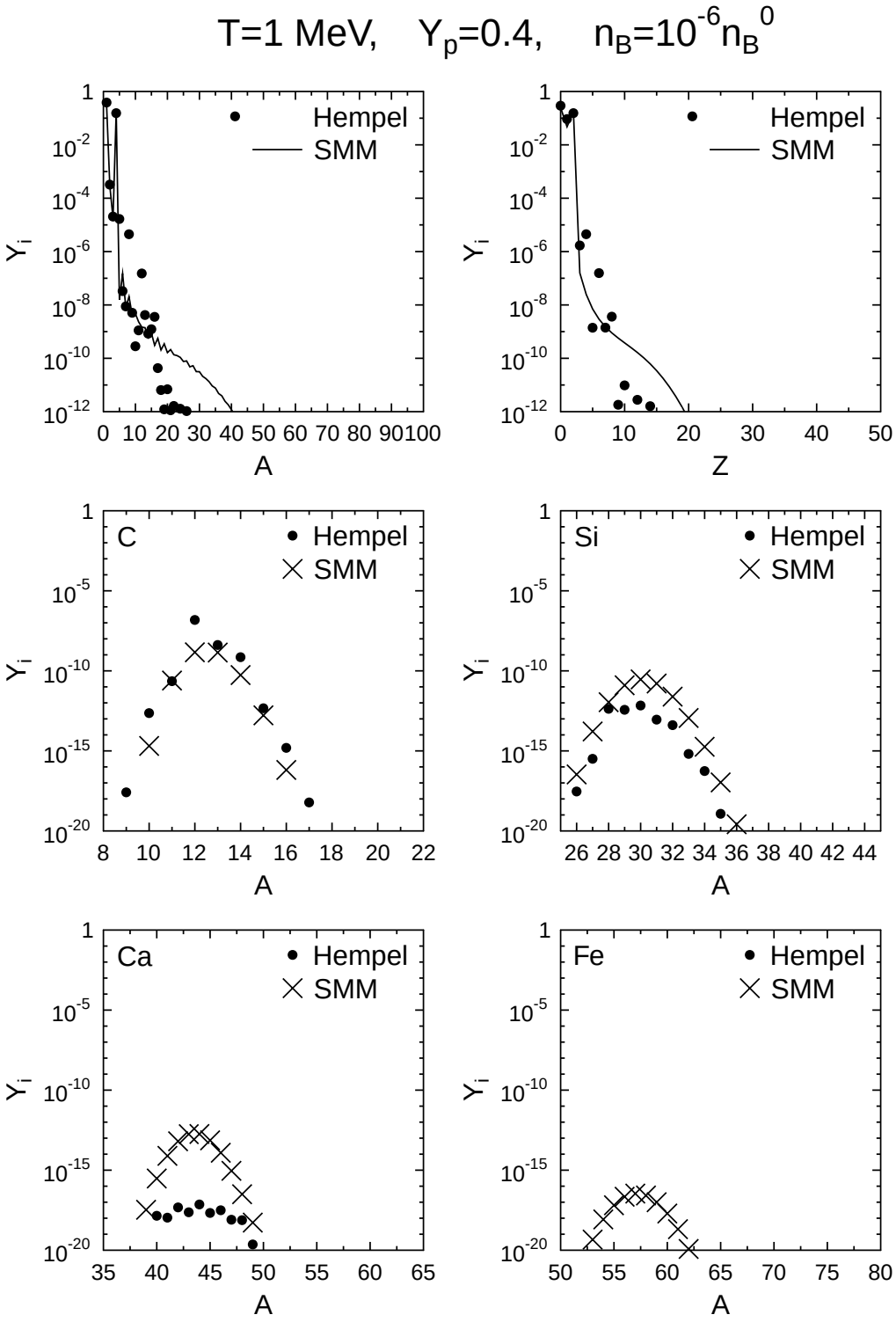

Figure 8.27: Comparison of the excluded volume NSE model with the SMM model [BBI$^+$95, BM04, BM05, Mis08, BM08] at $T = 1$ MeV, $Y_p = 0.4$ and $n_B = 10^{-6} n_B^0$. The upper left panel shows the summed yields of nuclei with mass number A, the upper right of nuclei with charge number Z. The lower four panels show the isotope distributions of $_6$C, $_{14}$Si, $_{20}$Ca, and $_{26}$Fe.

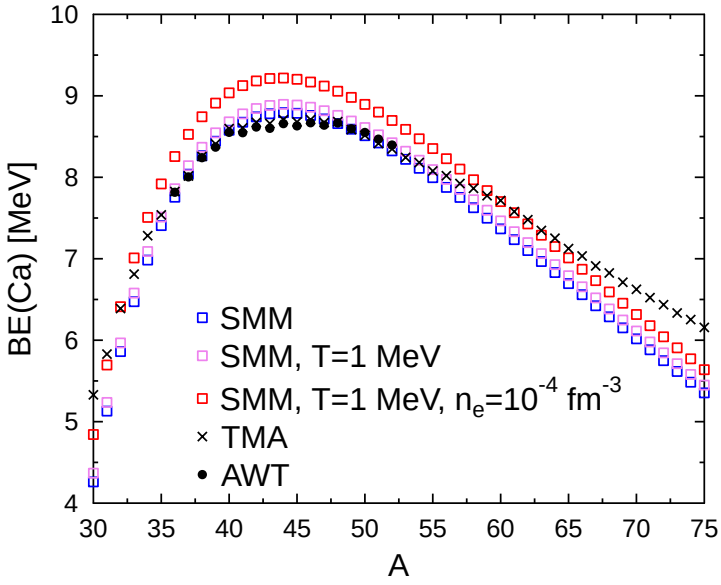

Figure 8.28: The binding energy per nucleon of calcium isotopes. Blue squares show the liquid drop formula of the SMM model of Ref. [BM08] at $T = 0$ and without electron background, violet squares at $T = 1$ MeV and red squares if an electron background is assumed in addition. Black crosses show the results of the theoretical mass table of Ref. [GTM05] and black circles the experimental measured values of Ref. [AWT03].

considered, for all other nuclei the mass formula is used. We find that the fractions of the aforementioned nuclei agree very well and differences appear only for the more heavy nuclei.

The mass formula which is used in the SMM is a continuous function of A and Z because the pairing energy is not included. The even-odd staggering which is observed in the mass number distribution comes from the fact, that the nuclei have discrete mass and charge numbers, and that only nuclei with an even number of nucleons can be symmetric. In contrast, if the nuclei are shown as a function of Z this staggering disappears, because for each Z there is a symmetric nucleus. In the ExV NSE model the scattering is larger, because the used binding energies are based on nuclear structure calculations or experimental measurements. Thus pairing and shell effects are taken into account.

One observes a faster decline of the mass and charge distribution in the ExV NSE model. The distribution looks very much like an exponential, whereas the SMM contains a small broader power-law-like contribution. This is also visible in the isotope distributions. For low charge, the magnitude of the yields are similar, whereas a strong reduction of the more heavy isotopes is seen in the ExV NSE model.

To understand the isotope distributions and the differences of the two models we first want to discuss the binding energies further. For each element there is a most stable isotope. The symmetry energy shows a quadratic behavior in $2Z/A$ with the minimum for $Z = N$. The Coulomb and surface energy however both decrease with A, thus the most stable nucleus shifts to more asymmetric nuclei. This effect becomes more and more important for the heavier nuclei, due to the increasing Coulomb energy. Figure 8.28 shows the binding energies of calcium isotopes calculated with the SMM mass formula of Eq. (8.58). In this model ^{44}Ca is the nucleus with the largest binding energy. As a function of mass number, the binding energy behaves very asymmetric. This is on the one hand due to the increasing contribution of the surface and Coulomb energy towards low A, but on the other hand caused by the symmetry energy. The symmetry energy per nucleon behaves quadratically around $N = Z$ only as a function of Z/A. For a constant Z thus the parabola is squeezed by a factor $1/A$, leading to a linear decrease of the binding energy for $A > 2Z$.

However, if we look at the isotope distributions in Fig. 8.27, we see that only nuclei close to the most stable nucleus are being populated. Very asymmetric nuclei do not appear. Thus mainly the quadratic behavior of the binding energy is probed, and the isotope distributions are in most cases very close to Gaussians. However, the ExV NSE model includes shell effects and pairing and thus the binding energies are in general no monotonous functions of A and Z. This can e.g. seen by the increase of the yield of ^{12}C. As another example, the yields of nuclei from ^{40}Ca to ^{46}Ca are all very similar because the experimentally measured binding energies are almost constant between $A = 40$ and 46. For $A = 40$ the neutron and proton magic shell are filled. The neutrons which are added in addition only give a slight increase of the binding energy. This effect of the shell closures then manifests itself also in the yields and the distribution becomes flat instead of a Gaussian.

Figure 8.28 shows also the temperature and density dependence of the SMM mass formula. The temperature enters the volume term of the binding energy quadratically, i.e. in the way of a Fermi gas. The surface energy is also temperature dependent and is constructed in such away, that the surface energy vanishes for $T = 18$ MeV, so that nuclei will disappear for larger temperatures. However, at $T = 1$ MeV the volume effect is more important and leads to a shift of the binding energies of 63 keV. The inclusion of the electron screening of the Coulomb energy has a stronger effect on the binding energy, even though calcium is a rather small nucleus. For larger nuclei it has the effect of stabilizing highly charged nuclei, thus nuclei become less asymmetric. However, at the presented temperature and density none of the effects lead to a significant different functional behavior of the binding energy.

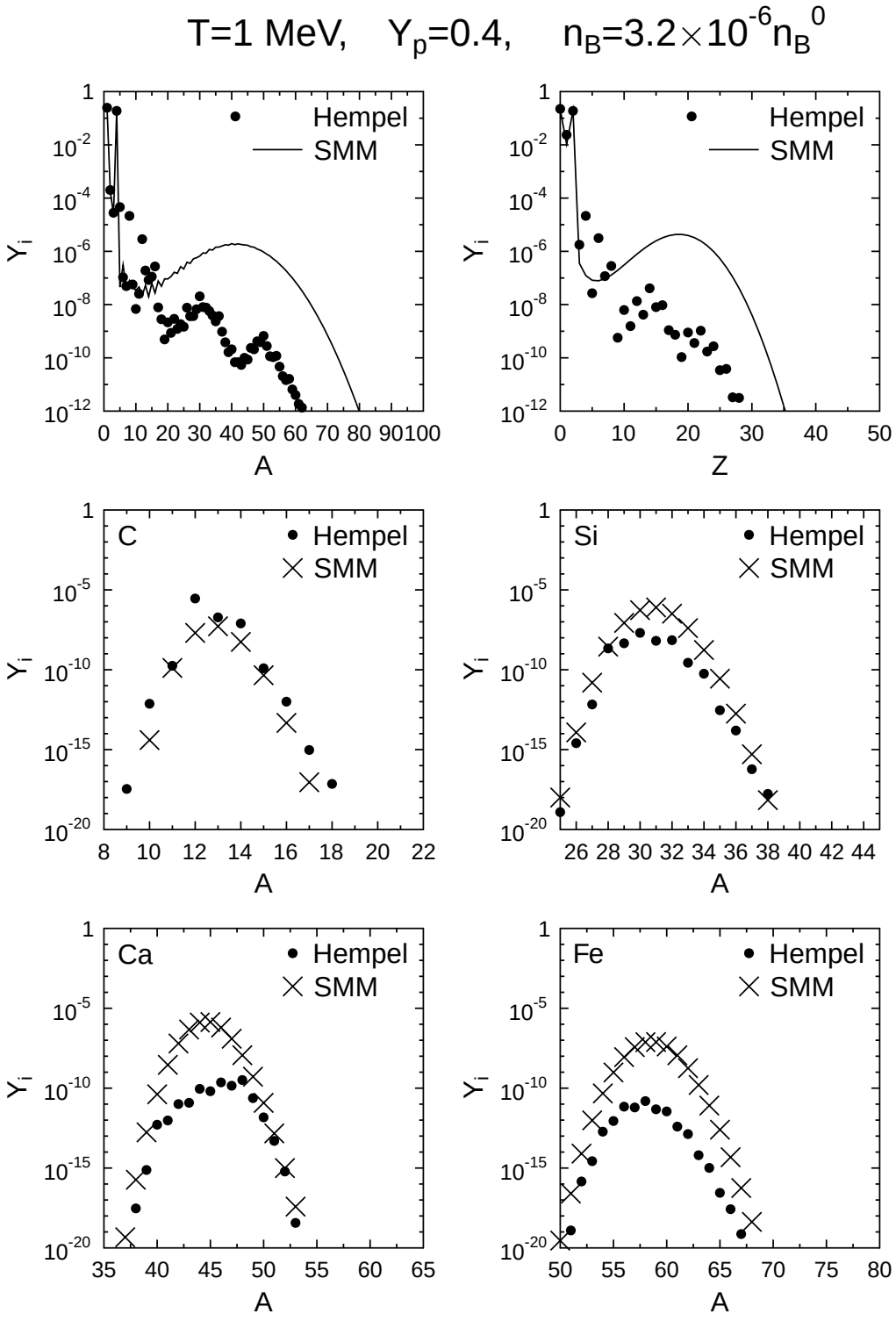

Figure 8.29: As Fig. 8.27, but for $n_B = 3.2 \times 10^{-6} n_B^0$.

Figure 8.29 gives the distributions for the same conditions, apart from a slightly increased density. In both models the yields of more heavy nuclei are increased on expense of the light clusters and nucleons. The change from exponential to power-law-like and finally u-shaped distributions which we observe here is usually interpreted as a consequence of the crossing of the liquid-gas phase transition line. The SMM still tends to larger nuclei, and has a maximum around $A = 40$. Contrary, some of the intermediate nuclei are enhanced by several orders of magnitude in the ExV NSE model. The use of experimental binding energies leads to an increase of ^{12}C, ^{8}Be and nuclei with $A = 5$ among others. Furthermore, in the ExV NSE model the distributions show a very non-monotonic behavior due to shell effects. Two maxima around A 30 and A 50 appear.

Also in the isotope distribution of the four selected elements one can see, that the fraction of heavy nuclei is increased compared to Fig. 8.29. The distributions of Si and Fe have a similar gaussian shape in the two models. The enhanced binding energy of ^{12}C and the plateau of the calcium isotopes are still visible. We note that even though the mass and charge distributions look very different, there is no systematic shift of the isotope distributions.

In Figure 8.30 the density is further increased. Now the typical u-shaped distribution around the minimum at $A = 10$ to 20 is clearly visible. The overall shape of the mass and charge distribution is now rather similar in the two models. However, the increased yields of intermediate mass elements and shell effects in the ExV NSE remain as major differences. The overall magnitudes of the isotope distributions are indeed very close to each other. In detail one finds that the ExV NSE develops a slightly increased tail of very neutron-rich isotopes.

In Figure 8.31 the density is increased further by two orders of magnitude. The free nucleon and light cluster yields have decreased by at least two orders of magnitude, and approximately only a fraction of 1% of free nucleons (almost only neutrons) remains. At the same the yields have been shifted to larger nuclei, giving an increased mass fraction of the heavy nuclei. Due to the negligible role of light clusters, where the largest differences had been observed before, now the two mass and charge distribution are even more similar. The differences could be interpreted as shell effects in the ExV NSE model on top of the continuous mass and charge distribution of the SMM. Also regarding the isotope distributions, the two models give similar predictions. Besides small changes for single nuclei the distributions look a bit broader in the ExV NSE model.

In Figure 8.32 the effect of the total proton fraction is studied. The lowering of Y_p to 0.2 has an interesting effect on the distributions. As was discussed in the analysis of

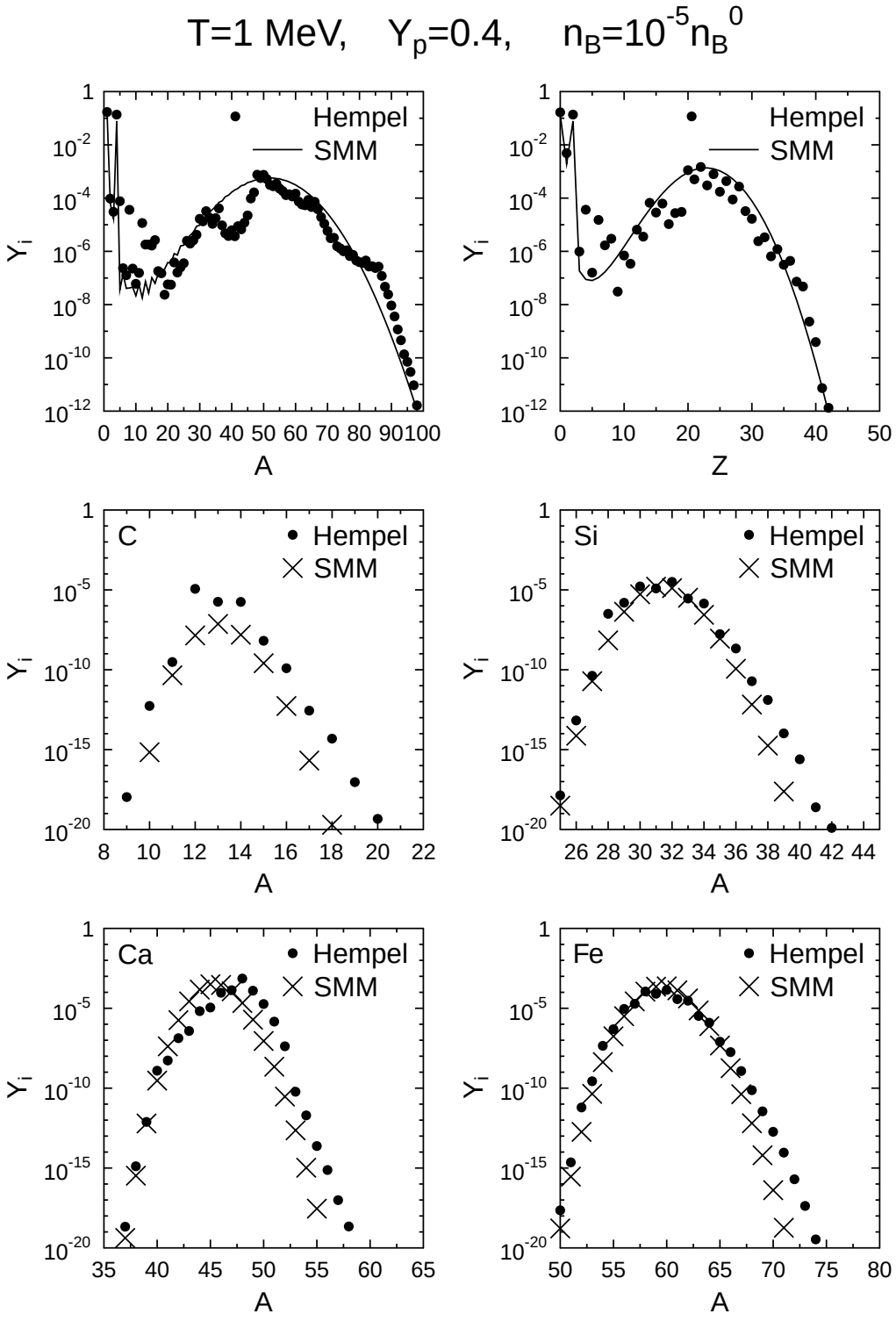

Figure 8.30: As Fig. 8.27, but for $n_B = 10^{-5} n_B^0$.

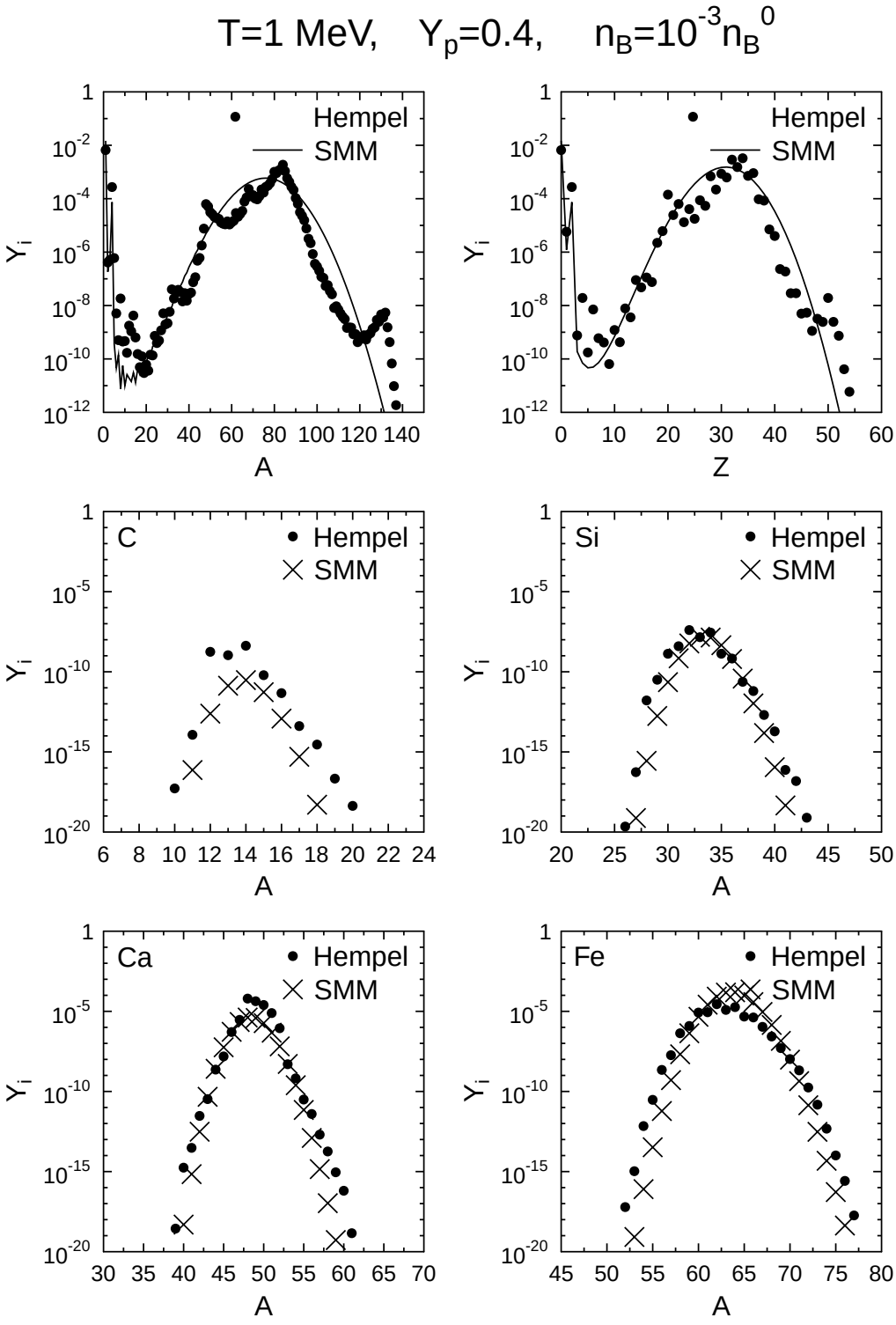

Figure 8.31: As Fig. 8.27, but for $n_B = 10^{-3} n_B^0$ and with a rescaled axis.

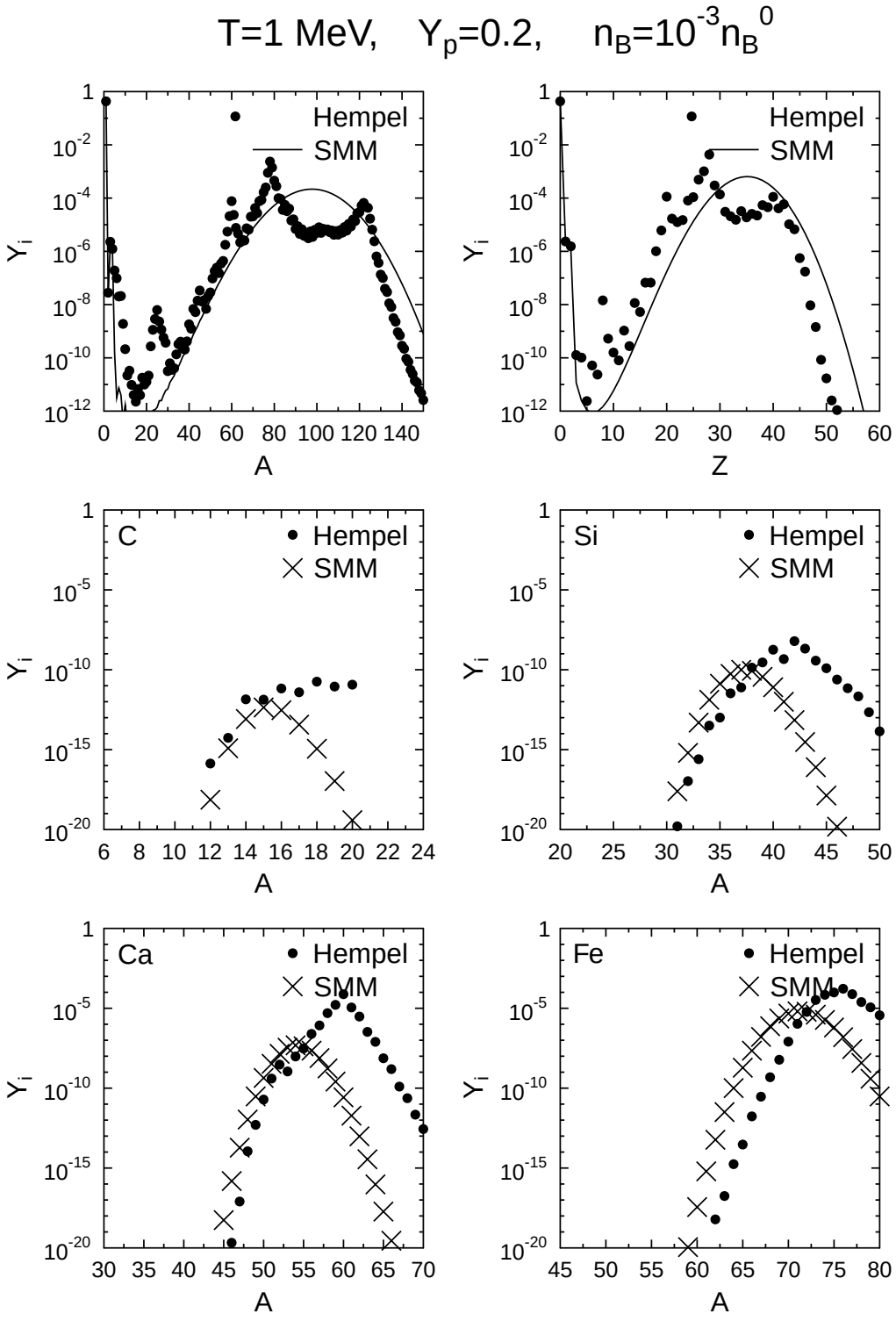

Figure 8.32: As Fig. 8.27, but for a reduced proton fraction $Y_p = 0.2$.

Fig. 8.8, in the ExV NSE model there is a critical proton fraction of $Y_p^{crit} = 0.3$ below which the neutron drip occurs. From this point of view, Fig. 8.32 shows a different physical situation then the previous graphs. There is a huge portion of free neutrons, $Y_n = 0.430$ in the ExV NSE and $Y_n = 0.443$ in the SMM model. In the ExV NSE could the excluded volume corrections disfavor large nuclei for large nucleon pressures, see Eq. (8.48). This could explain the shift to smaller mass numbers. The remaining protons and neutrons are bound in heavy nuclei. The average charge to average mass ratio of nuclei is thus $< Z > / < A >= Y_p^{tot}/(1 - Y_n)$ which gives 0.351 in the ExV NSE and 0.359 in the SMM model. The different neutron densities in the two models lead to slightly more symmetric nuclei in the SMM model.

In the isotope distributions now some significant differences appear. For carbon the isotope distribution increases towards the most asymmetric isotopes. The maxima of the distribution of the other elements are shifted to heavier nuclei by ~ 10 in mass number. It is interesting to see, that the distribution of calcium drops from ^{60}Ca to both sides exponentially. It is not completely clear where these effects come from. They could be connected to a larger baryo-chemical potential in the ExV NSE. In addition to the different implementation of excluded volume effects, in the SMM Fermi-Dirac statistics and the degeneracy of the nucleons are not taken into account. Also the form of the symmetry energy or the interactions of the nucleons could play a role.

In Figure 8.33 the same proton fraction as in Figs. 8.27 – 8.31 is shown. The density is the same as in Fig. 8.31, but this time the temperature is raised to 2 MeV. In general we find, that increasing the temperature has a similar effect as lowering the density. The shape of the distribution resembles a bit the situation shown in Fig. 8.29. Light clusters dominate, but the u-shaped dip starts to develop and there is already a small contribution of the heavy nuclei. This time the ExV-NSE model extends to larger values of Z and A. This could be an indication of the different description of temperature effects in the two models, which we will discuss in more detail later. As already found before, the ExV NSE gives an increased fraction of some of the intermediate nuclei. Compared to Fig. 8.31 the shell effects in the mass distribution are much less pronounced and almost not visible in the charge distribution any more.

The isotope distributions of the two models again look similar. The fraction of Carbon isotopes is increased, whereas Calcium is decreased, even though the latter is a magic nucleus. The shown isotope distributions are broader in the ExV NSE model than in the SMM.

In conclusion we found a good agreement of the two models. The main differences come from the shell effects in the ExV NSE which lead to peaks on top of the smooth

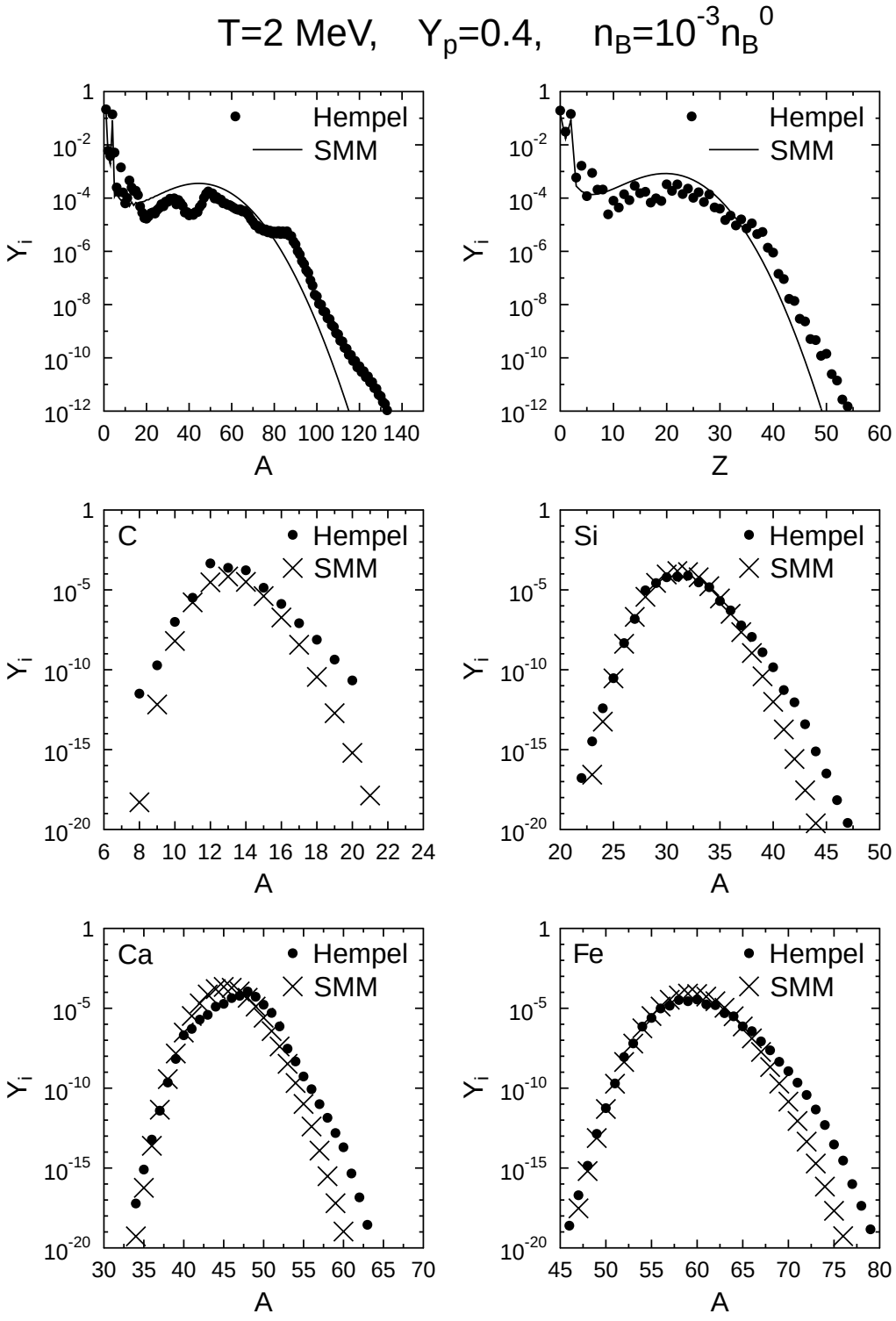

Figure 8.33: As Fig. 8.27, but for $n_B = 10^{-3} n_B^0$ and $T = 2$ MeV.

distributions found in the SMM. In the transition region from light to heavy clusters, the two models give different predictions, because the composition is dominated by light and intermediate nuclei, for which the liquid drop formulation of the binding energy shows larger differences to the experimental data. Only for the light clusters with $A \leq 4$ experimentally measured masses are included in the SMM. Regarding the isotope distributions, the experimental values lead to deviations from the typical gaussian distributions. Interestingly, we only find significant systematic differences when the neutron drip is reached, i.e. the chemical potential of the nucleons becomes positive. Possible explanations could be the different form of the excluded volume, missing degeneracy of the nucleons in the SMM, interactions in the ExV NSE or different nuclear symmetry energies.

8.5 Excited States

In this section we want to address the role of excited states in the supernova EOS further. The internal partition function was already introduced in Paragraph 8.2.3, Eq. (8.3). In the previous section we only considered excited states with energies below the binding energy. As an additional case we include excitation energies up to infinity. We want to compare the function $g^{FR}_{A,Z}(T)$ from Fai and Randrup (FR) with and without cutoff with a more elaborated model, namely the detailed internal partition functions in tabular form of Rauscher [RTK97, RT00, Rau03]. These tables are based on a backshifted Fermi-gas model and directly take into account most of the known experimental levels. As another reference, we use the internal degeneracy calculated with excited states known from experiment for nuclei with $Z \leq 5$, and the four nuclei ^{55}Fe, ^{56}Fe, ^{57}Ni, and ^{58}Ni. We present them in the same manner as the internal partition functions by showing the factor

$$g^{Exp}_{A,Z} = \sum_i g_i (1 + \Delta E^*_i / M_0)^{3/2} \exp(-\Delta E^*_i / T) \; , \tag{8.62}$$

where i denotes the sum over all known states. If the spin of the state is available, we also use this information in the case labeled 'Exp' later. As another reference we take the temperature dependent part of the binding energy of the SMM (Eq. (8.58)) expressed in the following way:

$$\begin{aligned} g^{SMM}_{A,Z} &= \frac{n_{A,Z}(F_{A,Z}(T))}{n_{A,Z}(F_{A,Z}(T=0))} \\ &= \exp\left(\frac{T}{\varepsilon_0} A - \frac{\beta_0}{T} A^{2/3} \left(\left(\frac{T_c^2 - T^2}{T_c^2 + T^2} \right)^{5/4} - 1 \right) \right) \; . \end{aligned} \tag{8.63}$$

For $T > T_c$ we take the second quotient to be zero. The part proportional to β_0 in the equation above comes from the temperature dependence of the surface energy, whereas the first part is the total excitation energy of a bulk Fermi-Dirac gas. For the identification of the surface effects, we also show this part separately:

$$g^{FD}_{A,Z} = \exp\left(\frac{T}{\varepsilon_0} A \right) \; . \tag{8.64}$$

Equation (8.32) shows that the internal degeneracy function, i.e. the excited states, gives a direct contribution to the EOS. We introduce the energy coming from the internal

partition function of a certain nucleus:

$$\Delta E = \frac{\partial g}{\partial T}\frac{T^2}{g} \; . \tag{8.65}$$

If excited states are explicitly taken into account these give a similar contribution:

$$\Delta E^{exp} = \frac{\sum_i g_i (1+\Delta E_i^*/M_0)^{3/2} \exp(-\Delta E_i^*/T)\Delta E_i^*}{\sum_i g_i (1+\Delta E_i^*/M_0)^{3/2} \exp(-\Delta E_i^*/T)} \; . \tag{8.66}$$

In the SMM we get the following expression for the excess of energy per nucleus between finite and zero temperature:

$$\begin{aligned} \Delta E^{SMM} &= F_{A,Z}(T) - F_{A,Z}(0) - T\frac{\partial F_{A,Z}}{\partial T} \\ &= \frac{T^2}{\varepsilon_0}A + \beta_0 A^{2/3}\left(\left(\frac{T_c^2 - T^2}{T_c^2 + T^2}\right)^{5/4}\left(1 + 5\frac{T^2 T_c^2}{T_c^4 - T^4}\right) - 1\right) \; . \end{aligned} \tag{8.67}$$

For a Fermi-Dirac gas without surface energy one obtains:

$$\Delta E^{FD} = \frac{T^2}{\varepsilon_0}A \; . \tag{8.68}$$

Figure 8.34 depicts the degeneracy factor for $T = 10^{10}$ K. Regarding the light clusters, FR agrees reasonably well with the experimental levels, because the degeneracies are small. The observed differences are mainly due to the use of known experimental values for the groundstate angular momentum instead of assuming $J = 1/2$ for odd and $J = 0$ for even nuclei which is used in the NSE model and the case FR. The model of Rauscher connects very well with the experimentally known excited states.

However, the shown levels only give a lower bound for the degeneracy, as the experimental knowledge may be incomplete, and additional levels could exist. Especially close to the continuum, the level density becomes very large, so that it is very difficult to identify single levels. Furthermore, only for the minority of the levels the angular momentum has been determined. The true angular momentum may be much larger than the assumed values, and thus would lead to an increase of g.

The experimental degeneracy for the four heavy nuclei is one order of magnitude larger than for FR, and lies in the region predicted by Rauscher. Rauschers model gives a much larger contribution to the excited states for the heavy nuclei compared to FR. In the model of FR only for large nuclei with $A > 150$ an significant increase of the degeneracy is visible at all. The model of FR not only shows a lower value of g but also has a different mass number dependence. We note that for $T = 10^{10}$ K no effect

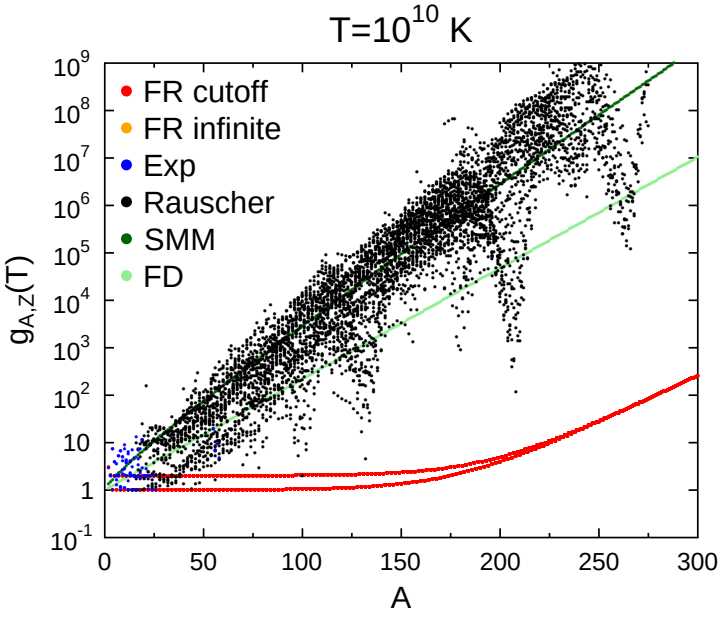

Figure 8.34: The degeneracy factor $g_{A,Z}(T)$ as a function of mass number A at $T = 10^{10}$ K. Shown are the detailed internal partition function of Rauscher [RTK97, RT00, Rau03], the simple semi-empirical expression of Fai and Randrup (FR) [FR82] with and without cutoff, known experimental levels of nuclei with $Z \leq 5$, and of the four nuclei ^{55}Fe, ^{56}Fe, ^{57}Ni, and ^{58}Ni, and the multiplication factor of the SMM [BM08] and a bulk Fermi-Dirac (FD) gas. For details see text.

of the cut-off in FR is observed. For SMM, we find that the general trend of Rauschers model is well reproduced by considering the bulk and surface energy to be temperature dependent. Only around the magic shells the degeneracy behaves very differently in Rauschers model and drops to very low values.

The total excitation energy of the nuclei is depicted in Fig. 8.35. Also for this quantity one finds that Rauscher connects to the experimental data. For the four heavy nuclei, we observe that the energy contribution in Rauschers model is above the experimental values, but in a similar range. Compared to the FR model, the different mass number dependence is striking, which leads to an overestimation of the energy of the excited states for light and very heavy nuclei. The SMM gives the largest total excitation energies and shows a larger deviation from Rauscher than a pure Fermi gas. This means that the entropy contribution $-\partial F_{A,Z}/\partial T$ is somehow overestimated in SMM.

Figures 8.36 and 8.37 show the same quantities as the previous two, but for the larger temperature of $\sim$ 10 MeV and for nuclei with lower mass numbers ($A < 60$), because heavier nuclei are not relevant at this temperature. For the very light nuclei with $A < 20$ the model of FR is a good approximation of $g_{A,Z}$ of the experimentally known excited states. At the depicted temperature the cutoff leads to a slightly reduced degeneracy of

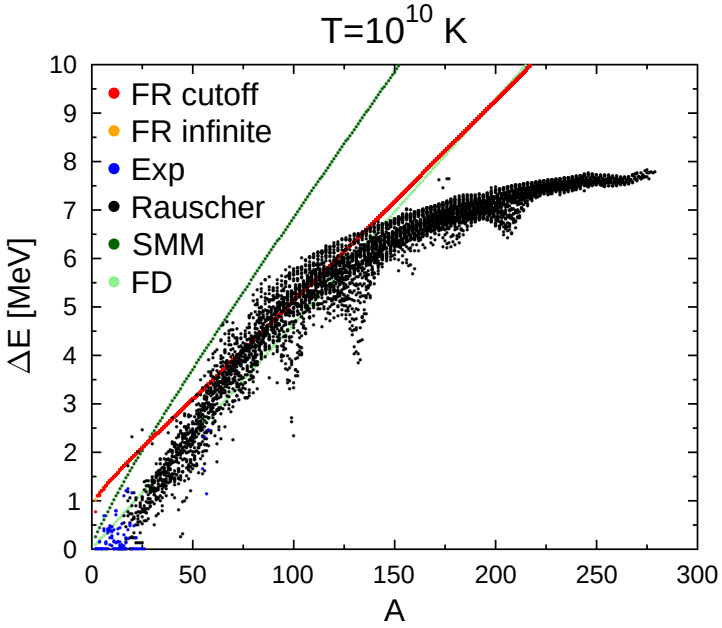

Figure 8.35: The total excitation energy ΔE of a certain nucleus of mass number A at $T = 10^{10}$ K. The same models as in Fig. 8.34 are shown.

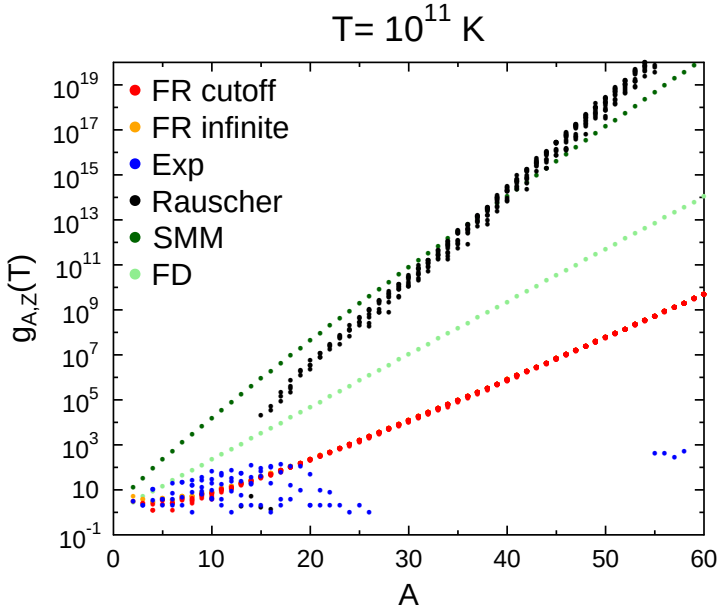

Figure 8.36: As Fig. 8.34, but now for $T = 10^{11}$ K.

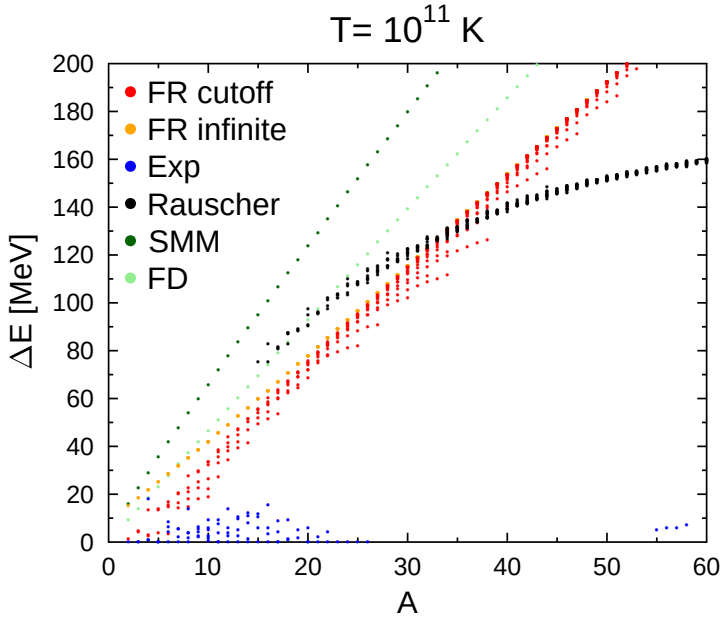

Figure 8.37: As Fig. 8.35, but now for $T = 10^{11}$ K.

the lightest nuclei. For heavy nuclei, the cutoff energy is so large that it has no effect, as very large excitation energies are exponentially suppressed due to the Boltzmann factor. For nuclei with $A > 20$ the different mass number dependence of Rauscher and FR is obvious, Rauscher predicts a much larger effect of the excited states. Rauscher and SMM agree rather well, only a slightly different mass-number dependence is observed. At this temperature the experimental degeneracy of the four heavy nuclei is well below all the other models. Furthermore their degeneracy is not even much higher than of the light nuclei. We attribute this to the lack of knowledge of excited states close to the continuum, where the states are so close that they go over to a band of excited states. Thus the few experimentally known excited states represent only a lower limit for the degeneracy.

In Fig. 8.37 an influence of the cutoff on the total excitation energy can be seen. It leads to lower total excitation energies. The effect of the cutoff on the total excitation energy is more important than for the internal degeneracy, as can be expected. Compared to the integral over the excitation energies E^* for the internal degeneracy, in the integral for the total excitation energy the additional factor E^* appears. Thus the larger excitation energies have a larger contribution to the total excitation energy than to the internal degeneracy. As an outcome, the cutoff energy is relevant for ΔE for nuclei up to $A \sim 20$. We see that especially for the lightest nuclei with $A < 10$ the FR model without cutoff leads to an significant overprediction of the total excitation energies compared to the experimental data. With the cutoff FR gives results which are similar to

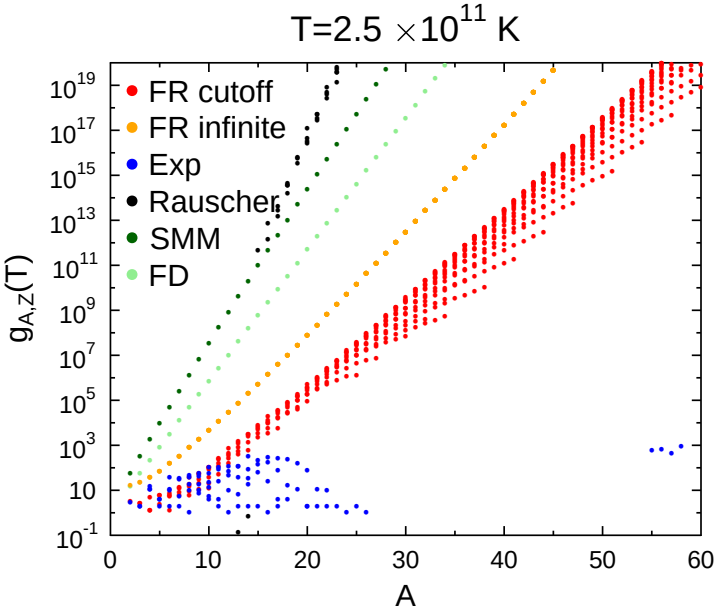

Figure 8.38: As Fig. 8.34, but now for $T = 2.5 \times 10^{11}$ K.

the experimental values. For nuclei with $A > 15$ Rauscher achieves much larger excitation energies. FR and SMM have a similar mass-number dependence, whereas the total excitation energies are very large in the SMM, as before. In Rauschers model the total excitation energy increases much more slowly with mass number and in a non-linear way.

At $T \sim 25$ MeV, which is shown in Fig. 8.38, the effect of the cutoff of lowering the degeneracy is very pronounced. Due to the different cutoffs, nuclei with the same mass number but different binding energies get a different degeneracy. Strongly bound nuclei get a larger degeneracy. Only with the cutoff the FR model connects well with the experimentally known excited states. The degeneracy in Rauschers Model is several orders of magnitude larger and has a larger slope with respect to the mass number. The difference between SMM and Rauscher has also further increased.

By studying Fig. 8.39, which shows the excitation energy, the necessity of introducing the cutoff can be seen. We remind the reader that actually only very light nuclei $A < 10$ are relevant at such large temperatures. Without the cutoff the excitation energy can reach several hundreds of MeV, even though many of the light nuclei are only slightly bound. Excited states far above the binding energy contribute significantly to the excitation energy. However, also in Rauschers model large excitation energies for nuclei with $A > 20$ are predicted. Only at $A > 60$ the FR model with cutoff and Rauscher become more similar again. Note the interesting effect that the surface energy now decreases the excitation energy of SMM.

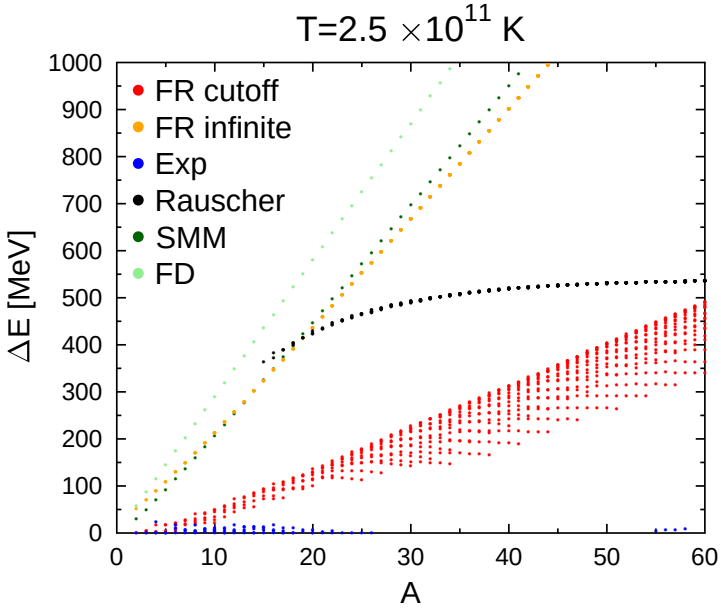

Figure 8.39: As Fig. 8.35, but now for $T = 2.5 \times 10^{11}$ K.

From this study we conclude the following. Even if only experimentally known excited states are taken into account, they lead to an important contribution to the internal degeneracy. For the light clusters the FR model with cutoff is in reasonable agreement with the experimental data. In most cases it gives a lower value for the internal degeneracy. However, we don't see this as a disadvantage, as a quantum treatment of the medium effects could lead to a suppression of the excited states. Thus it could be, that the effect of the excited states of the light clusters will be reduced at large densities. For heavy nuclei with $A > 60$ FR is orders of magnitude below the other models investigated here. Thus FR represents a rather conservative model for the role of the excited states. Regarding the excitation energy, FR gives an overprediction for $T \sim 1$ MeV for the light nuclei. At larger temperatures there is an agreement with the experimental data, if the cutoff is used.

Even though the model of FR (with the cutoff) is very simple, we chose it for the description of excited states, instead of neglecting them completely. We showed that the excited states have an important effect on the EOS as they contribute significantly to the energy density and other quantities. Without the cutoff the high temperature behavior would be pathologic. In preliminary hydrodynamic simulations of core-collapse supernovae we found that the use of FR without the cutoff even does not lead to the formation of the shock in the expected form. Rauschers model is much more sophisticated, but it is based on a certain model for the nuclear masses and only a selection of nuclei is available in tabular form. Still it would be interesting to use these detailed internal

partition functions and to compare the results for the EOS with the results of FR which have been shown in the previous section. The study presented here is by no means complete, see e.g. also [NY04] and the aspect of excited states has to be investigated further.

8.6 Medium Effects on Light Clusters

In this section we want to compare the excluded volume approach with two many-body theories, the quantum statistical (QS) model and a generalized relativistic mean field (gRMF) model. The gRMF model had been introduced in Ref. [TRK+10]. In addition to the nucleons, the light clusters are included as quasiparticles which contribute as sources for the meson fields. Like the nucleons, also the light clusters get a mean-field self energy leading to a reduced effective mass and medium shifts of the chemical potentials. However, the light clusters are composite particles of nucleons. Thus, at large densities the light clusters do not behave as free quasiparticles, but feel the filled Fermi sea of nucleons. This effect is called Pauli blocking and leads to a shift in the binding energies which cannot be described by the gRMF model itself. It is included as a density dependent part of the nuclear masses, which is taken from the QS model in parameterized form.

The QS model is described in detail in Refs. [SR08, Roe09]. It is based on the thermodynamic Greens function method and uses an effective nucleon-nucleon interaction. Effects of the correlated medium such as Pauli blocking, Bose enhancement and self-energy are taken into account, leading e.g. to the merging of bound states with the continuum of scattering states with increasing density (Mott effect). In Ref. [TRK+10] the nucleon self energies in the QS model are evaluated with the RMF model. Then the medium modifications can be determined, such as the mass shift and the Mott densities, where the clusters get dissolved.

Fig. 8.40 shows the Pauli-blocking shift, derived with the QS model based on the RMF interactions. With increasing temperature the Pauli-blocking becomes less important, leading to larger Mott densities, at which the binding energy vanishes. The relative change of the binding energy decreases with mass number.

In the following we will compare the results of Ref. [TRK+10] with the excluded volume NSE model. For this comparison we will first only consider the following light clusters with $A \leq 4$, which are also used in Ref. [TRK+10]: neutrons, protons, deuterons ^{2}H, tritons ^{3}H, helions ^{3}He and alpha particles ^{4}He. To investigate the role of heavier clusters, we will then include all available nuclei in the ExV model. Finally we will study the role of excited states, by also considering the temperature dependent degeneracy function as presented in Sec. 8.2.3.

Figure 8.41 shows the comparison for $T = 2$ MeV. We note that the fraction of tritons is almost equal to the helion fraction, because they are isospin partners and we are investigating symmetric nuclear matter. The only differences arise due to Coulomb

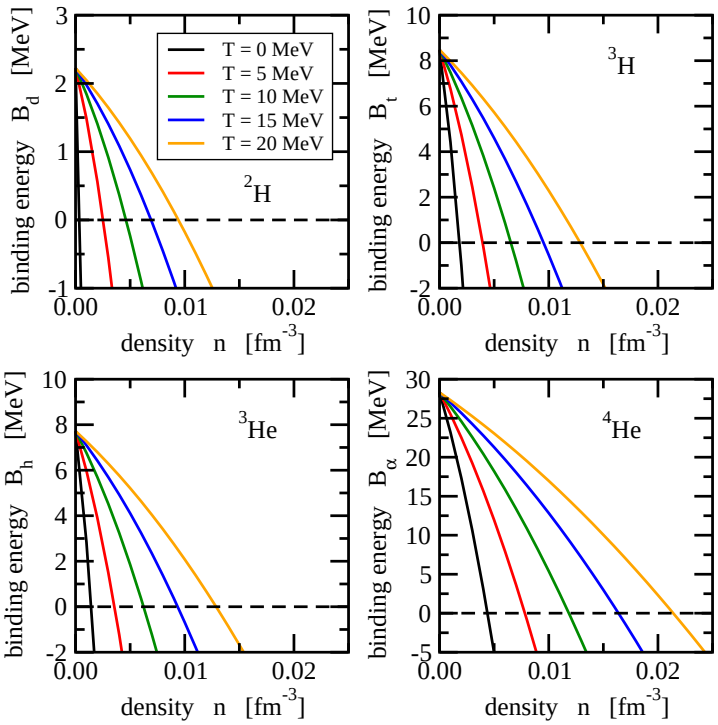

Figure 8.40: Figure taken from Ref. [TRK+10]. Change of the binding energy $B_i = B_i^0 + \Delta B_i$ of the clusters $i = d, t, h, \alpha$ in symmetric nuclear matter due to the binding energy shift ΔB_i in the generalized RMF model as a function of the total nucleon density of the medium for various temperatures T.

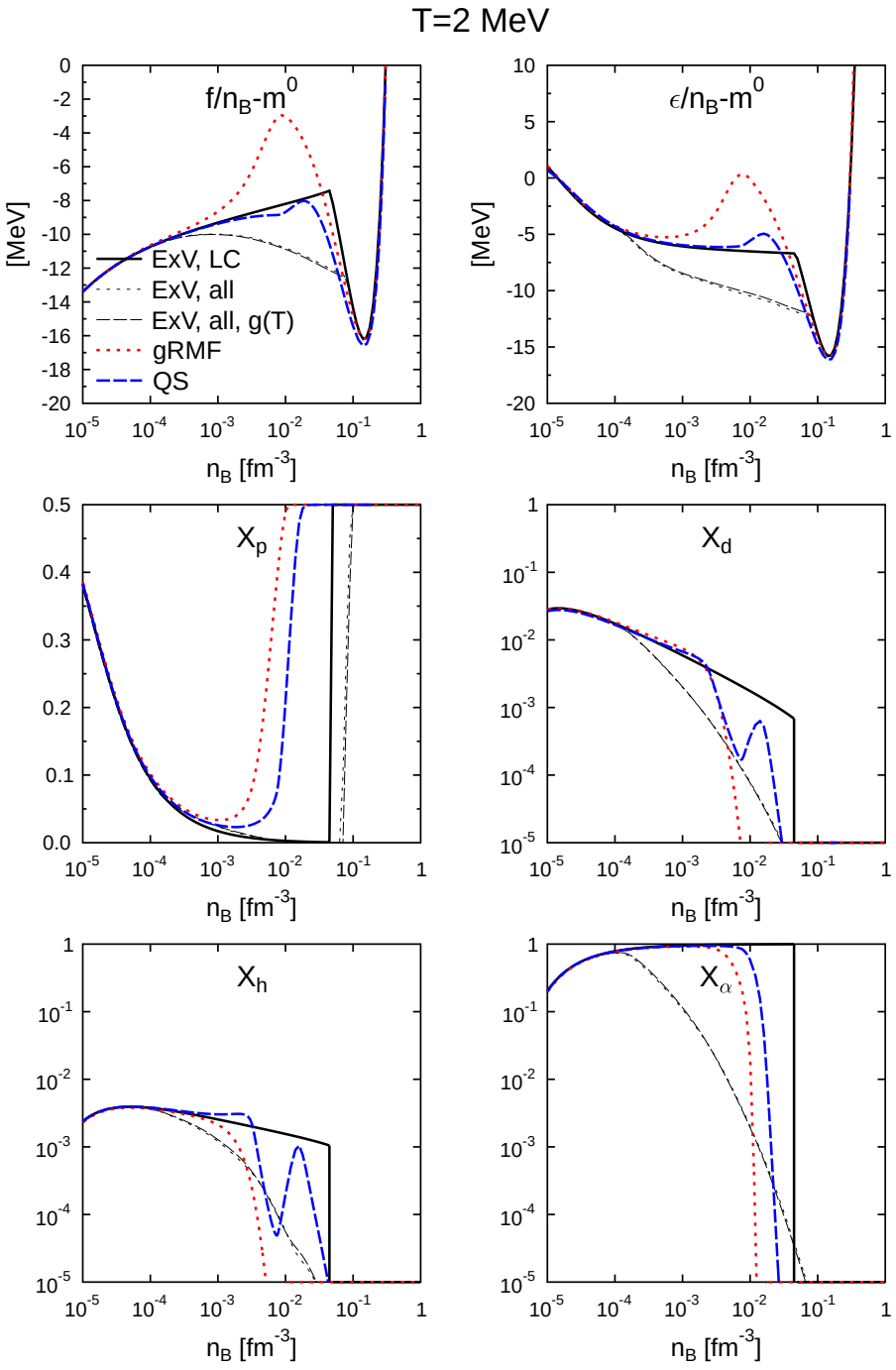

Figure 8.41: The free energy per baryon, energy per baryon and the mass fractions of protons, deuterons, helions and alphas, for symmetric nuclear matter at $T = 2$ MeV. The results of the generalized relativistic mean-field model gRMF and of the quantum statistical model QS from Ref. [TRK+10] are compared to the excluded volume NSE model ExV. "ExV, LC" shows the results if only the same light clusters with $A \leq 4$ as in Ref. [TRK+10] are considered and no excited states are taken into account. For "ExV, all" all available nuclei are used. "ExV, all, g(T)" also takes all available nuclei into account, but this time with the internal degeneracy function.

interactions and the mass difference. Similarly, the mass fraction of unbound neutrons is almost equal to the unbound proton fraction. Regarding the composition, up to $n_B \sim 10^{-3}$ fm $^{-3}$ the predictions of the different calculations which only consider the light clusters agree. It is interesting to note that even though the composition is still rather similar at $n_B \sim 10^{-3}$ fm $^{-3}$, the free energy in gRMF is increased compared to the other two models. In the QS and gRMF model above the Mott densities the light clusters start to dissolve due to the Pauli blocking. The binding energies of the light clusters are reduced gradually with density, which leads to an increasing proton fraction. Conversely, in the ExV model, the light cluster fraction increases until $\sim 0.3 n_B^0$, where a sudden turnover in the composition appears. The two quantum many-body models agree better with each other and do not show this behavior. Still they exhibit different features in detail, like e.g. the oscillatory behavior in the QS model. Even though the composition is more similar in the QS and gRMF model, the free energy and binding energy of QS is more similar to the ExV model. When uniform nuclear matter is reached, smaller deviations of the three models remain, as they are based on different forms of the nuclear interactions. One can conclude, that a similar behavior of the composition does not imply in general that other thermodynamic quantities also behave similarly.

The excluded volume approach gives a very crude representation of the medium modifications at this low temperature. However, it is enlightening to study the contribution of the heavy nuclei, which are taken into account in the thin black lines. In comparison with the light cluster NSE (thick solid black line), one sees that already at very low densities $n_B \sim 10^{-4}$ fm^{-3} the light clusters are actually replaced by heavy nuclei. The sum of the mass fractions of the light clusters with $A \leq 4$ and the nucleons drops below 0.10 for densities above 2×10^{-3} fm^{-3}. Thus the comparison with QS and gRMF at larger densities is not very significant, because the composition is dominated by heavy nuclei there. The fraction of the light clusters is reduced considerably by the appearance of heavy nuclei, before the Mott densities are reached. Also the energy and free energy density changes significantly, if the heavy nuclei are included. Deviations appear already at $n_B \sim 10^{-4}$ fm^{-3} and become similar large as the differences between the QS and gRMF model.

The dashed thin black line also uses all available nuclei but takes excited states by the use of the internal degeneracy function into account. As expected, at this low temperature the inclusion of excited states is not significant and almost no differences are observed.

Figure 8.42 shows the results of the three models at $T = 10$ MeV. There is no sudden turnover of the composition in the ExV model any more, but the clusters are dissolved

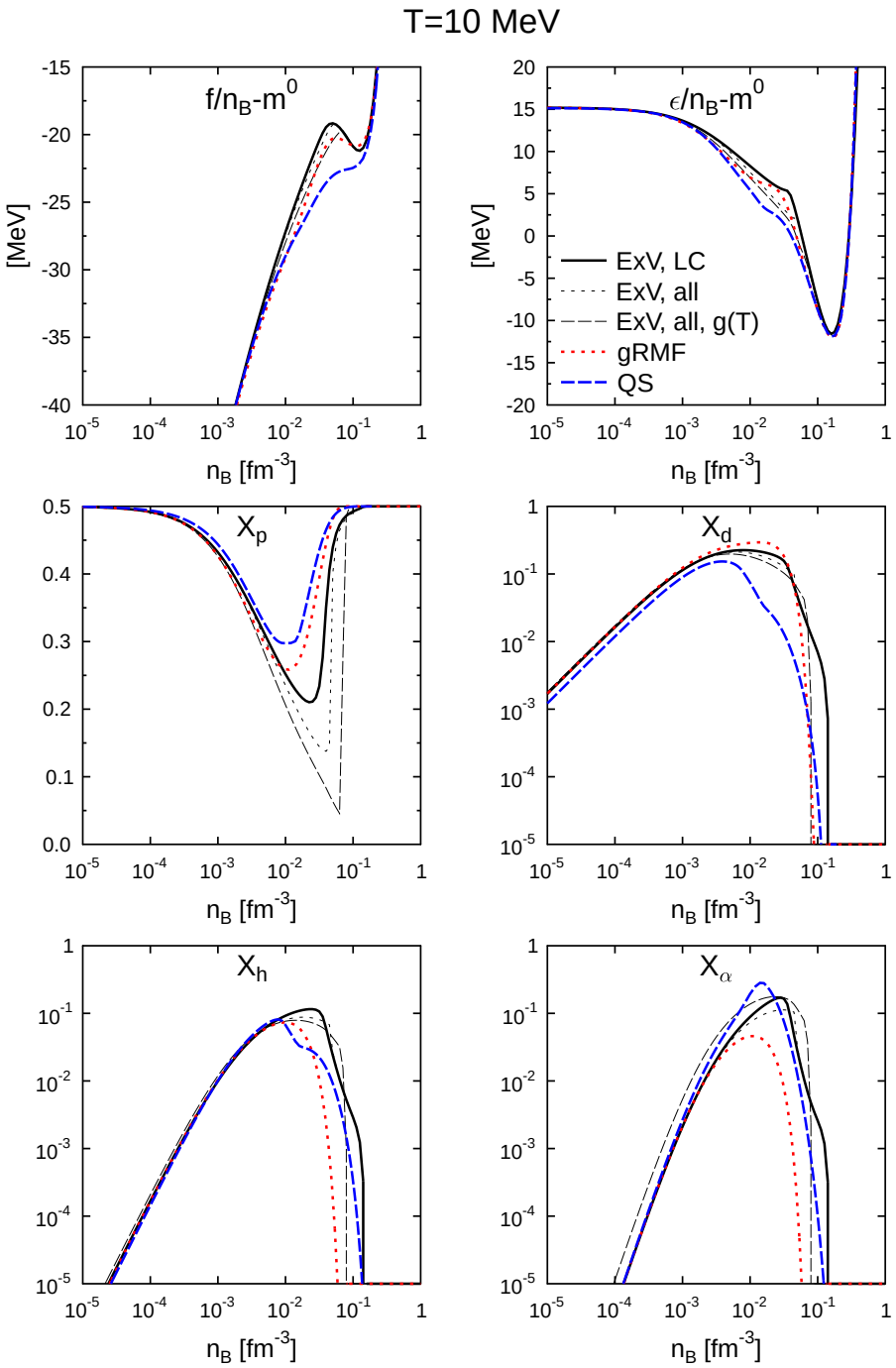

Figure 8.42: As Fig. 8.41, but now for $T = 10$ MeV.

continuously. At this temperature the composition of the ExV model agrees much better with the two quantum models. The maximum deuteron and alpha-particle fractions lie between the results of gRMF and QS, the maximum helion-fraction is a bit larger. The total cluster fraction is lower in the ExV model, as can be seen from the proton fraction. The densities at which the light clusters disappear are slightly larger in the ExV model, and are closer to the QS model. The differences of the two quantum models are of similar size as the differences to the ExV model. Thus we can conclude that the ExV model mimics the quantum medium effects reasonably well at $T = 10$ MeV.

We explain the better agreement at large temperatures by the following aspects. First, the unbound nucleon density is in general larger at larger temperatures, and clusters appear with lower fractions. This is a trivial reason for the better agreement. Second, the excluded volume corrections give a contribution to the free energy density proportional to $T \ln(\kappa)$, see Eq. (8.32). Thus the excluded volume has a larger effect at larger temperatures. On the other hand, also the Pauli-blocking gets weaker at larger temperatures, see. Fig. 8.40.

If one looks at the free energy and the internal energy in Fig. 8.42, it is apparent that they are increased in the ExV model at almost all densities, even though the composition is similar. As noted before, the direct contribution of the excluded volume is proportional to T and increases the free energy. However, the excluded volume does not add to the energy density directly which is also increased. We have a possible explanation for these deviations: Regarding the mean-field there are important conceptual differences in the three models: In QS and gRMF all nucleons (bound in clusters and unbound) contribute as sources for the meson fields. Furthermore, the light clusters get a mean field self energy. These effects are absent in the ExV model, where the mean field is given only by the unbound nucleons because the interacting nucleons are assumed to be outside of the light clusters. It would be interesting to compare the effective mass of the nucleons of the three models directly, to identify the origin of the observed differences further. Deviations between the QS and the gRMF model arise, because in gRMF the back-reaction of the composition on the energy shifts is self-consistently taken into account, whereas in the QS model only the total nucleon densities are used. Furthermore, the continuum states of the deuteron are treated in a more elaborated way in the QS model, leading to reduced deuteron fractions in general.

In the calculation with all nuclei (dotted thin black line), one finds that the heavy nuclei are not as important as before for $T = 2$ MeV. The maximum fractions of the light clusters are reduced only slightly and the transition density to uniform nuclear matter remains similar. The maximum mass fraction of heavy nuclei with $A > 4$ is ~ 0.40, which is reached at $n_B \sim 5 \times 10^{-2}$ fm^{-3}.

At $T = 10$ MeV the inclusion of excited states has a noticeable effect on the EOS and the composition. The formation of heavy nuclei is favored because of their large internal degeneracy. Their maximum mass fraction is increased to ~ 0.74 and uniform nuclear matter occurs at slightly larger densities. The degeneracy function acts differently on the abundances of the light clusters as can be seen by comparing the dotted with the dashed thin black line in Fig. 8.42: The helion and deuteron fractions are reduced, whereas the alpha-particle fraction is increased. This change in the composition is also present at very low densities. The deuteron is only very weakly bound, thus the cutoff for the maximum excitation energy is rather low, so that the internal degeneracy remains small, in contrast to the strongly bound alpha particle. Even though the degeneracy function leads to visible changes in the composition, its effect on the free energy and energy is almost negligible, compared to the direct contribution of the heavy nuclei.

For $T = 20$ MeV, which is shown in Fig. 8.43, the composition of the ExV model agrees very well with the results of gRMF and QS. The maximum mass fractions of the individual clusters are between the results of the two other models, and the maximum densities at which the single clusters disappear are in a similar range. This supports the conclusion which we have drawn before. The reduced deuteron fraction in the QS model is now even more pronounced. As already mentioned, it is due to the more elaborated treatment of the continuum states. There are important differences in the EOSs, where light clusters appear in large concentrations. All the three models have a rather different behavior, whereas the ExV model gives the largest energy and free energy.

In Fig. 8.43 one sees that heavy nuclei play almost no role at $T = 20$ MeV, as there are only very small differences between the solid and the dotted black line. Conversely, the effect of the degeneracy function on the composition is significant. Due to the large temperature, now the alpha particles profit the most from the inclusion of the excited states, as their cutoff energy is very large. The fractions of the other light clusters remain almost unaffected. Still, the effect of the internal degeneracy function on the EOS is rather small. As we showed in Sec. 8.5 this is not the case, if no cutoff in the integral over the excited states is used: Then all possible excitation energies contribute, and with increasing temperature the contribution to the energy would become arbitrary large.

Conclusions Regarding the composition with only light clusters we conclude, that the excluded volume description can imitate the complicated quantum medium effects relatively well at large temperatures. Contrary, at low temperatures the ExV model behaves very similar to an ideal gas and thus shows crucial deviations. However, in this case we found that the heavy clusters are the most abundant particles before the

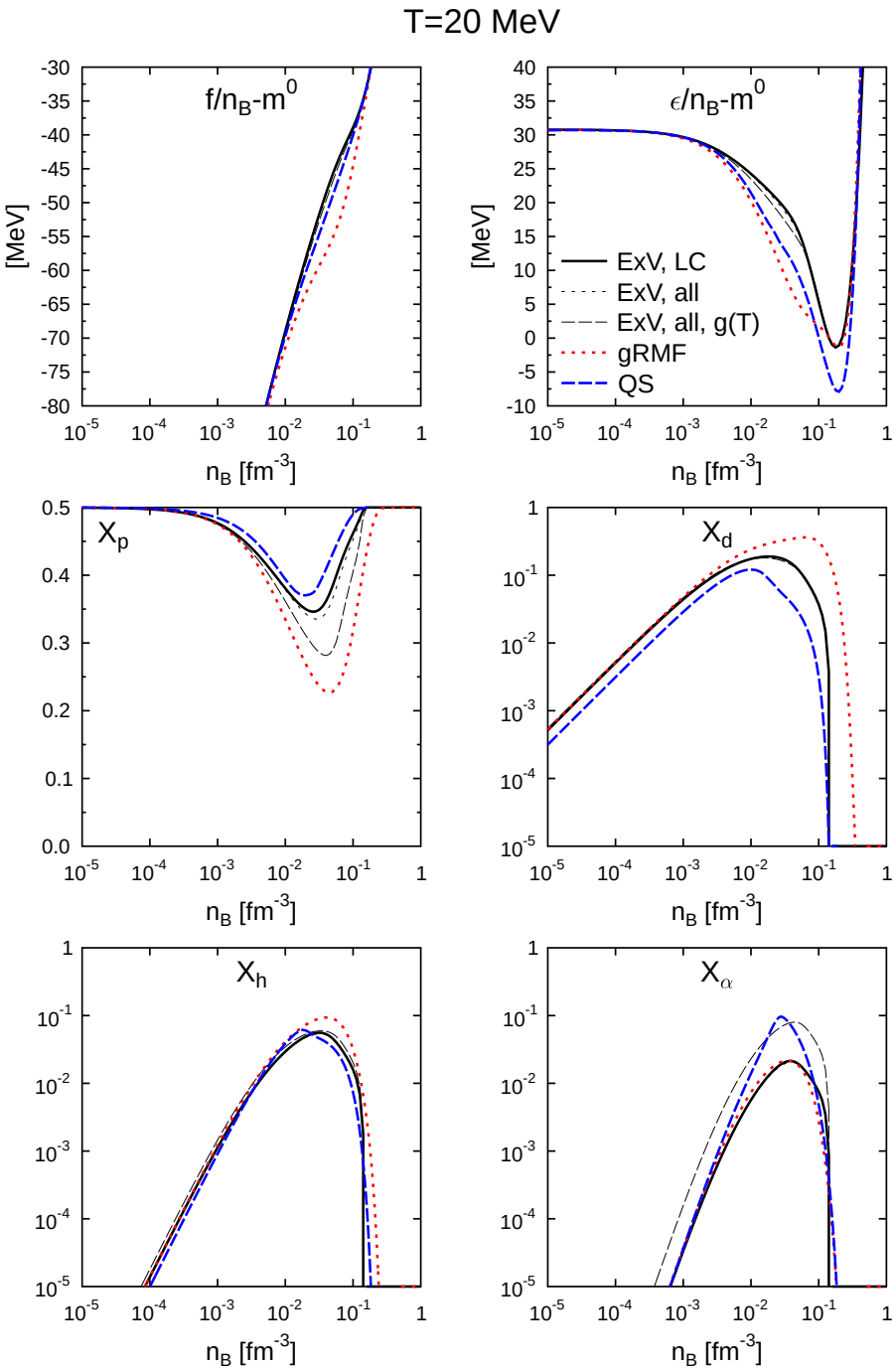

Figure 8.43: As Fig. 8.41, but now for $T = 20$ MeV.

medium effects of the light clusters become very strong. The better agreement at large temperatures could partly be due to the logarithmic term proportional to T in Eq. (8.32), and the reduced Pauli-blocking at large temperatures. Regarding the EOS we found that it is not possible to correlate thermodynamic variables like the energy density directly with the composition. Even if two different models show a very similar density dependence of the composition, the EOS can be notably different.

For the three models investigated here, there remain differences in the predictions for the EOS and the composition. There are even still some uncertainties within the two quantum many-body models. We showed that the results of the excluded volume approach are not so far away from the more sound but also more complicated quantum many-body models. Obviously, due to its phenomenological character, the excluded volume concept can always only mimic the true quantum effects. On the other hand, this simpler approach allows to include other aspects, like excited states or the distribution of heavy nuclei in a simple fashion, which are more demanding to implement into the quantum many-body theories.

8.7 Application in Core-Collapse Supernovae

The main motivation for the development of the NSE model is its application in astrophysical simulations, especially for core-collapse supernovae. In this section we show some first exploratory studies of the implications of the NSE model in simulations which have been performed by Tobias Fischer from the group of Prof. Matthias Liebendörfer in Basel. The applied core collapse model `Agile-Boltztran` is based on general relativistic radiation hydrodynamics in spherical symmetry, using three-flavor (anti)neutrino Boltzmann transport. For details see Refs. [MB93b, MB93a, MB93c, MM99, LMT$^+$01b, LMT01a, LMM$^+$04]. The following weak reactions are incorporated in the form of Ref. [Bru85]:

$$\begin{aligned} e^- + p &\longleftrightarrow n + \nu_e \\ e^+ + n &\longleftrightarrow p + \bar{\nu}_e \\ e^- + < A, Z > &\longleftrightarrow < A, Z-1 > + \nu_e \\ \nu + e^\pm &\longleftrightarrow \nu + e^\pm \\ \nu + N &\longleftrightarrow \nu + N \,, \end{aligned} \tag{8.69}$$

where N denotes nucleons or nuclei. Nucleon-nucleon Bremsstrahlung is also included, based on Ref. [TB01a]:

$$N + N \longleftrightarrow N + N + \nu + \bar{\nu} \,. \tag{8.70}$$

The formation of μ/τ neutrinos

$$\nu_e + \bar{\nu}_e \longleftrightarrow \nu_{\mu/\tau} + \bar{\nu}_{\mu/\tau} \tag{8.71}$$

is implemented according to Ref. [Hor02].

In the reactions listed above, only the average nucleus of the single nucleus approximation is considered. As a first step we also use this simplification and do not take the distribution of nuclei into account. This would require different physical concepts and tremendous changes in the numerical implementation. Instead we use the average nucleus $< A, Z >$ as specified by Eqs. (8.51) and (8.52). In the same way, we do not take the distribution of the light clusters into account but treat all light clusters as alpha-particles. In the simulation, only the light cluster fraction X_a and the heavy cluster fraction X_A is used, as defined in Eqs. (8.49) and (8.50).

The general scenario of a delayed explosion in a core-collapse supernova can be split into four phases with the *collapse phase* at the beginning. The collapsing star can be divided into a subsonic homologously collapsing inner core and the outer layers which are accreted with supersonic infall velocities. Initially this infalling matter has a low entropy per baryon ~ 1 and consists of heavy nuclei. Due to the compression and the raising electron degeneracy, electron captures occur, leading to more and more neutron rich nuclei. The weak reactions listed above are essential to determine the evolution of the total proton fraction Y_p.

When nuclear saturation density is reached in the center, the increasing compressibility leads to the core rebounce in the *bounce phase*. A stagnation wave forms which travels subsonically outwards until it reaches the supersonically infalling outer layers. The wave turns into a shock wave which heats and dissociates the accreting matter. Free protons appear which capture electrons very rapidly, causing an energetic neutronization burst at 2 - 5 ms after bounce.

The moment of the bounce is shown in Fig. 8.44 for the collapse of a 15 $M_\odot$ progenitor star. Three different EOSs are applied, which allow a systematic comparison of different aspects of the EOS. As a standard reference, we apply the Shen et al. EOS, shown by the black lines. The red lines show the results for the NSE model, if TM1 is used for the interactions of the nucleons which is also used in the Shen EOS. Thus NSE TM1 is identical to Shen, when uniform nuclear matter is reached. Because we do not have a mass table for TM1 at hand, we apply the mass table for TMA from Ref. [GTM05]. The blue lines show the EOS if the same mass table is combined with the TMA parameterization for the nuclear interactions. By comparing "Hempel, TM1" with "Hempel, TMA" we can directly identify the role of the uniform nuclear matter EOS because the description of the non-uniform matter phase and nuclei is identical in the two NSE EOSs.

Let us first discuss the main aspects of the simulation at bounce, which all three models have in common. The homologous core encloses a mass of 0.6 $M_\odot$, and the accreting layers with negative velocities extend up to 1.6 $M_\odot$, see Fig. 8.44 (a). The inner core has densities larger than 10^{14} g/cm^3, whereas a sharp density drop is present at the shock front. Regarding the entropy (Fig. 8.44 (c)) we see that the shock represents an irreversible process which increases the entropy from ~ 1 to ~ 3. Initially, the accreting matter is mainly heated by compression to $T \sim 4$ MeV. Then the shock causes the huge increase of the temperature above 12 MeV. We observe that the core is almost isothermal.

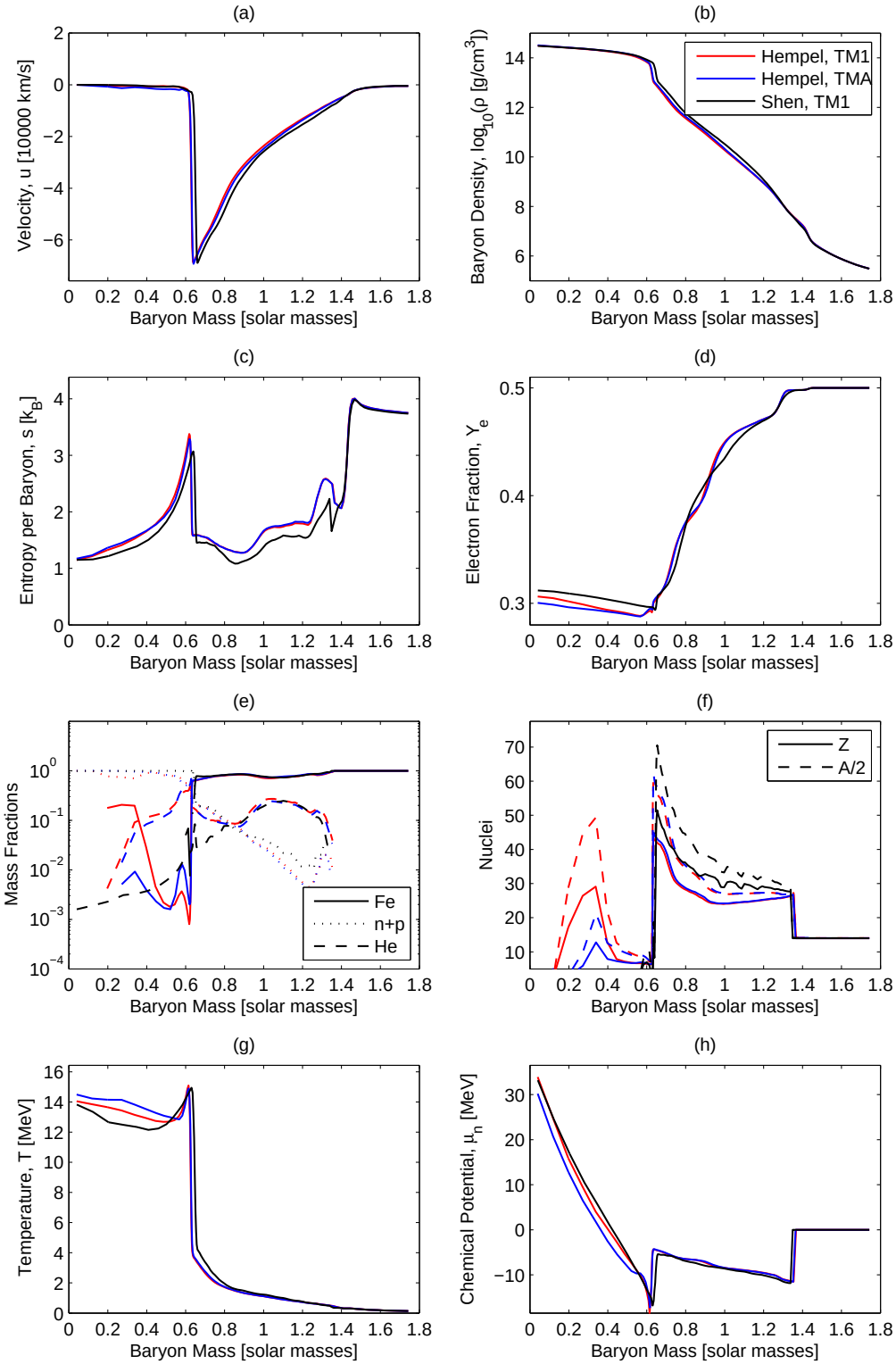

Figure 8.44: Results for the simulation of the collapse of a 15 $M_\odot$ progenitor star at bounce. Three different EOSs are applied, the Shen et al. EOS based on TM1 [STOS98a, STOS98b], the NSE EOS based on TM1 and the EOS based on TMA. In plot (e), "Fe" corresponds to the heavy mass fraction X_A and "He" to the light cluster mass fraction X_a in the NSE EOSs.

The composition can be studied by Fig. 8.44 (d) - (f). The unprocessed matter in the outermost layers corresponds to ^{28}Si. During the infall, below $M = 1.4$ M$_\odot$, electron captures take place and reduce the electron fraction, see Fig. 8.44 (d). The emitted neutrinos carry away some of the initially entropy $s \sim 4$, see Fig. 8.44 (c). Due to the compression, the nuclei become more asymmetric and increase in size, which is seen in Fig. 8.44 (f). The adiabatic compression leads to increasing temperatures with density so that the alpha particle fraction increases, Fig. 8.44 (e), when approaching the shock at $M = 0.6$ M$_\odot$ from above. Behind the shock, matter is mainly composed of free neutrons and protons.

Let us now turn to the role of the EOS. In general, the differences between NSE TM1 and NSE TMA are much less than the differences to the Shen EOS. Thus we first focus on the common differences between Shen and the two NSE models. The composition of the infalling matter above 0.8 M$_\odot$ regarding light and heavy nuclei and nucleons is rather similar in Shen and the NSE model. The temperature curves lie on top of each other in this range, but the entropy is slightly increased. By carefully looking at Fig. 8.20 one finds that the Shen EOS predicts indeed lower entropies at $T = 1$ MeV. For the infalling matter, the evolution of the electron fraction proceeds similar in the three EOSs, whereas small deviations occur. The average mass and proton number exhibit an unexpected oscillatory behavior in the Shen EOS. In the NSE models this does not occur, instead some smooth bumps are observed, which can also be identified in the electron fraction. This could be due to shell effects in the NSE description.

Between 0.6 and 0.8 M$_\odot$the light cluster fraction increases with density in the NSE model, but decreases in the Shen EOS. This could be due to the alpha particle approximation in the Shen EOS. The nucleon fraction remains similar, so that the light cluster fraction is increased on cost of the heavy nuclei. The light cluster give a contribution to the entropy and thus lower the temperature for an adiabatic compression, which is seen in Fig. 8.44 (g).

Also below the shock some differences are visible, which may be even more important. In the NSE model the light cluster fraction close to the shock is above 10 % and two orders of magnitude larger than in Shen. We already found in Fig. 8.17 that at temperatures $T > 10$ MeV the deuterons are more important than the alphas. The increased light cluster fraction occurs already in front of the shock but is even more pronounced behind it. The different predictions for the light clusters are the most evident differences between Shen and the NSE EOSs. Furthermore, the temperature and entropies behind the shock are larger in the NSE model, indicating a softer EOS with a more compact proton-neutron star (PNS) core. This can also be seen directly by the position of the shock.

In the comparison of the electron fraction of the Shen and the NSE EOSs one sees that the NSE models give a significant lower value of Y_e in the core. Because the degenerate electrons give the main contribution to the pressure, Y_e determines to large extent the compactness of the PNS. Thus the lower value of Y_e is connected to the larger entropy and temperature in the PNS and the deeper position of the shock front.

It is surprising that even the TM1 NSE model leads to lower Y_e because it differs from the Shen EOS only by the description of the nuclei and the model for the non-uniform matter phase. By considering the additional light cluster degrees of freedom like the deuteron one expects that the system tends to larger values of Y_e, but the opposite is observed here. Thus the reason for the lower electron fraction must come from somewhere else and has to be even stronger than the effect of the deuterons.

The neutrinos are trapped in the inner core, and the presence of neutrinos in general increases the electron fraction. Thus the lower Y_e could be explained by a faster diffusion of the neutrinos out of the core, leading to lower lepton and electron fractions. A faster deleptonization is obtained by larger mean free paths. Maybe it is the reduced fraction of nucleons and the increased light cluster fraction (see Fig. 8.44 (e)) below the shock which leads to the smaller neutrino cross sections and the faster deleptonization. This aspect has to be studied further to fully understand the origin of the reduced electron fraction of NSE TM1.

If weak equilibrium is achieved, then the electron fraction at a given density is directly set by the symmetry energy of the EOS. This effect can be studied by comparing TM1 with TMA. TM1 has a significantly larger symmetry energy and lower compressibility. However, in the discussion of Fig. 2.3 we showed, that the single value of K at saturation density does not give very much information about the EOS. In our case, TM1 has a larger pressure than TMA at almost all densities, despite the lower value of K. By looking at Fig. 8.44 (b) we see that the density profile of the core, which develops from the interplay of the compressibility and the symmetry energy, looks very similar in the two EOSs. Thus the electron fraction at a given radius is mainly a result of the symmetry energy. At low densities, the symmetry energy of the two NSE models is rather similar due to the presence of light clusters and nuclei. However, at large densities only the uniform nuclear matter contribution remains. Indeed, we find that the larger symmetry energy of TM1 drives the core to larger values of Y_e.

This aspect can also be identified in Fig. 8.44 (h). Below the shock, NSE TM1 gives similar values for the neutron chemical potential as Shen, as they are based on the same nuclear interactions. By approaching the center of the supernova, the electron fraction of the two models also come closer to each other. NSE TM1 has a larger neutron chemical

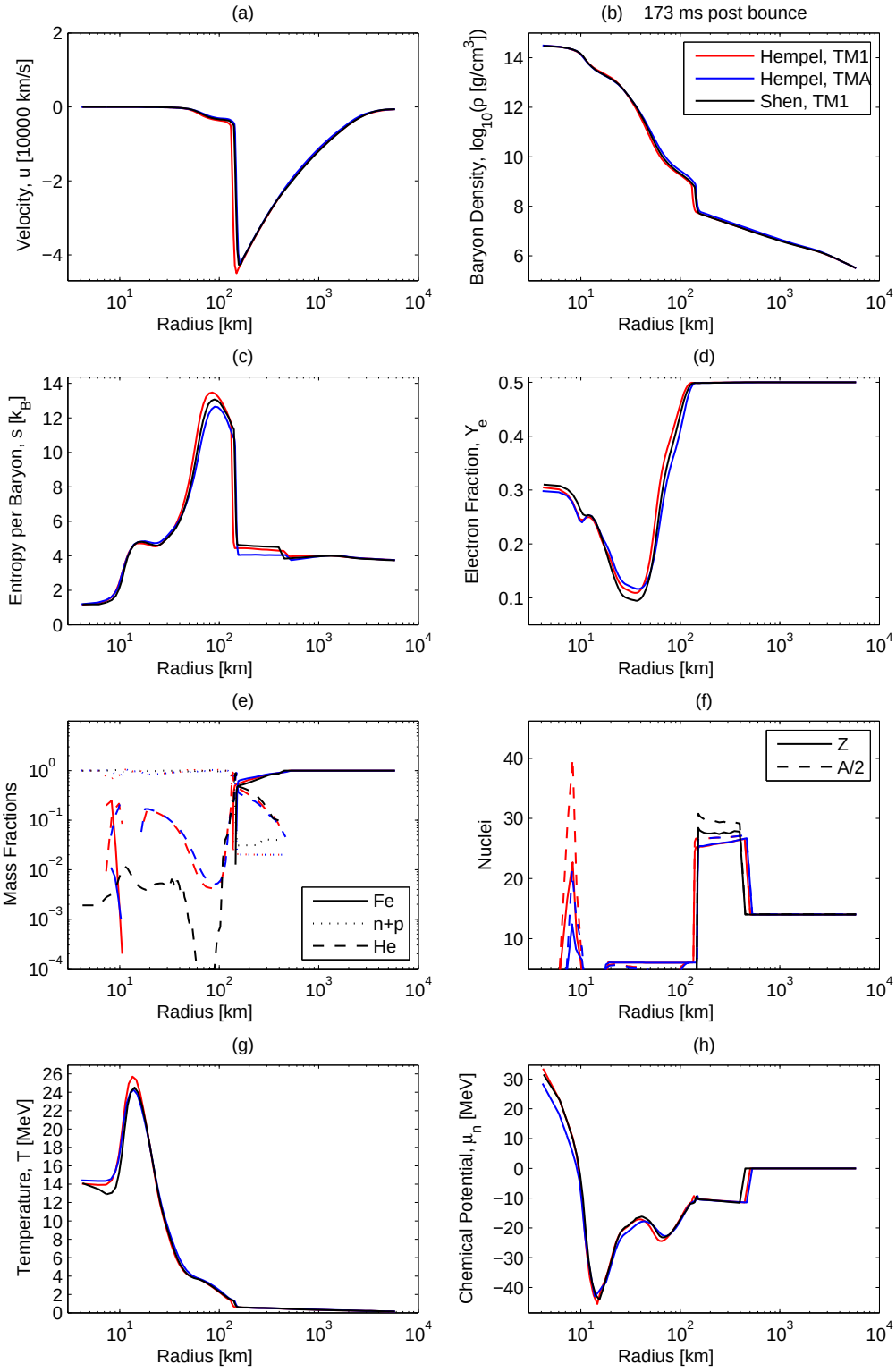

Figure 8.45: As Fig. 8.44, but at 173 ms after bounce.

potential of several MeV than TMA, meaning that it is more difficult to neutronize the matter which also reflects the larger symmetry energy.

After the bounce the so-called *accretion phase* begins. While matter is still accreting onto the PNS the dynamic shock turns into a hydrostatically expanding accretion front. This accretion front divides the cold accretion flow from the hot dissociated matter piling up on the PNS. In Fig. 8.45 we show the simulation at the later time of 173 ms after bounce. Again, we first want to discuss the most important common features and then turn to the detailed differences of the three EOSs.

We see that the accretion front has traveled outside to a radius of 200 km and much lower densities $\sim 10^8$ g/cm^3. The infalling matter has entropies of ~ 4, the matter behind the shock is heated up to $12-14$, corresponding to temperatures of 25 MeV. The center of the PNS remains still rather cold with an entropy per baryon of 1 and a temperature of $\sim$ 14 MeV, which is similar as at bounce. In the same way, the electron fraction remains rather constant in the core, because the neutrinos are completely trapped. Only further outside at the surface of the PNS their diffusion becomes important. After some neutrinos have escaped, the electron fraction can decrease further to lower the degeneracy of the electrons. The electron fraction has its minimum at $R \sim 40$ km with a value of 0.1.

The radial profile of the composition still shows some similarities to the situation at bounce. The infalling matter heats up and dissociates partly into light clusters. When the accretion front is reached it encounters a strong shock heating, so that also the light clusters are dissolved, and almost only free nucleons remain. Further inside the PNS the compression becomes strong enough that the light cluster fraction increases again. The formation of nuclei is also favored because the entropy decreases towards the center of the PNS behind the shock. In the innermost zones of the PNS almost only free nucleons remain, because the densities are too large to allow the presence of nuclei.

By looking at the electron fraction in more detail, one sees that the core below 10 km still behaves similar as during the bounce. NSE TM1 and Shen come closer to each other when approaching the center, whereas the two NSE model are closer to each other at lower densities further outside. In Fig. 8.45 (h) it is also evident that the NSE TM1 EOS gives the same neutron chemical potentials like the Shen EOS in the core, but that the two NSE models lie on top of each other in the outermost layers for $R > 100$ km. At the bounce we observed that Shen always gave larger values of Y_e below the shock. Now we find that the NSE models cross the electron fraction of the Shen EOS at $R \sim 10$ km and have a larger electron fraction further outside. This could now be allocated to the larger symmetry energy due to the inclusion of the additional light clusters besides the alpha-particle in the NSE models.

We see in Fig. 8.45 (e) that the light cluster fraction behind the shock is roughly two order of magnitudes larger than in the Shen EOS. At $R \sim 20$ km the light cluster fraction increases above 10 % in the NSE models, but jumps to zero between 10 and 20 km. This does only occur, because we neglect all nuclei in the EOS for $T > 20$ MeV for simplicity.

At 10 km another qualitative difference of the NSE models compared to the Shen EOS occurs. Before uniform nuclear matter is reached, some heavy clusters appear in a very narrow density region. This can be seen as the beginning of the uniform nuclear matter phase and part of the transition to uniform nuclear matter. In the Shen EOS, the alpha particles extend down to the center of the PNS. In this model, due to the different description of the excluded volume effects, alpha-particles can also exist above saturation density which is not physical.

Next we want to compare the NSE TM1 with the NSE TMA EOS in more detail. The core of the PNS is cooler in TM1 than in TMA. On the other hand, the maximum temperature of the envelope of the PNS is larger in TM1 and it shows more heating (in terms of entropy) after the shock. At bounce we mainly observed differences in the innermost layers and only behind the shock. Now we see some small differences arising in layers which are still in front of the shock. The accreted matter has now slightly larger entropies in TM1 than in TMA. Heat is transported to the outer layers by neutrinos, thus the increased entropy of the infalling matter might be caused by the larger shock heating in TM1. It is difficult to further explain the differences in the shock heating and the other small differences which are observed. These differences result from the complex interplay between neutrino transport, hydrodynamics and different aspects of the EOS like composition, compressibility and symmetry energy, integrated over the entire simulation time.

Figure 8.46 shows the simulation at 400 ms after the bounce. The system has continued its evolution similar as from the bounce to 173 ms postbounce. Neutrinos in the core are still trapped, so that the electron fraction in the center has almost not changed. The deleptonization in the layers further outside has continued and the electron fraction has decreased below 0.1. The surface of the PNS has contracted further, so that the entropy has increased above 16 and the temperature above 30 MeV. Now we observe also a slight increase of the temperature in the center of the PNS. The accretion front has moved further inside to $R \sim 180$ km during this contraction. The compression has also lead to the complete disappearance of the heavy clusters below the shock which were present in the NSE models before.

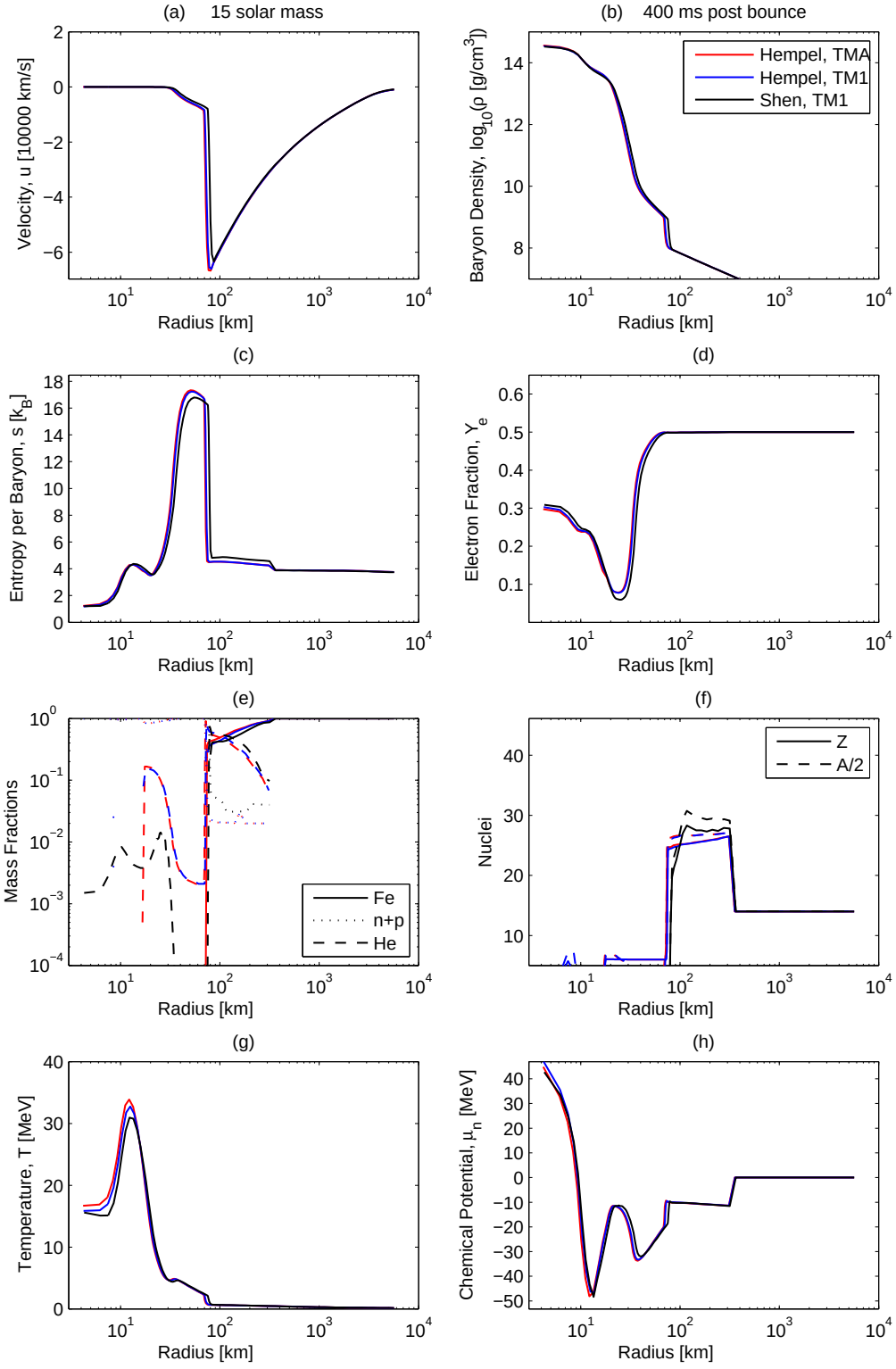

Figure 8.46: As Fig. 8.44, but at 400 ms after bounce. Note the different color coding for TM1 and TMA compared to Fig. 8.44.

It is interesting that the two NSE models look now again more similar than they did at 173 ms. The compression has again leveled off some of the characteristic features of the two EOSs. The biggest difference occurs in the neutron chemical potential and the temperature, with the latter being 1 to 2 MeV larger in TMA, indicating that TMA is the softer EOS with the lower maximum mass.

After the accretion phase has lasted for roughly 500 ms one expects that the explosion sets in, which marks the beginning of the *explosion phase*. The hot accumulated matter drives the shock to larger radii into the outer layers leading to a supernova explosion and the ejection of matter. A part of the matter is still falling onto the PNS or fills the space between the surface and the ejecta in form of a neutrino driven wind. However, so far explosions in spherical symmetry have only been obtained for one particular 8 $M_\odot$ ONeMg progenitor star. The differences which we observe for the different EOSs are rather small. Thus we do not expect that the new EOSs lead to important changes in the subsequent (short-time) evolution of the supernova.

However, from this study and in particular from the comparison between NSE TM1 and Shen, we can conclude that the model for the description of the non-uniform matter phase is more important than a change of the parametrization of the nuclear interactions. Even though the compressibility and the symmetry energy of nucleon matter are significantly different in TM1 and TMA, different effects cancel each other, so that the simulation looks almost identical at 400 ms postbounce time. E.g. the consideration of additional light clusters like the deuteron is more important than the particular form of the nuclear interactions.

Furthermore, we want to remind the reader that the NSE EOSs were used in a form which is equivalent to the Shen EOS, i.e. all light clusters are treated as alpha-particles and only the average nucleus of the distribution of heavy nuclei is considered. Thus we only probed the thermodynamic differences of the Shen and the NSE EOSs. Actually it is convenient, that only reasonably small differences occurred. Based on these results one could now start to include additional nuclear effects into the simulations. For example it would be interesting to implement the deuterons and their weak reactions or to take into account the distribution of the heavy nuclei.

To study the impact of the progenitor and to probe different conditions of the EOS, we also performed simulations for a 40 $M_\odot$ progenitor star. The results at bounce are shown in Fig. 8.47. By comparing with Fig. 8.44 we see that the shock is located at a very similar position and that the matter in the core which has passed through the shock has developed to similar conditions. However, in more detail we find, that a larger baryon

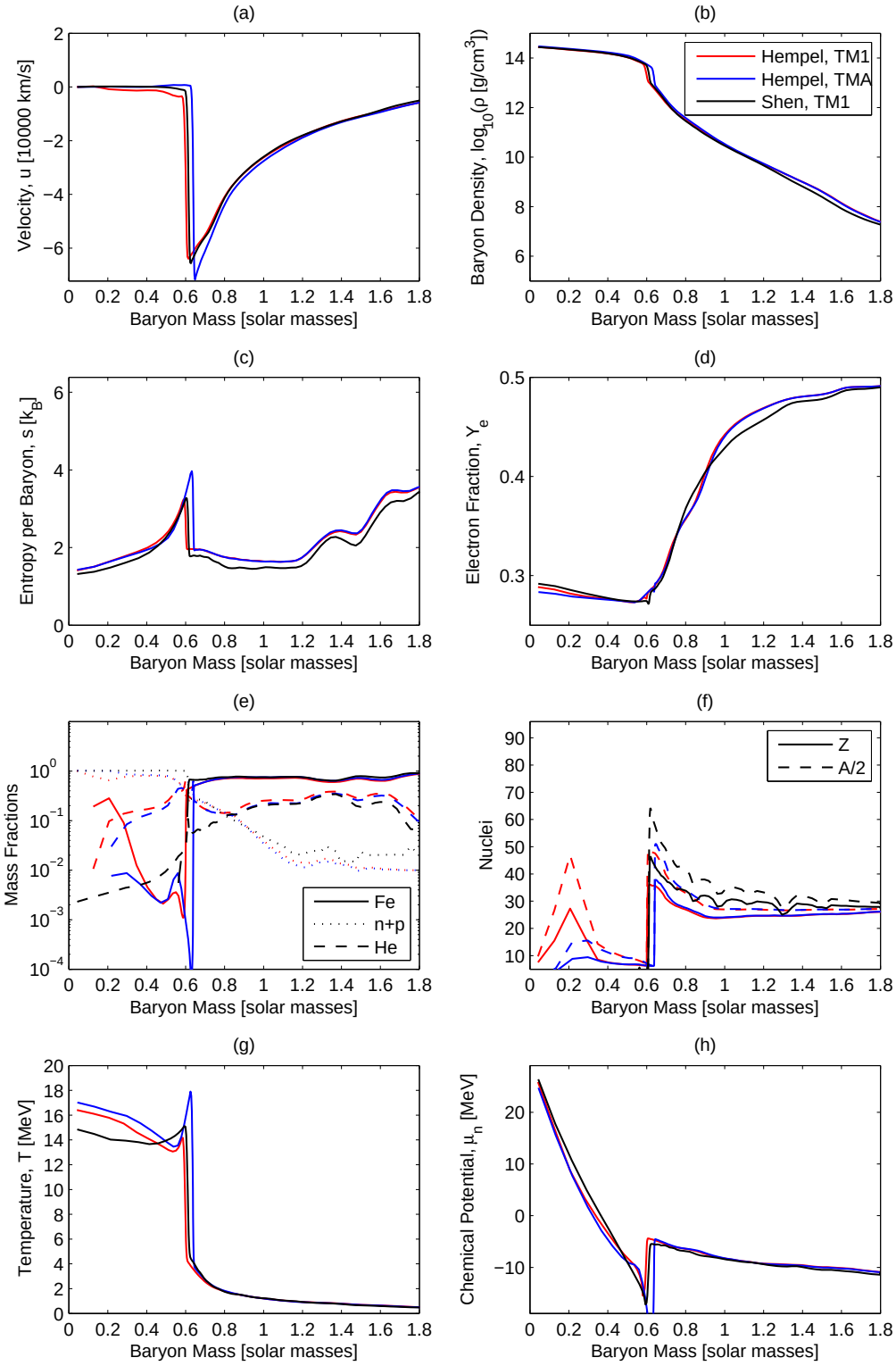

Figure 8.47: Results for the simulation of the collapse of a 40 $M_\odot$ progenitor star at bounce. Three different EOSs are applied, the Shen et al. EOS based on TM1 [STOS98a, STOS98b], the NSE EOS based on TM1 and the EOS based on TMA.

mass has negative velocities, i.e. more matter is infalling. Furthermore, the temperature of the core is increased by several MeV and has a slightly lower electron fraction.

Regarding the composition we find the same results as before, namely that the NSE and the Shen EOS mainly differ below and close to the shock by a significantly increased light cluster fraction in the NSE models. Furthermore, the transition to uniform nuclear matter occurs via the appearance of heavy nuclei, which does not happen in the Shen EOS. The Y_e profiles exhibit the same features as discussed before. At low densities the two NSE models give the same results, only in the most central part the NSE TM1 EOS goes over to the Shen EOS, which gives larger electron fractions than TMA due to the larger symmetry energy. In general the two NSE EOSs lead to rather similar results. Interestingly, only directly at the shock some larger differences occur between NSE TM1 and NSE TMA. The shock is located a little bit further outside in TMA, the accreting matter has a larger infall velocity and the entropy increase after the shock is larger.

In Figure 8.48 we show the results for the 40 $M_\odot$ progenitor at 218 ms postbounce time, i.e. at a similar stage as Fig. 8.45 for the 15 $M_\odot$ progenitor. By comparing the results for the two progenitor stars we find that the shock is still located at a similar position. The temperature in the case of the more massive progenitor is significantly larger and reaches almost 40 MeV at the envelope of the PNS. Thus uniform nuclear matter extends to lower densities than for the 15 $M_\odot$ progenitor. As the temperature in front of the shock is now slightly larger, the contribution of the light clusters is further enhanced and even prevails the heavy clusters. In front of the shock the light clusters are mainly alpha-particles, and thus the results of the Shen and the NSE EOSs coincide. Below the shock the missing other light clusters in the Shen EOS lead to considerably different results.

It is interesting to see, that exactly in the region from 10 to 100 km where the light cluster fraction is different, also the electron fraction deviates in the Shen and the NSE EOSs. The contribution of the additional light clusters increases the symmetry energy and thus leads to larger values of Y_e below saturation density. The electron fraction in the core is still the largest in the Shen EOS, due to the different evolution. This could be seen as the reason for the slightly more compact PNS core and the larger temperature in the core. Above 11 km, the temperature profiles of the three EOSs are similar. This leads to the increased entropy in the two NSE models, because of the additional degrees of freedom which are considered.

Also from the study of the 40 $M_\odot$ progenitor we conclude, that the model for the low-density EOS is more important than the change of the parametrization of the nuclear interactions. At this stage of the evolution, the dynamics seem to be dominated by the

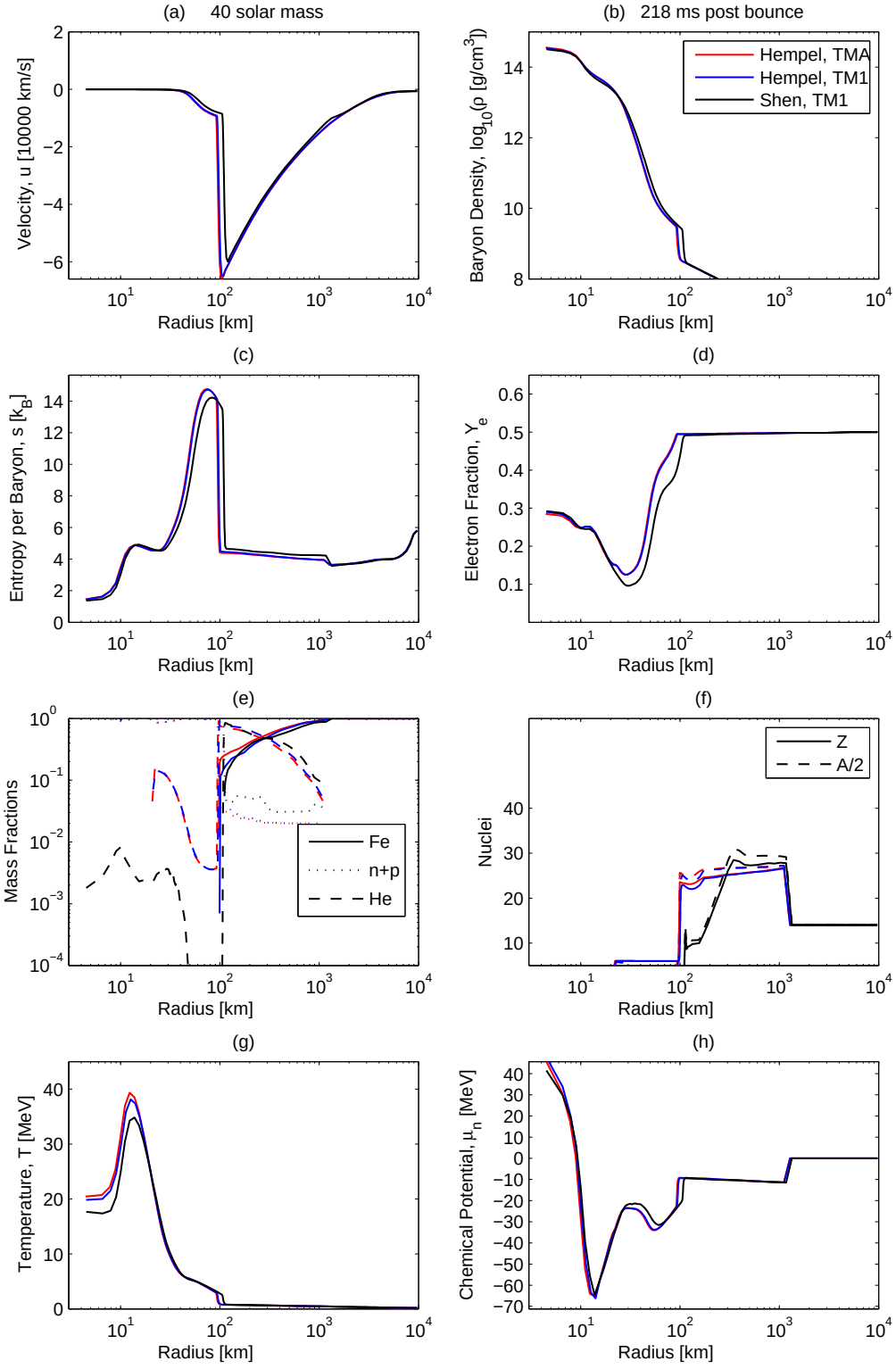

Figure 8.48: As Fig. 8.47, but at 218 ms after bounce. Note the different color coding for TM1 and TMA compared to Fig. 8.47.

EOS below saturation density and not so much by the EOS of the core. As a further study it would be interesting to use a consistent NSE EOS for TM1, i.e. an EOS which utilizes a mass table which is also based on TM1. The NSE TM1 EOS which was shown here used the same mass table as in the TMA EOS. Thus we cannot estimate the impact of the change of the nuclear masses due to the use of different nuclear interactions.

For both progenitors, in the comparison of Shen and NSE TM1 some small but interesting differences were found. Again, we want to emphasize that these differences only arise due to the different model assumptions for the description of nuclei and non-uniform nuclear matter. It would also be interesting to calculate and apply an NSE EOS with nuclear interactions which are significantly different compared to TM1 or TMA. This could lead to more pronounced effects of the uniform nuclear matter EOS in the simulation.

For a future simulation, especially the FSUgold interactions are interesting, because of the well constrained behavior of the symmetry energy. The inclusion of the ω-ρ-coupling is much more important than the change from TM1 to TMA which can also seen by the drastic reduction of the maximum mass of FSUgold to only 1.67 $M_\odot$. Due to the low symmetry energy at large densities we expect that the electron fraction will be further decreased in the core with the FSUgold EOS. Thus a larger gravitational binding energy is in principle available for the explosion. Furthermore, low symmetry energies at large densities imply in most cases larger symmetry energies at low densities below saturation density. Then the electron fraction in the region below the shock would be slightly increased. This could lead to larger neutrino heating below the shock so that it might be possible that a larger energy will be deposited in the shock. Additional energy deposition below the shock is one of the key ideas how to achieve an explosion. However, these expectations need to be verified by simulations, because many other effects can be counteracting, e.g. the neutrino transfer. By understanding the impact of the EOS in core-collapse supernovae further, one might find some more insight which aspects of the EOS help to achieve a robust supernova-mechanism.

Chapter 9

The Quark-Hadron Phase Transition

9.1 Signals in Core-Collapse Supernovae

In this section we show results for the investigation of the implications of the hadron-quark phase transition in the dynamical environment of a core-collapse supernova, which was published in [SHP+09]. So far only few detailed numerical studies have been performed to this scenario (see Sec. 2.3 for the literature review), because very often it is expected, that the phase transition occurs at later stages of the evolution, either in the protoneutron star stage or as a cold neutron star. Furthermore, a core-collapse supernova represents one of the most complex scenarios of astrophysics and its proper description requires extensive numerical simulations.

As we aim to study the basic effects from quark matter phase transitions on core-collapse supernovae, we take the very simple but widely applied quark bag model for the description of quark matter, see Sec. 2.5. We choose the bag constant such that we obtain an early onset for the phase transition at the density n_{crit} and a maximum mass of more than 1.44 $M_\odot$, without enabling absolutely stable strange quark matter. Within this narrow range we select $B^{1/4} = 162$ MeV (*eos1*) and 165 MeV (*eos2*), and a strange quark mass of 100 MeV as indicated by the Particle Data Group [Par04]. For the hadronic EOS we use the table of Shen et al. [STOS98a].

For the phase transition to quark matter we assume only global charge neutrality, thus Case V of Table 7.2 gives the conditions for chemical equilibrium. For the sake of simplicity, we have neglected finite size effects and Coulomb interactions within the mixed phase. Supernova timescales are in the range of ms and therefore long enough to establish equilibrium with respect to weak interactions that change the strangeness on the timescales of micro-seconds or less. Thus we assumed that strangeness is not conserved, leading to zero strangeness chemical potential, see Sec. 6.4. The phase diagram using *eos1* for different proton fractions Y_p is shown in Fig. 9.1. Because several

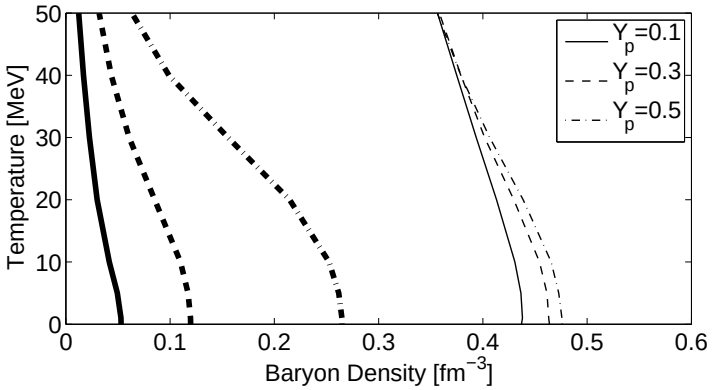

Figure 9.1: The onset (thick lines) and the end (thin lines) of the mixed phase from the QCD phase transition from nuclear matter to quark matter using *eos1*.

globally conserved charges exist (four), the phase transformation is continuous and very smooth. The mixed phase extends over a very broad range in density. It would be interesting to repeat the following study, by using different equilibrium conditions, e.g. for the assumption of local charge neutrality (given by case IV). Additional local constraints would lead to larger critical densities and decrease the density range of the mixed phase. Consequently the pressure would increase more slowly with density.

We remark that larger values for the bag constant result in higher critical densities. The two choices of the bag constants lead to critical densities of ~ 0.12 fm^{-3} and ~ 0.16 fm^{-3}, respectively (for $T = 0$ and proton fraction $Y_p = 0.3$). However, the small obtained values for the critical density close to saturation density are not in contradiction with heavy ion data. In contrast to heavy-ion collisions high-density supernova matter is isospin-asymmetric with a proton fraction $Y_p \sim 0.3$. Furthermore the typical expansion timescale in a relativistic heavy ion collision of 10^{-22} s, does not allow the equilibration of any weak reactions. Strangeness is conserved with total strangeness zero. Contrary, in supernovae the net strangeness can be produced to lower the Fermi momenta of the other quarks. The additional strange quark degree of freedom and the large asymmetry energy allow one to obtain small values for n_{crit} and lead to an early appearance of quark matter (see Fig. 9.1).

Our choice of parameters is also compatible with the still most precise neutron star mass measurement of 1.44 $M_\odot$ for the Hulse-Taylor pulsar [LP04]. With *eos1* and *eos2*, we obtain values for the maximum gravitational mass of 1.56 and 1.50 $M_\odot$ respectively. Note that higher neutron star masses can be achieved with more sophisticated models of quark matter [ABD$^+$07]. For $B^{1/4}$=162 and 165 MeV, almost the entire star is composed of quark matter, surrounded by a mixed quark-hadronic phase, which is enclosed by a thin pure hadronic crust.

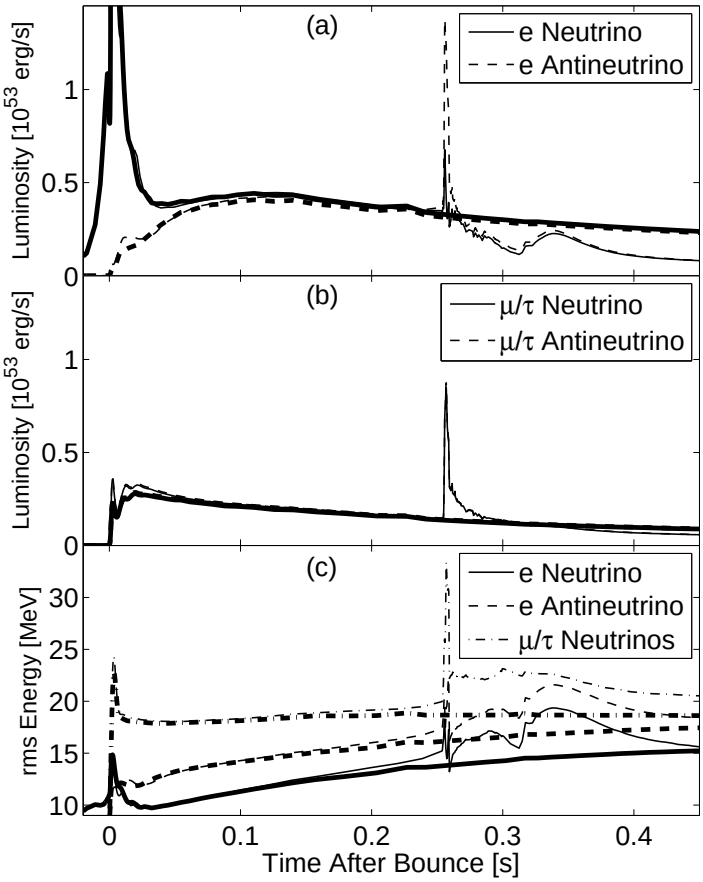

Figure 9.2: Neutrino luminosities (a) and (b) and rms-energies (c) calculated at 500 km radius for a 10 $M_\odot$ progenitor model. The results of the quark EOS *eos1* (thin lines) are compared to the results of the pure hadronic EOS [STOS98a] (thick lines). A second neutrino burst is clearly visible at $\sim$ 260 ms after bounce.

For the accurate prediction of the three-flavor neutrino signal, general relativistic effects may be important. Hence, we choose for our investigation the well-tested general relativistic description of the neutrino radiation hydrodynamics in spherical symmetry, that is based on Boltzmann neutrino transport. The simulation is based on the same computer code which was introduced at the beginning of Sec. 8.7. Quark matter appears only in optically thick regimes where neutrinos are in thermal and chemical equilibrium with matter. Thus for this first proof-of-principle study, we use the hadronic weak interaction rates for the corresponding reactions in the quark phase. The quark chemical are translated into hadronic chemical potentials by the use of Eq. (5.17) so that weak equilibrium for neutrinos in quark matter is obtained. Our simulations are launched from a 10 and a 15 $M_\odot$ progenitor model from Ref. [WHW02].

The standard core-collapse scenario leads to core bounce at nuclear saturation density and the formation of a shock. This expanding shock looses energy due to the dissociation

Prog. [$M_\odot$]	EOS	t_{pb} [ms]	M_Q [$M_\odot$]	M_{mix} [$M_\odot$]	M_{PNS} [$M_\odot$]	E_{expl} [10^{51}erg]	BE [10^{53}erg]	M_G [M_G]
10	*eos1*	255	0.850	0.508	1.440	0.44	3.40	1.25
10	*eos2*	448	1.198	0.161	1.478	1.64	3.19	1.30
15	*eos1*	209	1.146	0.320	1.608	0.42	4.08	1.38
15	*eos2*	330	1.496	0.116	1.700	–	4.28	1.46

Table 9.1: Baryon masses of the quark core, M_Q, the mixed phase, M_{mix}, the total PNS, M_{PNS}, in a late stage when the explosion energies, E_{expl}, are positive. BE is the gravitational binding energy of the corresponding cold hybrid star and M_G its gravitational mass. The pure quark phase first appears at postbounce time t_{pb}. For the 15 $M_\odot$ progenitor and *eos2* at t_{pb} a black hole forms.

of nuclei and the emission of the ν_e-burst at ~ 10 ms after bounce (see Fig. 9.2 (a)) and therefore turns into a standing accretion shock (SAS). The SAS could be revived by neutrino heating [BW85]. However, explosions in spherically symmetric models with accurate neutrino transport have only been obtained for a 8 $M_\odot$ ONeMg progenitor star [KJH06]. The collapse of more massive progenitors leads to an extended postbounce phase, during which the central protoneutron star (PNS) contracts due to mass accretion.

In our models that allow a transition to quark matter, the onset of the mixed phase ($n_B \sim 0.1$ fm^{-3}, $T \simeq 10$ MeV, $Y_e \sim 0.3$) is already achieved at core bounce. The initially reached quark matter fraction at the center of the PNS remains small during the first 50 ms after bounce. In the subsequent compression, the quark matter fraction rises again and an increasing central region of the PNS enters the mixed phase. The reduced adiabatic index causes the PNS to collapse.

PNS collapse: At a central density of 4 - 5 times nuclear saturation density the collapse halts due to the stiffening of the EOS in the pure quark phase. A large fraction of the PNS is composed of quarks, enclosed by a mixed hadronic-quark phase, which is surrounded by the infalling hadronic envelope (see Table 9.1). The mixed phase region shrinks gradually during the PNS collapse as more and more matter converts from the mixed into the pure quark phase. On this short time scale of ~ 1 ms, the SAS remains almost unaffected by this dynamical evolution inside the PNS (see Fig. 9.3). However, the change in the chemical potentials and the increasing density during the phase transition establish weak equilibrium at a lower electron fraction $Y_e \leq 0.1$, while the mean energy of the trapped ν_e increases above 200 MeV.

Shock formation and early shock propagation: A subsonic accretion front forms at the interface between the hydrostatic pure quark phase and the infalling mixed phase

(thick dashed line Fig. 9.3). The accretion front propagates through the mixed phase, meets the supersonically infalling hadrons at the sonic point and turns into an accretion shock (thick dash-dotted line). The high temperature and densities at the shock front lead to a rapid conversion of hadronic matter into the mixed phase. As the accreted layers become less dense, the second accretion shock detaches from the mixed phase boundary and propagates into the pure hadronic phase. This phase was deleptonized by the continued emission of electron neutrinos after the first neutronization burst. Weak equilibrium is achieved at an electron fraction ~ 0.1. When the second shock runs across this matter, the electron-degeneracy is lifted by shock-heating and the weak equilibrium is restored at higher values of the electron fraction ($Y_e \geq 0.2$). The larger adiabatic index of the hadronic phase turns the accretion shock into a dynamic shock with positive matter velocities (see thin solid line Fig. 9.3).

Explosion: As the second shock propagates across the steeply declining density gradient in the outer layers of the PNS the shock wave is strongly accelerated. Up to this point, neutrino transport plays a negligible role since neutrinos are trapped. This changes when the second shock reaches the neutrino spheres. A second neutrino burst of all neutrino flavors is released (see Fig. 9.2), dominated by $\bar{\nu}_e$ stemming from positron captures that establish the above-mentioned increase in Y_e. Due to its compactness the PNS releases (μ/τ) - neutrinos with significantly higher mean energies as illustrated in Fig. 9.2 (c). As soon as the expanding second shock merges with the outer SAS, the scenario resembles the situation of a neutrino-driven explosion mechanism (thin dashed line in Fig. 9.3), except for the large matter outflow with velocities $\sim 10^5$ km/s. Behind the expanding matter, a region with matter inflow develops due to neutrino cooling (thin dash-dotted line). The matter inflow becomes supersonic and produces another standing accretion shock at the surface of the PNS at a radius of ~ 50 km. The corresponding accretion luminosity explains the transient increase of the electron neutrino flavor luminosities in Fig. 9.2 (a) ~ 340 ms after bounce. The neutrinos emitted from this cooling region are partly absorbed behind the expanding shock. After the onset of the explosion the neutrino luminosities decrease again.

In general, the models with *eos1* and *eos2* evolve in a qualitatively similar manner. However, the models with the larger bag constant show a longer PNS accretion time before the onset of the phase transition due to the larger critical density. This results in a more massive PNS with a steeper density cliff at its surface. The higher postshock internal energy and the larger density gradient lead to a stronger second shock acceleration at the density cliff and explain the larger explosion energies. In comparison to the simulations using *eos1*, the second neutrino burst appears several 100 ms later and is found to have a larger peak-luminosity. The more massive progenitor stars give an

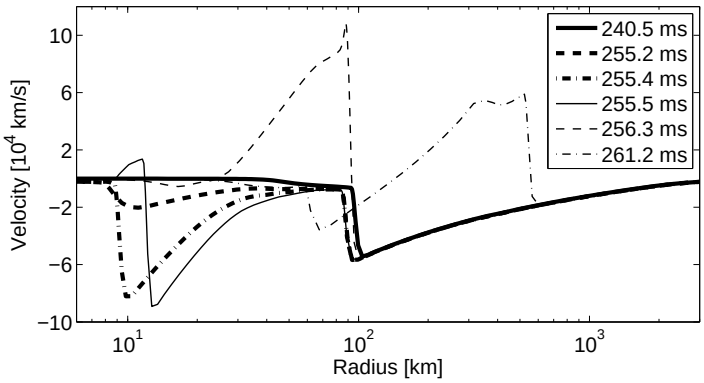

Figure 9.3: Velocity profiles at different times during the postbounce evolution of a 10 $M_\odot$ progenitor model based on *eos1*, illustrating the development of the explosion through different stages.

earlier onset of the phase transition and result in a more massive PNS with a shallower density cliff. A special case is the dynamical evolution of the PNS of the 15 $M_\odot$ progenitor model using *eos2*. Almost simultaneously with the formation of the second shock, the more compact quark core collapses to a black hole.

The goal of this investigation is to predict the general effects of a phase transition to quark matter in core collapse supernovae. The main result is a strong signature of the formation of quark matter, if it occurs during the postbounce phase. A second shock forms inside the PNS, that affects significantly the properties of the emitted neutrinos. We note that the formation of a second shock caused by the phase transition was already found in the investigative study of Ref. [GAM+93]. For a Galactic core-collapse supernova, the second neutrino burst should be resolvable by the present neutrino detectors. Unfortunately, the time sequence of the neutrino events from SN1987A [K. 88] was statistically not significant. While the binding energies of the remaining cold hybrid stars are in agreement with theoretical estimates for the energy release in SN1987A [Bet90] further analysis and improvements of the EOS would be required to optimally reproduce the temporal structure of the neutrino signal. The magnitude and the time delay of the second neutrino burst provide correlated information about the critical density, the EOS in different phases and the progenitor model. For low and intermediate mass progenitor models, the energy of the second shock becomes sufficient to drive an explosion even in spherical symmetry. We obtain explosion energies of several 10^{50} erg (see Table 9.1). The explosion is powered by the accretion of matter into the deep gravitational potential followed by the shock acceleration at the surface of the PNS. The ejecta contain neutron-rich material that expands on a fast timescale and should be investigated as a possible site for the r-process. With respect to the remnant, the narrow range of PNS masses

found in Table 9.1 may provide an explanation for the clustering of the observed neutron star masses (gravitational) around 1.4 $M_\odot$ (see e.g. [LP04]). The discussed direct black hole formation at the phase transition could be investigated further in light of the observed connection between supernovae and γ-ray bursts [Pir05, BBD$^+$03, MHB$^+$03].

The presented analysis should be complemented by multi-dimensional simulations, to explore the impact of known fluid instabilities that can not be treated in spherical symmetry. Another interesting scenario would be a weak neutrino driven explosion, followed by a fallback-induced QCD phase transition. Since the QCD phase diagram shows a large variety of color-superconducting phases [RWB$^+$05, SB07], a more sophisticated quark matter EOS should be adopted. This could lead to a second phase transition within the quark core of the PNS and would be an interesting extension of the present study.

9.2 A New Possible Quark-Hadron Mixed Phase in Protoneutron Stars

As another application we want to study the quantitative properties of the phase transition for one of the cases of Chap. 7 by applying the general conditions to specific equations of state for hadronic and quark matter. For case IIb of Sec. 7.3 we will analyze the consequences for the protoneutron stars' evolution during the cooling process and its stability. We follow the discussion of Ref. [PHSB09] which represents the first study of a locally charge neutral mixed phase in the context of compact stars.

We assume that the surface tension between the quark and hadron phase is so large, that the two phases are almost charge neutral, for details see Subsec. 7.1.1. Let us consider the interface between the two phases: a charge separated interface is formed with a size of the order of the Debye screening length, ~ 10 fm, with a layer of positively charged, electron depleted, hadronic matter on one side and a layer of quark matter with an excess of the electron on the other side (as discussed in [ARRW01] for the CFL phase). The interface is stabilized by the resulting electric field.

A calculation of finite size and charge screening effects in the mixed phase for protoneutron star matter, which has fixed entropy per baryon and fixed lepton fraction, has not yet been performed. Instead of including finite size effects we model this situation by requiring strict local charge neutrality. This introduces different chemical potential of charged particles in the two phases, e.g. for electrons. Notice that neutrinos, being not affected by the electric field, can freely stream across the interface. Consequently, lepton number is conserved only globally. This additional globally conserved quantum number has similar effects as the global charge neutrality condition adopted to model the phase transition for vanishing values of the surface tension.

We already showed that local charge neutrality implies a constant-pressure mixed phase for cold and catalyzed matter. This is not the case for the hot and lepton rich matter formed in a protoneutron star due to the conservation of lepton number and entropy. These additional conserved extensive variables lead to the appearance of a new kind of mixed phase during the stage of neutrino trapping and its gradual disappearance during deleptonization. The disappearance of the mixed phase at the end of deleptonization might lead to a delayed collapse of the star into a more compact configuration containing a core of pure quark phase. In this scenario, a significant emission of neutrinos and, possibly, gravitational waves is expected.

We consider here the "standard" conditions of a newly born neutron star, see Sec. 6.2 and Ref. [SPL00]: the matter has a fixed lepton fraction $Y_L = (n_e + n_\nu)/n_B = 0.4$ and

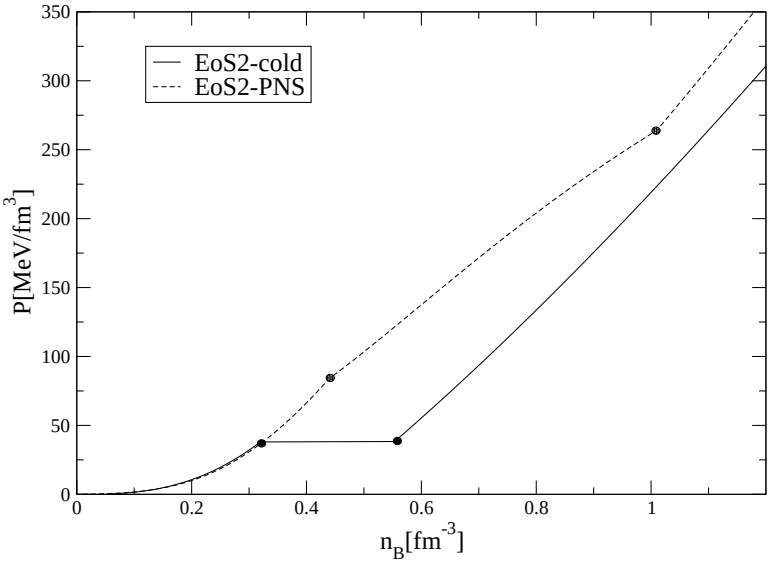

Figure 9.4: The equations of state are shown for the case of EOS2 for protoneutron star matter (dashed line) and for cold and catalyzed star matter (solid line). The dots indicate the onset and the end of the mixed phase in both cases.

fixed entropy per baryon $S/N_B = 1$ where n_e, n_ν and n_B are the electron, neutrino and baryon number densities and S is the entropy. The equilibrium conditions in protoneutron stars for local charge neutrality are given in Table 7.2 by case IIb. In addition we have pressure and thermal equilibrium. The two phases are locally charge neutral, so that only the entropy and the lepton number can be shared by the two phases:

$$(1-\chi)(n_e^h + n_\nu) + \chi(n_e^q + n_\nu) = Y_L n_B \tag{9.1}$$

$$(1-\chi)s^h + \chi s^q = S/N n_B \ . \tag{9.2}$$

The index h denotes the hadronic phase, q the quark phase, and s^α the local entropy density. We used that the neutrino densities are equal in the two phases. χ denotes the share of the quark phase of the total volume. The last two equations allow to fix χ and together with temperature and chemical equilibrium the system of equations can be solved.

To calculate the equations of state of hadronic matter and quark matter we adopt the relativistic mean field model with the parameterization TM1 for the former [STOS98a] and the MIT bag model including perturbative corrections for the latter [FPSB01, ABPR05]. We set the masses of up and down quarks to zero and the mass of the

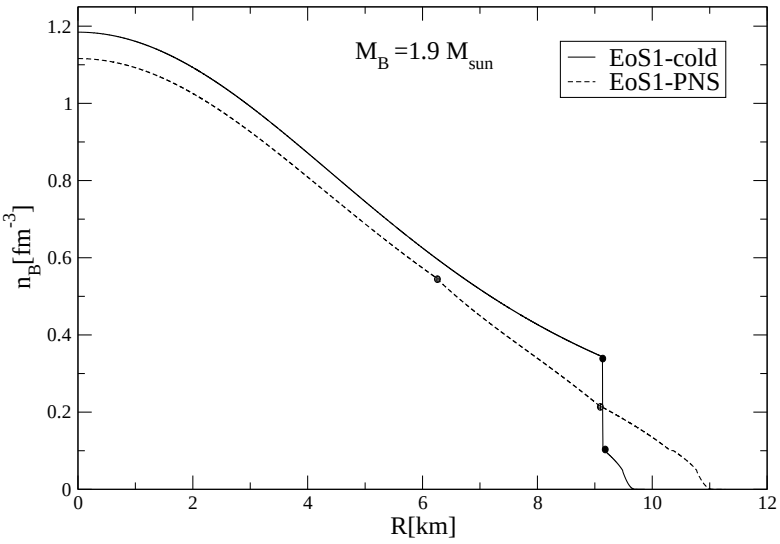

Figure 9.5: Density profiles for a star with a baryon mass of $1.9 M_\odot$ for the protoneutron star stage and the cold configuration. The dots mark the onset and the end of the phase transition.

strange quark to 100 MeV. We fix the constant which simulates the QCD perturbative corrections $c = 0.2$, and we select two values of the effective bag constant $B_{\rm eff}$ in order to have a critical density for the phase transition in protoneutron star matter of $\sim n_0$ and $\sim 3n_0$ (where $n_0 = 0.16$ fm^{-3} is the nuclear saturation density), corresponding to $B_{\rm eff}^{1/4} = 155$ MeV and $B_{\rm eff}^{1/4} = 170$ MeV. The two equations of state are labeled as EOS1 and EOS2 for the two choices of the effective bag constant. In Fig. 9.4 we show the equations of state for matter in a protoneutron star (indicated with PNS) and for cold and catalyzed matter (indicated with "cold"). The remarkable result is that within the mixed phase, the pressure increases as a function of the density and a large range of density is occupied by the mixed phase. During deleptonization the pressure in the mixed phase gradually flattens and finally for deleptonized and cold matter one finds the usual result of a Maxwell construction with a constant pressure from the onset to the end of the phase transition. This is in complete agreement with the expectations of the preceding chapters.

We use now the above presented equations of state to study the structures of protoneutron stars and cold stars. In Fig. 9.5 we show the density profile for a protoneutron star and the corresponding cold configuration (assuming total baryon number conservation during the cooling and deleptonization of the newly born star). The mixed phase,

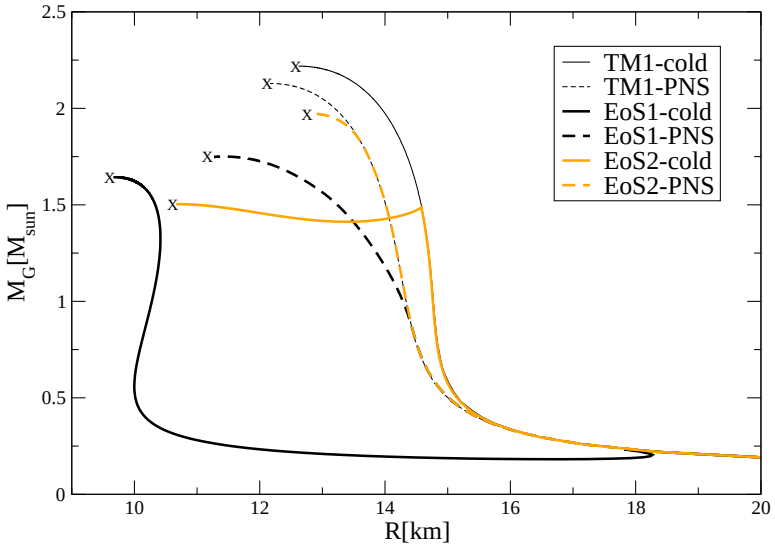

Figure 9.6: The mass-radius relations are shown for the different equations of state, EOS1, EOS2 and TM1 and for protoneutron stars and cold stars configurations (colors online). The crosses correspond to the maximum mass configurations.

initially present in a ~ 2 km large layer of the star, gradually shrinks during the deleptonization of the star and finally disappears in the cold configuration. As a result, a sharp interface separating hadronic matter from quark matter is obtained with a sizable jump of the baryon density. This shows nicely the evolution from a continuous to a discontinuous phase transformation during the cooling.

In Fig. 9.6 we show the mass-radius relations for the different cases. The black and orange thick dashed lines correspond to hybrid protoneutron stars (EOS1 and EOS2 respectively), the black and grey (orange online) thick solid lines correspond to the cold configurations. Neutron stars mass-radius relations are also shown for comparison (thin curves labeled with TM1). The new mixed phase appears in a protoneutron star because the pressure increases with the density. Therefore, we obtain stellar configurations with a core of pure quark matter, a layer of mixed phase and a layer/crust of hadronic matter for the case of EOS1 and hybrid stars with only a core of mixed phase in the case of EOS2. The mixed phase cannot appear anymore in the star for cold and catalyzed matter because the pressure is constant and only configurations with pure phases are obtained. As discussed before, a sizable jump of the density occurs at the interface separating the two pure phases which affects the stability of the stars: at the onset of the phase transition the stars are gravitationally unstable and only if a sizable volume of the star is

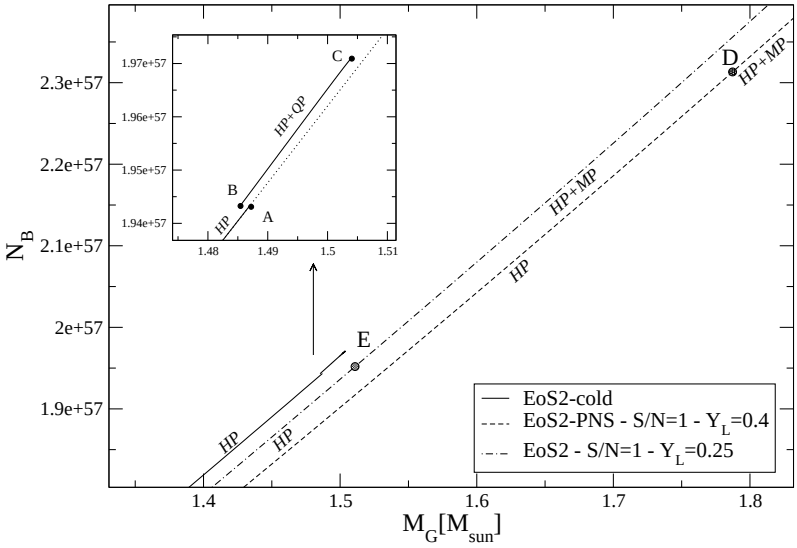

Figure 9.7: The total baryon number of compact stars as a function of the gravitational mass for EOS2 at different stages of the temporal evolution: protoneutron star (PNS, Y_L=0.4, $S/N = 1$), an intermediate stage with $Y_L = 0.25$, $S/N = 1$ and the cold configurations (cold). In the insert we show a magnification of the third family branch (solid line) and we also show the result for neutron stars (dotted line). *HP*, *MP* and *QP* denote the hadronic phase, the mixed phase and the quark phase respectively.

occupied by the quark phase the stars are stable. The mass-radius relations in this case correspond to the so called "third family" solutions, see [Ger68, SGST00, SHSG02, BB03] for a detailed discussion of the properties of these stars.

Concerning phenomenology, an interesting possibility is a delayed transition of a protoneutron star in a third family star during/after deleptonization, which is outlined in Fig. 9.7. The plot shows the baryon number of the stars as a function of the gravitational mass for protoneutron stars (dashed line) and cold stars (solid line). For the sake of discussion an intermediate configuration is also included (dotted-dashed line) corresponding to partially deleptonized matter with $Y_L = 0.25$. The insert shows a magnification of the third family branch of cold hybrid stars. The letter A in the plot denotes the configuration of a cold neutron star which is unstable with respect to the collapse to a third family star, indicated by the letter B, with the same baryon number. The energy released in such a collapse (the difference between the gravitational masses of the two configurations at fixed baryon number) is of the order of 10^{51} erg similar to values found in Ref. [MHB$^+$03]. The letter C marks the maximum mass of cold hybrid

stars. The letter D stands for the configuration of a protoneutron star for which the central density is equal to the density of the onset of the phase transition and a core of mixed phase is formed; the core of mixed phase increases with the central density and therefore with the mass of the stars. Stellar configurations with a baryon number lower than A are always composed of purely hadronic matter during the evolution of the star. Since C is smaller than D, for stellar configurations having baryon number between the labels A and C the corresponding protoneutron stars do not have quark matter in the core (neither pure phase nor mixed phase) but during the deleptonization, since the onset of the phase transition decreases, at a certain point a core of mixed phase forms (e.g. at point E). As the deleptonization proceeds the mixed phase gradually shrinks, a pure quark phase core starts to form and finally for fully deleptonized matter the mixed phase disappears and an hybrid star with pure phases is obtained. Depending on the detailed dynamics of the formation of the pure quark phase core and the disappearing of the mixed phase it is possible that the evolution towards the final cold hybrid star configuration, for stars having a baryon number close to A, proceeds through a gravitational collapse (similarly to the transition from A to B). In that case the gravitational potential energy is released in a short amount of time and a burst of neutrinos and gamma rays can be produced as proposed in Ref. [MHB$^+$03] for the collapse to third family stars. In such a fast dynamics also gravitational waves might be emitted if non-radial modes are excited. On the other hand it is also possible that the evolution of the star proceeds through hydrostatical equilibrium configurations, most probably for stars having a baryon number close to C, and the gravitational potential energy is released gradually. No strong signature is expected in this case unless finite size effects do play an important role for the nucleation of the new phase and the hadronic star can be in a metastable state before converting into a hybrid star [DPP$^+$08]. Finally, stars having baryon number larger than C will develop a core of mixed phase during deleptonization and will collapse to a black hole after the full deleptonization (similarly to the results of Ref. [PSPL01]).

We used here the simple MIT bag model to compute the equation of state of quark matter but our system of equations for the mixed phase has a general validity. Nevertheless, it would be important to repeat the calculations by using others models like for instance the NJL model [RWB$^+$06b, SB07, PS08]. We close with remarks about the interesting properties of the new mixed phase. Because of local charge neutrality no Coulomb lattice with charged finite structures of the two phases can form. Furthermore, to minimize the surface energy spherical structures are always favored, which excludes the occurrence of complex pasta structures. Additionally, the charge neutral structures can lower there energy by merging. Such locally charge neutral structures can grow

almost arbitrary in size so that asymptotically a full separation of the two phases will be obtained.

Thus one can expect significant changes of dynamical properties like the neutrino emissivities and opacities or the thermal conductivity. In such a mixed phase no coherent scattering of neutrinos with pasta structures can take place [RBP00], as the neutrino wavelength is much smaller than the size of the structures. A detailed simulation of neutrino transport within this new mixed phase would be extremely interesting for the possible implications on the neutrino signal of the changes of the structure of the star during deleptonization. Also the motion and the interactions of the drops/bubbles within the mixed phase, in presence of turbulence, might represent an interesting source of gravitational waves [Meg08]. Finally, the effects of the formation of this new mixed phase should be investigated quantitatively in supernova simulations and in calculations of neutrino transport in protoneutron stars.

Chapter 10

Summary

Within my PhD studies I investigated the EOS for hot and dense matter in astrophysics, with a particular focus on first order phase transitions. My research on the EOS can be splitted into two parts: on the one hand general thermodynamic concepts, and on the other hand the concrete application of these concepts to specific models.

We started with an introduction to nuclear astrophysics in Chap. 1 where we addressed stellar evolution, core-collapse supernovae, neutron stars and nucleosynthesis. In Chap. 2 we discussed general aspects of QCD, the theory of the strong interactions. We illustrated that it is not possible to use the QCD Lagrangian directly for applications in astrophysics because the relevant regime is non-perturbative and also a numerical solution on the lattice is yet not possible. Depending on the state of matter one wants to describe one has to choose a suitable phenomenological or effective model for the interactions of the particles so that one can calculate the EOS of bulk matter, i.e. in the thermodynamic limit. For nucleons I used different relativistic mean-field models, see Sec. 2.4. They are well-established models for the properties of nuclei and nuclear matter around saturation density. For larger densities, I applied the quark bag model, Sec. 2.5, to describe quark matter and the principle effects of deconfinement.

It is possible that a bulk EOS exhibits a first order phase transition. This happens e.g. at densities below saturation density in the liquid-gas phase transition of nuclear matter. At densities above saturation density one expects that the first order chiral and deconfinement transition from hadrons to quarks occurs, see Sec. 2.2. Besides using a specific model for the bulk EOS, one needs a model for the description of the phase transition.

In Chap. 3, I presented a system-independent, general classification of first order phase transitions with arbitrary many components. First order phase transitions can manifest themselves in two qualitatively different forms, namely as a continuous or a

discontinuous phase transformation. So far, this aspect has not been worked out in detail, and sometimes lead to confusion in the literature. In the context of compact stars there is usually only the distinction between the Maxwell and the Gibbs transition, and quite often restricted to the case of zero temperature and beta-equilibrium. In a continuous phase transformation the phase transition occurs via an extended mixed phase, and the thermodynamic variables change continuously. There is no latent heat involved in such a phase transformation. In a discontinuous phase transformation one jumps directly from the first to the second phase, leading to the discontinuous change of at least one of the extensive variables. Such a phase transformation requires the release or absorption of latent heat. We could show that first order phase transitions in an isolated system are always continuous. It was derived that the type of a first order phase transformation depends only on the number of phases $\mathcal{K}$ involved in the phase transformation, and the number of extensive thermodynamic variables $\mathcal{E}$ which are used as control parameters. The choice of the control parameters depends on how the system is manipulated to trigger the phase transition. If $\mathcal{E} \geq \mathcal{K}$ the phase transformation is continuous, for $\mathcal{E} < \mathcal{K}$ discontinuous. This classification is general and can be applied to any first order phase transition, e.g. also to heavy ion collisions. As an example we discussed the typical phase transformations and the phase diagram of a substance like water, for three different sets of control parameters.

In Chap. 4 we turned to some off-equilibrium aspects of first order phase transitions. The classical thermal nucleation of a multicomponent system was investigated, for different forms of finite-size effects. So far, there is no general formalism for multi-component nucleation in compact stars, and different approaches are used in the literature. Based on simple thermodynamic arguments I showed, that the most likely nucleation occurs via a state which is in unstable equilibrium with the heat and particle bath. Nevertheless all quantum numbers of the entire system are conserved. This has important consequences. For example, one does not have to assume locally fixed fractions to take into account flavor conservation in the process of deconfinement, which was done in several published articles. As examples for the particular form of finite-size effects, in Sec. 4.4 we first considered the case of a constant surface tension. We got a nucleation rate in agreement with the standard result of a one-component system. In Sec. 4.5 we also took the Coulomb energy of a homogeneously charged sphere into account which lead to a novel expression for the nucleation rate.

In Chap. 5 we showed how local constraints and internal degrees of freedom can be taken into account in a phase transition, and how they affect the equilibrium conditions. In the subsequent Chapter 6, we went away from the general concepts and introduced the typical state variables which are used for the description of the different stages of the

evolution of a compact star, from its birth in the supernova, over the cooling protoneutron star to the cold and deleptonized neutron star. In Chap. 7 we then discussed the phase transitions which can occur in these systems in great detail. It became clear that under certain conditions one might prefer to use local constraints for the description of the mixed phase, like e.g. local charge neutrality. We showed that additional local constraints do not change the general results of Chap. 3. But additional local constraints may allow a simplified thermodynamic description. For example in case of a strong surface tension and small screening lengths with the assumption of local charge neutrality one does not need to consider any finite-size effects. Additional local constraints can also change a continuous to a discontinuous phase transformation, so that no mixed phase has to be calculated. In this chapter we also presented all the relevant different kind of mixed phases which can occur in compact stars, and discussed the general features of the corresponding phase transformations.

The detailed study of the thermodynamics of first order phase transitions lead to the discovery of some new effects which have not been discussed in the literature so far. It was anticipated that it is not possible to form a sharp (macroscopic) interface between quark and hadronic matter (a discontinuous phase transformation) in protoneutron stars. Instead a hadron-quark mixed phase must always exist, which can disappear potentially only after the deleptonization and the cooling of the star. This idea was then studied quantitatively in Sec. 9.2 where we applied the quark-bag model. We investigated the possible effects on the temporal evolution of newly born hybrid stars in the scenario of a delayed transition of a neutron star to a third family star.

One of the most important topics of the thesis is the development of a complete supernova EOS, the excluded volume nuclear statistical equilibrium (ExV-NSE) model which was presented in Chap. 8. The approach is a phenomenological model for nuclear matter below saturation density which gives a detailed description of the liquid-gas phase transition. The interactions of the unbound nucleons are described with the relativistic mean-field model and two different parameter sets TM1 and TMA. All nuclei are treated as separate particle species, using the experimental mass table of Ref. [AWT03] and the theoretical nuclear structure calculations of Ref. [GTM05]. A simple description of excited states and Coulomb energies was implemented. Most importantly, we derived a new thermodynamic consistent formulation of the medium effects on light clusters and heavy nuclei by the excluded-volume approach. This approach assures that nuclei can not exist above saturation density and that the unmodified RMF description is achieved if nuclei are not present. Furthermore, the RMF interactions of the nucleons are coupled to the nuclei via chemical equilibrium. The ExV-NSE generalizes the model for the outer crust of cold neutron stars which I studied in my diploma thesis, see

Ref. [RHS06, HS08, GHSM07], to finite temperatures and arbitrary densities. It gives a consistent bridge from ordinary nuclei like they exist here on earth, to the densities where quark matter is expected to appear.

After presenting the model we discussed the composition and the EOS for typical supernova conditions and compared the results with the two commonly used supernova EOSs of Lattimer and Swesty, and Shen et al. The EXV-NSE model contains innovative features, which are not contained within the two other EOSs. Most important is the inclusion of all light clusters and the entire distribution of heavy nuclei. Thus it represents the first consistent model beyond the single nucleus approximation. We showed that the light clusters play a particular role at large temperatures and that the alpha-particle approximation fails under many conditions. The distribution of nuclei leads to some important differences in thermodynamic variables in the transition region from unbound nucleons to nuclei. We compared the ExV-NSE with the statistical multifragmentaion model (SMM) of Botvina and Mishustin in Sec. 8.4. Due to the shell effects in the nuclear masses, the ExV-NSE gives peaks around the magic nuclei on top of the smooth distributions of the liquid-drop formulation used in the SMM. Otherwise the two models lead to similar results for the mass, charge and isotope distributions. Only for conditions where the neutron drip has occurred, significant differences were found, which were most apparent in the isotope distributions. In Sec. 8.5 we studied the role of the excited states of nuclei further, by comparing with the internal partition functions of Rauscher et al., some experimental data and the temperature dependent part of the binding energies of the SMM. It was found that the simple degeneracy function used in the ExV-NSE gives a rather conservative estimate for the effects of excited states. Most importantly, we figured out that it is necessary to introduce a cutoff for the maximal excitation energy, otherwise the contribution of excited states to the energy density can become arbitrary large, leading even to an unphysical behavior of the EOS. In Sec. 8.6 we compared the excluded volume approach with two quantum many-body models. The agreement was satisfactory, and the most important qualitative features are reproduced with the ExV-NSE. The differences among the three models are of similar size. Only at very low temperatures significant differences are observed for the light clusters with the ExV-NSE model. However, it was shown that under these conditions, the composition is actually dominated by heavy nuclei, which are not included in the quantum many-body models.

With the EXV-NSE model one can calculate new EOS tables rather quickly. This allows to explore the role of certain aspects of the EOS in simulations, like e.g. different nuclear interactions which give different symmetry energies. In Sec. 8.7 we presented results of some first preliminary supernova simulations which were done in collaboration

with the Basel group around Matthias Liebendörfer and Tobias Fischer. Two different ExV-NSE EOSs and the Shen EOS were compared. With this comparison we could identify the impact of different aspects of the EOS in supernovae. We only got small differences, which is convenient, because only the thermodynamic differences of the EOS had been taken into account. Still we came to the conclusion that the model for the low-density EOS is more important than the change of the parameterization of the nuclear interactions. In more detail, the important effect of the additional light clusters in the ExV-NSE became apparent in the core-collapse supernova simulations.

As a very exciting example of the role of the EOS and first order phase transitions in core-collapse supernova, in Sec. 9.1 we found that an early phase transition to quark matter can lead to a successful energetic explosion. After quark matter appears a second shock wave forms, which merges with the standing accretion front and finally triggers the explosion. A second anti-neutrino burst is released which gives information about the critical density for the onset of deconfinement.

Chapter 11

Outlook

There exist important experimental constraints on the EOS at low and high densities which should be fulfilled by a realistic equation of state. It is important to study these constraints further. For example, there are some recent measurements of the low-density symmetry energy, which can only be explained if the cluster formation in nuclear matter is taken into account [KNS+07, NRT+10]. From a theoretical point of view, the comparison with the quantum many-body models of Röpke and Typel given in Sec. 8.6 is an important benchmark regarding the high temperature EOS which is dominated by light clusters. To probe different conditions it would be good to compare the ExV-NSE with a detailed calculation of the inner crust of a cold neutron star, using the same nuclear interactions. This would be a perfect check for the low temperature EOS where heavy nuclei are embedded in a free neutron gas and changes of the nuclear structure can be expected.

We just started with the application of the EXV-NSE model in core-collapse supernovae. It would be interesting to examine different nuclear interactions, which result in more pronounced differences of the high-density part of the equation of state than TM1 and TMA. In this context, the role of the symmetry energy is of particular interest. Especially the FSUgold parameterization of the relativistic mean-field model is promising, because of the well constrained behavior of the symmetry energy. As discussed at the end of Sec. 8.7 we expect that FSUgold would release more gravitational binding energy which is deposited more easily in the shock. By understanding the impact of the EOS in core-collapse supernovae further, one might find some more insight which aspects of the EOS help to achieve a robust supernova mechanism.

Furthermore, the EXV-NSE model contains some new nuclear physics aspects which could be investigated further. One possibility would be the consideration of the distribution of nuclei for the electron and neutrino capture rates. One had to study the

underlying weak reactions and how they can be implemented into simulations. Such a project would naturally give a direct connection to nucleosynthesis calculations and would require close collaborations with people who do simulations. It is convenient that the same nuclear input of the ExV-NSE model is also used in nucleosynthesis calculations. Thus it can give a better connection between supernova and nucleosynthesis calculations than the existing equations of state.

The model for the low-density equation of state itself could also be developed further. For example a more detailed treatment of the Coulomb energy of a multi-component plasma at finite temperature could be implemented. Another aspect would be the more detailed description of the excited states of nuclei. I already started to study a different formulation of the excluded volume effects, which might be more physical and could help to resolve the difficulties in the transition to uniform nuclear matter. Another future project could be to combine a quantum many-body model for the medium effects of the light clusters with the excluded volume approach for the heavy nuclei in a new NSE model.

One has just started to analyze the consequences of phase transitions in the context of core-collapse supernovae. There are still plenty of exciting scenarios which have not been studied so far. For example one could investigate the implications of different descriptions of the mixed phase of quarks and hadrons. To take the dynamics of the nucleation of the quark phase into account, one had to implement estimated nucleation timescales into supernova simulations and had to consider the possible occurrence of metastable states in the EOS. This would be a nice application of the nucleation rates which have been derived in Chap. 4. A non-equilibrium phase transition is connected with the release of latent heat and a discontinuous behavior of the equation of state. This would directly cause the formation of shocks and the phase transition would be much more violent.

The inclusion of strange degrees of freedom both in the hadronic and quark part of the equation of state would also be interesting. As was shown in Ref. [SHP$^+$09] the additional strange quark degrees of freedom can significantly lower the critical density for the onset of deconfinement. So far, weak equilibrium with respect to strangeness changing reactions was always assumed in such studies. Instead one could explicitly take the strangeness conservation during the deconfinement process into account. To achieve a consistent description it would be necessary to include strange hadronic degrees of freedom in the equation of state as well, which would be an interesting study by its own.

A unified supernova equation of state which includes quark and hadronic degrees of freedom in a consistent manner is very desirable. A further extension could be the consideration of finite size effects in the hadron-quark phase transition, which then also fix the size of the quark bubbles in the hadronic phase. So far, for quark matter only the quark bag model was applied in the context of core-collapse supernovae. One of the next steps could be the use of more microscopic models than the quark-bag model and thus to deal more with the quantum field theoretical aspects. For example the (Polyakov-loop) NJL model for the quarks would be a significant improvement as it contains chiral symmetry restoration and further (first order) phase transitions to color-superconducting phases.

Apart from nuclear astrophysics, also the connection to neighboring areas like nuclear physics or heavy ion physics is of interest, as they provide important experimental constraints. So far, in high-energy heavy ion collisions only the cross-over region of the QCD phase diagram is explored, which is phenomenological very different to a first order phase transition. In the future, at the FAIR facility at GSI one tries to reach the first order region. Then the physics of heavy ions and neutron stars will come closer together. The concepts for the description of the phase transition and mixed phases in neutron stars might then also become relevant for heavy-ion collisions. At lower energies, radioactive ion beams at FAIR and other facilities will allow the measurement of very exotic neutron rich nuclei in the future. This will constrain the supernova EOS further.

Obviously, the comparison with astronomical data is of great importance. Hopefully, some new observations of neutron stars will finally lead to stringent constraints which rule out some of the exceedingly many different scenarios for the high-density behavior of the EOS. Especially the observation of a galactic supernovae with modern telescopes and neutrino detectors seems to be promising to give new information about the two "Science Questions for the next century", which were cited in the introduction. A galactic supernova could help to resolve the quests for the understanding of the supernova mechanism, the site of nucleosynthesis and the possible phase transition to quark matter.

Bibliography

[AB00] B. Alex Brown. Neutron radii in nuclei and the neutron equation of state. *Phys. Rev. Lett.*, 85(25):5296–5299, Dec 2000.

[ABD+07] M. Alford, D. Blaschke, A. Drago, T. Klähn, G. Pagliara, and J. Schaffner-Bielich. Astrophysics: Quark matter in compact stars? *Nature*, 445, January 2007.

[ABPR05] M. Alford, M. Braby, M. Paris, and S. Reddy. Hybrid Stars that Masquerade as Neutron Stars. *Astrophys. J.*, 629:969–978, August 2005.

[ADRM09] E. B. Abdikamalov, H. Dimmelmeier, L. Rezzolla, and J. C. Miller. Relativistic simulations of the phase-transition-induced collapse of neutron stars. *Mon. Not. R. Astron. Soc.*, 392:52–76, January 2009.

[AMO+08] A. Arcones, G. Martínez-Pinedo, E. O'Connor, A. Schwenk, H.-T. Janka, C. J. Horowitz, and K. Langanke. Influence of light nuclei on neutrino-driven supernova outflows. *Phys. Rev. C*, 78(1):015806, July 2008.

[Apa98] J. M. Aparicio. A Simple and Accurate Method for the Calculation of Generalized Fermi Functions. *Astrophys. J. S.*, 117:627, July 1998.

[ARRW01] M. Alford, K. Rajagopal, S. Reddy, and F. Wilczek. Minimal color-flavor-locked-nuclear interface. *Phys. Rev. D*, 64(7):074017, October 2001.

[AWT03] G. Audi, A. H. Wapstra, and C. Thibault. The Ame2003 atomic mass evaluation (II). Tables, graphs and references. *Nucl. Phys. A*, 729:337–676, December 2003.

[BB03] Sarmistha Banik and Debades Bandyopadhyay. Color superconducting quark matter core in the third family of compact stars. *Phys. Rev. D*, 67(12):123003, Jun 2003.

[BBD+03] Z. Berezhiani, I. Bombaci, A. Drago, F. Frontera, and A. Lavagno. Gamma-Ray Bursts from Delayed Collapse of Neutron Stars to Quark Matter Stars. *Astrophys. J.*, 586:1250–1253, April 2003.

[BBI+95] J. P. Bondorf, A. S. Botvina, A. S. Iljinov, I. N. Mishustin, and K. Sneppen. Statistical multifragmentation of nuclei. *Phys. Rep.*, 257:133–221, June 1995.

[BDM+06] S. W. Bruenn, C. J. Dirk, A. Mezzacappa, J. C. Hayes, J. M. Blondin, W. R. Hix, and O. E. B. Messer. Modeling core collapse supernovae in 2 and 3 dimensions with spectral neutrino transport. *Journal of Physics Conference Series*, 46:393–402, September 2006.

[Bet90] H. A. Bethe. Supernova mechanisms. *Reviews of Modern Physics*, 62:801–866, 1990.

[BFG+05] D. Blaschke, S. Fredriksson, H. Grigorian, A. M. Öztaş, and F. Sandin. Phase diagram of three-flavor quark matter under compact star constraints. *Phys. Rev. D*, 72(6):065020, September 2005.

[BGMG00] K. A. Bugaev, M. I. Gorenstein, I. N. Mishustin, and W. Greiner. Exactly soluble model for nuclear liquid-gas phase transition. *Phys. Rev. C*, 62(4):044320, October 2000.

[BGMG01] K. A. Bugaev, M. I. Gorenstein, I. N. Mishustin, and W. Greiner. Statistical multifragmentation in thermodynamic limit. *Physics Letters B*, 498:144–148, January 2001.

[BGP01] D. Blaschke, H. Grigorian, and G. Poghosyan. Phase Diagram for Spinning and Accreting Neutron Stars. In D. Blaschke, N. K. Glendenning, and A. Sedrakian, editors, *Physics of Neutron Star Interiors*, volume 578 of *Lecture Notes in Physics, Berlin Springer Verlag*, page 285, 2001.

[BHR03] M. Bender, P.-H. Heenen, and P.-G. Reinhard. Self-consistent mean-field models for nuclear structure. *Reviews of Modern Physics*, 75:121–180, January 2003.

[Bis71] G. S. Bisnovatyi-Kogan. The Explosion of a Rotating Star As a Supernova Mechanism. *Soviet Astronomy*, 14:652, February 1971.

[BL84] A. Burrows and J. M. Lattimer. On the accuracy of the single-nucleus approximation in the equation of state of hot, dense matter. *Astrophys. J.*, 285:294–303, October 1984.

[BL85] A. Burrows and J. M. Lattimer. The prompt mechanism of Type II supernovae. *Astrophys. J.*, 299:L19–L22, December 1985.

[BLD+06] A. Burrows, E. Livne, L. Dessart, C. D. Ott, and J. Murphy. An acoustic mechanism for core-collapse supernova explosions. *New Astronomy Review*, 50:487–491, October 2006.

[BM04] A. S. Botvina and I. N. Mishustin. Formation of hot heavy nuclei in supernova explosions. *Phys. Lett. B*, 584:233–240, April 2004.

[BM05] A. S. Botvina and I. N. Mishustin. Multifragmentation reactions and properties of stellar matter at subnuclear densities. *Phys. Rep.*, 72(4):048801, October 2005.

[BM08] A. S. Botvina and I. N. Mishustin. Statistical approach for supernova matter. *arXiv eprints*, 0811:2593, November 2008.

[BMG07] T. J. Bürvenich, I. N. Mishustin, and W. Greiner. Nuclei embedded in an electron gas. *Phys. Rev. C*, 76(3):034310, September 2007.

[BMG10] A. Bhattacharyya, I. N. Mishustin, and W. Greiner. Deconfinement phase transition in compact stars: Maxwell versus Gibbs construction of the mixed phase. *Journal of Physics G Nuclear Physics*, 37(2):025201, February 2010.

[Bod71] A. R. Bodmer. Collapsed Nuclei. *Phys. Rev. D*, 4:1601–1606, September 1971.

[BP08] G. F. Burgio and S. Plumari. Structure of hybrid protoneutron stars within the Nambu Jona-Lasinio model. *Phys. Rev. D*, 77(8):085022, April 2008.

[BPRS09] S. I. Blinnikov, I. V. Panov, M. A. Rudzsky, and K. Sumiyoshi. The equation of state and composition of hot, dense matter in core-collapse supernovae. *arXiv eprints*, 0904:3849, April 2009.

[BQB+82] J. Bartel, P. Quentin, M. Brack, C. Guet, and H.-B. Håkansson. Towards a better parametrisation of Skyrme-like effective forces: A critical study of the SkM force. *Nucl. Phys. A*, 386:79–100, September 1982.

[Bru85] S. W. Bruenn. Stellar core collapse - Numerical model and infall epoch. *Astrophysical Journal Supplement Series*, 58:771–841, August 1985.

[BS09] T. Boeckel and J. Schaffner-Bielich. A little inflation in the early universe at the QCD phase transition. *arXiv:0906.4520*, June 2009.

[BV81] P. Bonche and D. Vautherin. A mean-field calculation of the equation of state of supernova matter. *Nuclear Physics A*, 372:496–526, December 1981.

[BW85] H. A. Bethe and J. R. Wilson. Revival of a stalled supernova shock by neutrino heating. *Astrophys. J.*, 295:14–23, August 1985.

[BZ34a] W. Baade and F. Zwicky. On Super-novae. *Proceedings of the National Academy of Science*, 20:254, 1934.

[BZ34b] W. Baade and F. Zwicky. Supernovae and cosmic rays. *Phys. Rev.*, 45:138, 1934.

[CHB06] O. L. Caballero, C. J. Horowitz, and D. K. Berry. Neutrino scattering in heterogeneous supernova plasmas. *Phys. Rev. C*, 74(6):065801, December 2006.

[CotPotU03] National Research Council Committee on the Physics of the Universe. *Connecting Quarks with the Cosmos: Eleven Science Questions for the New Century*. National Academies Press, Washington, D.C., 2003.

[CT65] F. E. Clifford and R. J. Tayler. The equilibrium distribution of nuclides in matter at high temperatures. *Memoirs of the Royal Astronomical Society*, 69:21, 1965.

[DCG06] C. Ducoin, P. Chomaz, and F. Gulminelli. Role of isospin in the nuclear liquid gas phase transition. *Nuclear Physics A*, 771:68–92, May 2006.

[DCG07] C. Ducoin, P. Chomaz, and F. Gulminelli. Isospin-dependent clusterization of neutron-star matter. *Nuclear Physics A*, 789:403–425, June 2007.

[DHN+07] C. Ducoin, K. H. O. Hasnaoui, P. Napolitani, P. Chomaz, and F. Gulminelli. Anomalous thermodynamics and phase transitions in neutron star matter. *Phys. Rev. C*, 75(6):065805, June 2007.

[DL09] Pawel Danielewicz and Jenny Lee. Symmetry energy i: Semi-infinite matter. *Nuclear Physics A*, 818(1-2):36 – 96, 2009.

[DLL02] P. Danielewicz, R. Lacey, and W. G. Lynch. Determination of the Equation of State of Dense Matter. *Science*, 298:1592–1596, November 2002.

[DPP+08] A. Drago, G. Pagliara, G. Pagliaroli, F. L. Villante, and F. Vissani. Formation of quark phases in compact stars and sn explosion. *SIXTH INTERNATIONAL CONFERENCE ON PERSPECTIVES IN HADRONIC PHYSICS*, 1056(1):256–263, 2008.

[DPS08] A. Drago, G. Pagliara, and J. Schaffner-Bielich. Formation of quark phases in compact stars and their connection to gamma-ray-bursts. *Journal of Physics G Nuclear Physics*, 35(1):014052, January 2008.

[DS10] V. A. Dexheimer and S. Schramm. Novel approach to modeling hybrid stars. *Phys. Rev. C*, 81(4):045201, April 2010.

[DT99] Alessandro Drago and Ubaldo Tambini. Finite temperature quark matter and supernova explosion. *Journal of Physics G: Nuclear and Particle Physics*, 25(5):971–979, 1999.

[EE91] C. A. Engelbrecht and J. R. Engelbrecht. Fermi gas descriptions of nuclear level densities. *Annals of Physics*, 207:1–37, April 1991.

[EH80] M. F. El Eid and W. Hillebrandt. A new equation of state of supernova matter. *Astronomy and Astrophysics Supplement Series*, 42:215–226, November 1980.

[EMCT06] Tomoki Endo, Toshiki Maruyama, Satoshi Chiba, and Toshitaka Tatsumi. Charge screening effect in the hadron-quark mixed phase. *Progress of Theoretical Physics*, 115(2):337–353, 2006.

[FHR+08] Y. Funaki, H. Horiuchi, G. Röpke, P. Schuck, A. Tohsaki, and T. Yamada. Density-induced suppression of the α-particle condensate in nuclear matter and the structure of α-cluster states in nuclei. *Phys. Rev. C*, 77(6):064312, June 2008.

[FML+06] C. Fröhlich, G. Martínez-Pinedo, M. Liebendörfer, F.-K. Thielemann, E. Bravo, W. R. Hix, K. Langanke, and N. T. Zinner. Neutrino-Induced Nucleosynthesis of A>64 Nuclei: The νp Process. *Physical Review Letters*, 96(14):142502, April 2006.

[FMMT96] H. Fujii, T. Maruyama, T. Muto, and T. Tatsumi. Equation of state with kaon condensates and neutron stars. *Nuclear Physics A*, 597:645–671, February 1996.

[FPSB01] Eduardo S. Fraga, Robert D. Pisarski, and Jürgen Schaffner-Bielich. Small, dense quark stars from perturbative qcd. *Phys. Rev. D*, 63(12):121702, May 2001.

[FR82] G. Fái and J. Randrup. Explosion-evaporation model for fragment production in medium-energy nuclear collisions. *Nucl. Phys. A*, 381:557–576, June 1982.

[Fre09] P. C. C. Freire. Eccentric Binary Millisecond Pulsars. *arXiv eprints*, 0907:3219, July 2009.

[FW98] C. L. Fryer and S. E. Woosley. Gamma-Ray Bursts from Neutron Star Phase Transitions. *Astrophys. J.*, 501:780, July 1998.

[FWM+09] T. Fischer, S. C. Whitehouse, A. Mezzacappa, F. -K. Thielemann, and M. Liebendörfer. Protoneutron star evolution and the neutrino driven wind in general relativistic neutrino radiation hydrodynamics simulations. *arXiv eprints*, 0908:1871, August 2009.

[FYH+08] Y. Funaki, T. Yamada, H. Horiuchi, G. Röpke, P. Schuck, and A. Tohsaki. Alpha-Particle Condensation in Nuclear Systems. *arXiv eprints*, 0809:0542, September 2008.

[GAM+93] N. A. Gentile, M. B. Aufderheide, G. J. Mathews, F. D. Swesty, and G. M. Fuller. The QCD phase transition and supernova core collapse. *Astrophys.*

J., 414:701–711, September 1993.

[Ger68] Ulrich H. Gerlach. Equation of state at supranuclear densities and the existence of a third family of superdense stars. *Phys. Rev.*, 172(5):1325–1330, Aug 1968.

[GHSM07] L. Guo, M. Hempel, J. Schaffner-Bielich, and J. A. Maruhn. Triaxial nuclear models and the outer crust of nonaccreting cold neutron stars. *Phys. Rev. C*, 76(6):065801, December 2007.

[GKS87] C. Greiner, P. Koch, and H. Stocker. Separation from strangeness from antistrangeness in the phase transition from quark to hadron matter - Possible formation of strange quark matter in heavy-ion collisions. *Physical Review Letters*, 58:1825–1828, May 1987.

[Gle92] N. K. Glendenning. First-order phase transitions with more than one conserved charge: Consequences for neutron stars. *Phys. Rev. D*, 46:1274–1287, August 1992.

[Gle01] N. K. Glendenning. Phase transitions and crystalline structures in neutron star cores. *Phys. Rep.*, 342:393–447, March 2001.

[Gol68] T. Gold. Rotating Neutron Stars as the Origin of the Pulsating Radio Sources. *Nature*, 218:731, 1968.

[GP95] N. K. Glendenning and S. Pei. Crystalline structure of the mixed confined-deconfined phase in neutron stars. *Phys. Rev. C*, 52:2250–2253, October 1995.

[GPW97] N. K. Glendenning, S. Pei, and F. Weber. Signal of Quark Deconfinement in the Timing Structure of Pulsar Spin-Down. *Physical Review Letters*, 79:1603–1606, September 1997.

[Gro90] D. H. E. Gross. REVIEW: Statistical decay of very hot nuclei-the production of large clusters. *Reports on Progress in Physics*, 53:605–658, May 1990.

[GS98] N. K. Glendenning and J. Schaffner-Bielich. Kaon Condensation and Dynamical Nucleons in Neutron Stars. *Physical Review Letters*, 81:4564–4567, November 1998.

[GS99] N. K. Glendenning and J. Schaffner-Bielich. First order kaon condensate. *Phys. Rev. C*, 60(2):025803, August 1999.

[GTM05] L. Geng, H. Toki, and J. Meng. Masses, Deformations, and Charge Radii–Nuclear Ground-State Properties in the Relativistic Mean Field Model. *Prog. Theor. Phys.*, 113:785–800, April 2005.

[GZDA01] Z. Gong, L. Zejda, W. Däppen, and J. M. Aparicio. Generalized Fermi-Dirac functions and derivatives: properties and evaluation. *Computer Physics Communications*, 136:294–309, May 2001.

[HBP+68] A. Hewish, S. J. Bell, J. D. Pilkington, P. F. Scott, and R. A. Collins. Observation of a Rapidly Pulsating Radio Source. *Nature*, 217:709, 1968.

[HM81] W. Hillebrandt and E. Mueller. Computer simulations of stellar collapse and shock wave propagation. *Astron. Astrophys.*, 103:147–153, November 1981.

[HMM+03] W. R. Hix, O. E. Messer, A. Mezzacappa, M. Liebendörfer, J. Sampaio, K. Langanke, D. J. Dean, and G. Martínez-Pinedo. Consequences of Nuclear Electron Capture in Core Collapse Supernovae. *Physical Review Letters*, 91(20):201102, November 2003.

[HNW84] W. Hillebrandt, K. Nomoto, and R. G. Wolff. Supernova explosions of massive stars - The mass range 8 to 10 solar masses. *Astron. Astrophys.*, 133:175–184, April 1984.

[Hor02] C. J. Horowitz. Weak magnetism for antineutrinos in supernovae. *Phys. Rev. D*, 65(4):043001, February 2002.

[HP82] P. Haensel and M. Proszynski. Pion condensation in cold dense matter and neutron stars. *Astrophys. J.*, 258:306–320, July 1982.

[HPS93] H. Heiselberg, C. J. Pethick, and E. F. Staubo. Quark matter droplets in neutron stars. *Physical Review Letters*, 70:1355–1359, March 1993.

[HPS09] M. Hempel, G. Pagliara, and J. Schaffner-Bielich. Conditions for phase equilibrium in supernovae, protoneutron, and neutron stars. *Phys. Rev. D*, 80(12):125014, December 2009.

[HS06a] C. J. Horowitz and A. Schwenk. Cluster formation and the virial equation of state of low-density nuclear matter. *Nuclear Physics A*, 776:55–79, September 2006.

[HS06b] C. J. Horowitz and A. Schwenk. The virial equation of state of low-density neutron matter. *Physics Letters B*, 638:153–159, July 2006.

[HS08] M. Hempel and J. Schaffner-Bielich. Mass, radius and composition of the outer crust of nonaccreting cold neutron stars. *Journal of Physics G Nuclear Physics*, 35(1):014043, January 2008.

[HS10] M. Hempel and J. Schaffner-Bielich. A statistical model for a complete supernova equation of state. *Nuclear Physics A*, 837:210–254, June 2010.

[HSS09] S. Heckel, P. P. Schneider, and A. Sedrakian. Light nuclei in supernova envelopes: A quasiparticle gas model. *Phys. Rev. C*, 80(1):015805, July 2009.

[HW85] W. Hillebrandt and R. G. Wolff. Models of Type II Supernova Explosions. In W. D. Arnett & J. W. Truran, editor, *Nucleosynthesis : Challenges and New Developments*, page 131, 1985.

[IMN+78] A. V. Ignatiuk, I. N. Mikhailov, R. G. Nazmitdinov, B. Nerlo-Pomorska, and K. Pomorski. Equilibrium properties of fast-rotating headed nuclei. *Physics Letters B*, 76:543–546, July 1978.

[IOS03] C. Ishizuka, A. Ohnishi, and K. Sumiyoshi. Liquid-gas phase transition of supernova matter and its relation to nucleosynthesis. *Nucl. Phys. A*, 723:517–543, August 2003.

[IRR+08] N. D. Ippolito, M. Ruggieri, D. H. Rischke, A. Sedrakian, and F. Weber. Equilibrium sequences of nonrotating and rapidly rotating crystalline color-superconducting hybrid stars. *Phys. Rev. D*, 77(2):023004, January 2008.

[Ito70] N. Itoh. Hydrostatic Equilibrium of Hypothetical Quark Stars. *Progress of Theoretical Physics*, 44:291–292, July 1970.

[JMMS08] H.-T. Janka, A. Marek, B. Müller, and L. Scheck. Supernova Explosions and the Birth of Neutron Stars. In C. Bassa, Z. Wang, A. Cumming, & V. M. Kaspi, editor, *40 Years of Pulsars: Millisecond Pulsars, Magnetars and More*, volume 983 of *American Institute of Physics Conference Series*, pages 369–378, February 2008.

[K. 88] K. S. Hirata et al. Observation in the kamiokande-ii detector of the neutrino burst from supernova sn1987a. *Phys. Rev. D*, 38(2):448–458, Jul 1988.

[KJH06] F. S. Kitaura, H.-T. Janka, and W. Hillebrandt. Explosions of O-Ne-Mg cores, the Crab supernova, and subluminous type II-P supernovae. *Astron. Astrophys.*, 450:345–350, April 2006.

[KNS+07] S. Kowalski, J. B. Natowitz, S. Shlomo, R. Wada, K. Hagel, J. Wang, T. Materna, Z. Chen, Y. G. Ma, L. Qin, A. S. Botvina, D. Fabris, M. Lunardon, S. Moretto, G. Nebbia, S. Pesente, V. Rizzi, G. Viesti, M. Cinausero, G. Prete, T. Keutgen, Y. E. Masri, Z. Majka, and A. Ono. Experimental determination of the symmetry energy of a low density nuclear gas. *Phys. Rev. C*, 75(1):014601, January 2007.

[Kt07] F. Karsch and the RBC-Bielefeld Collaboration. Transition temperature in QCD with physical light and strange quark masses. *Journal of Physics*

G Nuclear Physics, 34:627, August 2007.

[KTUY05] H. Koura, T. Tachibana, M. Uno, and M. Yamada. Nuclidic Mass Formula on a Spherical Basis with an Improved Even-Odd Term. *Progress of Theoretical Physics*, 113:305–325, February 2005.

[Lan32] L. D. Landau. On the theory of stars. *Physik. Zeits. Sowjetunion*, 1:285, 1932.

[LAN07] LAND Collaboration, A. Klimkiewicz et al. Nuclear symmetry energy and neutron skins derived from pygmy dipole resonances. *Physical Review C (Nuclear Physics)*, 76(5):051603, 2007.

[LB98] G. Lugones and O. G. Benvenuto. Effect of trapped neutrinos in the hadron matter to quark matter transition. *Phys. Rev. D*, 58(8):083001, October 1998.

[LC05] Bao-An Li and Lie-Wen Chen. Nucleon-nucleon cross sections in neutron-rich matter and isospin transport in heavy-ion reactions at intermediate energies. *Phys. Rev. C*, 72(6):064611, Dec 2005.

[LCC+06] L.-M. Lin, K. S. Cheng, M.-C. Chu, , and W.-M. Suen. Gravitational waves from phase-transition-induced collapse of neutron stars. *The Astrophysical Journal*, 639(1):382–396, 2006.

[LCK08] Bao-An Li, Lie-Wen Chen, and Che Ming Ko. Recent progress and new challenges in isospin physics with heavy-ion reactions. *Physics Reports*, 464(4-6):113 – 281, 2008.

[LD91a] J. M. Lattimer and F. Douglas Swesty. A generalized equation of state for hot, dense matter. *Nucl. Phys. A*, 535:331–376, December 1991.

[LD91b] J. M. Lattimer and F. Douglas Swesty. A generalized equation of state for hot, dense matter. *Nucl. Phys. A*, 535:331–376, December 1991.

[LDGS10] G. Lugones, T. A. S. Do Carmo, A. G. Grunfeld, and N. N. Scoccola. Deconfinement transition in protoneutron stars: Analysis within the Nambu-Jona-Lasinio model. *Phys. Rev. D*, 81(8):085012, April 2010.

[LL69] L. D. Landau and E. M. Lifshitz. *Statistical physics. Pt.1.* 1969.

[LLPR83] D. Q. Lamb, J. M. Lattimer, C. J. Pethick, and D. G. Ravenhall. Phase transitions in cold and warm dense matter. *Nuclear Physics A*, 411:449–473, December 1983.

[LM00] K. Langanke and G. Martínez-Pinedo. Shell-model calculations of stellar weak interaction rates: II. Weak rates for nuclei in the mass range A=45-65 in supernovae environments. *Nuclear Physics A*, 673:481–508, June 2000.

[LMM+04] Matthias Liebendorfer, O. E. Bronson Messer, Anthony Mezzacappa, Stephen W. Bruenn, Christian Y. Cardall, and F.-K. Thielemann. A finite difference representation of neutrino radiation hydrodynamics in spherically symmetric general relativistic spacetime. *The Astrophysical Journal Supplement Series*, 150(1):263–316, 2004.

[LMS+03] K. Langanke, G. Martínez-Pinedo, J. M. Sampaio, D. J. Dean, W. R. Hix, O. E. Messer, A. Mezzacappa, M. Liebendörfer, H.-T. Janka, and M. Rampp. Electron Capture Rates on Nuclei and Implications for Stellar Core Collapse. *Physical Review Letters*, 90(24):241102, June 2003.

[LMT01a] M. Liebendörfer, A. Mezzacappa, and F.-K. Thielemann. Conservative general relativistic radiation hydrodynamics in spherical symmetry and comoving coordinates. *Phys. Rev. D*, 63(10):104003, May 2001.

[LMT+01b] M. Liebendörfer, A. Mezzacappa, F.-K. Thielemann, O. E. Messer, W. R. Hix, and S. W. Bruenn. Probing the gravitational well: No supernova explosion in spherical symmetry with general relativistic Boltzmann neutrino transport. *Phys. Rev. D*, 63(10):103004, May 2001.

[LP04] J. M. Lattimer and M. Prakash. The Physics of Neutron Stars. *Science*, 304(5670):536–542, 2004.

[LW70] J. M. LeBlanc and J. R. Wilson. A Numerical Example of the Collapse of a Rotating Magnetized Star. *Astrophys. J.*, 161:541, August 1970.

[MB93a] A. Mezzacappa and S. W. Bruenn. A numerical method for solving the neutrino Boltzmann equation coupled to spherically symmetric stellar core collapse. *Astrophys. J.*, 405:669–684, March 1993.

[MB93b] A. Mezzacappa and S. W. Bruenn. Stellar core collapse - A Boltzmann treatment of neutrino-electron scattering. *Astrophys. J.*, 410:740–760, June 1993.

[MB93c] A. Mezzacappa and S. W. Bruenn. Type II supernovae and Boltzmann neutrino transport - The infall phase. *Astrophys. J.*, 405:637–668, March 1993.

[MCM79] A. B. Migdal, A. I. Chernoutsan, and I. N. Mishustin. Pion condensation and dynamics of neutron stars. *Physics Letters B*, 83:158–160, May 1979.

[MCST07] T. Maruyama, S. Chiba, H.-J. Schulze, and T. Tatsumi. Hadron-quark mixed phase in hyperon stars. *Phys. Rev. D*, 76(12):123015, December 2007.

[MCST08a] T. Maruyama, S. Chiba, H.-J. Schulze, and T. Tatsumi. Properties of a hyperon quark mixed phase in compact stars. *Journal of Physics G*

Nuclear Physics, 35(10):104076, October 2008.

[MCST08b] T. Maruyama, S. Chiba, H.-J. Schulze, and T. Tatsumi. Quark deconfinement transition in hyperonic matter. *Physics Letters B*, 659:192–196, January 2008.

[Meg08] A. Megevand. Gravitational waves from deflagration bubbles in first-order phase transitions. *Phys. Rev. D*, 78(8):084003, October 2008.

[MHB+03] I. N. Mishustin, M. Hanauske, A. Bhattacharyya, L. M. Satarov, H. Stöcker, and W. Greiner. Catastrophic rearrangement of a compact star due to the quark core formation. *Physics Letters B*, 552:1–2, January 2003.

[Mis08] I. N. Mishustin. From nuclear multifragmentation reactions to supernova explosions. *arXiv eprints*, 0803:1388, March 2008.

[MJ09] A. Marek and H.-T. Janka. Delayed Neutrino-Driven Supernova Explosions Aided by the Standing Accretion-Shock Instability. *Astrophys. J.*, 694:664–696, March 2009.

[MLB79] T. J. Mazurek, J. M. Lattimer, and G. E. Brown. Nuclear forces, partition functions, and dissociation in stellar collapse. *Astrophys. J.*, 229:713–727, April 1979.

[MLF06] G. Martínez-Pinedo, M. Liebendörfer, and D. Frekers. Nuclear input for core-collapse models. *Nuclear Physics A*, 777:395–423, October 2006.

[MM99] A. Mezzacappa and O. E. B. Messer. Neutrino transport in core collapse supernovae. *Journal of Computational and Applied Mathematics*, 109:281–319, September 1999.

[MP07] L. McLerran and R. D. Pisarski. Phases of dense quarks at large N_C. *Nuclear Physics A*, 796:83–100, November 2007.

[MS90] W. D. Myers and W. J. Swiatecki. A Thomas-Fermi model of nuclei. Part I. Formulation and first results. *Annals of Physics*, 204:401–431, December 1990.

[MS95] H. Müller and B. D. Serot. Phase transitions in warm, asymmetric nuclear matter. *Phys. Rev. C*, 52:2072–2091, October 1995.

[MSTV90] A. B. Migdal, E. E. Saperstein, M. A. Troitsky, and D. N. Voskresensky. Pion degrees of freedom in nuclear matter. *Phys. Rep.*, 192:179–437, September 1990.

[MTV+05] T. Maruyama, T. Tatsumi, D. N. Voskresensky, T. Tanigawa, and S. Chiba. Nuclear "pasta" structures and the charge screening effect. *Phys. Rev. C*, 72(1):015802, July 2005.

[MTV+06] T. Maruyama, T. Tatsumi, D. N. Voskresensky, T. Tanigawa, T. Endo, and S. Chiba. Finite size effects on kaonic "pasta" structures. *Phys. Rev. C*, 73(3):035802, March 2006.

[Mue97] H. Mueller. The deconfinement phase transition in asymmetric matter. *Nuclear Physics A*, 618:349–370, February 1997.

[Mur80] M. J. Murphy. The equation of state near beta equilibrium for a collapsing stellar core. *Astrophysical Journal Supplement Series*, 42:385–420, March 1980.

[NBBS06] O. E. Nicotra, M. Baldo, G. F. Burgio, and H.-J. Schulze. Hybrid protoneutron stars with the MIT bag model. *Phys. Rev. D*, 74(12):123001, December 2006.

[NRT+10] J. B. Natowitz, G. Röpke, S. Typel, D. Blaschke, A. Bonasera, K. Hagel, T. Klähn, S. Kowalski, L. Qin, S. Shlomo, R. Wada, and H. H. Wolter. Symmetry Energy of Dilute Warm Nuclear Matter. *Physical Review Letters*, 104(20):202501, May 2010.

[NS09] W. G. Newton and J. R. Stone. Modeling nuclear "pasta" and the transition to uniform nuclear matter with the 3D Skyrme-Hartree-Fock method at finite temperature: Core-collapse supernovae. *Phys. Rev. C*, 79(5):055801, May 2009.

[NSY08] K. Nakazato, K. Sumiyoshi, and S. Yamada. Astrophysical implications of equation of state for hadron-quark mixed phase: Compact stars and stellar collapses. *Phys. Rev. D*, 77(10):103006, May 2008.

[NY04] D. K. Nadyozhin and A. V. Yudin. Equation of State under Nuclear Statistical Equilibrium Conditions. *Astronomy Letters*, 30:634–646, September 2004.

[NY05] D. K. Nadyozhin and A. V. Yudin. The Influence of Coulomb Interaction on the Equation of State under Nuclear Statistical Equilibrium Conditions. *Astronomy Letters*, 31:271–279, April 2005.

[OGH+07] E. O'Connor, D. Gazit, C. J. Horowitz, A. Schwenk, and N. Barnea. Neutrino breakup of A=3 nuclei in supernovae. *Phys. Rev. C*, 75(5):055803, May 2007.

[Par04] Particle Data Group, S. Eidelman et al. Review of Particle Physics. *Physics Letters B*, 592:1–5, July 2004.

[PBP+97] M. Prakash, I. Bombaci, M. Prakash, P. J. Ellis, J. M. Lattimer, and R. Knorren. Composition and structure of protoneutron stars. *Phys. Rep.*, 280:1–77, 1997.

[PCL95] M. Prakash, J. R. Cooke, and J. M. Lattimer. Quark-hadron phase transition in protoneutron stars. *Phys. Rev. D*, 52:661–665, July 1995.

[PGW06] D. Page, U. Geppert, and F. Weber. The cooling of compact stars. *Nucl. Phys. A*, 777:497–530, October 2006.

[PHSB09] G. Pagliara, M. Hempel, and J. Schaffner-Bielich. New possible quark-hadron mixed phase in protoneutron stars. *Physical Review Letters*, 103(17):171102, 2009.

[Pie04] J. Piekarewicz. Unmasking the nuclear matter equation of state. *Phys. Rev. C*, 69(4):041301, April 2004.

[Pir05] Tsvi Piran. The physics of gamma-ray bursts. *Rev. Mod. Phys.*, 76(4):1143–1210, Jan 2005.

[PMP04] P. K. Panda, D. P. Menezes, and C. Providência. Stellar matter in the quark-meson-coupling model with neutrino trapping. *Phys. Rev. C*, 69(5):058801, May 2004.

[PRE+00] J. A. Pons, S. Reddy, P. J. Ellis, M. Prakash, and J. M. Lattimer. Kaon condensation in proto-neutron star matter. *Phys. Rev. C*, 62(3):035803, September 2000.

[PS08] G. Pagliara and J. Schaffner-Bielich. Stability of color-flavor-locking cores in hybrid stars. *Phys. Rev. D*, 77(6):063004, March 2008.

[PSPL01] J. A. Pons, A. W. Steiner, M. Prakash, and J. M. Lattimer. Evolution of Proto-Neutron Stars with Quarks. *Physical Review Letters*, 86:5223–5226, June 2001.

[Ran09] J. Randrup. Phase transition dynamics for baryon-dense matter. *Phys. Rev. C*, 79(5):054911, May 2009.

[Rau03] T. Rauscher. Nuclear Partition Functions at Temperatures Exceeding 10^{10} K. *Astrophysical Journal Supplement Series*, 147:403–408, August 2003.

[RBP00] S. Reddy, G. Bertsch, and M. Prakash. First order phase transitions in neutron star matter: droplets and coherent neutrino scattering. *Physics Letters B*, 475:1–2, February 2000.

[Rei89] P.-G. Reinhard. REVIEW ARTICLE: The relativistic mean-field description of nuclei and nuclear dynamics. *Reports of Progress in Physics*, 52:439–514, April 1989.

[RGSG91] Dirk H. Rischke, Mark I. Gorenstein, Horst Stoecker, and Walter Greiner. Excluded volume effect for the nuclear matter equation of state. *Z. Phys.*, C51:485–490, 1991.

[RHS06] S. B. Rüster, M. Hempel, and J. Schaffner-Bielich. Outer crust of nonaccreting cold neutron stars. *Phys. Rev. C*, 73(3):035804, March 2006.

[Roe09] G. Roepke. Light nuclei quasiparticle energy shifts in hot and dense nuclear matter. *Phys. Rev. C*, 79(1):014002, January 2009.

[RPW83] D. G. Ravenhall, C. J. Pethick, and J. R. Wilson. Structure of Matter below Nuclear Saturation Density. *Phys. Rev. Lett.*, 50:2066–2069, June 1983.

[RT00] T. Rauscher and F.-K. Thielemann. Astrophysical Reaction Rates From Statistical Model Calculations. *Atomic Data and Nuclear Data Tables*, 75:1–2, May 2000.

[RTK97] T. Rauscher, F.-K. Thielemann, and K.-L. Kratz. Nuclear level density and the determination of thermonuclear rates for astrophysics. *Phys. Rev. C*, 56:1613–1625, September 1997.

[RWB+05] Stefan B. Rüster, Verena Werth, Michael Buballa, Igor A. Shovkovy, and Dirk H. Rischke. Phase diagram of neutral quark matter: Self-consistent treatment of quark masses. *Phys. Rev. D*, 72(3):034004, Aug 2005.

[RWB+06a] S. B. Rüster, V. Werth, M. Buballa, I. A. Shovkovy, and D. H. Rischke. Phase diagram of neutral quark matter: The effect of neutrino trapping. *Phys. Rev. D*, 73(3):034025, February 2006.

[RWB+06b] S. B. Rüster, V. Werth, M. Buballa, I. A. Shovkovy, and D. H. Rischke. Phase diagram of neutral quark matter: The effect of neutrino trapping. *Phys. Rev. D*, 73(3):034025, February 2006.

[Saw05] R. F. Sawyer. Effects of ion and electron correlations on neutrino scattering in the infall phase of a supernova. *Physics Letters B*, 630:1–6, December 2005.

[SB07] F. Sandin and D. Blaschke. Quark core of protoneutron stars in the phase diagram of quark matter. *Physical Review D (Particles, Fields, Gravitation, and Cosmology)*, 75(12):125013, 2007.

[SGST00] K. Schertler, C. Greiner, J. Schaffner-Bielich, and M. H. Thoma2. Quark phases in neutron stars and a third family of compact stars as signature for phase transitions. *Nucl. Phys. A*, 677:463–490, September 2000.

[Sha09] M. M. Sharma. The breathing-mode giant monopole resonance and the surface compressibility in the relativistic mean-field theory. *Nuclear Physics A*, 816:65–88, January 2009.

[SHGS06] I. Sagert, M. Hempel, C. Greiner, and J. Schaffner-Bielich. Compact stars for undergraduates. *European Journal of Physics*, 27:577–610, May 2006.

[SHP+09] I. Sagert, M. Hempel, G. Pagliara, J. Schaffner-Bielich, T. Fischer, A. Mezzacappa, F.-K. Thielemann, and M. Liebendörfer. Signals of the QCD Phase Transition in Core-Collapse Supernovae. *Physical Review Letters*, 102(8):081101, February 2009.

[SHSG02] J. Schaffner-Bielich, M. Hanauske, H. Stöcker, and W. Greiner. Phase Transition to Hyperon Matter in Neutron Stars. *Physical Review Letters*, 89(17):171101, 2002.

[SKC06] S. Shlomo, V. M. Kolomietz, and G. Colò. Deducing the nuclear-matter incompressibility coefficient from data on isoscalar compression modes. *European Physical Journal A*, 30:23–30, October 2006.

[SLB10] A. W. Steiner, J. M. Lattimer, and E. F. Brown. The Equation of State from Observed Masses and Radii of Neutron Stars. *ArXiv e-prints*, May 2010.

[SPL00] A. W. Steiner, M. Prakash, and J. M. Lattimer. Quark-hadron phase transitions in young and old neutron stars. *Physics Letters B*, 486(3-4):239 – 248, 2000.

[SR07] J. R. Stone and P.-G. Reinhard. The Skyrme interaction in finite nuclei and nuclear matter. *Progress in Particle and Nuclear Physics*, 58:587–657, April 2007.

[SR08] K. Sumiyoshi and G. Röpke. Appearance of light clusters in post-bounce evolution of core-collapse supernovae. *Phys. Rev. C*, 77(5):055804, May 2008.

[SSL+09] S. R. Souza, A. W. Steiner, W. G. Lynch, R. Donangelo, and M. A. Famiano. Comparison of Statistical Treatments for the Equation of State for Core-Collapse Supernovae. *Astrophys. J.*, 707:1495–1505, December 2009.

[ST94] Y. Sugahara and H. Toki. Relativistic mean-field theory for unstable nuclei with non-linear σ and ω terms. *Nucl. Phys. A*, 579:557–572, October 1994.

[STOS98a] H. Shen, H. Toki, K. Oyamatsu, and K. Sumiyoshi. Relativistic equation of state of nuclear matter for supernova and neutron star. *Nucl. Phys. A*, 637:435–450, July 1998.

[STOS98b] H. Shen, H. Toki, K. Oyamatsu, and K. Sumiyoshi. Relativistic Equation of State of Nuclear Matter for Supernova Explosion. *Progress of Theoretical Physics*, 100:1013–1031, November 1998.

[SV09a] V. V. Skokov and D. N. Voskresensky. Hydrodynamical description of a hadron-quark first-order phase transition. *Soviet Journal of Experimental and Theoretical Physics Letters*, 90:223–227, October 2009.

[SV09b] V. V. Skokov and D. N. Voskresensky. Hydrodynamical description of first-order phase transitions: Analytical treatment and numerical modeling. *Nuclear Physics A*, 828:401–438, September 2009.

[SWS+08] H. Sonoda, G. Watanabe, K. Sato, K. Yasuoka, and T. Ebisuzaki. Phase diagram of nuclear "pasta" and its uncertainties in supernova cores. *Phys. Rev. C*, 77(3):035806, March 2008.

[TB01a] T. A. Thompson and A. Burrows. Neutrino processes in supernovae and the physics of protoneutron star winds. *Nuclear Physics A*, 688:377–381, May 2001.

[TB01b] S. Typel and B. A. Brown. Neutron radii and the neutron equation of state in relativistic models. *Phys. Rev. C*, 64(2):027302, August 2001.

[TBP03] T. A. Thompson, A. Burrows, and P. A. Pinto. Shock Breakout in Core-Collapse Supernovae and Its Neutrino Signature. *Astrophys. J.*, 592:434–456, July 2003.

[TDF+10] F.-K. Thielemann, I. Dillmann, K. Farouqi, T. Fischer, C. Fröhlich, A. Kelic-Heil, I. Korneev, K.-L. Kratz, K. Langanke, M. Liebendörfer, I. V. Panov, G. Martinez-Pinedo, and T. Rauscher. The r-, p-, and νp-Process. *Journal of Physics Conference Series*, 202(1):012006, January 2010.

[THS+95] H. Toki, D. Hirata, Y. Sugahara, K. Sumiyoshi, and I. Tanihata. Relativistic many body approach for unstable nuclei and supernova. *Nuclear Physics A*, 588:357, May 1995.

[TRK+10] S. Typel, G. Röpke, T. Klähn, D. Blaschke, and H. H. Wolter. Composition and thermodynamics of nuclear matter with light clusters. *Phys. Rev. C*, 81(1):015803, January 2010.

[TS88a] M. Takahara and K. Sato. Supernova explosions and the soft equation of state. *Astrophys. J.*, 335:301–305, December 1988.

[TS88b] Mariko Takahara and Katsuhiko Sato. Phase transitions in the newly-born neutron star and neutrino emissions from sn1987a. *Progress of Theoretical Physics*, 80(5):861–867, 1988.

[TZD+09] M. B. Tsang, Y. Zhang, P. Danielewicz, M. Famiano, Z. Li, W. G. Lynch, and A. W. Steiner. Constraints on the Density Dependence of the Symmetry Energy. *Physical Review Letters*, 102(12):122701, March 2009.

[VYT03] D. N. Voskresensky, M. Yasuhira, and T. Tatsumi. Charge screening at first order phase transitions and hadron-quark mixed phase. *Nuclear Physics A*, 723(1-2):291–339, July 2003.

[Wal74] J. D. Walecka. A theory of highly condensed matter. *Ann. Phys. (N.Y.)*, 83:491–529, April 1974.

[WHW02] S. E. Woosley, A. Heger, and T. A. Weaver. The evolution and explosion of massive stars. *Rev. Mod. Phys.*, 74(4):1015–1071, Nov 2002.

[Wit84] E. Witten. Cosmic separation of phases. *Phys. Rev. D*, 30:272–285, July 1984.

[WMS+05] Gentaro Watanabe, Toshiki Maruyama, Katsuhiko Sato, Kenji Yasuoka, and Toshikazu Ebisuzaki. Simulation of transitions between "pasta" phases in dense matter. *Phys. Rev. Lett.*, 94(3):031101, Jan 2005.

[YK09] N. Yasutake and K. Kashiwa. Lepton effects on the protoneutron stars with the hadron-quark mixed phase in the Nambu Jona-Lasinio model. *Phys. Rev. D*, 79(4):043012, February 2009.

[YKaHY07] Nobutoshi Yasutake, Kei Kotake, Masa aki Hashimoto, and Shoichi Yamada. Effects of qcd phase transition on gravitational radiation from two-dimensional collapse and bounce of massive stars. *Physical Review D (Particles, Fields, Gravitation, and Cosmology)*, 75(8):084012, 2007.

[YT01] M. Yasuhira and T. Tatsumi. Protoneutron stars with kaon condensation and their delayed collapse. *Nuclear Physics A*, 690:769–789, July 2001.

[ZBHG06] J. L. Zdunik, M. Bejger, P. Haensel, and E. Gourgoulhon. Phase transitions in rotating neutron stars cores: back bending, stability, corequakes, and pulsar timing. *Astron. Astrophys.*, 450:747–758, May 2006.